SAPIENZA
UNIVERSITÀ DI ROMA

# Smart Grids for Power Quality Improvement

*PhD Course in Engineering and Applied Science for Energy and Industry*

*XXXII cycle*


Tutors:

**Prof. Alberto Geri**

**Ing. Massimo Cresta**

International Co – tutor:

**Prof. Mihai Sănduleac**

Candidate:

**Tommaso Bragatto**


A.A. 2018-2019

# Table of Contents

# List of Figures

# List of Tables

# 1 Introduction

## 1.1 Motivation and context

In the context of an increasing penetration of Distributed Generators, Distribution System Operators of any size are facing the transition to the Smart Grid, investigating how its role will change in the future. This work will present a comprehensive analysis of how a DSO would face the Power Quality issue in the future thanks to the technologies of the smart grids.

The activities have been carried out in collaboration with the DSO of the city of Terni, namely ASM Terni S.p.A. (ASM) and its productivity unit Terni Distribuzione Elettrica (TDE) which owns and manages the distribution network in the municipality. During the work lifespan, there has been the opportunity to evaluate smart technologies and carry out grid analysis in a real environment, notably, the Medium Voltage distribution network of TDE and the living laboratory at ASM headquarters. Some activities have been totally developed within this work whilst others have been carried out in the context of some European projects that have been founded or cofounded by the Innovation and Research & Innovation actions for Energy sector established by the European Commission and involve ASM as consortiums' partner. The consortiums of these projects have designed, produced and installed in the ASM facilities cutting-edge devices and software solutions for the distribution network and the electrical customers; this work has evaluated their contribution on the power quality.

Firstly, it is worth defining Smart Grid in the context of this work. Even if its definition in currently under discussion because the variety of actors involved, the most common definitions have been collected in [1] and the most suitable for this work has been provided by U.S. Department of Energy (DOE). The U.S. Department of Energy has defined the smart grid in terms of seven features:

- Optimize asset utilization and operating efficiency.
- Accommodate all generation and storage options.
- Provide power quality for the range of needs in a digital economy.
- Anticipate and respond to system disturbances in a self-healing manner.
- Operate resiliently against physical and cyber-attacks and natural disasters.
- Enable active participation by consumers.
- Enable new products, services, and markets.

Therefore, the definition of Smart Grid according to DOE is as follows, [2]:

"The smart grid is the electricity delivery system, from point of generation to point of consumption, integrated with communications and information technology for enhanced grid operations, customer services, and environmental benefits. A smart grid is self-healing, enables active participation of consumers, operate resiliently against attack and natural disasters, accommodate all generation and storage options, enable introduction of new products, services and markets, optimize asset utilization and operate efficiently, provide power quality for the digital economy."

Considering Smart Grid definition, it is important to understand what is currently Power Quality for a DSO; in this respect, the main objective of a DSO is to reduce the interruptions, secondly

abnormal voltages are also an issue as well as the reduction of technical losses (i.e., increasing the energy efficiency). However, DSOs are focused on outages since it means the lack of its main services to the users, namely, electrical energy, which also dramatically affects other crucial services such as Telecommunication, heating, cooling, water, industrial processes.

Moreover, the Italian DSOs, which have been studied in this work, receive monetary incentives or have to pay penalties if the outages, recorded in a year, are less than defined objectives or more than these. Investigating on reduction of outages implies an increase of resilience of the distribution network, as the ability of a DSO to promptly react when a foreseen event and rapidly restore the network to the normal status.

## 1.2 Objectives

The reduction of outages are investigated in this work considering contributions on the network development plans and on real time operations. Therefore, in a first stage, the analysis of a component widely installed in the Italian distribution networks has been carried out; notably thermal analysis of MV cable and joint is performed in order to investigate on the anomalous number of faults on this component that have been recorded in summer during last years.

Moreover, the distribution network of TDE has been analyzed with a Resilience assessment software and its related procedures for improving and validating the development plan of the distribution network. The homemade software, developed during this work lifespan, can be used for any networks and the resilience can be assessed for any type of treats.

The last stage consists of theoretical evaluations and demonstration activities of innovative solutions that could help the DSO to reduce congestions in the network during real time operation (i.e., to prevent and foreseen outages). The enabling tools that have been used are Real time Smart Meters installed in the networks and proper management software. In this respect, main concern of this work has been the interaction between DSO and Aggregator who manages a pool of users in the Demand Response campaigns. The evaluated mechanisms allow DSO to increase hosting capacity of the network in respect of Photovoltaic plants (PV) and Electrical Vehicles (EV). Moreover, this work presents assessment on cooperation mechanism between DSO and a rural microgrid by means of a proper ICT infrastructure.

In the context of power quality improvement thanks to the Smart Grids, further technologies have been evaluated in this work. With respect to the energy efficiency and voltage control, the support from storage systems have been studied by means of tests on the field, as well as it has been assessed the support from EV charging stations coordinate with the implementation of smart contracts leveraging on blockchain technology.

## 1.3 Thesis organization

The contents of the thesis are organized in 4 Chapters, each of them contains Sections and several Subsections. A brief abstract for each chapter is reported.

*Chapter 2 – Pillars of the Smart Grid: state of the art*

This chapter reports some the major trends for the Smart Grids, highlighting also the most notable features currently available in a distribution network. Each section deals with a different pillar of the Smart Grid, notably Section 2.1 reports the metering infrastructures available for the DSO to manage the grid; Section 2.2 deals with energy storage systems and their current status as for the integration with the prosumers (i.e., consumers able to self-produce energy); Section 2.3

analyzes the most adopted solutions for Demand Response (DR), reporting the obstacles and barriers in their adoption; Section 2.4 describes the challenges of electric mobility.

*Chapter 3 – Terni: real-life pilot for research applied on Smart Grids*

As anticipated in previous section, the activities of this work have leveraged on the facilities and assets of ASM and TDE, notably, the features of the distribution network are reported in Section 3.1 highlighting the impact of the distributed generators whilst Section 3.2 presents a focus on the behavior of the prosumers connected to the grid in Terni.

*Chapter 4 – Network Planning for continuity of supply*

In the context of Smart Grid technologies, software for the analysis of the grids and their components can be used for improving power quality. This chapter presents the analysis carried out for improving DSO awareness about the network vulnerability, aiming to improve the distribution grids in the development plans aiming at reduce the number of outages and improving the resilience of the infrastructure.

This objective has been reached analyzing key components that are currently subject to anomalous failure rates, notably, the cold – shrinkable MV joints, analyzed in Section 4.1. This section presents a full 3D model of grounded cable and joints which have been developed and compared with two different experimental setups (i.e., one in a laboratory environment and another one applying real conditions on the component); the model has been used for evaluating the effect of different conditions on temperature aiming at investigate which may be the causes for the anomalous number of faults recorded in the last 5 years.

Section 4.2 deals with a resilience assessment carried out with a homemade software which implements network topology and assets vulnerability for evaluating the effects of extreme weather events as well as other treats in terms of disconnected users. The goal of the analysis is to validate and improve the development plan of the DSO.

*Chapter 5 – Real – time operations for Power Quality Improvement: Flexibility Sources and their management*

This Chapter deals with the contribution of the Smart Grid technologies, actually implemented in the aforementioned pilot site, on Power Quality improvement.

Section 5.1 reports the enabling technologies, highlighting the features of the real time Smart Meters, developed over Nobel GRID project, [3], and the related software for managing DR campaigns and the distribution networks. Details about the storage system are provided, notably it consists of Second Life Batteries which were used for the mobility purpose. Finally, an overview of cutting edge technologies is reported.

Section 5.2 presents the results of the demonstration activities and theoretical analysis dealing with the improvement of energy efficiency, notably, the usage of batteries and microgrid resources have been evaluated in this work.

Section 5.3 shows the main results of the demonstration of activities carried out in a real environment, evaluating how the implemented solutions could improve the electrical parameters. In this respect, the provision of ancillary services from storage systems have been assessed as well as the effect of DR on hosting capacity and energy efficiency.

*Published materials*

Some contents of this thesis have been published during the lifespan of the work and they are properly cited in the text. The complete list of publications is provided by Section 7.

# 2 Pillars of the Smart Grid: state of the art

## 2.1 Grid trends: challenges and opportunities

During WiseGRID project, the main grid trends have been collected in [4]; according to World Economic Forum [5], innovation has the potential to reshape the energy sector, while benefiting not only the industry actors, but also their customers and the environment. Several promising technical options have become or are becoming viable: distributed RES generation (already quite common), distributed generation combined *in situ* with distributed storage, consumer side options technologies such as smart meters, smart appliances and electric vehicles. While there are significant distributed RES installed, independent storage facilities together with V2G technologies are emerging. However, a wider adoption of these technologies would be possible only with a strong interest of the consumers that should be driven by market levers or specific incentives (e.g. tax credits) together with a "going-green" lifestyle shift.

Three major trends are affecting the electricity system (*Figure 1*), [5]:

**1. Electrification**: more equipment is becoming electrically supplied, domestic heating and transportation (electric vehicles) being the two most relevant examples. Coupled with increased RES generation, this will reduce the use of fossil fuels. Increasing electrification also provides opportunities to enhance the flexibility and efficiency of electricity systems.

**2. Decentralization:** to decentralize part of the generation and storage, moving from the high voltage grid to medium and low voltage area. Distributed generation can benefit customers and the system, supplying electricity directly and supporting load growth. Distributed storage offers a way to flatten out the peaks and valleys of supply and could be a viable alternative to "peaker plants".

**3. Digitization:** the increasing use of IT and digital technologies. Smart energy systems can enable demand-response measures. Smart meters and smart appliances allow demand management and provide incentives for consumers to play an active role in providing flexibility to the energy systems.

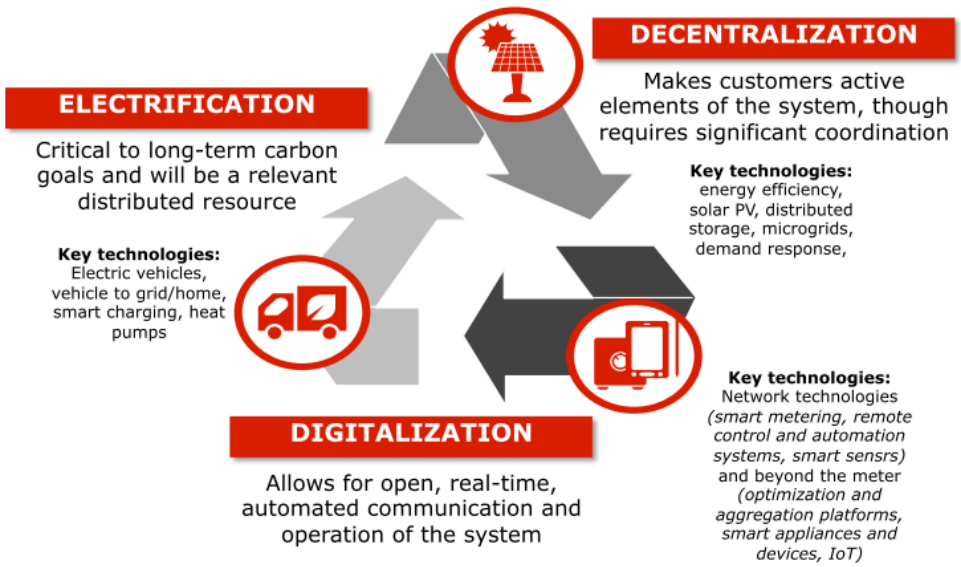


*Figure 1 – Major grid trends* [5]

These trends pave the way towards a system where traditional boundaries between producers, distributors and customers are blurred, increasing the complexity of system governance and posing many challenges to the distribution grid:

- Increasing presence of renewable power,
- Increasing presence of Distributed Energy Resources (DER) RES, storage, PHEV,
- Bi-directional flow of energy ("Prosumers"),
- Increasing distributed energy resources require real-time management of bidirectional power flows - "Prosumers", since intermittent energy sources, such as wind and solar, must be counter-balanced by "smarter" grid and energy storage that may provide capacity to the grid when demand is peaking, reducing supply and demand mismatch,
- Shifting from centralized to decentralized generation and control architecture,
- Automation of distribution management,
- Situational awareness and grid predictability is becoming more critical,
- New applications/services based on smart devices and more active network,
- Smart devices/resources with distributed intelligence,
- Coordinated decision making,
- Big Data,

Shifting from centralized to decentralized grid management, while maintaining grid stability and security, implies the need of real-time grid monitoring and new application/services gathering data from interconnected smart devices that replace or integrate traditional equipment, in order to improve the automation of distribution management operations.

Undoubtedly, the electric distribution system has been considerably affected by grid modernization. The "smart grid" has transformed the electric distribution systems from dated processes to electronic and computer-managed decision making with a high level of automation. The core of this transformation is the Distribution Management System (DMS), which is a set of integrated computer and communication systems whose purpose is to assist the Distribution System Operator (DSO), electrical engineers, and other electric utility technicians in monitoring and controlling the distribution system in an optimal way without compromising safety, stability or systems' protection, [6], [7], [8] and [9].

The DMS can cover an entire distribution grid or just a subset of the whole system, such as a number of substations of the distribution grid. The DMS generally has full capability for the overall operation of the entire grid or part of the grid. Most of the today's DMS are designed to meet operational requirements for the automation and administration of traditional distribution grids. The fundamental characteristics of the traditional distribution systems are passive networks and radial configurations. These characteristics are the base for today's DMS planning and implementation; grid modelling, data structures, and advanced application algorithms are key features of a modern DMS. An ordinary DMS is generally consisted of several subsystems and software modules. Although the overall architecture of a DMS with these components may still work fine for a new distribution grid with a high penetration of DER and microgrids, the contents of these components may need to be extended or updated significantly by incorporating the impacts of the transition from passive to active networks in the distribution grids.

A typical Distribution System consists of a DMS, SCADA, GIS, AMR and ERP systems.

### 2.1.1 *Supervisory Control And Data Acquisition (SCADA)*

A power transmission system transports the electric power from production to the loads by using transmission lines and distribution substations. Implementing a SCADA system for the power distribution not only reduces manual operation but also facilitates automatic operations with reduced disruptions offering a smoother and more reliable operation.

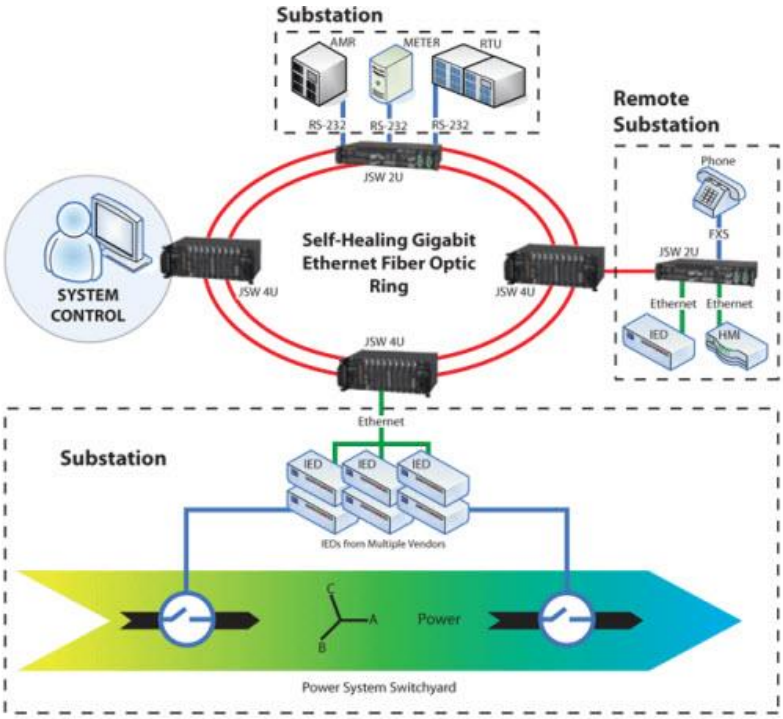


*Figure 2 – SCADA system overview* [10]

*Figure 2* shows the structure of a SCADA in a power system, where it collects data from different electrical substations (even at remote locations) and correspondingly processes the data. Programmable logic controllers monitor substation components in real time and transmit data to a centralized SCADA system. If any failure of electrical power occur, SCADA detects the exact location of the fault, reducing the waiting time for calls from customers. SCADA immediately alarms system operators for identification, allowing faster system healing. Also in substations, SCADA automatically controls isolator switches and circuit breakers for exceeding parameter limits, thereby continuous inspection of parameters is performed without a line worker. Some of the functions of SCADA in power distribution system are:

- Improving power system efficiency by maintaining an appropriate range of power factor
- Reducing peak power demand
- Continuous monitoring, controlling of various electrical parameters and improvement of operation under both normal and unstable conditions
- Alarming operators by addressing the problem
- Historic data querying
- Response to customer service interruptions

The advantages of Implementing SCADA systems for Electrical Distribution are the following:

- Due to faster recognition of faults, equipment damage can be avoided
- Monitoring and control of distribution network can be performed remotely
- Saves work cost by eliminating manual operation
- Reduce outage time by generating alarms to quickly address problems
- Improves the constancy of service by restoring power after the occurrence of temporary faults
- Automatically improves the voltage profile due to power factor correction and VAR control
- Facilitates the view of historical data in various ways
- Reduces the labor cost by reducing the staff required for meter reading

The major components in a SCADA system are the following:

- **Remote Terminal Units (RTUs)**

RTU is the main component in a SCADA system because it has a direct connection with various sensors, meters and actuators associated with a control environment.

RTUs are real-time programmable logic controllers (PLCs) which are responsible for properly converting remote station information to digital form, sending and receiving signals from a master unit to control process equipment through actuators and switchboxes.

- **Master Terminal Units (MTUs)**

A central host server is called Master Terminal Unit, sometimes also called SCADA center. It communicates with several RTUs by executing reading and writing operations. In addition, it performs control, alarming, networking with other nodes, etc.

- **Communications System**

The communication network transfers data between central host computer servers and field data interface devices and control units. The network link can be cable, radio, telephone, satellite or any combination of them.

- **Operator Workstations**

These are the computer terminals presenting a Human Machine Interface software. These workstations are operator terminals that request and send the information to host client computer in order to monitor and remotely control the field parameters.

### 2.1.2 *Automatic meter reading (AMR) and new techniques based on real time metering data from Unbundled Smart Meter*

The Automatic Meter Reading (AMR) and Meter Data Management (MDM) systems refer to equipment and applications that enable the provider to control remote smart meters, store their data and process it for pricing, troubleshooting, and analysis purposes. The AMR system can provide metering data and information about the consumer's energy profile and other elements that may be useful for different actors, such as DMS or other applications.

The latest technological developments are challenging for finding new solutions to mitigate the massive integration of renewable-based electricity generation in the electrical networks and to support new and dynamic energy and ancillary services markets. One challenge is, for instance, the massive (small) PV roof-based installations, which demand a solution to solve observability in such

sites. Smart meters are becoming ubiquitous equipment in the low voltage grid, enabled by the decision made in many countries to support massive deployments.

The smart meter is the only equipment mandatory to be mounted when supplying a grid connected user, as it primarily has the function to measure delivered and/or produced energy on its common coupling point with the network, as a technical and legal support for billing. Active distribution networks need new functionalities to cope with bidirectional energy flows on the grid, and many smart grid requirements need to be implemented in the near future. However, there is no real coupling between smart meter systems and smart grids, as there is not yet a synergy using the opportunity of the high deployment level in smart metering.

Currently, an innovative approach, evaluated and implemented in this work, is to manage the smart metering and smart grid orchestration proposes a new general design based on an unbundled smart meter (USM) concept *Figure 3*, labelled as a next generation meter with a design from scratch accommodating both SMM and SMX, and having the name SLAM (Smart Low cost Advanced Meter). SLAM is intended to be deployed everywhere at the prosumer's interface to the grid is, as it is usually now, the case with standard meters. Furthermore, rich data acquired by the SLAM will be used to demonstrate the potential of providing real-time data for improving DSO operations, *Figure 4*. The information sent to the DSO is only non-sensitive data from a privacy perspective, and is therefore able to be applied everywhere in the grid, down to the end-customer level, where a citizen's personal data protection is an important aspect.

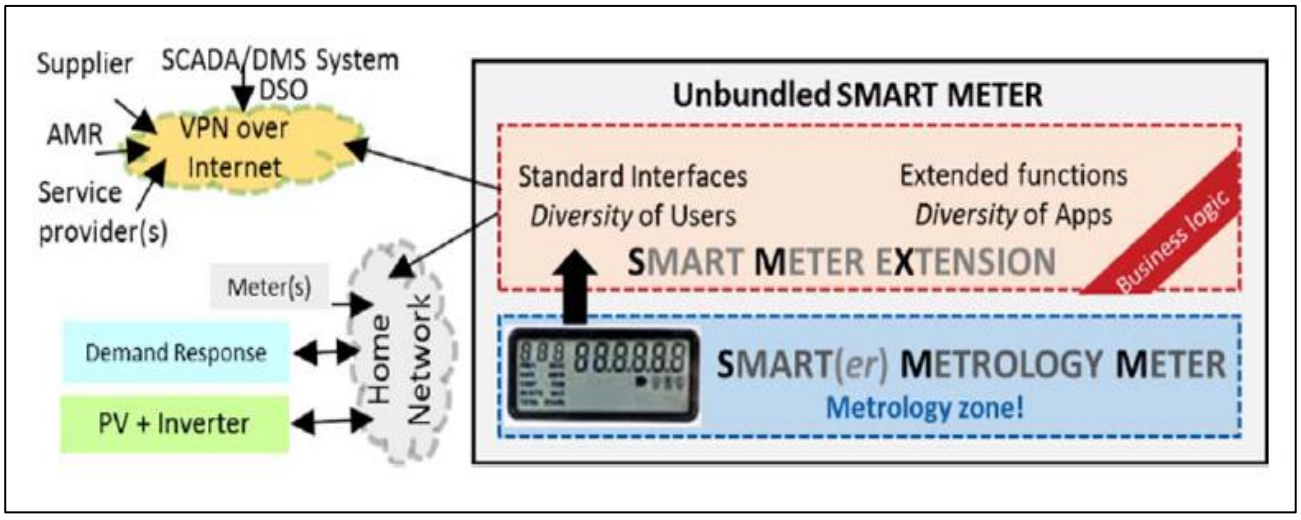


*Figure 3 Unbundled Smart Meter Architecture,* [11]

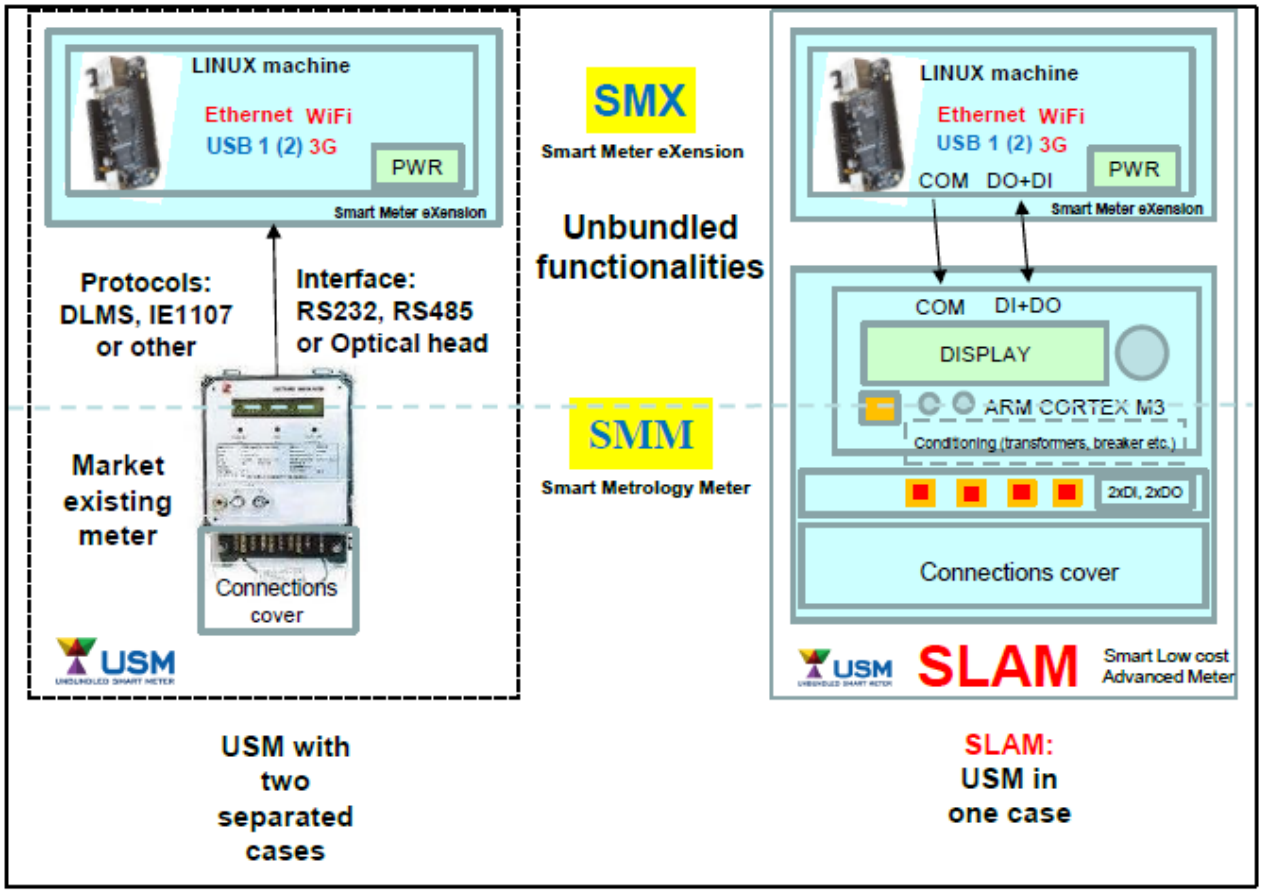


*Figure 4 Unbundled Smart Meter in the Nobel GRID project,* [11]

Today, electricity grids face multiple challenges due to high renewable penetration and to the dynamic evolution of the markets of energy and energy services. Some of the challenges related to renewables are: the stochastic behaviour of renewable energy production, the possible change of power flow direction in the distribution networks (initially designed to have only one-way power flow and a passive/loads only behaviour) and the temporal mismatch between production and load. These challenges are being widely considered in the scientific community and have been treated in many papers (e.g., [12], [13], [14], [15]). Smart metering (SM) is the new technical solution for evolving markets and the smart grid is the new paradigm where the power network and its generic prosumers are highly linked by information and communication technologies (ICT) solutions, expecting to improve the overall network functionality. But at producer or consumer level, high levels of smart metering deployment still do not support the emerging smart grid functionalities.

Both smart metering and smart grids must also face cyber-security threats. Security aspects related to smart meters deployment have been analysed from different perspectives, e.g., by the authors of [16] and [17].

Today, the state-of-the-art smart meters are characterized by complex functionalities:

- Active and reactive energy measurement with metrology certification, such that they can be used for official billing purposes (meters without such certification are not legally enforced to provide information valid for invoicing).
- Complex tariff implementations.

- Design based on communication with the most important actor, which is managing the billing data: the DSO (distribution system operator)—as market facilitator in most EU countries, or the independent central hub—as third party market facilitator [18].
- The communication path is implemented in most cases through the PLC (power line carrier, considered to bring no or very low operational losses) and in some cases through GPRS (general packet radio service)/3G.
- Usual protocols for the data readout from smart meters are specialized for AMR/AMI (automatic meter reading/advanced metering infrastructure) data collection, e.g., DLMS/COSEM (device language message specification/companion specification for energy metering) protocol and its associated data model.
- Smart meters are able to provide, on request, instrumentation measurements at high reporting rates, between 1 and 10 s, as a possible support for SCADA (supervisory control and data acquisition) functionalities. This instrumentation data (e.g., voltage u, current i, active power p, reactive power q) is still not used at its full potential, for various reasons: the communication path is too slow (valid especially for PLC communication), protocol is not appropriate for SCADA, etc.;
- Load profiles (LP) of energy, instrumentation and of other data can be stored for medium to long periods, such as one month to several months, depending on the selected time period for LPs memorization; usually for LP periods of 15 minutes between consecutive records, the LP time depth is more than one month.
- Some electrical energy smart meters have functionalities to collect data from other local meters: gas, water or heat meters; this architecture enables multi-utility/multi-service smart metering [19], allowing improvements in energy and market efficiency.
- A small number of electrical energy smart meters have a local interface to communicate with local devices, thus enabling different services for final users.
- A small number of electrical energy smart meters have a local interface to communicate with end-users [20], thus enabling energy awareness and supporting different services for final users.

The Smart Low-cost Advanced Meter (SLAM), developed within NOBEL GRID project [21], implements in an enhanced way all these functionalities and much more:

- Complex tariffication is helped also by a nearly real-time possibility of communication with the supplier or with the spot market, thus allowing to take advantage of real-time opportunities such as small or negative prices due to temporary excess of RES energy (curtailment in the case of excess energy may be avoided if additional RES production is paired with additional consumption, if possible).
- The SLAM communication is simultaneously multi-user and multi-protocol, which allows that all energy actors can access the metering data;
- A powerful role-based access control (RBAC) functionality allows that each actor is accessing the data with his particular rights, based on its role in providing services; for instance, DSO has access at non-private real-time data such as voltage level, but not to the real-time active power, which can disclose private activity; an ESCO or aggregator can have access to more fine-grained data if their service requires it and if a specific data protection contract has been signed between the parts.

- Smart Grid is helped with real-time data down to one second reporting time, which gives similar or better performance compared with traditional SCADA, while the measurements accuracy is in most cases superior.
- To allow this flexibility of communication, IP-based communication is used on public networks, such as internet, which gives easy access directly to the meter data; it means that today PLC is not a choice, as it is not publicly available (but only to DSO) and does not have enough dynamics to allow real-time exchange of data for all the meters (only very few and selected meters in a LV metering pool may have a certain real-time behaviour).
- Cyber security is high, based on multiple VPN pathways, a different one for each type of actors; this allows a high level of security for the transmission of data; additional improvements of data security may be possible by extending the security level with Physical Unclonable Function (PUF), which is developed in [22].
- The meter allows different types of local interface in order to communicate with local devices, thus enabling different services such as demand response. Different communication means can become operational by adding e.g. through the USB a radio dongle to interact with loads / intelligent white appliances through Wi-Fi or ZigBee); the interoperability is enabled by a specific driver (or agent) in SMX, which can be added during the runtime, and not only during the initial deployment.

  The meter has a local interface to communicate with end-users, which can access it through a web browser on the smartphone, tablet, laptop or stationary PC; energy awareness is highly boosted and allows important savings based on the real-time monitoring.
- The fine granularity in voltage measurement (each second) allows to monitor voltage level quality, as part of a more complex PQ measurement support.
- SLAM supports measurements of voltage harmonics up to the 42$^{nd}$ harmonic, being able to monitor and assess the pollution of the grid with the harmonics at the level of all meters. Complex IEC-based measurements can be done with specific and expensive equipment only in special situations when there is a specific request or for grid analysis.
- SLAM allows to run on the SMX side different software agents which allow new functionalities such as local renewables and storage support for the upcoming prosumers as well as a better accommodation of home EV charging,
- SLAM is unleashing and improving all businesses which need energy measurement over different time periods (slots) from each hour down to each minute. It is also improving functionalities for smartening the grid, as it is able to provide real-time grid data to actors such as DSO and aggregators, in order to improve different specific functionalities. The high reporting rate, down to each second, is competing with the classic RTU, while this comes with smart meter needed for billing purposes.
- The data security is a killing factor for smart grids, meaning that if it is not well implemented, the smart grid functionality should be not implemented as well. With high data-security based equipment such as SLAM, the real-time data as well as the energy records used for billing energies and energy services become trustful and allow both high security and enhanced privacy by design.

## 2.2 Demand and services of energy storage system for the DSO

### 2.2.1 *Classification and types of Storage systems*

There are several types of energy storage technologies that can be deployed in an energy system, [23]. In general, one can distinguish different categories of storage technologies such as electrochemical, chemical, thermal, mechanical and electromagnetic. Also a combination of different technologies, the so called hybrid technologies, is possible. *Figure 5* gives an overview of existing technologies.

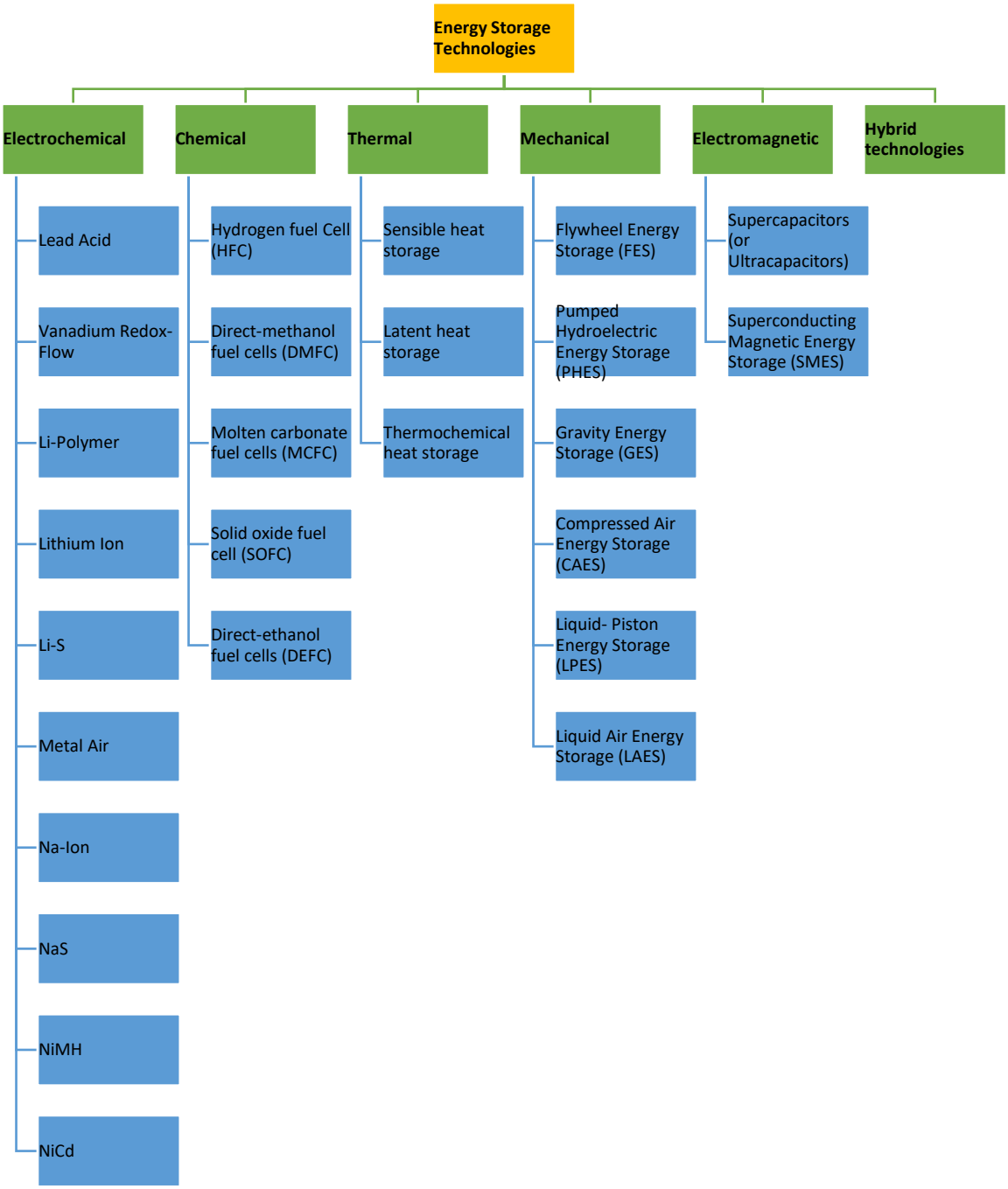


*Figure 5 - Types of energy storage technologies*

In general, such systems store energy that is produced at one time for use at a later time. While doing so, one energy form is often converted into another, e.g. in the case of electrochemical

storage systems electricity is converted into electrochemical energy and vice versa. As illustrated in Figure 5 each category features several sub-technologies which again differ in the used material compositions like in the case of electrochemical storage systems or in the functional principle, e.g. the pumping of water into a reservoir or the compression of air. Besides the functional principle the storage duration is one important characteristic. Some technologies are used for short-term storage (minutes to hours) and some are used for long-term storage (days or even weeks). Further important characteristics include the efficiency, the lifetime and the costs.

### 2.2.2 *Current role of energy storage systems in the energy system*

With the increase of installed renewable energy sources in Europe, energy storage systems are gaining more and more importance. Energy storage system can cover a variety of applications in the energy system and can be installed at different locations. *Figure 6* illustrates how utility services, customer services, and market services are related across sectors.

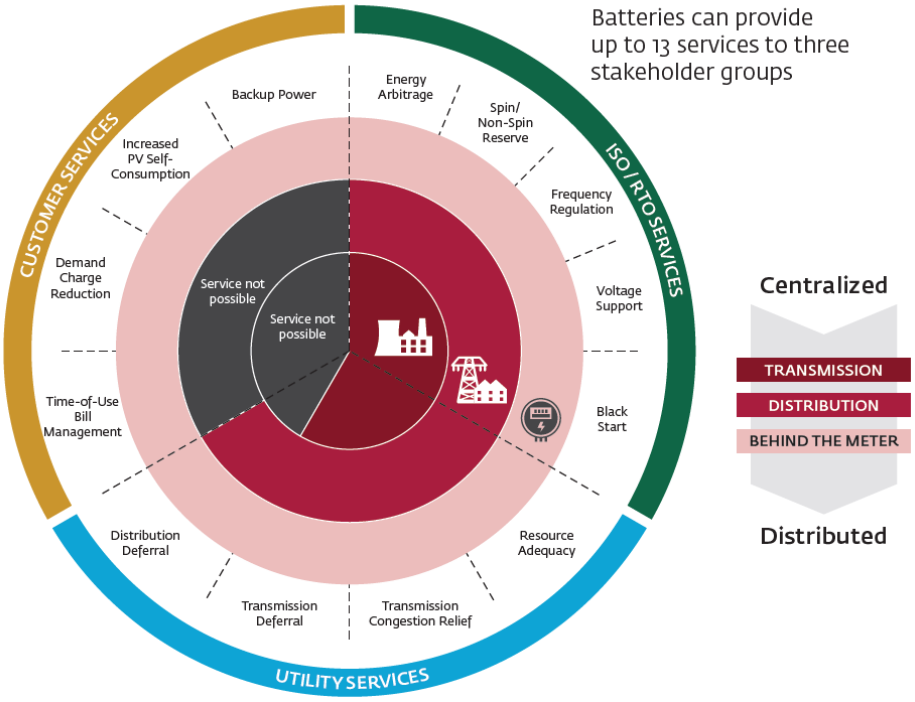


*Figure 6 - Services of storage systems* [24]

As shown in *Figure 6*, energy storage systems can increase the self-consumption of the consumers respectively prosumers. In that specific application, Energy storage systems are installed in family homes or industries and are operated in combination with RES. By deploying energy storage, the surplus energy that is produced during the day can be stored. At night or in the evening the stored energy can be used in order to cover the load. The self-consumption has several benefits; notably avoiding curtailment of renewable energy; energy consumption from the grid and payment of grid fees and taxes.

The market for such solar energy storage systems is currently focused in several European countries the role of self-consumption. Another application where energy storage systems is frequency regulation in the European Energy system. Due to their short response time and the ability to absorb or inject power to the grid, most of the known energy storage systems have a great ability to perform this service.

Moreover energy storage systems can be used for peak-shaving purposes. However information regarding the deployment in peak-shaving applications is quite unknown. Depending on the grid situation, energy storage systems may also help to prevent transmission congestion and consequently defer the necessity for grid upgrades (e.g. the change of overloaded transformers) on distribution as well as transmission level. As a consequence the feed-in of renewable energy sources during peak times doesn't have to be curtailed and the amount of electrical energy they provide can be increased.

Last but not least, the energy storage systems can provide a black start. Black start means: a power station restarts without the external electricity grid due to a total or partial shutdown of the transmission system. This means that the system is able to provide a V/f-controlled pre-specified voltage and frequency. Therefore it is also possible to do frequency regulation. Storage may be essential to reliably integrate power generated from renewable energy in systems that have weak interconnection. Energy Storage system can also be used as backup power device in case of blackout. In the distribution grid usually smaller decentralized energy storage systems are deployed, primarily for self-consumption and backup power purposes at household level. However, more centralized structures such as energy storage systems for powering a micro grid or an entire island grid can be observed as well [25] [26].

### 2.2.3 *Services of Energy Storage Systems*

The diagram in *Figure 7* is categorizing different storage technologies depending on power of the system and the time of discharge.

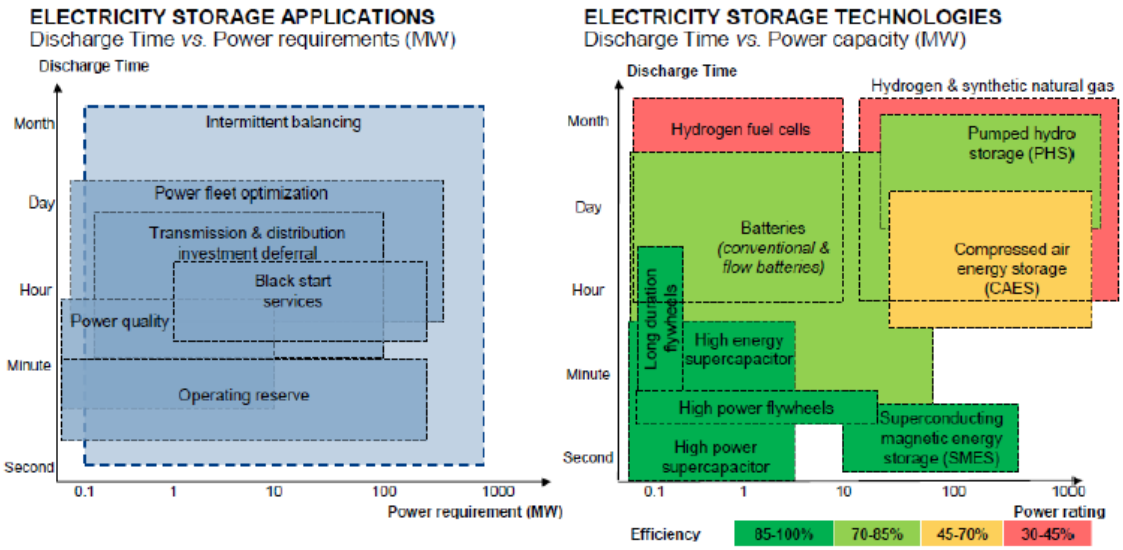


*Figure 7 - Electricity storage diagram* [27]

This diagram shows the different characteristics of diverse kinds of technologies. It shows also that the services that storage systems can provide do not need the same technical requirements. Depending on the characteristics, different storage systems are suitable for specific services and applications. To these services and applications different business cases are linked. In this diagram, the power and the discharging time (which can be assimilated to the energy stored) are illustrated, both are important characteristics of storage systems. Moreover other parameters can be taken into account such as installation costs, number of cycle, reliability, maintenance costs or efficiency.

In [28] the following services that ESS can provide are stated. There are several services to use a battery which depend on the market level where the battery is installed. In a first approximation,

it can be distinguished into two classes: Customer and Utility services as well as ISO (Independent System Operators) and RTO (Regional Transmission Organizations) services.

## 2.3 Existing Demand Response technologies

### 2.3.1 *DR strategies*

#### 2.3.1.1 *Classification of DR strategies*

In [29], the WiseGRID project, existing DR technologies have been analyzed; a broad classification of DR programs is provided in Table 1 according to three main classification criteria, i.e. control information, decision variable and motivation.

*Table 1 – Classification of DR programs according to three main classification criteria.*

| **Classification Criteria** | **DR Categories** |
|---|---|
| Control information | Centralized |
| | Distributed |
| Decision variable | Event scheduling |
| | Energy management |
| Motivation | Price-based |
| | Incentive based |

The motivation criterion has recently become the most dominant one, when distinguishing between the various DR programs. This is especially true regarding their marketing and how they are communicated to potential customers. A further – more detailed classification – breakdown of price and incentive-based DR techniques is presented below:

- Explicit DR (incentive-based DR)
    - Classical
        - Direct control
        - Interruptible / Curtailable loads
    - Market-based
        - Demand bidding
        - Emergency DR
        - Capacity market
        - Ancillary Services (AS) market
- Implicit DR (price-based DR)
    - Time of Use (ToU)
    - Critical Peak Pricing (CPP)
    - Extreme Day Critical Peak Pricing

- Extreme Day Pricing
- Real-time Pricing (RTP)
- Peak Time Rebates

These two main categories of DR programs are typically managed by different roles in the Smart Grid ecosystem.

Incentive-based DR aims to trigger demand profile modification at specific times and, potentially, at specific grid connections/lines with the main goal to support the grid and/or to provide real-time services to parties that must maintain portfolio energy balance. Such programs are usually managed by third-party demand-side aggregators that build up a portfolio of controllable demand assets.

The main purpose of price-based DR is to modulate the demand profile of a retailer customer portfolio according to the wholesale price of electricity. It is a valuable tool for retailers who want to manage their portfolio to minimize or avoid energy imbalances. The careful design of tariffs and rates has the potential to shift peak demand and help the retailer lower its cost structures by reducing hedging costs.

DR offers a wide range of benefits for all stakeholders involved:

**DR program/campaign participant**

- Incentive payments: the most obvious benefit for participants in explicit DR campaigns (and Peak Time Rebate implicit DR campaigns) is the remuneration they receive for successful response to DR signals.
- Energy cost savings: implicit DR campaigns offer the possibility to electricity consumers to significantly reduce their energy costs.
- Increased market power: participation of small electricity consumers –especially through any kind of federation schemes – gives them market power, i.e. the capability to affect prices according to their needs. This can be achieved via direct negotiations with utilities/aggregators or even through the establishment of cooperatives that act as electricity producers and retailers under the complete control of their members.

**Aggregators (explicit DR)**

- Financial benefits from capacity and ancillary service markets or Over-The-Counter (OTC) transactions with BRPs and/or Distribution/Transmission System Operators (DSOs and TSOs, respectively). This is the main revenue stream for the aggregator business model.

**Energy suppliers/utilities (implicit DR)**

- Portfolio imbalance risk hedging: the capability of suppliers to affect the aggregated demand profile of their clientele allows them to hedge against imbalances of demand versus electricity purchased in the wholesale market, which could lead to imbalance penalties.
- More predictable demand profile yields better forecasts and purchase strategies from the wholesale energy market: demand shaping also allows the supplier to improve their forecasting and wholesale purchasing strategies and – in an extreme case – lower their costs by shifting significant demand to times of cheaper electricity (i.e. by lowering night tariffs).

- Compliance to EU directives on energy efficiency: the EU Winter Package published at the end of 2016 foresees specific energy efficiency targets that must be met by suppliers. As a result, implicit DR provides them the necessary tools to comply with policy and regulatory requirements.
- Differentiated energy tariff programs, offering diversity: the capability to customize and personalize energy tariff schemes to the requirements of individual customers gives retailers an important tool to diversify and increase the attractiveness of their offerings.

**Market**

- Reduced energy prices: DR can lead to avoidance of electricity generation from costly generators that are low in the merit order and push the wholesale price upwards. This leads to an average reduction of energy prices, especially at times of peak demand.
- Increased capacity: capacity of the energy system refers to available reserves that can support the system in times of need. DR can become an important, since it is a cheap and practically already available source of capacity for the energy system.
- Participation of many consumers – especially federations of consumers - in energy markets increases market liquidity, reduces the market power of large buyers/sellers and yields lower and more stable electricity prices.

**Energy system**

- Increased reliability of the system as whole due to diversified sources of ancillary/balancing services that lead to reduced outages.
- Avoided/deferred infrastructure investment costs due to the decreased need for further network capacity to counter increased demand.
- DR can offer significant benefits to participants and the energy system as a whole, but also brings some costs for setting up and operation. These costs per stakeholder are indicated below:

**DR program participant (residential, business or industrial)**

**Set up**

- Purchase and installation of required enabling technology – in some cases the cost of this equipment can be borne by the program owner, but this depends on the respective commercial arrangement.
- Definition of response plan and processes. This is an important cost element, since a detailed execution plan needs to be put in place in order to reap the benefits of participation in DR campaigns with minimal disruption to the normal activities of the load owner/manager.
- Transaction costs in the process of identifying, screening and selecting the most beneficial offer for program owners for participation in DR programs.

**Running**

- Lost business: modification of the electricity demand profile may result in degradation in business operations. This has to be carefully evaluated so that it never outweighs the expected benefits from DR participation.

- Inconvenience or degradation of operational performance: any electricity demand profile modification is bound to cause some inconvenience or disruption. If an adequate response plan is in place, this disruption can be minimized or alleviated.
- Costs due to rescheduling energy-intensive processes: ramp-up/down of electricity hungry industrial processes can have significant overheads. The cost-benefit assessment performed prior to the enrolment in the DR program should take into account all these issues and verify a positive impact on the participant bottom line.
- Costs for onsite generation: local generation has been used as a backup power solution to avoid disrupting the load operations while actually complying with the DR signals and hence fulfilling the obligations to the aggregator or supplier. This solution is clearly costly, but still may be cost effective depending on the potential DR incentives or non-compliance penalties.

**DR program owner (aggregator/ supplier)**

**Set up**

- Installation of metering and communication infrastructure, and control infrastructure for explicit DR campaigns (direct load control): the cost of equipment for the facilitation of participation in DR program may fall on the program owner depending on the arrangements made with the DR participant. This cost can be significant.
- Availability of metering, reconciliation and billing capabilities: in the simple case price-based DR the program owner must be able to measure the actual demand profile of the client, calculate the energy cost and perform the necessary billing and financial transactions. In the case of explicit DR, things become more complicated. The baseline demand must be estimated in order to verify compliance to DR signals. This requires additional Information and Communications Technology (ICT) tools for the accurate estimation of a baseline.
- Participant recruitment, including costs for education/awareness-raising, etc.: building, maintaining and extending a portfolio of clients is a costly activity. Especially the intended participation of residential consumers in the energy markets will lead to huge increase in the necessary client numbers in order to reach the energy volumes required for market participation for aggregators. Given that DR is a very innovative concept and exposure of citizens to it is extremely limited, the necessary awareness raising and sales activities will be very challenging.

**Running**

- Administration, DR program management: significant effort is required for the successful implementation of DR programs, starting from program design all the way up to day-to-day management and assessment.
- Marketing & advertisement: maintaining and extending a healthy market share requires expenditures for advertisement and marketing, especially for services that target the public at large.
- Incentive payments to participants: this is the most obvious cost for the program owner, the incentive payments to their customers for the successful participation in DR campaigns. This mainly applies to explicit DR campaigns (and Peak Time Rebate implicit-DR programs to be exact), since in other cases the participant benefits from reduce energy costs rather than payments.

- Evaluation & monitoring: continuous monitoring and assessment of DR program/campaign performance as well as identification of possible improvements should be a permanent activity in order to improve the program for all stakeholders involved.

#### 2.3.1.2 *Major challenges for the successful roll out of DR programs*

##### *2.3.1.2.1 Explicit DR*

**Baselining**

Explicit DR programs – or more generally any DR program that directly remunerates the modification of electricity consumption profiles – faces a major challenge: how to accurately estimate the magnitude of the modification. The necessary prerequisite is that the original consumption pattern would be somehow known. This is however impossible and the best alternative is an estimation of this pattern: the baseline. The actual consumption pattern is then compared to the baseline to calculate the profile modifications (e.g. load shedding or shifting, generation) and establish the necessary remuneration.

In most realistic cases electricity consumption depends on a number of factors. Seasonal factors, such as the weather or daylight patterns, can have a very important impact. The impact of these factors on electricity consumption, however, can be estimated to a reasonable degree. Other factors have much higher volatility and much less predictability. Consumption patterns depending on human occupancy and activity – in the built environment for example - can be very unpredictable. A good example is household behaviors, which are seldom fully predictable even though the main activities of the residents are more or less similar on a day per day basis. The exact timing and combination of activities is very seldom the same, leading to electricity consumption patterns that cannot be accurately predicted.

Furthermore, baselining for DR cannot leverage the averaging effects that govern the grid-level demand predictions performed by the system operator. The baseline consumption of each individual electricity user (metering point) needs to be estimated in order to decide whether the user has responded to DR signals in an appropriate manner according to existing arrangements.

**Democratizing access to explicit DR**

DR programs are mainly targeted to large electricity consumers, i.e. industrial plants or large businesses/tertiary buildings and currently the low hanging fruits for participation in DR programs. The scale of their consumption means that a demand side aggregator can build the necessary portfolio volume for participation in the applicable markets with a limited number of customers. This is very important because customer acquisition and recruitment costs are quite high for aggregators. The whole process is still far from standardized and most arrangements are bespoke to suit the needs of individual arrangements. Furthermore and depending on the target market, the respective loads that will participate in the DR program may need to be qualified which adds additional costs and overheads to the process. The immediate implication is that it is currently prohibitive for aggregators to pursue small-scale customers and aggregate the small loads of many customers in order to reach the required volume for market participation.

Two ongoing developments that will alleviate this challenge include: a) the alteration of the legislative frameworks around Europe, which slowly reduce the minimum power volume that must be bid in markets, and b) the emergence of ICT tools and processes to manage DR campaigns.

This challenge also applies to explicit DR programs, since price-based DR benefits can be directly reaped by the electricity users as long as they modify their consumption patterns according to the price evolution.

**Minimum requirements for participation in ancillary service markets**

Current regulations typically impose minimum requirements on services in order for them to qualify for participation in wholesale markets. Examples include fixed trading charges (e.g. membership fees, entrance fees, etc.), minimum trading volume and minimum available capacity. These trading conditions may hinder the ability of smaller players (e.g. emerging aggregators) to participate.

The need for an appropriate definition of market structures and roles in all other Member States is emerging towards enabling the clear and direct access of consumers to aggregation service providers and ensuring free market competition around DR services. Any delay in this process would increase risks for all parties and enable abuse.

**New balance of roles and responsibilities of market actors**

Perhaps the greatest factor that needs to be considered concerns the roles and responsibilities of new and existing players on the electricity market. Current competences need to be reviewed and expanded where necessary, and DSOs, for instance, will likely need to play a more active role in the future. On top of this, a more thorough demarcation of the competences of aggregators is crucial given the importance of intermediaries when dealing with a large number of small consumers. Besides the need to establish new roles in energy market designs, the question arises as to how to deal with their interaction.

DR activations may have a significant impact on suppliers (e.g. their sales volume and costs) and the balancing exercise of balance responsible parties. The development of adequate compensation mechanisms is critical in this respect. Furthermore, accounting for the technical properties of the grid and the creation of priority rules between market and technical flexibility seem inevitable. For example, simultaneity of market signals in a local area could lead to network problems such as congestion, thereby requiring the DSO to define certain limits.

**Standardization**

Finally, standardization has an important impact on interest in investments and market competitiveness. With an increasing number of technologies being connected to the grid, interoperability is becoming a true challenge. However, there currently exist very few (inter)national smart grid standards. Fortunately, a number of European standardization organizations (CEN, CENELEC and ETSI) are developing smart grid standards. Besides standards, there is a need for clear legal definitions of new smart grid concepts, and for streamlining these definitions across different policy levels.

*2.3.1.2.2 Implicit DR*

**Consumer acceptance**

Electricity consumers around Europe – especially small consumers on the Low Voltage (LV) network – are used to fixed energy tariffs and pay-per-use programs. Dynamic prices bring a radical shift that requires significant awareness raising and training so that consumers enjoy the potential benefits. In general, most consumers are very reluctant to become exposed to volatile prices due to the inherent risk of energy cost increases if they fail to shape their electricity consumption profile accordingly. This reluctance seems to be part of human nature, they prefer to avoid downside risks rather than strive for a better situation with reduced energy costs.

Recent deployments of dynamic tariffs on a commercial scale in Finland and Sweden, however, show that consumers are able to leverage the dynamic prices to reduce their energy costs. Real electricity customers achieved reductions of 15% to 30% compared to their energy costs under flat tariffs [30] [31]. Research studies report similar results. A study [32] on 67 households in Germany reported consistent energy savings between 20% and 30% between households using a dynamic ToU tariff and smart appliances with limited intelligence (delay start until a price threshold is reached). Similar results are reported in the US [33]. All these results have been achieved without the use of intelligent automation at the building/home level.

**Price regulation**

Another aspect that comes into play is the distribution grid tariff. Nowadays, this tariff makes up a significant part of the final retail rate, and its design can therefore have an effect on the effectiveness of DR products based on dynamic pricing. For instance, the tariff structure can lead to the neutralization of market signals when there are conflicting interests between suppliers/aggregators and grid operators. More generally, a poorly designed tariff can lead to technical problems when it encourages sub-optimal grid usage (e.g. local overinvestment in Distributed Generation - DG). On the other hand, socio-economic problems ensue when the tariff leads to unacceptable cross-subsidization.

Moreover, active DR inevitably requires some form of signal to the consumer and/or (financial) compensation. Dynamic pricing (ToU) therefore plays an important role in its implementation, but at the moment it is substantially limited by national legal provisions around the EU. Having a pricing structure consisting of several time blocks with different prices during the day provided that adequate metering equipment is available, but continuous revision of these prices on a daily basis, for instance, is prohibited by regulations regarding variable contract types.

**Personal data security and privacy**

On the consumer side, although there already exists a broad legal framework on privacy and data security at several policy levels (EU, national), there is a lack of sector-specific rules regarding confidentiality and data handling and security in the context of DR for consumers. This factor may hamper consumer involvement and support. Current regulations are generally designed to support data processing for billing purposes, which typically takes place once a year. Active demand, however, will require a significant increase in processing frequency and data granularity.

#### 2.3.1.3 *Current state of European energy markets*

The situation in the European Union is much more complicated and fragmented due to the heterogeneity of national regulatory frameworks and market structures. However, it has to be pointed out that, during the last years, many important steps have been done towards the design, development and operation of an Internal Energy Market based on the principles of the so-called "Target Model" as well as on the European Guidelines (CACM, FCA, EB), which cover also the cross-border exchanges**.** The Joint Research Center of the European Commission provided in 2016 the following overview of the current situation of DR markets in the Member States [34].

The wholesale markets are by far the largest and (theoretically) most liquid markets in any given Member State. Here Retailers look to buy sufficient energy either from their own generators or from the market, to supply their customers. In order to maintain balance they should buy the same amount of energy for any given time period, as their customer's will consume.

This is part of their balance responsibility and each retailer will therefore have such a BRP, who will be responsible for the imbalances settlement of the BSPs, such as DR aggregators. Wholesale

markets include futures markets but also intra-day and spot markets, where energy is bought and sold 15-60 minutes prior to the time of consumption. After this point there is 'gate closure'. The wholesale market activity is at an end and the TSO is responsible to maintain balance from the time of gate closure to the microsecond prior to consumption. This is done through balancing markets and AS. BRPs with an uninstructed shortage pay money to the TSO, whereas BRPs with an uninstructed surplus receive money from the TSO. This is done through the BRP-TSO Imbalance Settlement process, where the calculation of charges/remuneration of BRPs for their imbalances can be conducted by using f.e. Single Pricing, Dual Pricing, Based on total costs, Alternative payment direction, Two-price settlement and Additive Component. The EB Guideline with expected entry into force in the beginning of December 2017, there is a clear preference for dual pricing and the harmonization of the Imbalance Settlement period to 15 minutes.

Retailers may be required to pay the TSO for these services according to the amount that they were off in their balancing calculations. However the company's generators may also earn from providing balancing and AS to the TSO. This mechanism is different in different Member States, but the principle remains the same.

ENTSO-E writes: 'Balancing refers to the situation after markets have closed (gate closure) in which a TSO acts to ensure that demand is equal to supply, in and near real time. '

Efficient balancing markets ensure the security of supply at the least cost. An important aspect of balancing is the approach to procuring AS. AS markets provide a range of capabilities, which TSOs contract so that they can guarantee system security. These include black-start capability (the ability to restart a grid following a blackout); frequency response (to maintain system frequency with automatic and very fast responses); fast reserve (which can provide additional energy when needed); the provision of reactive power and various other services."

Explicit DR is first established within the balancing and AS markets. These provide the best investment security and prices. The types of services required by the TSO also fit a consumer's capabilities well.

At national level, few Member States clearly engaged in the process of a wide integration of DR in the electricity markets. Some markets were fully open, in others some DR products were allowed to participate.

#### 2.3.1.4 *Outlook for DR in the EU*

Research [35] shows that there has been an overall increase of interest in enabling DR in many Member States. Regulatory changes have been implemented or are planned in many of the analyzed countries. Notably, in the countries where DR has traditionally been almost non-existent, such as Estonia, Spain, Italy, there has been at least some regulatory interest in exploring its potential. The European countries that currently provide the most conducive framework for the development of DR are Switzerland, France, Belgium, Finland, Great Britain, and Ireland. Nevertheless, there are still market design and regulatory issues that exist in these well-performing countries. Switzerland and France have detailed frameworks in place for independent aggregation, including standardized roles and responsibilities of market participants. In France, a new draft decree being reviewed by the Conseil d'Etat in early 2017 could provide for a new financial settlement framework whereby a significant of the payment to retailers with curtailed customers would be charged to retailers rather than to DR providers. However, issues persist around a standardized baseline methodology.

In both Belgium and Ireland upcoming legislation should help to increase the participation of DR. New legislation addressing the role of the aggregator and independent aggregation will soon be put in place in Belgium, which will help to provide an equal footing for all market actors; a strong

sign for the uptake of DR. However, there are still some issues regarding measurement and verification that inhibit the growth of DR. In Ireland, the new "Integrated Single Electricity Market" to be implemented in 2018, together with the DS3 program, will open a range of markets for demand side response, specifically the balancing market, and the wholesale market, as well as a newly designed Capacity Mechanism.

Great Britain continues to have a range of markets open to demand-side participation. Independent aggregators can directly access consumers for AS and capacity products, and the country recently has started considering a framework for independent aggregator access to the Balancing Mechanism. Yet, with relatively burdensome measurement and verification procedures in place for DR, it still has room to improve.

Finland stands out amongst the Nordic countries primarily as it allows independent aggregation in at least one of the programs in the AS, and due to its advanced provisions for measurement and verification. It will also be experimenting through pilot projects with independent aggregation in other parts of the balancing market starting in 2017.

Austria, Denmark, Germany, Netherlands, Norway, and Sweden performance falls behind that of the aforementioned Member States as regulatory barriers remain an issue and hinder market growth. Although several markets in these countries are open to DR in principle, program requirements continue to exist which are not adjusted to enable demand-side participation. Furthermore, a lack of clarity remains around roles and responsibilities of the different actors and their ability to participate in the markets. However, Germany, the Nordic countries and Austria have started processes to find a standard solution for the role of independent aggregation. One of the notable differences lately is that Germany is making significant efforts through product definitions have been updated or are about to be updated, and balancing reserve markets that are about to be opened for independent aggregation.

Slovenia, Italy, and Poland performance lies in the third tier with respect to DR facilitation efforts. In Slovenia and Poland, no major regulatory changes have been made within the past couple of years that would have allowed for further DR participation. Italy has slowly started to take the regulatory steps needed for a solid framework for DR. However, despite the gradual opening of markets, significant barriers still hinder customer participation. For example, major sections of the market are still closed off and they lack a viable regulatory framework for DR overall.

Spain, Portugal, and Estonia are laggards because aggregated demand-side flexibility is either not accepted as a resource in any of the markets or it is not yet viable due to regulation. Estonia may be an important country to watch in the future given that markets could open once they have disconnected from the IPS/UPS synchronous area.

Greece is currently in the process of a major re-structuring of its internal Market. The transition from the current model of the Day-Ahead Market and the mandatory pool to the new Market design that involves the balancing market is expected to be completed at the end of 2018. There is currently an interruptibility scheme, which is expected to be prolonged. However, this refers only to large customers. DR will be an important part of the new Balancing Market and consumers will be able to adjust their electricity through their aggregators. Until the end of April 2017 and for a period of 1 year there was a flexibility mechanism (Transitional Flexibility Remuneration Mechanism - TFRM), which helped to remunerate generating units (gas and hydro plants) for the services they provided (mainly referring to ramping), in the view of the absence of a balancing market. The goal of this remuneration was to respond to the flexibility needs of the power system, avoid generation units mothballing and reward them for providing this necessary service. The Greek Regulator has recently

done a Public Consultation on a new transitory flexibility mechanism, until Target Model is fully implemented.

## 2.4 Potential and challenges of the electrification of transport sector [36]

### 2.4.1 *E-mobility in EU*

### 2.4.2 *Strategy and actions in the last decade*

WiseGRID Consortium collected the potential and challenges of the electrification of transport sector in [36]. In 2010, a strategic memo from the European Commission (EC) sets the goal for Europe to be more resource efficient, with a greener and more competitive economy in 2020 [37]. Every day, the EU imports for about 500 million euro crude oil [38]. In the last decade, an estimated 84% of the crude oil was burnt to provide our societies with energy [39]. To lower the EU dependency on crude oil, which could result in avoiding costs, decreasing the related to health consequences and avoiding for geopolitical instability, the EU wants to promote novel cleaner energy production. Part of the solution to decarbonize our society is to promote 'zero emission vehicles' for transport. The goals and approach to achieve this are written down in the Clean Power for Transport package [40].

Investigating the approaches set forth by the EU, it can be identified two clear approaches pursued by the EU at the same time. The first is promoting clean and energy efficient vehicles, still based on conventional internal combustion engines (ICEs). The 2020 target is 95 g/km for those type of passenger cars [41]. The second approach is facilitating the deployment of breakthrough technologies in ultra-low-carbon vehicles, which include battery-electric vehicles (BEVs).

The EU is promoting action on different parallel levels, ranging from the production side by setting rules on vehicles requirements [42], over fiscal stimuli (purchase financial incentives, energy taxation directives, vehicle taxation) [43], extensive monitoring of the EV market [44] and labeling and consumer understanding and guidance [45]. A special emphasis always is made on preventing market-distorting rules when implementing measures.

The very first actions to promote electric vehicles are limited to 'electric and crash safety requirements'. These aspects and their importance are repeated in later communications (e.g. Memo 12/419 [46]). In this early strategic memo, emphasis is also put on charging infrastructure and smart charging. However, a lot of uncertainties had - and to a lesser extent still have - to be dealt with respect to help reaching the Clean Power for Transport package its goals and to validate the assumed environmental friendliness of BEV, causing first researching efforts mainly on extensive researching life cycle assessments of EVs and batteries (e.g. [47]).

In the meanwhile, in a vision for the automotive industry in 2020, dating from 2012, the EU confirms the focus on promoting classic internal combustion technologies as the way forward [46]. "A portfolio of propulsion technologies, dominated by the advanced combustion engine technology, although increasingly electrified" is a key characteristic of a strong and competitive automotive industry". The vision shows a hesitation in choosing fully for development of 'alternative fuels', as a big emphasis is repeatedly made on changing the status quo of vehicle production very slowly and gradually. This might be a result of a conservative attitude of the established automotive sector in redefining the tempo of the uptake of new technology.

In these early days, interesting thoughts are already being set forward about the charging of EVs, such as the 'recognition that charging of electric vehicles is expected to be performed mainly at home/work'. Nevertheless, the EU goal confirms in another recent directive to provide one public charging station for every 10 EVs [48]. The EU members are transforming these directives into locally applied action plans and legislation. [48]

Usually the appearance of new technologies, such as electric propulsion for cars, offers opportunities for new players to enter the market, expecting new EV manufacturers appearing in this transition to e-mobility. In Europe this has not yet happened on a large scale.

A part of the answer lies in the high regulatory boundaries for new automotive players that want to bring new vehicles to market. These rules are mostly set by the current industry players and enforced by EU legislation. The automotive sector is the largest industrial sector in the EU. Twenty four percent of all cars produced in the world are built in Europe. 16,5 million passenger cars were made in the EU in 2016 [49]. Another part of the answer to the question of the lack of new automotive players might lie in the fact that current industry players receive large financial support for investigating new technologies. The current industry players remark repeatedly in position papers that "anticipation of change should be holistic and respect all factors influencing the competitiveness and the long-term perspective of companies" [50].

The EU car manufacturers claim to be a key driver of knowledge and innovation. In 2016, R&D (Research and Development) investments in the EU were biggest in the automotive sector, leading with at least 25% more budget compared to other sectors. Moreover, no region in the world invested more in R&D into automotive than Europe, but it is not easy to find out which part goes to investment in electric vehicles [50]. Automotive R&D is currently mainly driven by stricter standards set by authorities on vehicle emissions and fuel consumption. Electro-mobility and further improving internal combustion engines will be key technology areas in which R&D in automotive is directed in the coming years [50].

As a result, more vehicle manufacturers will launch new EV models in the near future. It is to be expected that the launch of these new EV models increases EV market share, a goal of the Clean Power for Transport directive. In addition, the European Clean Power for Transport directive recommends that there should be one public available charging point for every 10 electric cars by 2020 [48]. It is to be expected that more countries will roll out public charging infrastructure projects, which will – together with the novel EV models – will also have a high impact on stimulating the uptake of EVs.

Besides the necessary market offerings, regarding EV models and charging infrastructure, public authorities set also forth financial and fiscal stimuli to increase the purchase and the use of cleaner vehicles. These stimuli are based on general desired performance criteria of cars set by the EU, such as threshold levels of $CO_2$ emissions [43]. Such stimulating measures need to be technology neutral, and avoid focus on one peculiar type of vehicle, such as electric mobility. In addition, EU is weary that financial incentives indirectly subsidy the manufacturing of the cleaner vehicles, so the financial incentives should not be bigger than the difference with the status-quo vehicles. [43]

Since the possible financial incentives proposed by the EU can be implemented in many ways by member states, there are a lot of different stimuli in different EU countries which are presented in Table 2 [51]. A common measure applied by nearly all countries are registration tax benefits and ownership tax benefits. [43]

As an example, it has been taken the Clean Power for Transport (CPT) program implemented by the Flemish authorities in Flanders [52]. The actions from this program consist of a) a subsidy

program to stimulate purchase of EVs for natural persons, which receive a grant in cash upon purchasing an EV, b) the exemption of taxes for purchasing new EVs, c) a yearly project call for investigating implementation of EVs in society on which diverse stakeholders can apply (in 2017 with a budget of 1M€ and maximal 150 k€ per project) and, d) by the roll out of charging infrastructure over Flanders with the goal to provide 2500 charging stations with each 2 connecting points by the end of 2020. The result of these actions should be a market share of 7,5% in 2020, and a number of charging stations that amounts to 10% of the BEV fleet.

Do these efforts to stimulate EV bear fruits? When examining battery electric vehicles, in 2012, the market expectations were 225.000 EVs to be sold in Europe in 2012, and 700.000 in 2015 [53]. But the reality shows lower numbers. Overall, the current sales figures are 3 times less, with approximately 200.000 sold EVs in 2015 in Europe, as is represented in Figure 8. The too optimistic forecast did apparently not take into account the only slowly growing political support of EVs in the EU by most of the member states, which is in stark contrast to some countries outside the EU, such as Norway.

Indeed, Norway has a market share of EVs for new vehicles of 19% nowadays. The EU countries in which EV have the largest share of all newly registered vehicles in 2017, are Austria and The Netherlands, both around 1,4%. In the ranking they are followed by France and Sweden, both around 1,1% market share. The remaining EU countries have similar market shares, averaging 0,4% of market share [54] presented in Figure 9.

The EV growth in Norway is supported by an extensive number of stimuli. Should the members of the EU have imposed all incentives as Norway has done starting in the '90s, the EU might have reached or even exceeded the estimates [55]. Even though, in this scenario it is still the question whether the production capacities of the EV suppliers and manufacturers could have met the forecast goals.

Looking at the sales figures of EV, although a remarkable stagnation in 2016, in 2017 EVs are again heading toward 0,6% of newly registered vehicles across the EU. The sales of EV are again speeding up during 2017 in the EU [56]. On average for the whole of the EU, sales of EV went up with 39% between 2016 and 2017, when comparing the totals for the same period for those years. Sales of EV do not show a steady increase however, and are still influenced heavily by political decisions. For example, Denmark is a specific case because it has an average market share of BEV of 0,6%, but EV sales dropped in 2017 by 40% [56]. This slowing down in Denmark was due to a change in tax policy for EV owners since 2017, a change which got a lot of media attention [57].

It can be argued that a very broad package of incentives and support, both fiscal, financial and structural and accompanying investments, was and is still clearly needed for reaching that initial forecast of 2012, even today in 2017.

Finally, it is worth remarking that the nature of the car market is slowly changing. Personal car use per person per year in several key European countries is in decline and there is some evidence that younger generations are less interested in car ownership and more open to alternative mobility solutions [58], such as car sharing or mobility-as-a-service. In addition, electric vehicles are perfectly suited for autonomous driving cars, one of the new paradigm shifts in mobility to be expected, which is expected to 'disrupt' the market in the next decade to come. Many new business models are therefore emerging in the coming years.

| Country | Registration Tax Benefits<br>Applied:21 times | Ownership Tax Benefits<br>Applied:21 times | Purchase Subsidies<br>Applied:16 times | Company Tax Benefits<br>Applied:13 times | Local Incentives<br>Applied:13 times | Infrastructure Incentives<br>Applied:7 times | Financial Benefits<br>Applied:3 times | VAT Benefits<br>Applied:1 times | Number of applied measures |
|---|---|---|---|---|---|---|---|---|---|
| Austria | 1 | 1 | 1 | 1 | 1 | | | 1 | 6 |
| Ireland | 1 | 1 | 1 | 1 | 1 | 1 | | | 6 |
| Malta | 1 | 1 | 1 | 1 | 1 | 1 | | | 6 |
| Spain | 1 | 1 | 1 | | 1 | 1 | 1 | | 6 |
| United Kingd | 1 | 1 | 1 | 1 | 1 | 1 | | | 6 |
| Denmark | 1 | | 1 | 1 | 1 | 1 | | | 5 |
| France | 1 | 1 | 1 | 1 | 1 | | | | 5 |
| Germany | | 1 | 1 | 1 | 1 | | 1 | | 5 |
| Portugal | 1 | 1 | 1 | 1 | 1 | | | | 5 |
| Belgium | 1 | 1 | 1 | 1 | | | | | 4 |
| Hungary | 1 | 1 | | 1 | 1 | | | | 4 |
| Romania | 1 | 1 | 1 | | | 1 | | | 4 |
| Greece | 1 | 1 | | | | | 1 | | 3 |
| Italy | | 1 | 1 | | | 1 | | | 3 |
| Latvia | 1 | 1 | | | 1 | | | | 3 |
| Luxembourg | | 1 | 1 | 1 | | | | | 3 |
| Netherlands | 1 | 1 | | 1 | | | | | 3 |
| Slovakia | 1 | | 1 | | 1 | | | | 3 |
| Slovenia | 1 | 1 | 1 | | | | | | 3 |
| Sweden | | 1 | 1 | 1 | | | | | 3 |
| Cyprus | 1 | 1 | | | | | | | 2 |
| Czech Repul | 1 | 1 | | | | | | | 2 |
| Finland | 1 | 1 | | | | | | | 2 |
| Lithuania | 1 | | | | 1 | | | | 2 |
| Croatia | 1 | | | | | | | | 1 |
| Bulgaria | | | | | | | | | 0 |
| Estonia | | | | | | | | | 0 |
| Poland | | | | | | | | | 0 |

*Table 2 – Overview of incentives implemented by the EU member states to promote EV uptake.* [51]

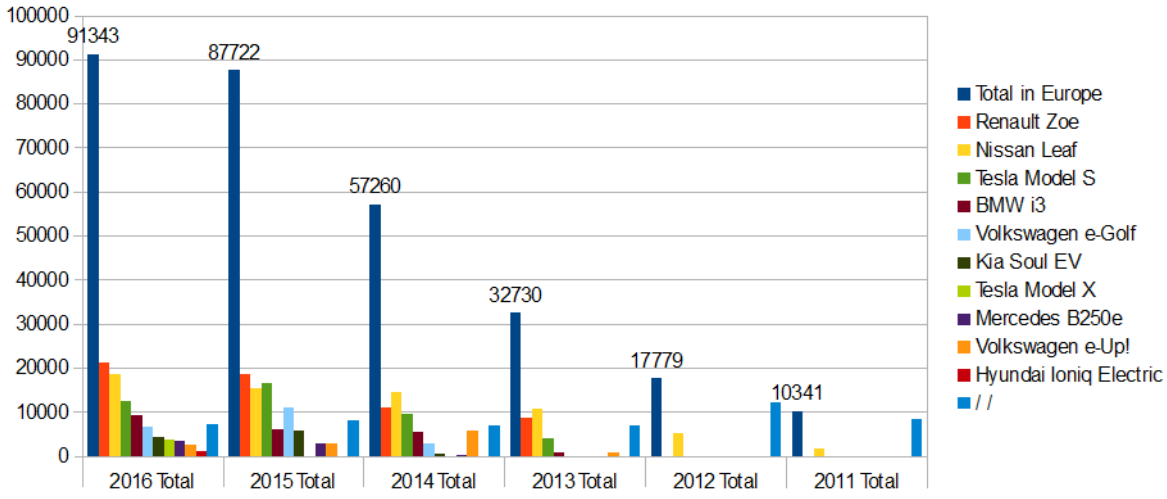


*Figure 8 – Total sales numbers of EV in Europe, subdivided by EV make and model.* [53]

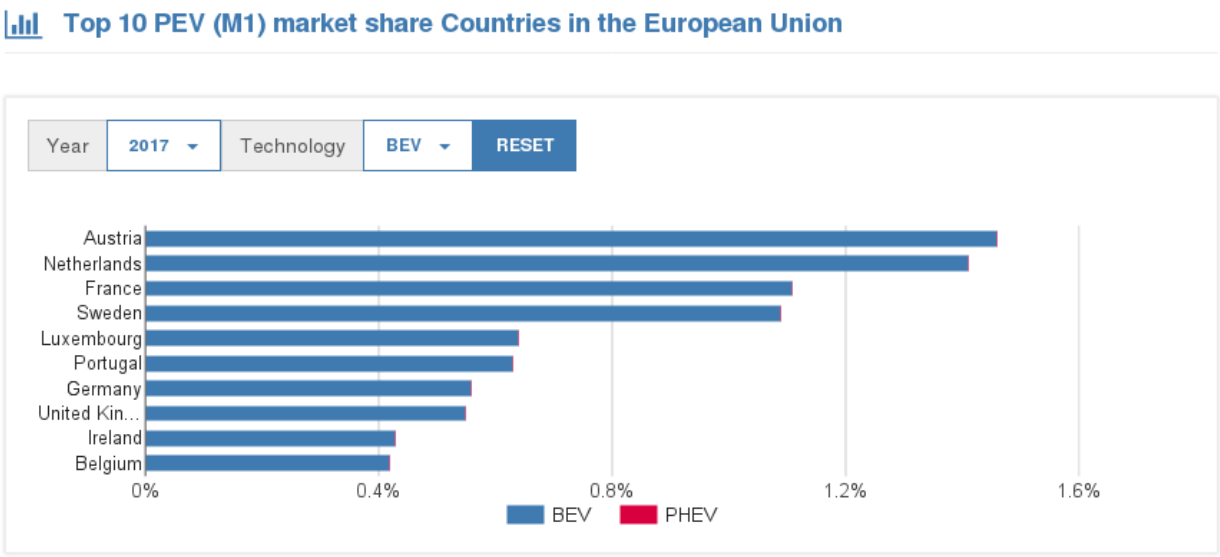


*Figure 9 – Overview of the EU countries with the highest market share in EV.* [54]

### 2.4.3 *Electric Grid Perspective*

Electric vehicle, as a new type of energy resource, has dual representation as it can have either static or dynamic behavior. In the static representation, electric vehicles are considered as mere loads adhering to the "plug-n-play" concept and their operation is similar to the one of conventional loads. In this case, the charging process of the EV battery starts as soon as the EV plugs into the grid. As far as the dynamic behavior is concerned, electric vehicles can be considered as manageable loads whose demand is flexible and it can be allocated among the non-commuting hours in respect to different business objectives. In a more ambitious scenario, electric vehicles can be considered as distributed storage units which are, additionally, capable of injecting energy back to the electricity grid (Vehicle-to-Grid services, V2G) in order to support grid operation and enhance its operational efficiency.

Irrespectively of the EV representation, the integration of electric vehicles into electricity grids poses an additional load to the system which modifies the system load curve. This demand must be served at any point of the grid, where an EV may be connected, similarly to the conventional one without any discrimination. There are several parameters defining the additional EV demand which can be separated into two categories as follows:

Constant parameters

*EV deployment level:* the size of the EV fleet that is connected to the electricity grid

*Charging station technologies*: the nominal charging power of the charging stations varies according to the technology from 3.2kW up to 300kW.

*Availability of charging stations*: the placement of the charging stations, i.e. home, workplace, public places, highways etc., affects significantly the demand profile of the charging

Probabilistic parameters

*Driving profile*: the energy consumption of the EV battery which fulfils the mobility needs of electric vehicles depends on the travel distance and the driving conditions (economic or dynamic driving, use of auxiliary loads such as air-condition etc.)

*EV connectivity:* electric vehicles are not available for charging unless they are connected to the electricity grid (either via charging cable or contactless). The start and the available duration of the charging process are defined by the arrival and departure time of EV user to and from the charging station.

The aforementioned parameters defines the additional charging demand that fulfills the e-mobility needs of an EV fleet. The way this demand will be imposed on the electricity network load curve depends on the implemented charging policy (dumb charging, multi-tariff charging, smart charging). An extended analysis on the impact of EV demand on the system load curve considering different charging policies has been performed in [59].

Based on this analysis, the dumb charging policy can lead to "worst case" scenarios. When EV charging remains completely uncontrolled, the profile of the charging demand is highly dependent on the time of return from the last journey of the day. Since home arrival normally coincides with increased residential consumption, the EV demand can be synchronized with the system peak load. Thus, dumb charging might result in local distribution network congestions and a higher share of EVs, might require premature grid investments [59]. The Figure 10 shows the impact of the "dumb charging" in the system daily demand in different European countries and for various EV penetration scenarios. The worst-case scenario in a typical winter day is presented.

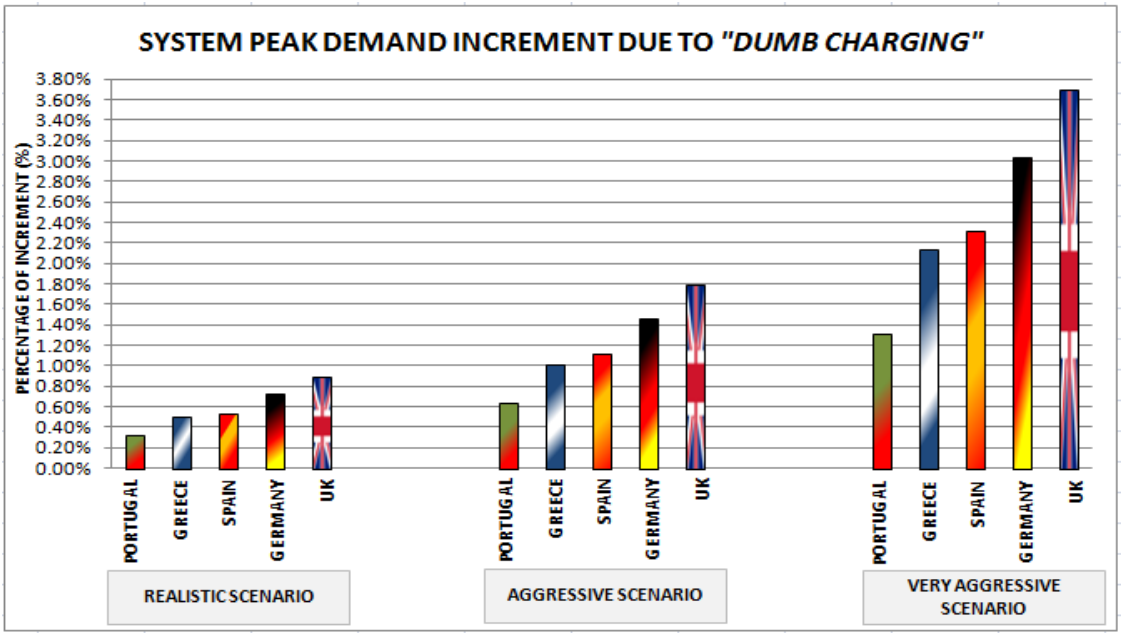


*Figure 10 – The increase in system peak demand in different European countries due to "dumb charging" for the three penetration scenarios.* [59]

The grid impacts of home charging can be limited by developing charging infrastructures at workplaces. In this case, part of the daily EV charging needs compensating the battery consumption for driving from home to work, can be fulfilled during morning hours at workplace, when the system demand is still relatively low.

Concerning the work charging, it was concluded that the demand peak of the home charging is reduced since the daily mobility energy requirements are partially fulfilled during morning hours. Moreover, in case of hybrid EVs the daily driving autonomy using the battery can be extended if intermediate charging sessions are occurred. However, the conclusion for this analysis is not to develop workplace charging infrastructure in order to reduce the peak demand of home charging

but wherever workplace charging infrastructure exists it can be utilized for intermediate charging sessions which can consequently reduce home charging demand peak. As the number of EVs charging at workplaces increases, the additional system peak demand due to EV "dumb charging" reduces.

Dual-tariff charging is more effective than dumb charging, since it enables the shifting of the EV demand from high loading hours to off-peak hours. However, this is likely to result in a sharp increase of EV demand at the beginning of the low energy price period which might affect the network operation.

Smart charging avoids high peak loads by allocating the EV demand during off-peak hours. The figure below (Figure 11) illustrates the effect of this load allocation to the system load factor. In smart charging, EV demand is managed in a way that reduces the system load variation between off-peak hours and high load hours. Smart charging is the most effective charging strategy, however its implementation is not straightforward and for a large number of vehicles it requires advanced control and management techniques.

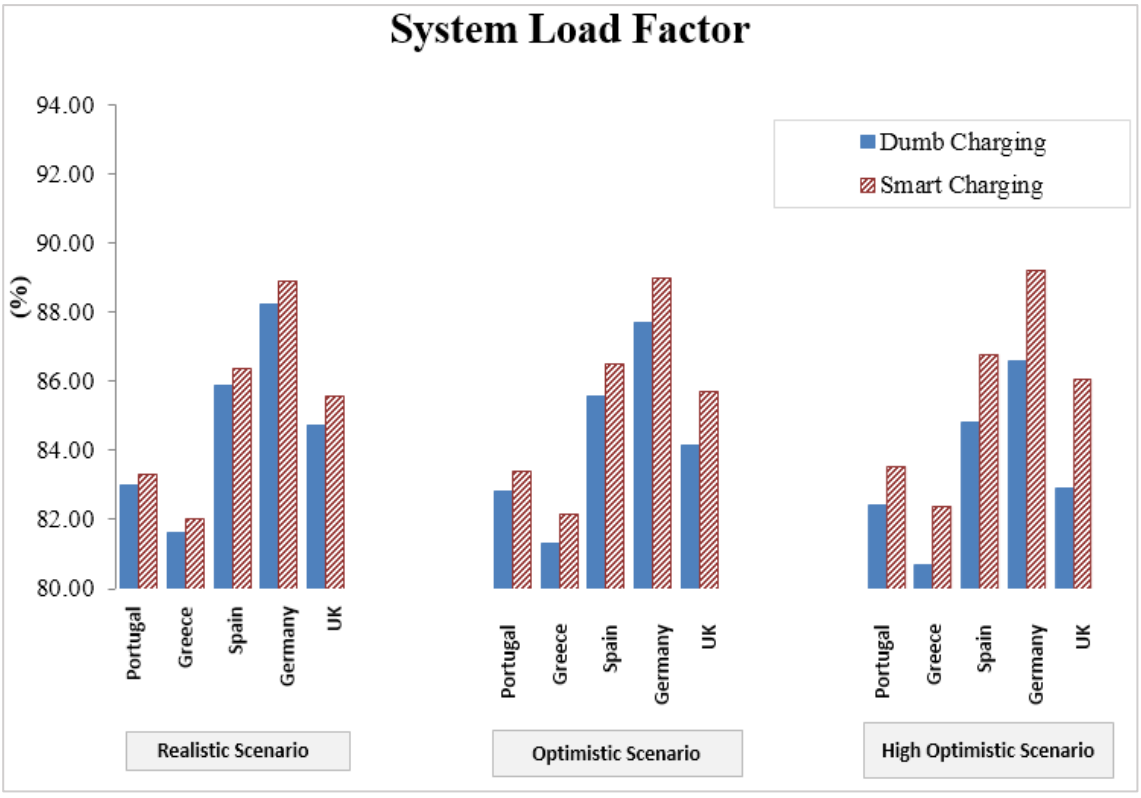


*Figure 11 – The increase of system load factor comparing "dumb charging" with "smart charging"* [60]

The additional demand of electric vehicles is expected to affect the operation of distribution networks depending on the EV penetration level as well as the adopted charging strategy. The integration of electric vehicles into electricity grids may provoke operational issues at local grid level, i.e. distribution network. Each distribution network can host a maximum number of electric vehicles without violating any network operational constraint [61], [62]. The maximum EV penetration level is called *EV hosting capacity* and it is defined based on the technical and operational characteristics of the respective distribution network. More specifically, MV urban distribution networks are densely populated and the network equipment loading is usually high. Thus, EV deployment is

expected to further burden network equipment. On the contrary, MV (Medium Voltage) rural networks comprise long lines provoking high voltage drops, while the network loading is relatively low. Consequently, the EV hosting capacity can be defined either based on the network loading or the voltage profile. The EV hosting capacity of a network can be increased by implementing advanced EV coordination mechanisms enabling more efficient exploitation of the grid capacity and local resources.

Finally, the charging equipment when connected to the local grid can also deliver grid services (V2G) for example, respond to a demand of the grid operator. Possible scenario's in which connected electric cars could favor grid stability by adjusting the charging power of the car, or deliver energy back from the car to grid. The EVs can be connected to grid via a private network (house or building) and also provide services there (Vehicle to Home/Building – V2H/B) such as energy cost reduction.

# 3 Terni: real-life pilot for research applied on Smart Grids

This chapter presents the distribution network and key assets which has been used for this work, notably a description of the distribution is provided in Section 3.1, Section 3.2 presents a focus on the prosumers' features whilst Section 3.3 provides information about the headquarters of the DSO in which some specific activities have been carried out.

## 3.1 The distribution network of Terni

ASM TERNI S.p.A. is an Italian multi utility company, established in 1960 and fully owned by the Terni municipality, specializing in water, gas, electricity and environmental services. It owns and operates the local power distribution network, covering a surface of 211 $km^2$ and delivering about 400 GWh to 65,500 customers annually. The ASM distribution network acquires electricity at High Voltage (HV) through 3 primary substations and supplies electricity to residential and business customers through 60 Medium Voltage (MV) lines (10kV to 20kV) and about 700 secondary substations. The peak power is about 70 MW and the total length of the power lines in the grid is about 2,400 kilometres (600 km MV and 1,800 km Low Voltage - LV).

Nowadays the ASM's electric grid is characterized by a large number of distributed renewable energy sources embedded in the MV and LV distribution networks: 1 biomass plant, 5 hydro power generators and 1,234 photovoltaic (PV) units are currently connected directly to the MV and LV distribution networks reaching the total installed capacity of around 70 MW. In this regard, it is worth pointing out that, based on this energy mix shown in *Figure 12*, 200 GWh of the 400 GWh absorbed yearly, are produced by DER systems connected to the MV/LV grid of ASM, 70 GWh of which are from intermittent RES.

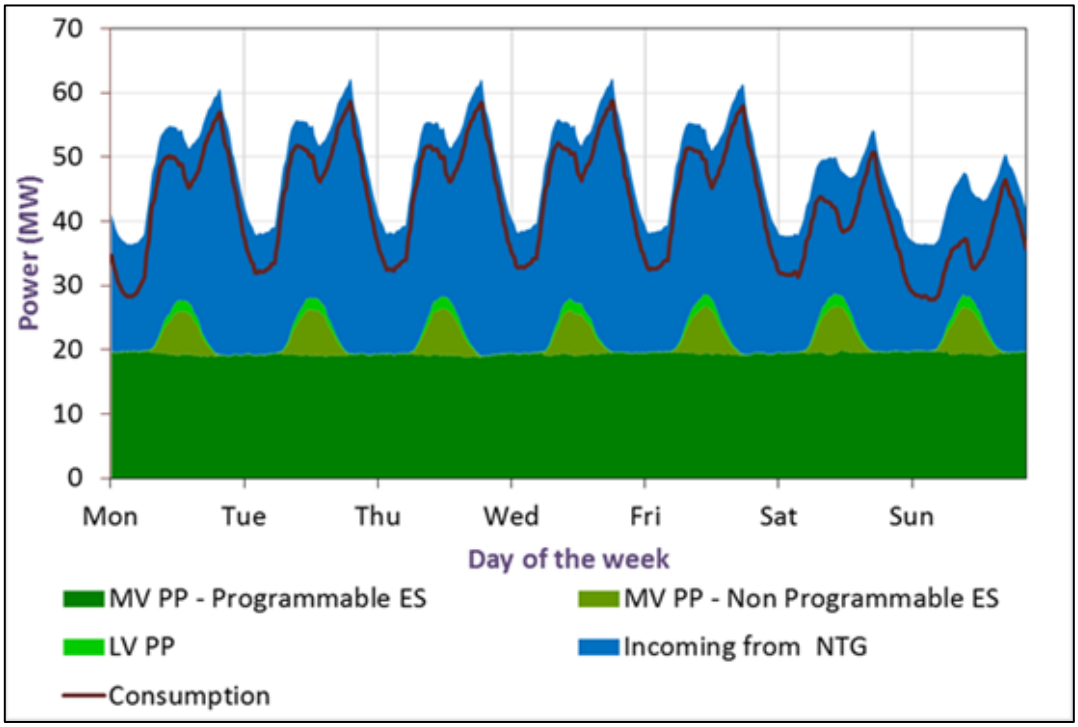


*Figure 12 Weekly average power profile for ASM distribution network (2016).*

In 2010 the deployment throughout the power network of smart meters with four data acquisitions per hour (each 15 minutes) was completed, reaching all the 65,500 end users. Moreover, both secondary substations and RES generators have been equipped with real time power automation devices (compliant to the IEC61850 protocol), allowing the real time measurements of at least active and reactive power, frequency, voltage and current.

The power distribution network is connected to HV grid through 3 substations. There are also 6 sorting MV/MV substations and 615 MV/LV substations. MV cable and overhead lines are long about 622 km, whereas LV lines length is about 1418 km. Nowadays the energy customers are about 65,500, 98% of which have an electronic meter. The ASM's power network topology is shown in Figure 2. In 2018 the energy consumption reaches 347 GWh, while the distributed production units connected to the MV / LV network (DER) generate 178 GWh (i.e. approximately 49% of the total demand).

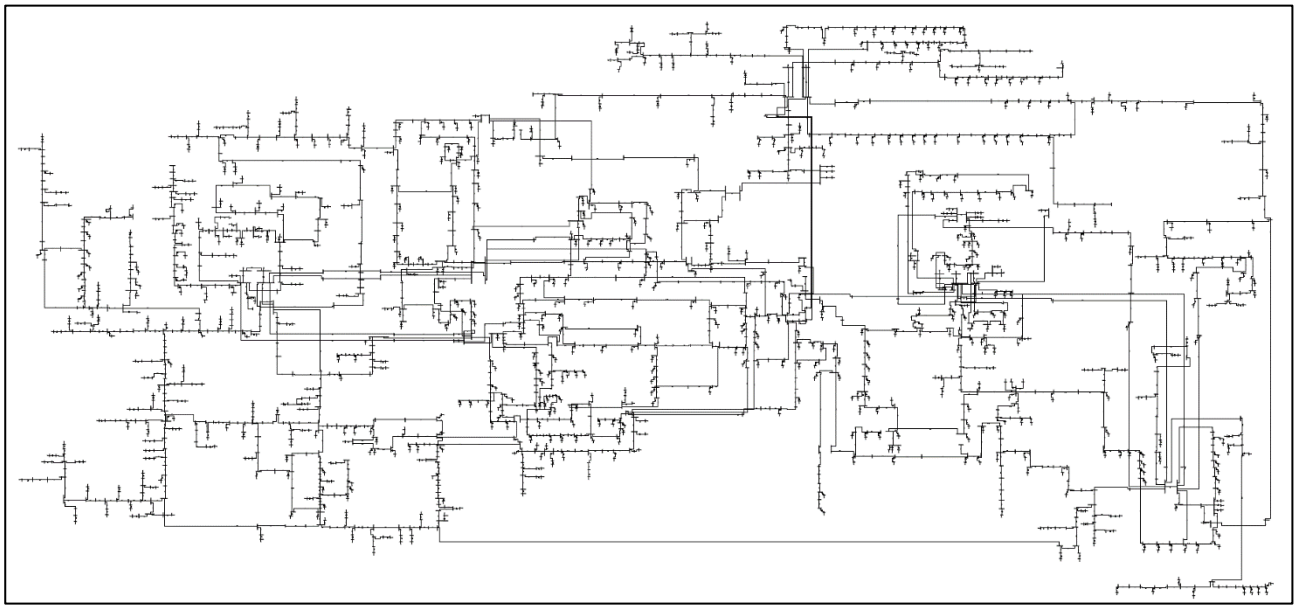

*Figure 13 Single line diagram of ASM's power network*

In 2018 about 50% of the total consumption was covered by RES. In actual fact in 2018 the local power network received renewable energy from 1,289 power generation plants (mainly PV arrays) using renewable sources, such as sunlight, water and biomass. In 2018 the total electric power generated from RES was as follows:

- 1278 PV arrays (31.5 MW) producing 32 GWh yearly
- 7 Hydro plants (10.0 MW) producing 71 GWh yearly
- 4 biomass/waste to energy plants (21.0 MW) producing 81 GWh yearly

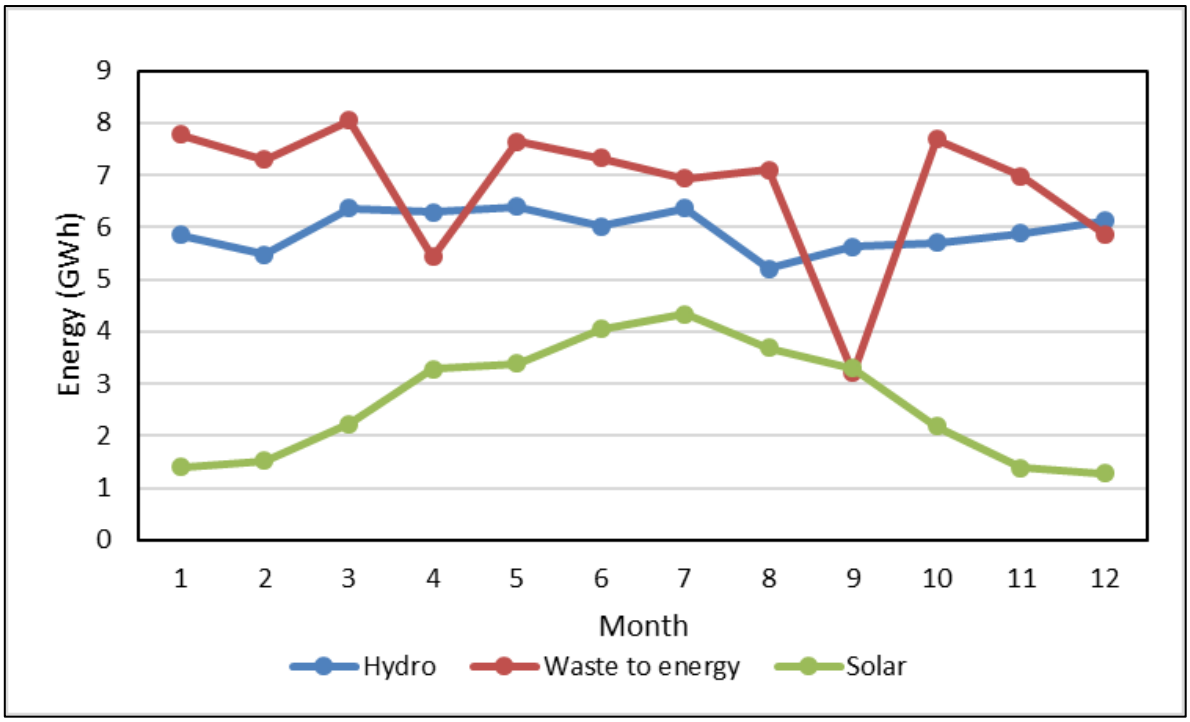


*Figure 14 Internal generation monthly based*

### 3.1.1 *Metering, monitoring and communication*

- **Smart meters**

As reported previously, almost all the electricity customers have smart meters installed in their premises. Based on the installed power capacity, different models of Landis+Gyr SMs have been chosen by ASM, as follows:

- Smart meter with PLC (Power Line Communication): for LV users with an installed power capacity ≤30kW;
- GME for LV (GSM/GPRS communication) ≥ 30kW;
- GME for MV customers (GSM/GPRS communication).

Moreover, in some critical points of the power network ASM TERNI has installed a certain number of new generation SMs able to get real-time measurements and support real-time operations in a Smart Grid (class A power quality analyzer - a 3-phase high-precision analyzer and recorder, power quality, power meter, fault recorder and energy meter). It is a three phase high-precision power quality analyzer compliant to Class A, according to IEC61000-4-30, and Class 0.2S for energy metering. It is capable of measuring the following parameters: voltages and currents; active, reactive and apparent power; active and reactive (4 quadrants) energy; power factor; frequency, flicker (Perception of flicker short term - PST and Perception of flicker long term - PLT); voltages and currents harmonics and interharmonics (up to 50° order); voltage unbalance; voltage dips and swells; voltage interruptions (short and long); rapid voltage changes and waveforms (window records with programmable pre and post-triggers).

- **Advanced Metering Infrastructure (AMI)**

In order to manage time-based data from smart meters, an AMI has been put in place, allowing to remotely turn power on or off to a customer, read usage information from a meter, detect a service outage, change the maximum amount of electricity that a customer may demand at any

time, detect "unauthorized" use of electricity and remotely shut it off, and remotely change the meter billing plan. ASM is currently using two different channels for the collection of data from the installed meters; one is exclusively used for the Point of Delivery (PoD) for customers with power installation up to 30 kW and the other for power consumption greater than 30 kW.

Data related to first channel are addressed via PLC; these are temporarily stored in a Electric energy meter concentrator (one for each 400 meters), extracted and transmitted via GPRS network towards ASM Terni servers. Data related to the second channel is extracted and transmitted via GSM/GPRS. The data related to the second channel are addressed via GSM / GPRS; these are transmitted to a meter data management software and analyzed with the aim to verify any problem in data transmission and finally temporarily stored in the ASM's server for at least five years.

- **SCADA system**

The whole Medium Voltage (MV) network is under the control of a SCADA system able to:

- communicate with the calculation platform which hosts all algorithms for status analysis, power flow calculation and voltage regulation;
- receive and send information from/to Main Station equipment;
- receive and send information from/to Substation equipment;
- carry out the anti-islanding function and, when needed, send disconnection requests to the Main Station equipment.

Remote Control System staff is using the Operator Terminals to display the grid (status and measurements), interact with it (controls and commands) and manage abnormal situations (alarms) by means of a Human-Machine Interface (HMI).

### 3.1.2 *Reverse Power Flow in the distribution network*

When power at high voltage comes off the transmission grid, it is stepped-down to lower voltage to the distribution network to power customers. Along these distribution systems are substations to transform voltage levels and, recently, several distributed generation plants connected on the LV or MV networks. This increasing integration of renewable energy sources such as hydro, wind and solar power has changed the energy paradigm, from the traditional unidirectional flow of energy and communication to a bidirectional power flow. Whilst in traditional power supply systems, power generation follows the load, in the future power consumption will follow generation.

Nowadays the DSO needs tools and solutions to efficiently manage internal energy production guaranteeing stability and avoiding imbalance in the grid. In actual fact, if the load is lower than the local energy production connected at the same MV bus, RPF from the distribution to the transmission network occurs.

From a technical point of view, RPF represents a change in the paradigm for both transmission and distribution operators. Analyzing the problem from the national point of view, the phenomenon is evident in some parts of southern Italy because of the high penetration of wind farms. Since the local load in these areas is significantly lower than the wind energy, a consistent RPF occurs. However this energy cannot flow in the reverse direction due to the constraints on the maximum loading of electrical energy distribution feeders in the National Transmission Grid (NTG) and therefore, although the rest of Italy, especially in the North, needs energy for their local consumption the wind farms are often disconnected [63].

To understand the current situation in the ASM's distribution grid the power drawn from the grid, the RPF and the internal load were investigated. In 2016, 370 GWh were delivered to the consumer, 230 GWh drawn from NTG and 193 GWh produced by DER plants connected to the ASM's power network; the yearly RPF measured in the substations reached 25 GWh and about 40% of the measures shows that the locally-produced energy overcomes energy drawn from the NTG, especially in the night because of hydro power plants.

*Figure 15* shows the load profile of the whole distribution network in 2016 for power flowing from TSO to DSO, or vice versa (RPF).

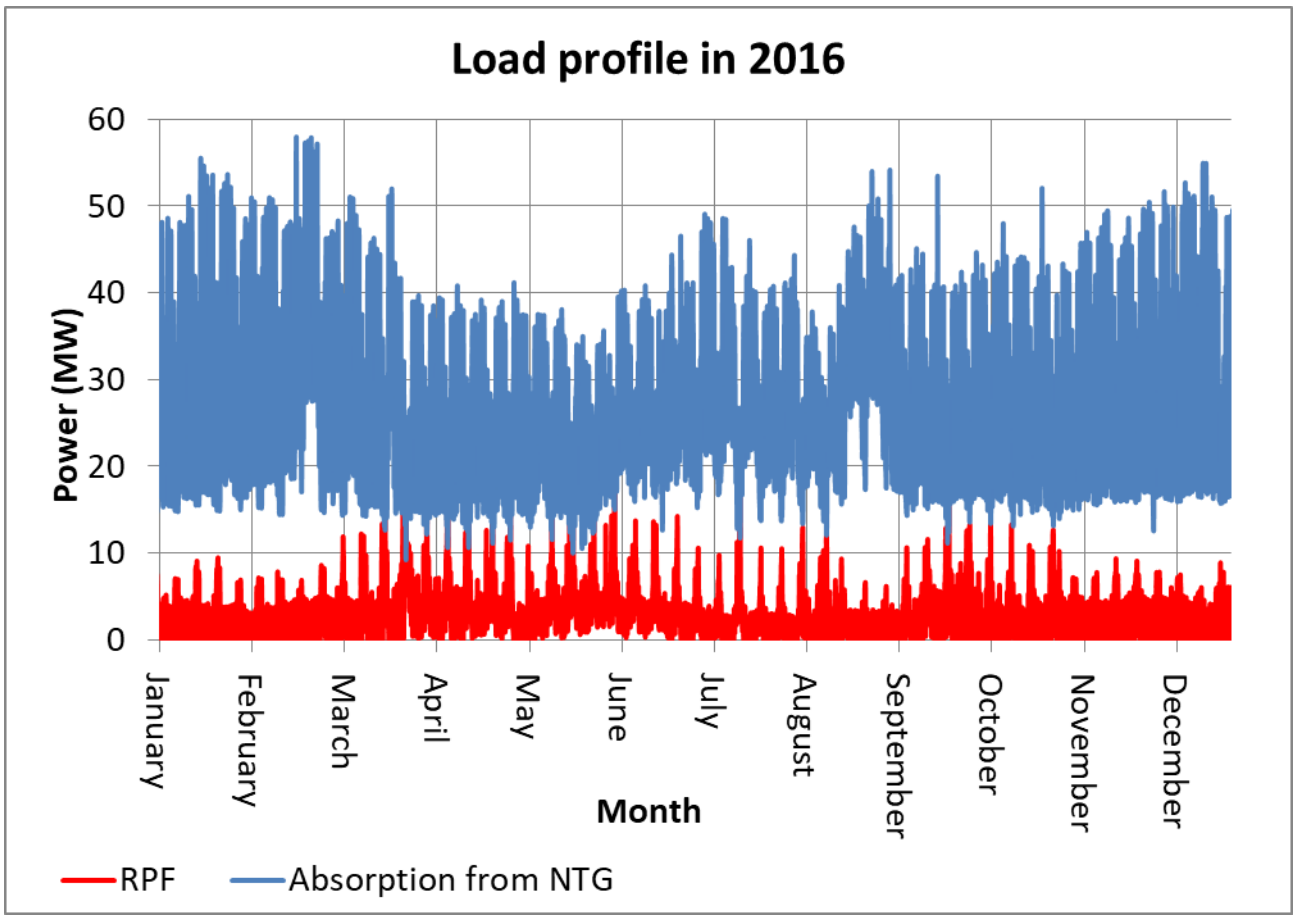


*Figure 15 Load profile (2016)*

In order to qualitatively define the impact of RPF in the distribution network, the ratios of RPF to the power absorbed from transmission grid (TG) and to the energy produced by distribution grid (DG) were calculated on hourly basis. The number of hours in 2016 when RFP overcomes the 25%, 50% and 100% of TG and DG power was calculated and expressed as a percentage (*Table 3*).

| Statement | n. of hours (Statement is true) / n. of hours in a year (%) | Statement | n. of hours (Statement is true) / n. of hours in a year (%) |
|---|---|---|---|
| **RPF > 0,25*TG** | 19,2% | **RPF > 0,25*DG** | 14,7% |
| **RPF > 0,50*TG** | 4,2% | **RPF > 0,50*DG** | 0,05% |
| **RPF > TG** | 0,55% | | |

*Table 3 Percentage of hours when RPF is higher than TG and DG (2016)*

In order to characterize more in detail the RPF profile in the distribution network, RPF was measured in five T/D connection points, namely the green and red buses at Terni Ovest (TO) substation, the green and red buses at Villa Valle (VV) substation and the bus at EX-SIT substation (*Figure 16*). Although the TSO could operate the substation's buses together or separately, in this assessment each bus was considered independent for fiscal and technical reasons. In actual fact, since every bus distributes and receives electric power from a specific distribution network, every calculation of energy transition were performed in each bus considering only the load and the production effectively connected to the bus bar.

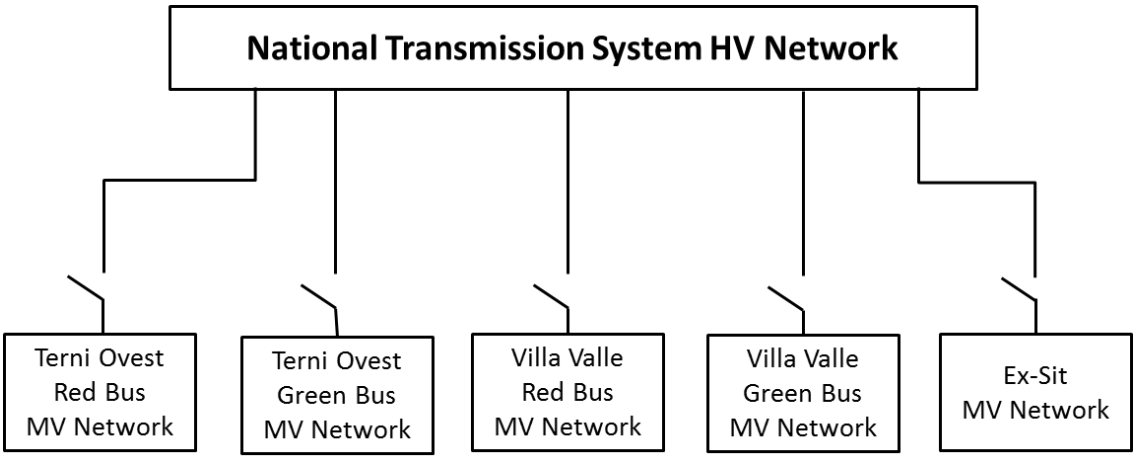


*Figure 16 The T/D connection points in the ASM's distribution network used for the ex-ante evaluation*

*Table 5* shows the total absorbed energy, the reverse energy, the absorption power peak and the reverse power peak measured in each bus in 2016. Moreover, the RPF rate in each bus was calculated and reported in the Table 3 as percentage of hours per year in which active power flows in the reverse direction (from DSO to TSO - $N_{h,RPF,year}$) and also when the hourly RPF is higher than the energy drawn from the HV grid ($N_{h,RPF>AE,year}$).

| | EX-SIT | VV-GB | VV-RB | TO-GB | TO-RB | ASM Network |
|---|---|---|---|---|---|---|
| **Absorbed energy (GWh)** | 29,33 | 2,62 | 100,56 | 32,35 | 65,31 | 230,17 |
| **Reverse energy (GWh)** | 5,37 | 19,62 | 0 | 0,35 | 0 | 25,35 |
| **Absorption power peak (MW)** | 20,74 | 17,23 | 21,85 | 10,76 | 16,48 | 57,98 |
| **Reverse power peak (MW)** | 11,71 | 6,96 | 0 | 3,72 | 0 | 22,24 |
| $N_{h,RPF,year}$ | 40,31% | 89,12% | 0% | 8,85% | 0% | 91,44% |
| $N_{h,RPF>AE,year}$ | 27,26% | 83,93% | 0% | 4,06% | 0% | 0,55% |

*Table 4 Yearly data at each bus bar (2016)*

Data reported in the table clearly shows that RFP occurs in EX-SIT, VV-GB and TO-GB, whilst in VV-RB and TO-RB this phenomenon is not detectable. That is due to the fact that i) all the hydro power plants are connected to the VV-GB bar so that RPF occurs because locally generated power often exceeds the local load and ii) the majority of PV power plants are connected to the TO-GB and the EX-SIT bus bars causing RPF for the local imbalance between production and consumption. It is worth highlighting that about 23% of RPF in ASM's distribution network is caused by the intermittent generation (mainly PV arrays connected to the TO-GB and the EX-SIT bus bars). Analysis will be focused more on this buses, because it will be shown that this RPF is due to a misocoordination between consumed energy and produced energy, so that a DR campaign is crucial in order to reduce it. Otherwise, RPF generated by hydro power plant is mainly due to a topology issue so that a DR campaign will be not effective in order to decrease it.

In order to understand typical events of RPF happening over the year, a weekly analysis focused on specific periods of the year (summer, winter, Easter) and specific buses was carried out.

Summer vs Winter – The seasonal variation of the local energy production and load and their impact on RPF and power drawn from the transmission grid were investigated. In accordance with the literature [5, 6], two weeks were chosen as representatives of the seasonal variation, namely 6-12 June (Figure 17) and 19-25 December 2016 (Figure 18). The comparison between the two graphs shows that during summer RPF occurs always during the day whilst in winter it happens only when the load is at its lowest level.

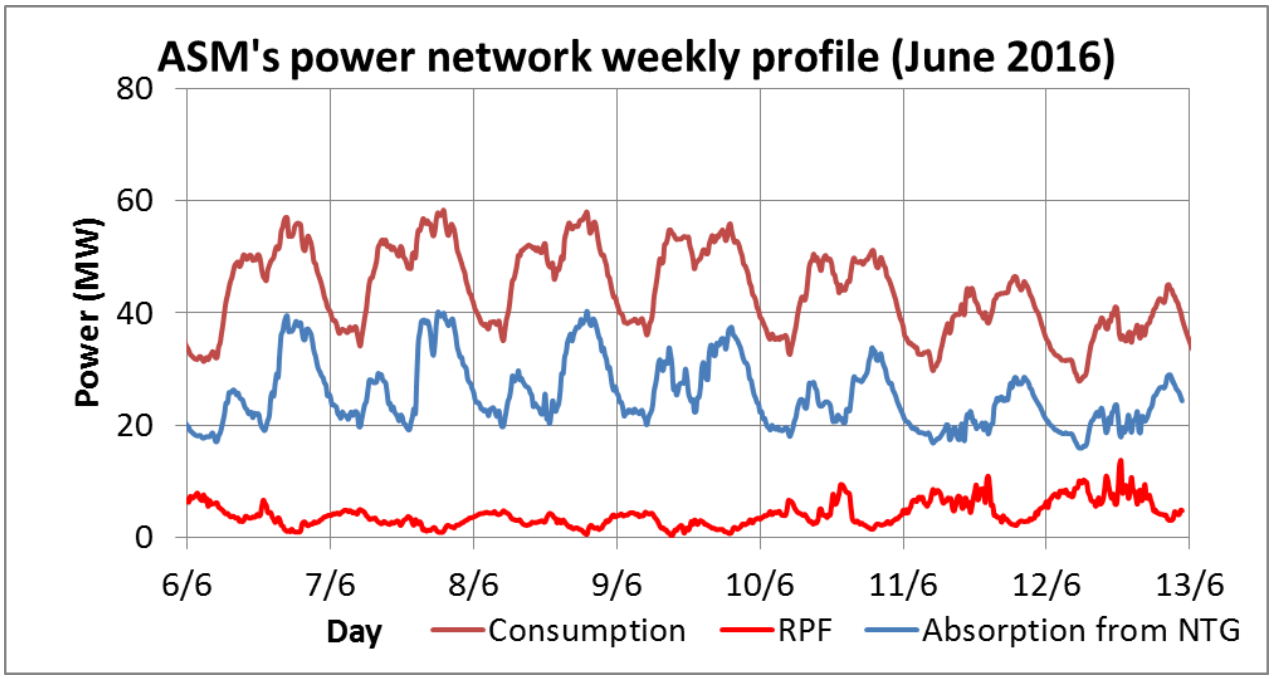


*Figure 17 Load profile in summer*

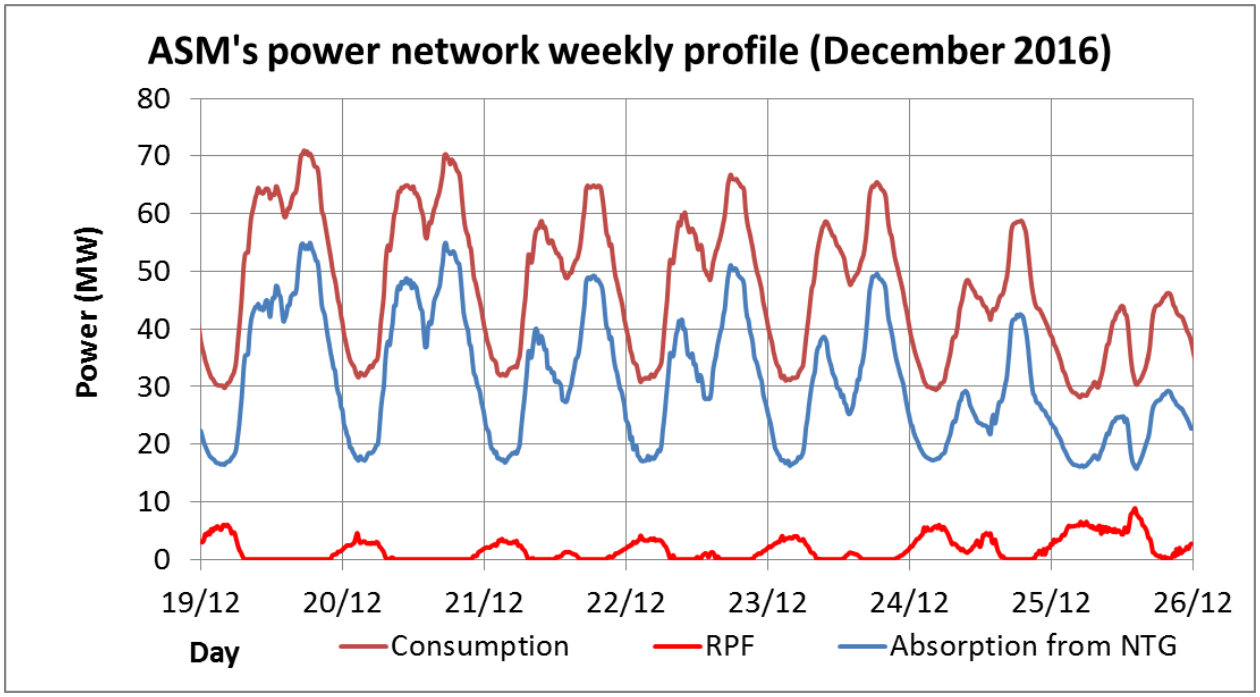


*Figure 18 Load profile in winter*

Since RPF is related to the distributed generation and based on the analysis shown in *Table 2* it happens only at three buses of the ASM distribution network, the load profiles were analysed separately, for TO-GB and EX-SIT, both characterised by the high penetration of PV and for VV-GB feeded by hydropower plants.

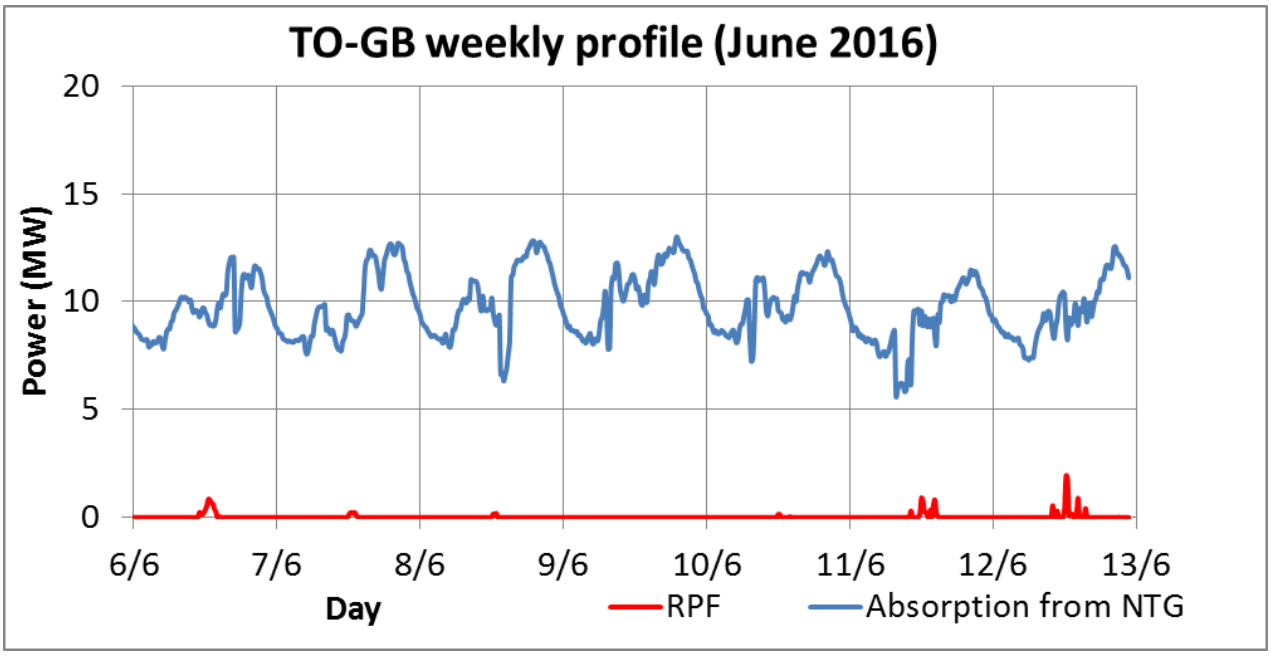


*Figure 19 TO-GB Load profile in summer*

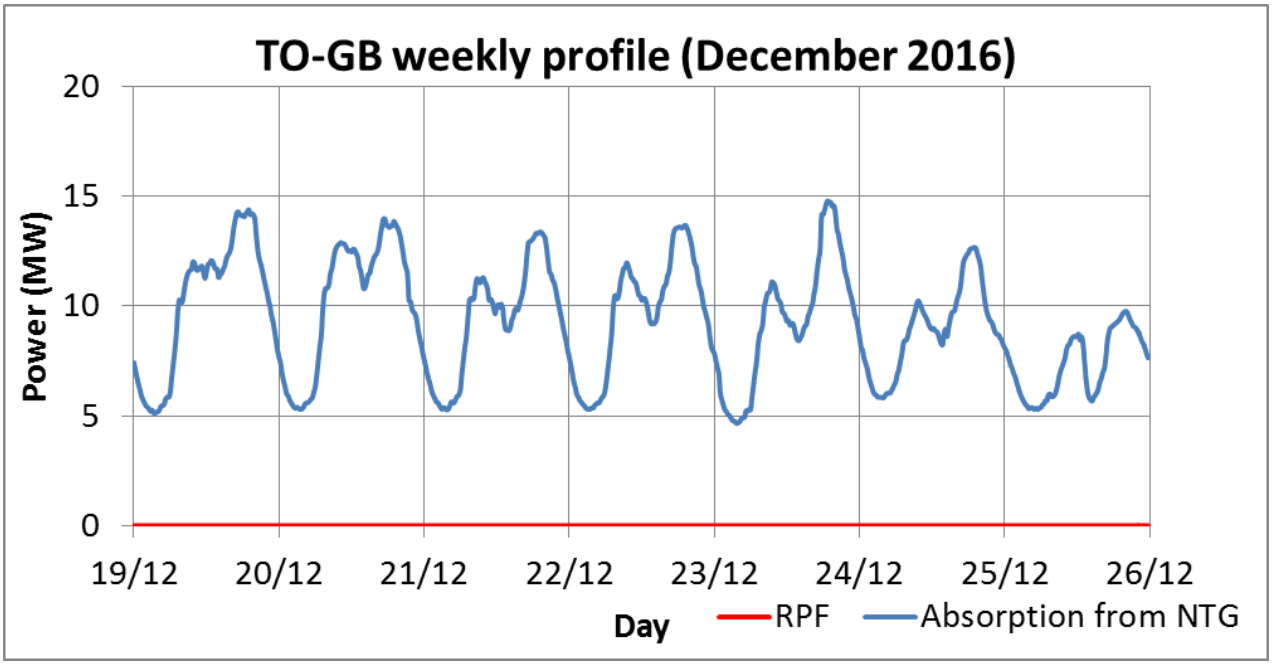


*Figure 20 TO-GB Load profile in winter*

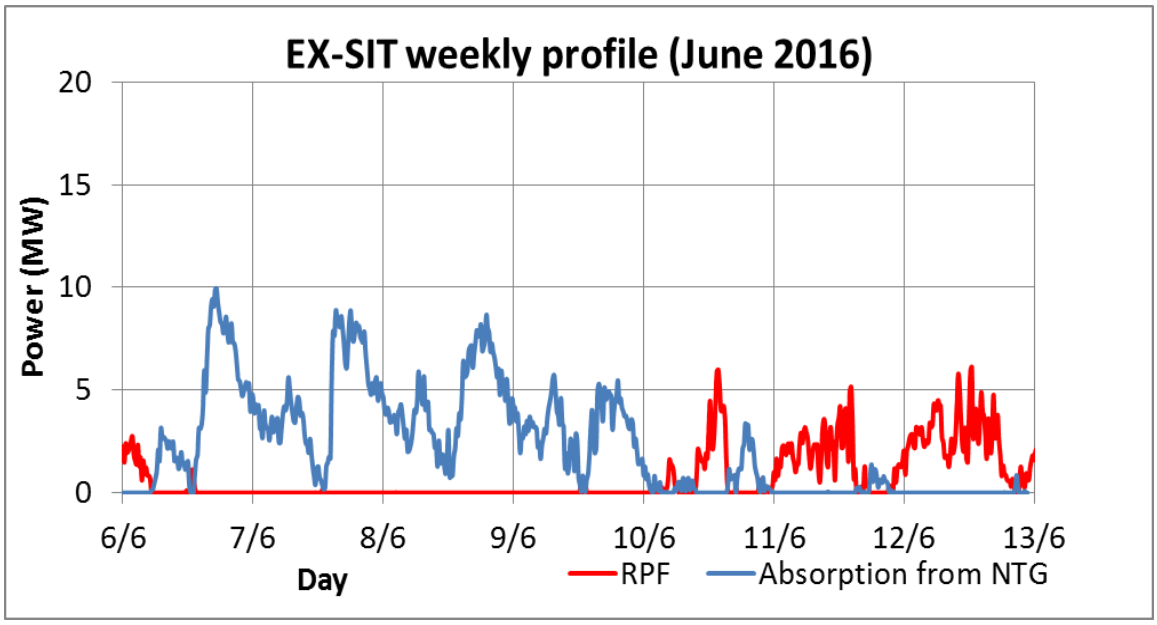


*Figure 21 EX-SIT load profile in summer*

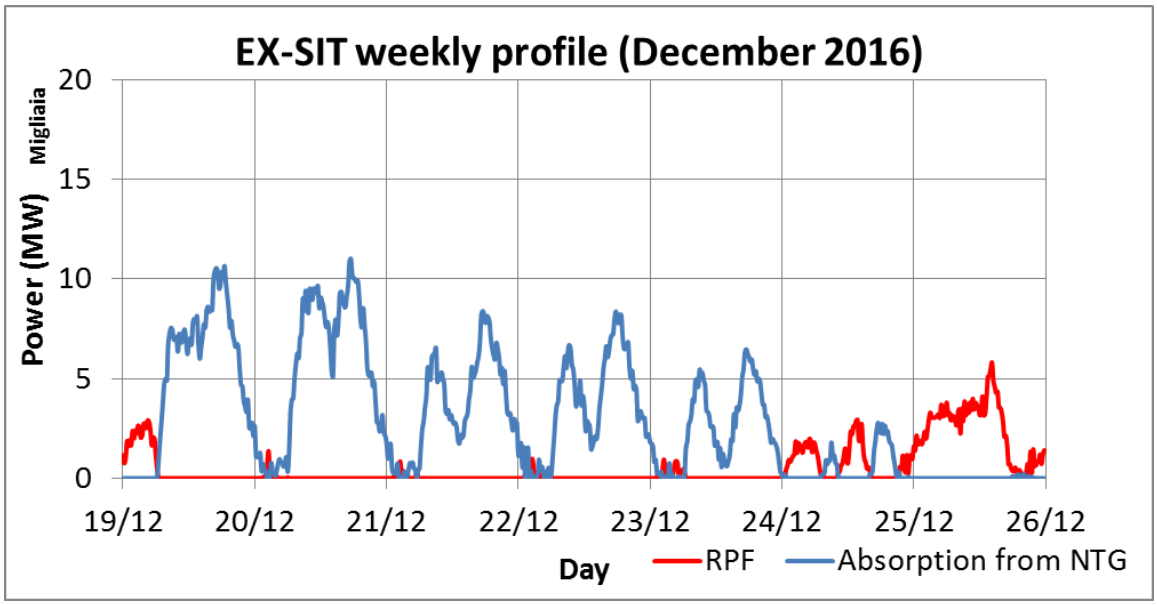


*Figure 22 EX-SIT load profile in winter*

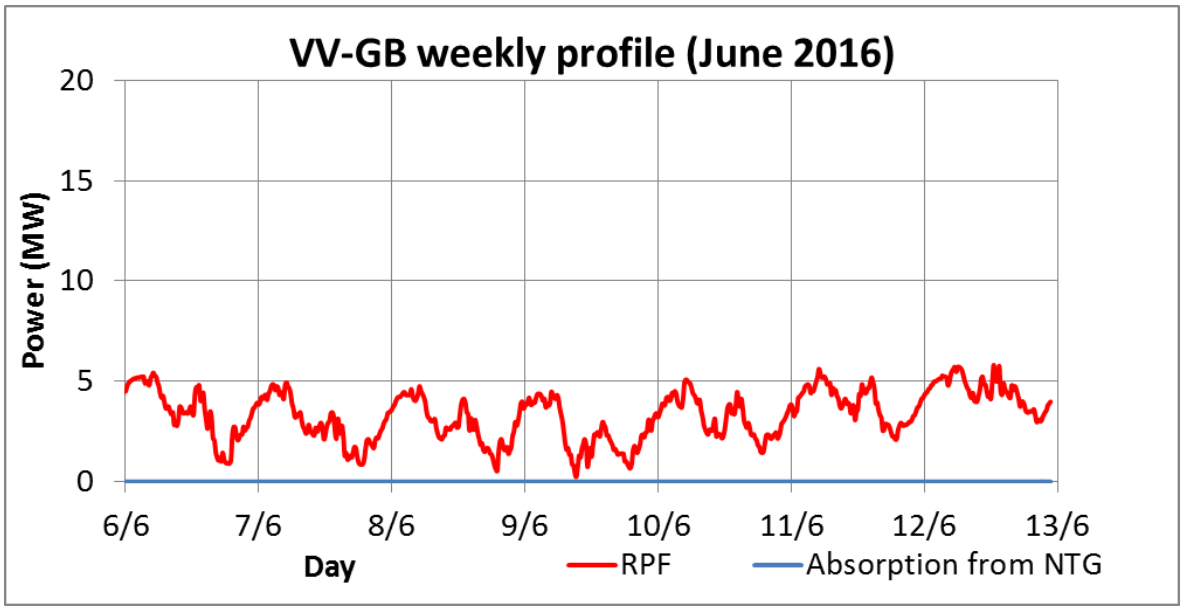


*Figure 23 VV-GB load profile in summer*

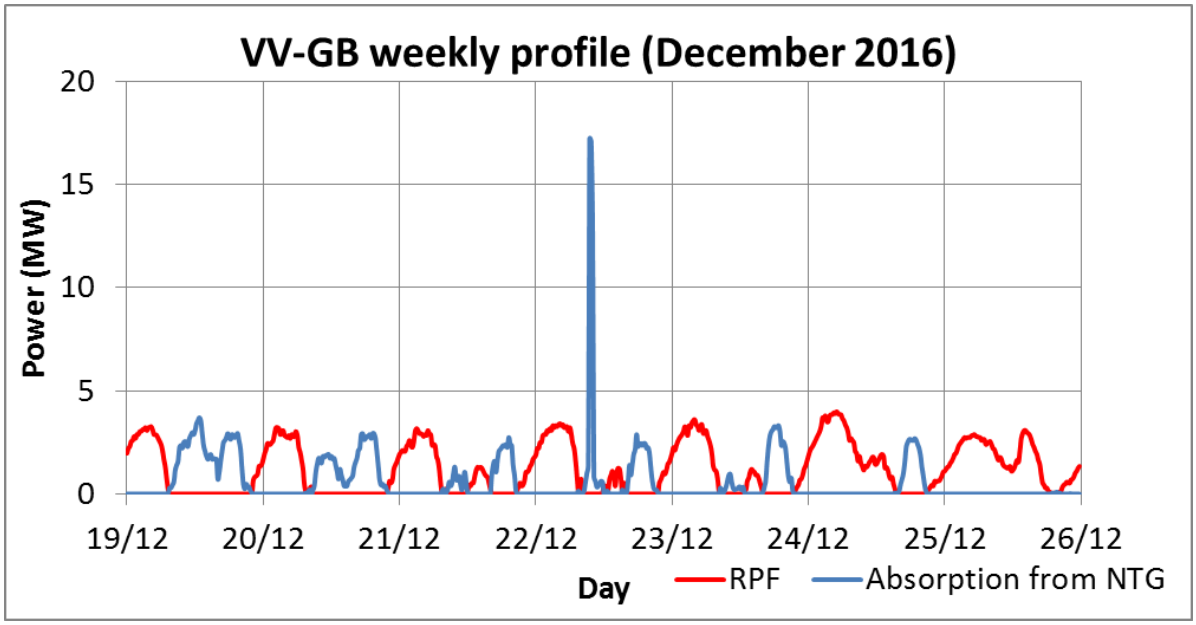


*Figure 24 VV-GB load profile in winter*

The data analysis of the three buses shows that in both TO-GB and EX-SIT, where the local production is mainly due to the solar energy, RPF occurs especially in the week-end with peaks when the sun is at its strongest. Moreover, it is interesting to point out that EX-SIT bus bar receives also energy from a thermoelectric plant so that the RPF profile is affected also during the night. As to the VV-GB seasonal profiles, whilst in summer energy flows only in the reverse direction showing a consistent imbalance of the local load, in winter, when the local consumption rises, RPF decreases.

***Easter week*** - Since 2014, during Easter week the ratio of PV production to local load is so high that TERNA (the Italian TSO) usually requires to reduce PV injection [5]. Therefore, as consequence of the imbalance between local energy consumption and DER production, a consistent RPF is expected over the period. The weekly profile of 2016 Easter week is reported in the *Figure 25*.

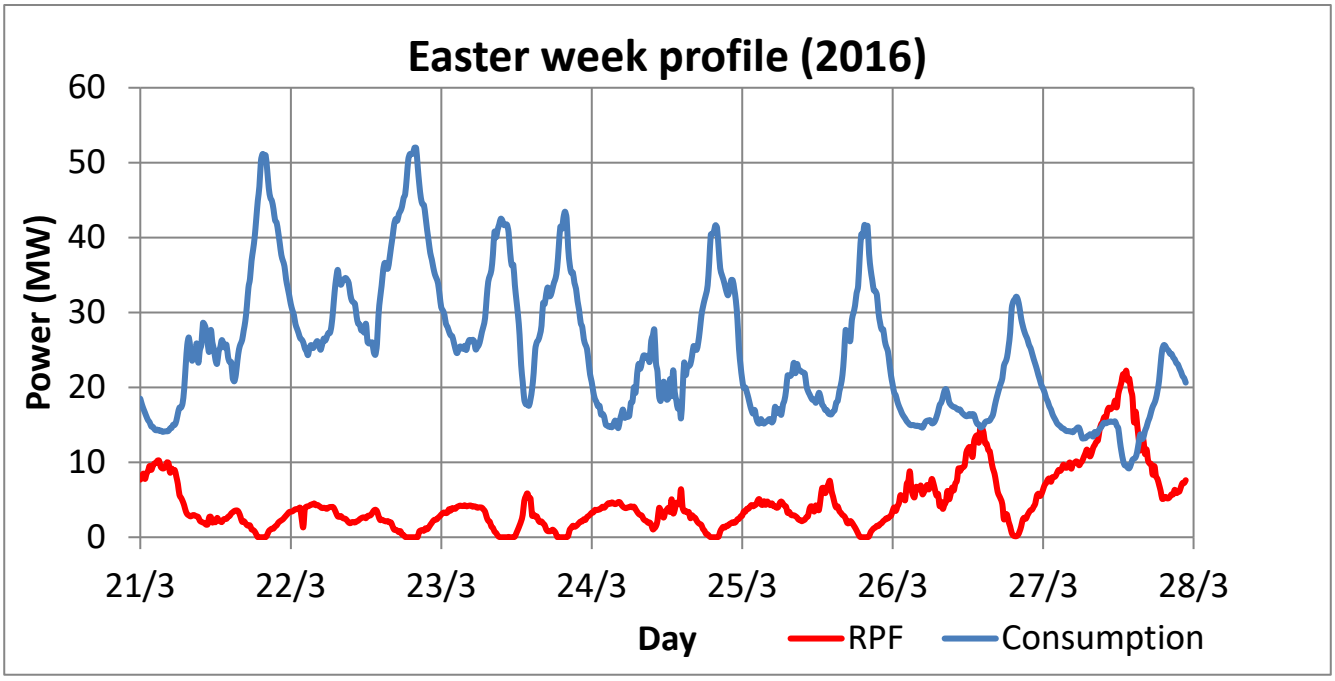


*Figure 25 Power flow during the Easter week in 2016*

The weekly profile shows that on the Easter weekend RPF is sometimes higher than the power drawn from the NTG; the peak was detected on Sunday at 02:15 PM. It is worth noting that over a year, considering a sampling time of 15 minutes, 192 times the energy drawn from the NTG is lower than RPF (about 0.05%). That was measured every Spring Sunday (from 20$^{th}$ of March to 5$^{th}$ of June 2016) and during some other public holidays, even though the ratio of RPF to the energy drawn from the NTG is lower than in Easter.

From the analysis outlined in *Table 4*, PV arrays are mostly connected to two buses, namely EX-SIT and TO-GB, where RPF has been detected. The analysis of the RPF peaks during Easter demonstrates that the RPF peak happened on Sunday at 14:15. The *Figure 26* underlines RPF (red line) and the power drawn from the transmission grid (blue line) at TO-GB.

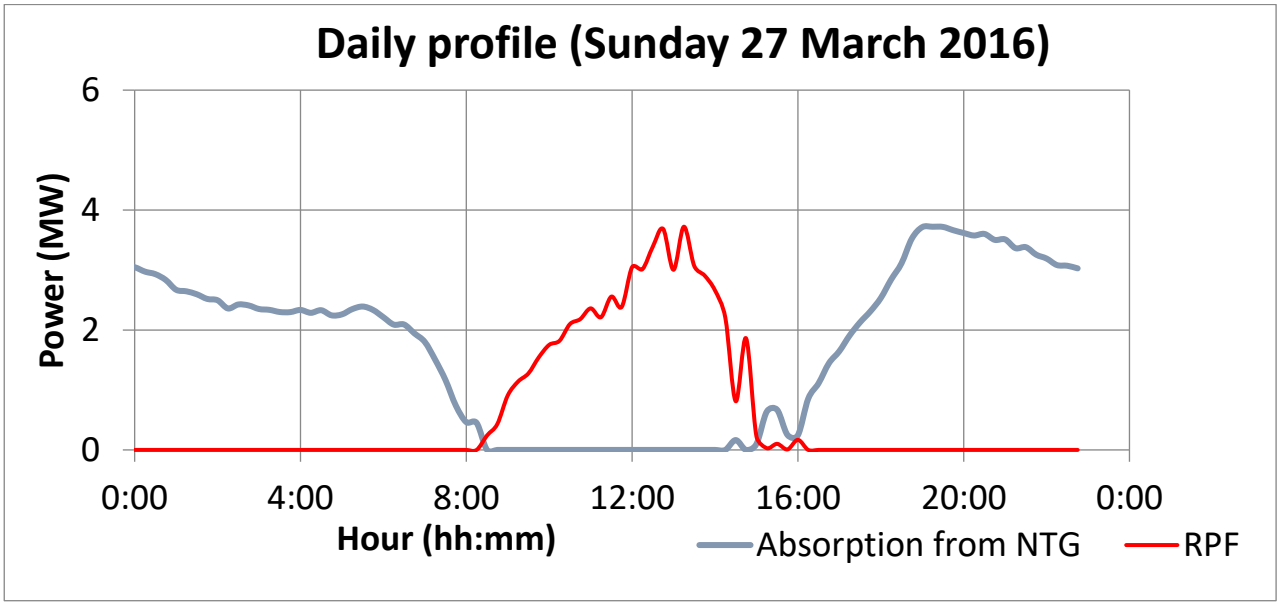


*Figure 26 TO-GB daily profile (27$^{th}$ of March 2016)*

In conclusion, based on the data reported in this technical analysis, it is evident how important is the mitigation of the RPF caused by the intermittent generation (mainly PV arrays) for improving power quality and efficiency, avoiding overvoltage on the feeder, protection miscoordination, increased fault currents, and incorrect operation of equipment.

## 3.2 Statistical analysis of the domestic prosumers over three year

This subsection presents and analyzes monthly aggregated data regarding PV prosumers connected to ASM distribution grid. Analyzes focus on years 2015 and 2016 and specifically concern domestic PV prosumers, aiming at evaluating some key topics about domestic prosumers.

In recent years, Italy and other countries in EU, as well as China and Japan, promoted and encouraged self-consumptions, for instance by means of feed-in tariffs and premiums dedicated to self-consumption, in some cases (i.e. Japan) specifically dedicated to domestic prosumers. In order to increase PV self-consumptions, technologies are actually available on the market, as a battery energy storage system coupled with the PV: in this case, PV generation is shifted by means of electric batteries to increase matching with load consumptions. Another action under study (in some cases put in operation in pilot projects) is demand side management (DSM): in this case, loads are shifted in order to increase matching with PV generation. Notably, DSM effectiveness is affected by the response of the domestic customer and so models of the customer's energy usage, also taking into account lifestyle factors affecting energy usage in houses [64], should be considered. Finally, many papers dealt with increasing self-consumption by using storage systems [65] - [66], DSM [67] - [68] or both [69] - [70].

Focusing only on domestic PV prosumers, such users are 774 until 31 December 2015 and 851 until 31 December 2016. The aggregate installed PV power and load contractual power were 3.2 MWp – 3.27 MW in year 2015 and 3.47 MWp – 3.67 MW in year 2016. During 2015, domestic PV prosumers produced 3.58 GWh and injected in the grid 2.56 GWh, whereas load consumptions were 2.12 GWh. Considering year 2016, domestic PV prosumers produced 3.63 GWh and injected in the grid 2.61 GWh, whereas load consumptions were 2.4 GWh. Table I and Table II summarize such data for year 2015 and 2016, respectively.

Finally, Figure 27 reports the statistical distribution of the ratio between the installed PV power, $P_{PV}$, and the contractual power, $P_C$, considering the 851 domestic PV prosumers connected in the ASM grid during 2016. The figure shows that the majority of domestic PV prosumers installed a PV plant comparable, even if lower, to the contractual power: the most probable value of $P_{PV}/P_C$ ratio is about 0.85, corresponding to 230 users.

*Table 5 Aggregate collected data in year 2015*

| | **PV producers + PV prosumers** | **Domestic PV prosumers** | **Domestic PV prosumers (%)** |
|---|---|---|---|
| # | 1066 | 774 | 72.61 |
| PV power (MWp) | 29.70 | 3.20 | 10.77 |
| Load contractual power (MW) | 18.51 | 3.27 | 17.67 |
| Produced energy (GWh) | 29.22 | 3.58 | 12.25 |
| Injected energy (GWh) | 25.74 | 2.56 | 9.95 |
| Absorbed energy (GWh) | 17.8 | 2.12 | 11.91 |
| Self-consumed energy (GWh) | 3.48 | 1.02 | 29.31 |

*Table 6 Aggregate collected data in year 2016*

| | **PV producers + PV prosumers** | **Domestic PV prosumers** | **Domestic PV prosumers (%)** |
|---|---|---|---|
| # | 1153 | 851 | 73.81 |
| PV power (MWp) | 30.75 | 3.47 | 11.28 |
| Load contractual power (MW) | 19.18 | 3.67 | 23.11 |
| Produced energy (GWh) | 32.88 | 3.63 | 11.04 |
| Injected energy (GWh) | 26.34 | 2.61 | 9.91 |
| Absorbed energy (GWh) | 19.52 | 2.40 | 12.30 |
| Self-consumed energy (GWh) | 6.54 | 1.02 | 15.60 |

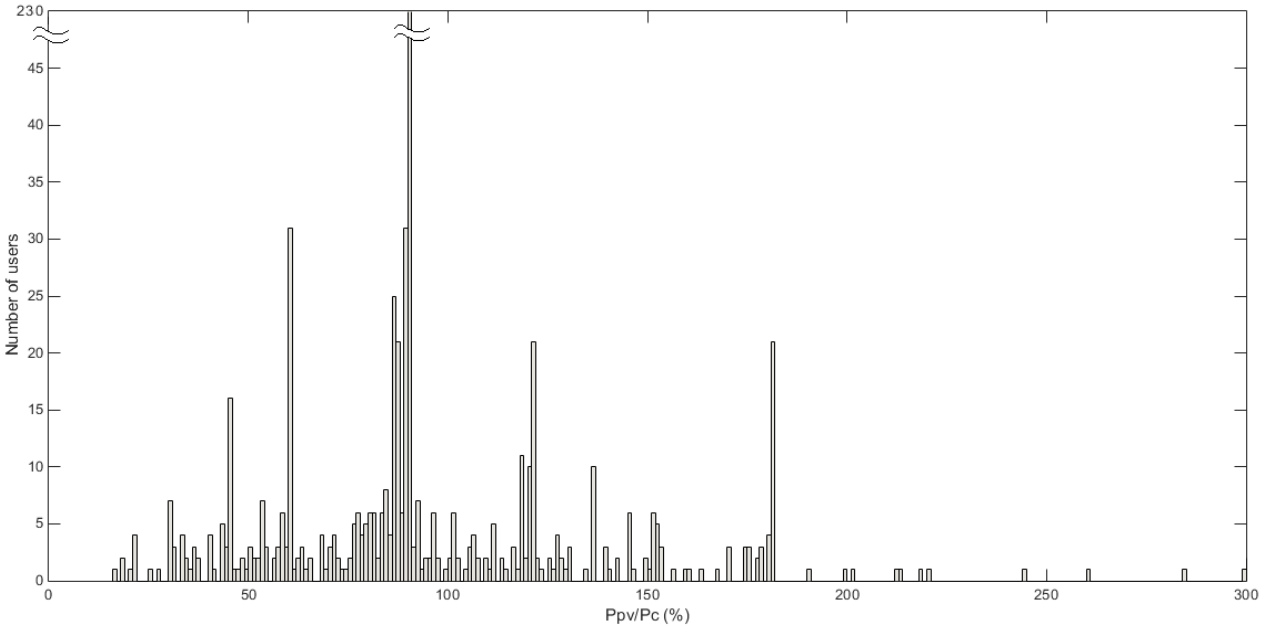


*Figure 27 Statistical distribution of PPV/PC ratio during year 2016.*

### 3.2.1.1 *Basic Definitions and Metrics*

For each i-th domestic PV prosumer, the equivalent operating hours, $H_{e,i}$, are evaluated by the following expression (1):

$$H_{e,i} = \frac{E_{g,i}}{P_{PVp,i}} \cdot \frac{12}{n_{m,i}} \tag{1}$$

where $E_{g,i}$ is the overall energy generated by the i-th PV during the year and $P_{PVp,i}$ is the peak power of the i-th PV. Equation (1) takes into account also PV plants which did not produce energy for all the 12 months of the year since they were not yet in operation ($n_{m,i}$ is the number of months in the year that $PV_i$ was in operation). The average $H_e$ for the aggregate $n$ prosumers is

$$H_e = \frac{1}{n} \sum_{i=1}^{n} H_{e,i} \tag{2}$$

For the i-th domestic PV prosumer, self-consumption rate $SCR_i$ is defined as the ratio between the PV energy directly utilized by the prosumer, $E_{u,i}$, and $E_{g,i}$. Finally, the average $SCR_{\%}$ for the aggregate $n$ prosumers is calculated as

$$SCR_{\%} = \left( \frac{1}{n} \sum_{i=1}^{n} SCR_i \right) \cdot 100 \quad (3)$$

For the i-th domestic PV prosumer, self-sufficiency rate $SSR_i$ is defined as the ratio between the PV energy directly utilized by the prosumer, $E_{u,i}$, and the total energy utilized by the prosumer, $E_{l,i}$, which is the sum of $E_{u,i}$ and the energy absorbed by the grid. Finally, the average $SSR_{\%}$ for the aggregate $n$ prosumers is calculated as

$$SSR_{\%} = \left( \frac{1}{n} \sum_{i=1}^{n} SSR_i \right) \cdot 100 \quad (4)$$

In the statistical analysis, three different databases are used, as listed in the following.

1. At first, all domestic PV prosumers connected to ASM network are considered (Case 1).
2. A filter is applied to PV prosumers of point 1, not considering prosumers with SCRi,% < 5% and/or He,i < 100 (Case 2). This filter is applied in order to exclude PV prosumers with very low load connected (in such case, the prosumer may be considered as a producer) or with PV disconnected for a very long time (due, for instance, to a protracted fault). In Case 2, 6% of Case 1 prosumers are excluded.
3. A further filter is then applied to prosumers of point 2, not considering prosumers with ratio between PPVp and load contractual power not in the range 0.85-1.15 (Case 3). With this filter, all prosumers with oversized/undersized PV with respect to the contractual power are thus excluded (in Case 3, 54% of Case 1 prosumers are excluded).

#### 3.2.1.2 *Results*

*Figure 28* and *Figure 29* show the statistical distribution of equivalent operating hours per domestic PV prosumer, $H_{e,i}$, in 2015 and 2016, respectively. Database 2 described in Section III.D has been used. A quite similar trend can be inferred in both cases: statistical distributions approximate quite well a normal distribution, with mode equal to 1200 h in 2015 and 1150 h in 2016.

*Figure 30* and *Figure 31* show the statistical distribution of self-consumption rate per domestic PV prosumer, $SCR_i$, in 2015 and 2016, respectively. Also in this case, database 2 described in Section III.D has been used.

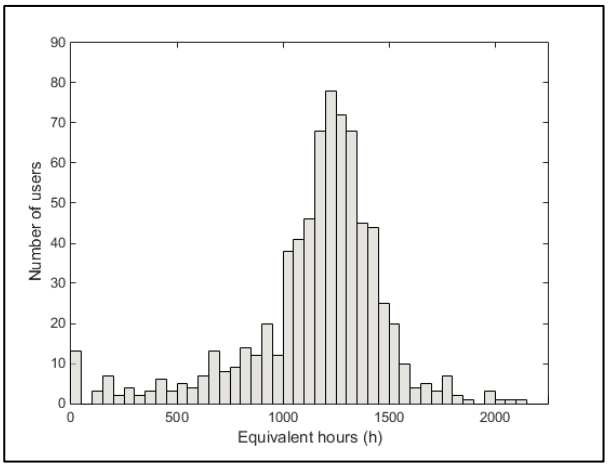


*Figure 28 Statistical distribution of equivalent hours per domestic PV prosumer (2015).*

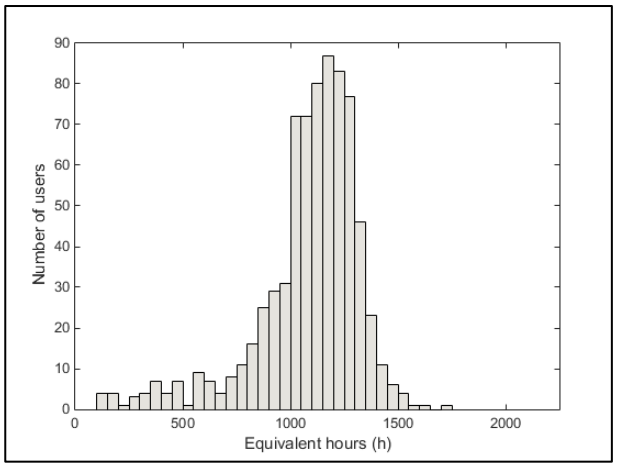


*Figure 29 Statistical distribution of equivalent hours per domestic PV prosumer (2016).*

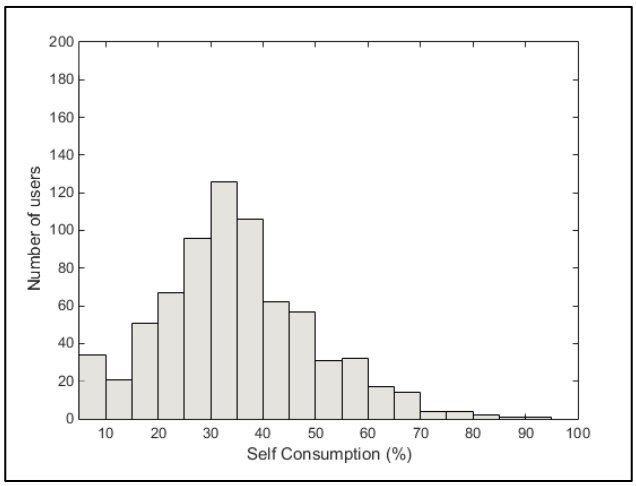


*Figure 30 Statistical distribution of self-consumption rate per domestic PV prosumer (2015).*

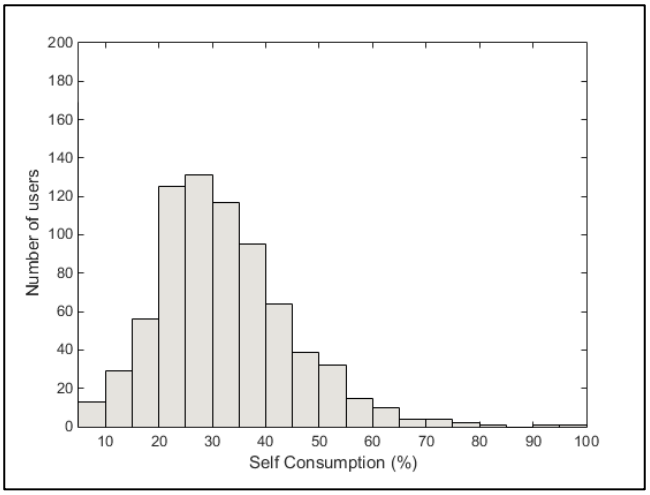


*Figure 31 Statistical distribution of self-consumption rate per domestic PV prosumer (2016).*

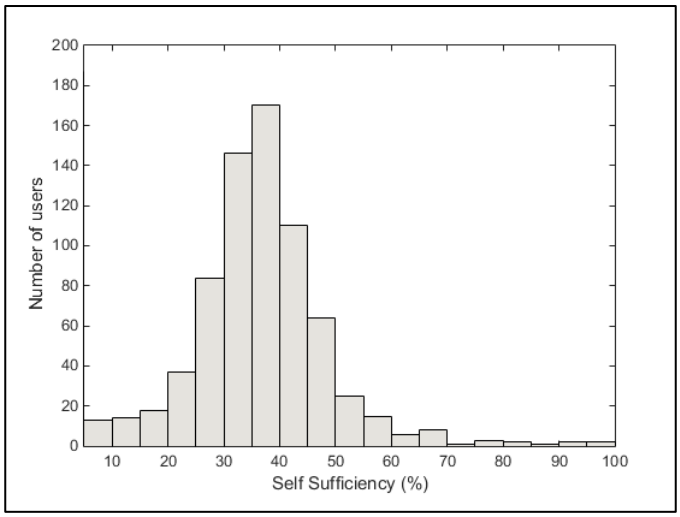


*Figure 32 Statistical distribution of self-sufficiency rate per domestic PV prosumer (2015).*

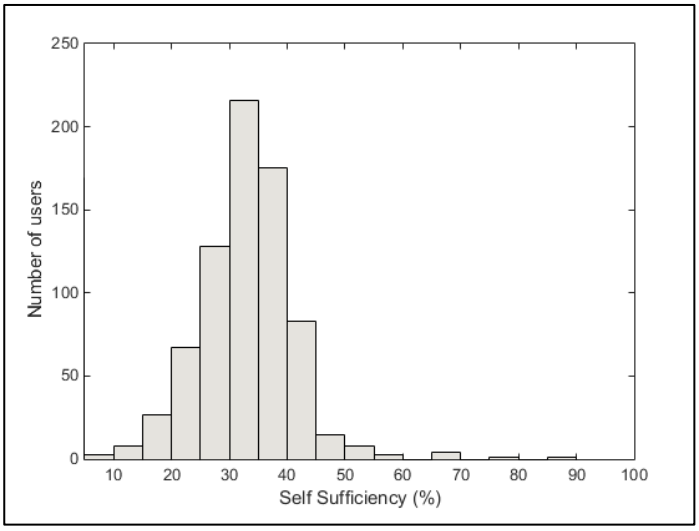


*Figure 33 Statistical distribution of self-sufficiency rate per domestic PV prosumer (2016).*

Results evidence a similar trend for the statistical distribution of self-consumption rates in 2015 and 2016, even if a small decrease in the most probable value, namely from about 30 % in 2015 to about 28 % in 2016, is observed.

*Figure 32* and *Figure 33* show the statistical distribution of self-sufficiency rate per domestic PV prosumer, $SSR_i$, in 2015 and 2016, respectively. Also in this case, as for previous cases, database 2 described in Section III.D has been used, i.e. by applying the first filter to the available measurements. The statistical distributions of self-sufficiency calculated show quite similar data in both 2015 and 2016. As observed for statistical distributions of equivalent hours and self-consumption rate per prosumer, also self-sufficiency rates have decreased in 2016 with respect to 2015, with the mode value dropped from about 38 % to about 35 %, respectively.

*Table 7* reports average values obtained for $H_e$, $SCR_{\%}$ and $SSR_{\%}$ in years 2015 and 2016 by applying the equations for all the three cases discussed in Section III.D. Both for Case 1 and Case 2 and Case 3, all considered indexes have decreased in 2016 with respect to year 2015, according to the same trend evidenced in the previous subsections. Remarkably, average $H_e$ and $SCR_{\%}$ results obtained for year 2016 in the ASM LV network perfectly match the corresponding results reported in [71] regarding Umbria region, thus validating the statistical analyses presented in the work. Several motivations could be proposed to explain such decreasing trend, for instance an average

ageing of PV plants during the years causing a deterioration of the PV performances with respect to the rated values. However, such behavior have to be more deeply investigated by considering aggregate data of years before 2015 and of year 2017 in order to advance any explanation.

Another important point directly related to the meaning of self-consumption and self-sufficiency may be inferred from *Figure 34*, which reports the statistical distribution of the ratio between energy load consumption and energy PV generation for the considered domestic PV prosumers during 2016. Generally speaking, the self-sufficiency index may be related to the user's benefit: the more $SSR_{\%}$ is high, the more the money saving in the electric bill is high. On the other hand, the self-consumption index may be related to the DSO's benefit, since the more $SCR_{\%}$ is high, the more the distribution grid is not affected by uncontrolled power injections. The maximization of both $SSR_{\%}$ and $SCR_{\%}$ is not a simple task. Load consumptions may be asynchronous with respect to PV generation: in this case both $SSR_{\%}$ and $SCR_{\%}$ decrease and a suitable load shifting is required (for instance, by means of energy storage systems or DSM strategies). PV plant may be undersized with respect to load consumption and its production cannot completely cover load consumptions: in this case, a high $SCR_{\%}$ may be achieved, but $SSR_{\%}$ cannot be maximized beyond a certain limit even if storage systems or DSM strategies are employed. Conversely, PV plant may be oversized so that load consumption cannot match the whole PV generation: in this case, a high $SSR_{\%}$ may be achieved, but $SCR_{\%}$ cannot be maximized beyond a certain limit, unless oversized and economically disadvantageous storage systems are employed. In order to maximize both $SCR_{\%}$ and $SSR_{\%}$, the main requirement is that the ratio between energy load consumption and energy PV generation for each domestic PV prosumer is as far as possible close to 1: the distribution reported in *Figure 34* shows that for the majority of prosumers such ratio ranges from 0.7 to 1.2, so that the installation of a PV system integrated with a properly sized storage system would give the possibility to the majority of domestic users to be full energy independent from the grid.

However, it is important to underline that there is also a seasonal mismatch between consumption and production, as evidenced in *Figure 35*. The figure shows that self-consumption increases in the winter months (October to February) while self-sufficiency decreases. In winter, production is small, so the denominator in the formulas of self-consumption is reduced, whereas total load consumption increases and therefore self-sufficiency decreases. It should be noted that the maximization of self-sufficiency is more easily reachable in summer months, while maximization of self-consumption is more easily reachable in winter months. In conclusion, even if the user is equipped with a properly sized storage system, summer PV production would in many cases overcome the user's energy demand, whereas winter PV production could be insufficient to completely cover load consumption. In such cases, during summer/winter there would still be injection/absorption of active power to/from the grid, normally undesirable.

*Table 7 $H_e$, $SCR_{\%}$ and $SSR_{\%}$ Values in Years 2015 and 2016*

| | **Case 1** | | **Case 2** | | **Case 3** | |
|---|---|---|---|---|---|---|
| | **2015** | **2016** | **2015** | **2016** | **2015** | **2016** |
| **He (h)** | 1171 | 1013 | 1205 | 1085 | 1233 | 1104 |
| **SCR%** | 33.32 | 29.88 | 34.88 | 32.44 | 32.44 | 31.52 |
| **SSR%** | 35.23 | 29.73 | 36.55 | 33.13 | 37.20 | 33.44 |

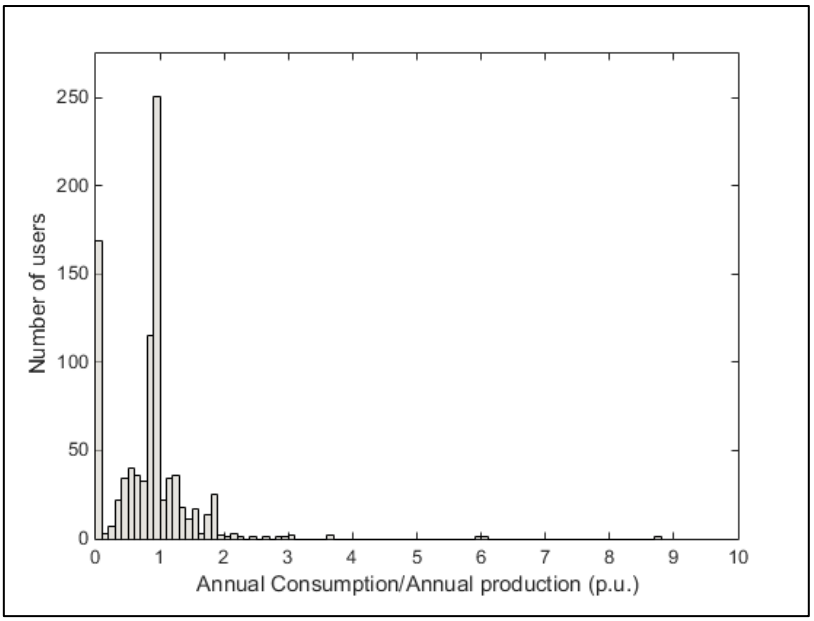


*Figure 34 Statistical distribution of annual consumption/annual production ratio during year 2016.*

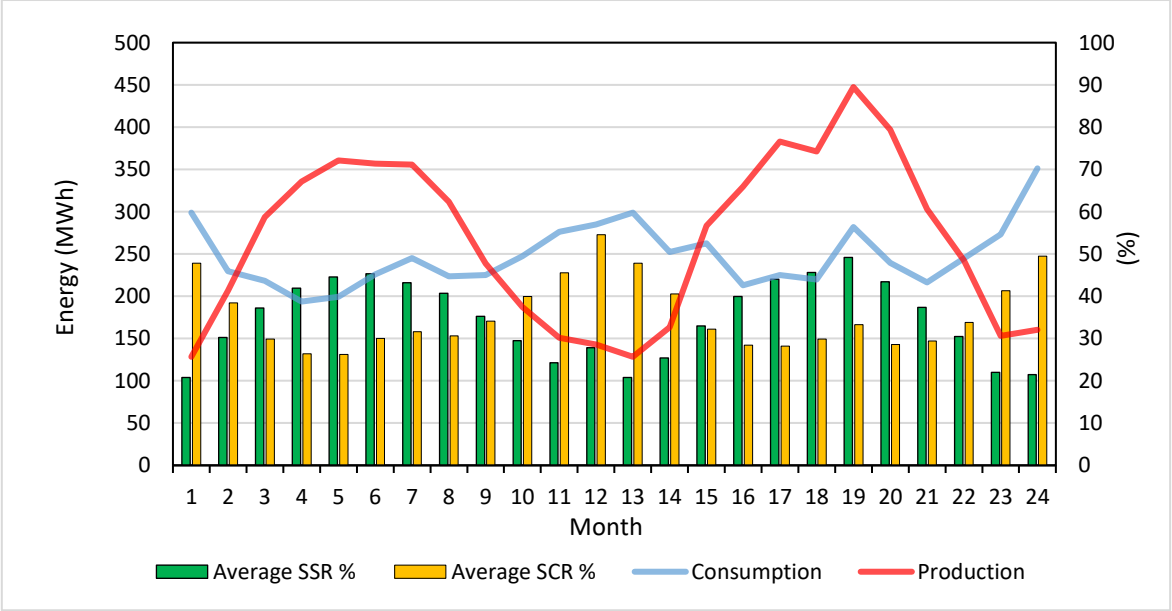


*Figure 35 Monthly average self-consumption and average self-sufficiency for domestic PV prosumers during years 2015-2016.*

## 3.3 ASM headquarters: a living lab of smart grid technologies

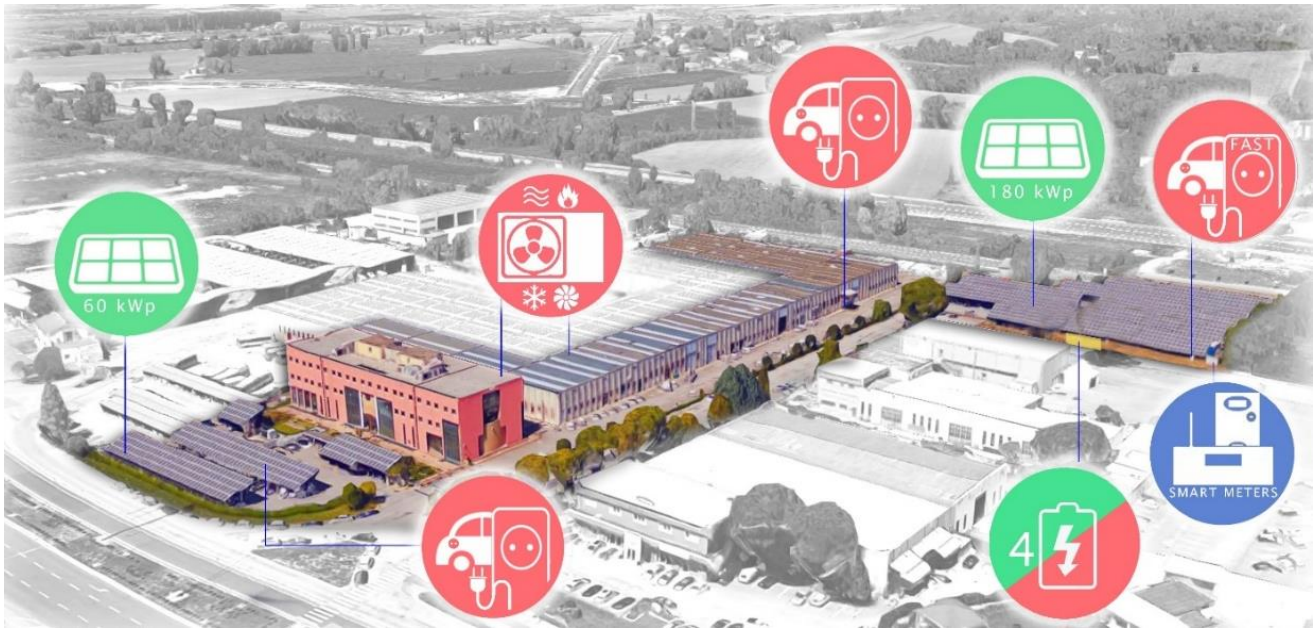


*Figure 36. ASM headquarters*

According to the general overview given in *Figure 36*, ASM district can be considered as a living lab because of the presence of advanced technologies already tested and in operation for the purpose of validating the main pillars of a smart grid (e.g. AMI, DR, Storage, EV integration, V2G). In particular, the district consists of the following block of energy units:

- Two PV arrays (180 kWp and 60 kWp), connected to the LV network;
- 72 kWh 2nd life Li-ion battery energy storage is the Block of Energy Unit (BoEU) providing the electric power storage and supply services. It is the BoEU that plays an important role in providing the district with the flexibility necessary to implement different services, especially ancillary services like Primary reserve, Dynamic reactive Power control and Reactive Power Compensation;
- ASM Terni buildings comprising a 4,050 $m^2$ three-storey office building, a 2,790 $m^2$ single-storey building consisting of technical offices, a computer centre and an operation control centre and a 1,350 $m^2$ warehouse; usually the base load varies between 50 kW and 90 kW and peak load is between 120 kW and 170 kW, depending on seasonal factors. A daily load profile is shown in Figure 37 as an example;
- Three smart charging stations (two SpotLink EVO and one Efacec QC45) and six electric vehicles (four Renault ZOE and two Nissan LEAF) will be part of the Terni pilot site. The 22 kWh/40 kWh lithium-ion batteries of Renault Zoe are charged at 22 kW SpotLink EVO charging station while a Efacec QC45 charging station, supplying up to 50 kW DC, is used to charge the 22 kWh lithium-ion batteries of Nissan LEAF.

This energy infrastructure is enhanced by an innovative metering system, made up of new generation smart meters (NORM [22]) able to collect real time data from the most crucial points of the district and transmit the data through the mobile network (GSM).

*Figure 38* shows the single line diagram of the ASM's living lab notably, the NORM devices are marked with green square.

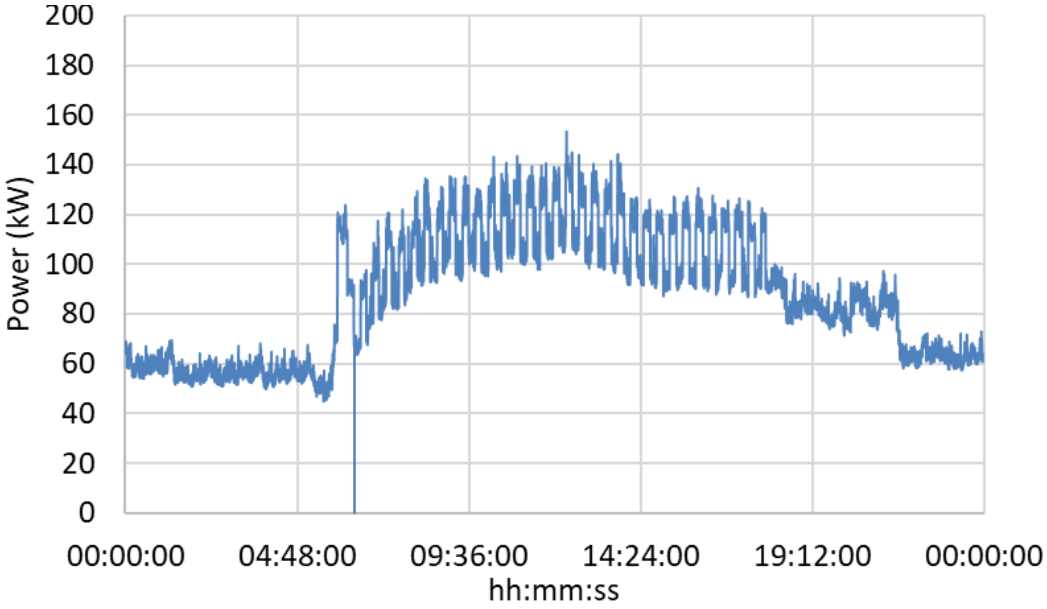


*Figure 37. Daily load profile of ASM buildings*

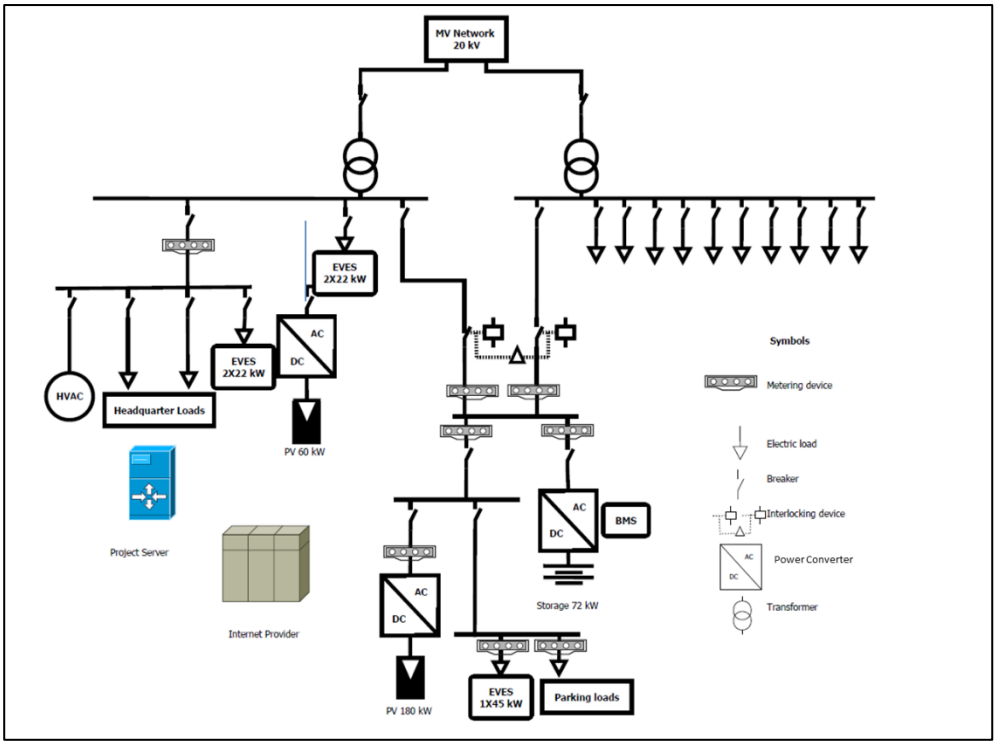


*Figure 38. Terni pilot site configuration*

During this work lifespan, many activities have been carried out thanks to the European research and innovation projects funded under the Horizon 2020 framework programme:

- Nobel GRID [72] and WiseGRID [73], demonstration of the active role of the Distribution System Operator in the management and supervision of network resources: Smart Metering (200 IoT meters for real-time monitoring of consumption) and Demand

Response (Campaigns for active participation in electricity consumption), definition of business models for new players in the smart grid;

- SUCCESS [22], development of an overarching approach to threat and countermeasure analysis with special focus on the vulnerabilities introduced by Smart Meters in the energy domain;
- DEFENDER [74], Validation of solutions and technologies for the defence of energy infrastructures, with reference to the distribution network, demonstration of the block-chain for crowdsensing and use of Phasor Measurement Units (PMU) with low cost fault localization;
- NRG-5 [75], integration between the 5G infrastructure and the smart grid in a real environment, as part of the 5G-PPP partnership;
- ELSA [76], installation of batteries that have exhausted their life cycle for electric mobility in order to increase the efficiency of energy distribution;
- inteGRIDy [77], management and integration of a micro-network to increase the quality of service;
- eDREAM [78], aims to the transfiguration of traditional market approaches and smart grid operations into novel decentralized and community-driven energy systems fully exploring local capacities, constraints, and Virtual Power Plants-oriented optimization in terms of local and secure grid nodes stabilization;
- SOFIE [79], aiming to enable creation of business platforms, based on existing IoT platforms and distributed ledgers, without needing to negotiate with any gatekeeper (neither technology- nor business wise).

# 4 Network Planning for continuity of supply

The electricity distribution network is the infrastructure that is the pillar of the services provided to citizens, and it is also the backbone of future smart cities. Therefore, increasing attention has to be paid to the electric power quality in terms of continuity of service.

In this context, the Italian Authority (ARERA, Italian Regulatory Authority for Energy, Networks and Environment [80], has established in [81] very ambitious benchmark values for the Key Performance Indicators (KPI), normally used to evaluate the quality of electric service [82] (i.e., the System Average Interruption Duration Index, SAIDI, and the System Average Interruption Frequency Index, SAIFI). In particular, for the LV users of the Distribution System Operator (DSO) of Terni (i.e., Terni Distribuzione Elettrica, TDE, which is a productivity unit of ASM Terni S.p.A.), the set targets are: for SAIDI 28 *minutes/user/year* in high density area and 68 *minutes/user/year* in rural area, respectively (computed with respect to long interruptions, i.e., longer than 180 s), while for SAIFI 2.62 *number of outages/user/year* in high density area and 6.01 *number of outages/user/year* in rural area, respectively (computed with respect both to long and short, i.e. longer than 1 s, interruptions). In 2017, the DSO has reached the following values: for SAIDI 28.963 *minutes/user/year* in high density area and 60.844 *minutes/user/year* in rural area, respectively; for SAIFI 1.477 *number of outages/user/year* in high density area and 3.976 *number of outages/user/year* in rural area, respectively. Although the performance indices set by the authority and achieved by the DSOs are very challenging (i.e., the quality of the electric service is already very good), the feeling that the users have about an electric outage is amplified by the loss of some essential services offered to citizens (e.g., heating, water, mobility, telecommunications, etc.), due to their dependence on the continuity of electricity supply, especially when emergency situations occur.

Therefore, the DSOs have crucial role for the improvement of the network; notably the development plans of the DSO has to be properly assessed for reducing interruptions; a first levers has been identified in the assessment of component reliability focusing on the most critical according to the present state of the art; on the other hand, a second lever is the a resilience assessment against extreme natural events [83], in order to reduce the global impact of electric service failures during these threats.

With respect to component assessment, in the last years, an increasing attention has been paid to faults occurring on cable lines. In 2015, particularly during the month of July, DSOs in Italy recorded an abnormal increase of MV cable failures (from two to three times if compared to previous years). Moreover, in case of cable lines, joint is the component more affected by faults.

Recently, Italian DSOs are reporting some experiences about faults on joints: in [84], UNARETI (DSO operating in Milan and Brescia, in the North of Italy) is working on a wide replacement of joints, substituting those already installed (with a 24 kV rated voltage) with new ones (with a 36 kV rated voltage). As an extreme consequence, authors in [85] propose to design the topology of MV networks in order to reduce the number of joints, since it is considered a weak component. Other works reported the dramatic increasing number of faults occurring on the joints, as in [86].

Chapter 4.1 presents a circuit model of MV joint carrying out a 3-D non-linear model and its experimental validation; the model has thus been applied for simulating one year of joint heating in real cable operations and laying conditions, [87] and [88]. The thermal effects related to the electric CR inside the joint due to the necessity to assure the screen continuity have been also assessed, evaluating the effects of ground faults on joint heating (i.e., those faults causing a current circulation

through the cable screens), taking into account the auto-reclosure schemes normally implemented by DSOs to provide continuity of supply, [89].

With respect to resilience assessment, in the last years, the main stakeholders of electric power systems are emphasizing issues about frequency and magnitude of extreme weather events which affect the distribution networks and customer supply. Whenever networks are designed and development plans are drawn, this new feature must be assessed and implemented.

In Chapter 4.2, a procedure to evaluate the resilience of a distribution network against flooding threats is presented. Starting from a detailed analysis about the resilience of each asset of the grid, the procedure implements the exploration of the network in order to evaluate the impact of interruptions (e.g., in terms of number of disconnected users) produced by the specific threat; then, it calculates the resilience indices of the whole system.

The procedure is applied with respect to different threats, on the distribution network of Terni. Referring to this case study, the proposed method suggests the countermeasures able to reduce the impact of flooding events and evaluates their benefits. Results point out that the remedial actions, identified by the procedure, are also able to improve the resilience of the network and, in addition, they are in agreement with the development plan already established by the DSO.

## 4.1 A 3-D nonlinear thermal circuit model of underground MV power cables and their joints

Due to their wide application, especially in urban areas, both at medium (MV) and low (LV) voltage level, underground power cables are an essential part of distribution networks. In the last two years, an abnormal increase of MV cable failures (two three times compared to previous years and practically all permanent failures) has occurred in Italy, especially during summer 2015 (the hottest year ever in Italy since 1880), dramatically worsening the continuity of service. Most of such failures occurred at cable joints, which are commonly considered the weakest parts of an underground cable. One of the probable cause that Distribution System Operators (DSOs) propose to explain joint failures is the overheating, which is also related to the ambient temperature. In order to study and verify such hypothesis, a thermal model able to represent the cable, the joint, the cable laying condition, as well as the heat exchange between the soil and the air is required.

Many models have been proposed in literature in order to calculate the temperature field of buried cables. Analytical methods in conjunction with empirical approximated formulas [90], [91], [92] and [93] were firstly proposed. Based on the electrical-thermal analogy, some authors proposed to represent the cable system by means of equivalent electric circuits [94] and [95]. In recent years, many numerical models solving the thermal problem by means of boundary element method [96], finite element method [97] and [98] and finite difference method [99] and [100] have been developed. Such models, however, mostly focus on the ampacity evaluation and do not consider the cable joint; moreover, the heat exchange between the soil surface and air is often oversimplified.

This work presents a circuit model, that is based on the electrical-thermal analogy and it is able to simulate the thermal behavior of an underground cable; a detailed representation of cable joints is also provided. The model takes into account different cable laying conditions and, notably, the thermal exchange between the upper surface and the surrounding environmental. The latter is due to the solar radiation absorbed by the soil surface, to the convective heat exchanged between soil

and air, to the heat flux due to the radiation emitted by the soil and, finally, to the heat flux due to the evaporation of the water in the soil. The proposed model refines the model previously presented by the authors and described in [101], and extends it by adding a full 3-D representation of the ground and thermal exchanges between ground surface and external environment. The developed model is able to simulate the thermal behavior of cables and joints buried in the ground for various operating conditions (laying, ambient temperature, solar radiance, relative humidity and sky temperature).

### 4.1.1 *Cold-shrinkable joint under test*

The schematic representation of the joint is provided in *Figure 39*. Two main parts may be identified: a central body, with an aluminum joint connecting two cable stretches and covered by a two-layer plate and high permittivity mastic layer (MNAC); a cold-shrinkable body, composed by a triple layer extruded Ethylene-Propylene Diene Monomer (EPDM) body, a copper stocking for cable screen continuity and an overall protective EPDM cover.

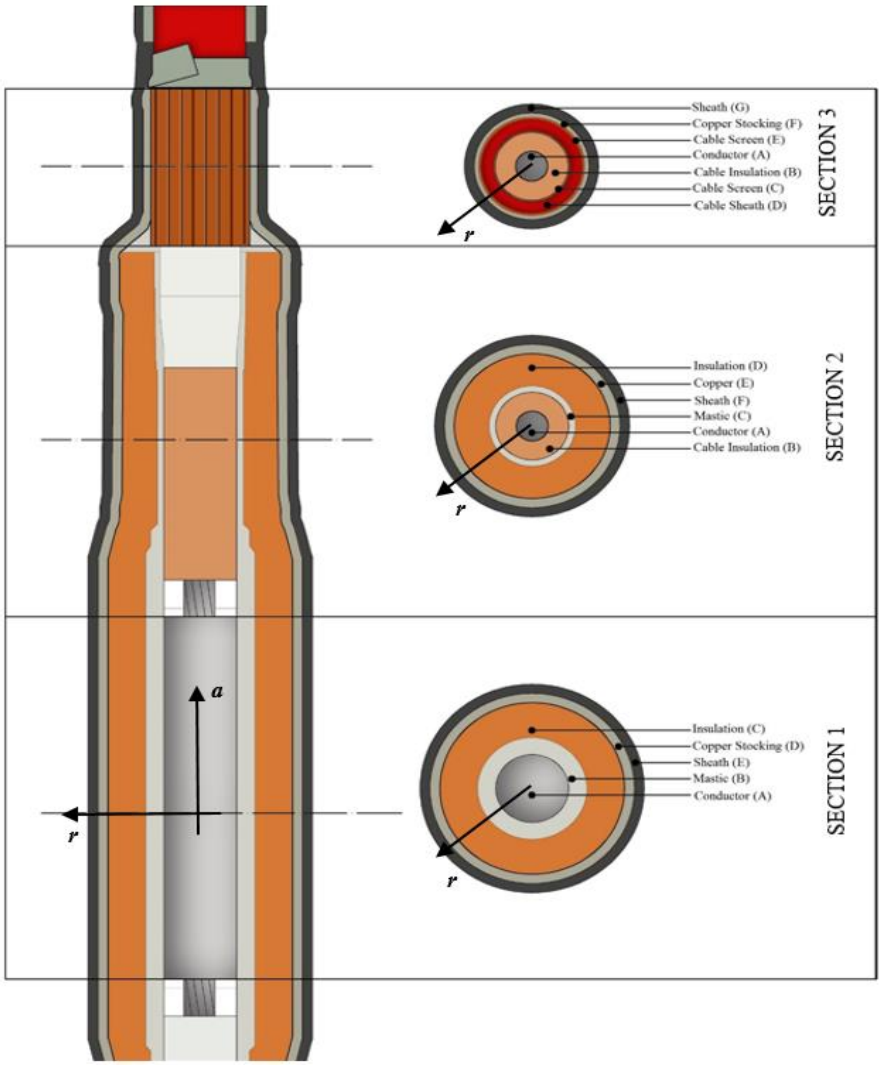


*Figure 39 The simulated cold-shrinkable joint (the cylindrical coordinate system used in the model is also shown).*

Five different sections have been defined in order to geometrically characterize the joint: a central one (Section 1 in *Figure 39*), two sections on the left (Sections 2 and 3 in *Figure 39*) and the symmetrical ones on the right (not represented in *Figure 39*). Physical and geometrical parameters

of each section, namely the external radius $r_e$, the length $L$, the thermal conductivity $\lambda$ and the volumetric heat capacity $c$, are listed in the following tables.

*Table 8 Parameters used in the simulations (section 1 of the joint)*

| Layer | Material | $r_e$ (mm) | L (m) | λ ($K^{-1}\cdot m^{-1}\cdot W$) | c ($J\cdot K^{-1}\cdot m^{-3}$) |
|---|---|---|---|---|---|
| **Conductor joint** | Aluminium | 16 | 0.144 | 237.022 | 2421630 |
| **Mastic** | MNAC | 21 | 0.144 | 0.2 | 2000000 |
| **Insulation** | EPDM | 29.1 | 0.144 | 0.2 | 2000000 |
| **Joint stocking** | Copper | 29.7 | 0.144 | 390.01 | 3434200 |
| **Sheath** | EPDM | 33.1 | 0.144 | 0.2 | 2000000 |

*Table 9 Parameters used in the simulations (section 2 of the joint)*

| Layer | Material | $r_e$ (mm) | L (m) | λ ($K^{-1}\cdot m^{-1}\cdot W$) | c ($J\cdot K^{-1}\cdot m^{-3}$) |
|---|---|---|---|---|---|
| **Conductor joint** | Aluminium | 8.25 | 0.15 | 237.022 | 2421630 |
| **Cable insulation** | HEPR | 13.75 | 0.15 | 0.2 | 2000000 |
| **Mastic** | MNAC | 15.8 | 0.15 | 0.2 | 2000000 |
| **Insulation** | EPDM | 26.5 | 0.15 | 0.2 | 2000000 |
| **Joint stocking** | Copper | 27 | 0.15 | 390.01 | 3434200 |
| **Sheath** | EPDM | 30.1 | 0.15 | 0.2 | 2000000 |

*Table 10 Parameters used in the simulations (section 3 of the joint)*

| Layer | Material | $r_e$ (mm) | L (m) | λ ($K^{-1}\cdot m^{-1}\cdot W$) | c ($J\cdot K^{-1}\cdot m^{-3}$) |
|---|---|---|---|---|---|
| **Conductor joint** | Aluminium | 8.25 | 0.066 | 237.022 | 2421630 |
| **Cable insulation** | HEPR | 13.75 | 0.066 | 0.2 | 2000000 |
| **Cable screen** | Copper | 14.55 | 0.066 | 390.01 | 3434200 |
| **Cable sheath** | PVC | 17.75 | 0.066 | 0.167 | 2000000 |
| **Cable screen** | Copper | 18.3 | 0.066 | 390.01 | 3434200 |
| **Joint stocking** | Copper | 19.2 | 0.066 | 390.01 | 3434200 |
| **Sheath** | EPDM | 22.6 | 0.066 | 0.2 | 2000000 |

#### 4.1.1.1 *A 3D Model of a cold shrinkable joint*

The well-known Fourier equation describes heat transfer within cables and joints:

$$w = -\nabla \cdot (\lambda \nabla T) + c\frac{\partial T}{\partial t} \tag{5}$$

being $\lambda$ the thermal conductivity, $c$ the volumetric heat capacity and $w$ the heat source of the temperature field, which is strictly related to the Joule losses of the conductor. In the thermal problem, moreover, the Fourier equation is coupled to the following one:

$$\rho(T) = \rho_{20°C} \cdot [1 + \alpha(T - 20)] \tag{6}$$

which states the dependence of $w$ on the conductor temperature $T$ by means of the electrical resistivity ρ. The problem is formulated in polar coordinates, due to the cable geometry, and is both non-homogeneous (since materials and layers composing the joint are different from those composing the cable) and non-linear (the dependence on temperature of the materials composing each layer is different). By taking advantage of the electrical-thermal analogy, in which temperature, heat flow, thermal resistance and thermal capacitance are represented by voltage, current,

electrical resistance and electrical capacitance, respectively, an equivalent electric network is used to solve the thermal problem, as described in the next subsections.

The system formed by the cable, its joint and the pipe (*Figure 39*), at first may be subdivided in *m* cylindrical sections, being *m* the number of different materials which form the considered part along the radial direction (*r* in *Figure 39*). Each cylindrical section is in turn subdivided into *n* equal parts, being *n* the fixed step of the discretization along the axial direction (*a* in *Figure 39*). Referring to the *i-th* cylindrical elementary volume (*Figure 40*), resistive bipoles $R_{ri}$ and $R_{ai}$ take into account the thermal conduction along the radial and axial directions, respectively; the capacitance Ci simulates the thermal capacity of the volume and the value of its initial voltage v(0) which defines the initial thermal condition for that volume. Lastly, the voltage controlled current generator $G_i$ simulates the heat source due to Joule losses inside the volume. The current, i.e. the heat flow due to Joule losses, generated by $G_i$ depends on the voltage, i.e. the temperature, and the electrical resistance, which vary with the temperature, of the metallic layer simulated by the i-th cylindrical elementary volume. In case the i-th cylindrical elementary volume does not simulate a metallic layer through which a current flows during the operation of the cable, $G_i$ is not connected. Dielectric losses are disregarded in this work, since in MV EPR insulated cables their effect is negligible with respect to Joule losses, as reported in [26].

Rri is calculated as

$$R_{ri} = \frac{1}{2\pi\lambda_i L_i} \ln \frac{r_{e,i}}{r_{i,i}} \tag{7}$$

where $\lambda_i$ is the thermal conductivity, $L_i$ is the length of the *i-th* part discretized along the axial direction, $r_{e,i}$ is the external radius and $r_{i,i}$ is the internal radius of the *i-th* cylindrical volume. $R_{ri}$ of copper and alluminium conductors have been neglected.

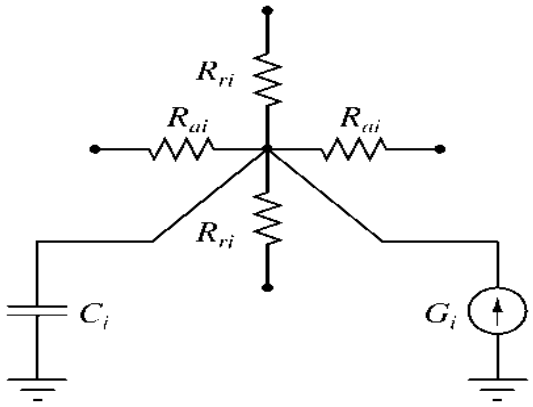


*Figure 40 Elementary cylindrical volume as simulated in the equivalent circuit model.*

$R_{ai}$ is evaluated with

$$R_{ai} = \frac{L_i}{\pi\lambda_i (r_{e,i}^2 - r_{i,i}^2)} \tag{8}$$

and $C_i$ with

$$C_i = \pi L_i c_i (r_{e,i}^2 - r_{i,i}^2) \tag{9}$$

being $c_i$ the volumetric heat capacity of the *i-th* volume. In the model, the electric contact resistance between cable screens and joint stocking (which should be simulated by another current generator) has been disregarded, i.e. the joint is considered as correctly installed. In case the cable

is not directly buried into the ground but it is laid in a pipe or a duct, a thermal resistance between cable and pipe must be considered. Referring to the *i-th* volume, such thermal resistance, named $R_{i,cp}$ which takes into account convective, radiating and conductive heat transfer, may be assessed by means of the empirical formula proposed in [102], [103] and [104]:

$$R_{i,cp} = \frac{U}{\left[1 + 0.1(V + Y\theta_{mi})D_{ei}\right] \cdot L_i} \tag{10}$$

where $U$, $V$ and $Y$ are constants whose values depend on the installation and are reported in [102], $\Theta_{mi}$ is the mean temperature of the air between the cable and the pipe (°C) and $D_{ei}$ is the equivalent external diameter (mm) of the volume. If more than one cable is simulated, an empirical coefficient multiplies $D_{ei}$ in order to take into account the mutual heating between cables into the pipe: according to [102], for three cables grouped in a pipe such empirical coefficient has been taken equal to 2.15.

If cable, joint and pipe are laid in open air, an equivalent thermal resistance, $R_{air}$, between the pipe and the air surrounding the pipe is connected to the ideal independent voltage generator $E_0$, used to set the ambient temperature. $R_{air}$ is evaluated by the formula [105]:

$$R_{air} = \frac{1}{hA} \tag{11}$$

being $h$ the convective heat transfer in air, taken as 4.5 $W \cdot K^{-1} \cdot m^{-2}$ (both radiative and conductive heat transfer are neglected), and $A$ the external surface of the pipe ($m^2$). Conversely, in case the system is buried into the ground, a soil thermal model is required, as described in the next subsection. Moreover, $R_{air}$ is replaced by a current generator simulating the convective thermal exchange between soil surface and the air surrounding the soil.

In real operating conditions, cables and joints are buried into the ground, so a soil thermal model has to be developed and coupled to the cable and joint model described in the previous subsection. As shown in *Figure 41*, the soil is simulated by a parallelepiped volume, whose dimensions along $x$, $y$ and $z$ axes are $L_x$, $L_y$ and $L_z$, respectively. Inside the parallelepiped, cable and joint, placed into the pipe, are buried at a certain depth.

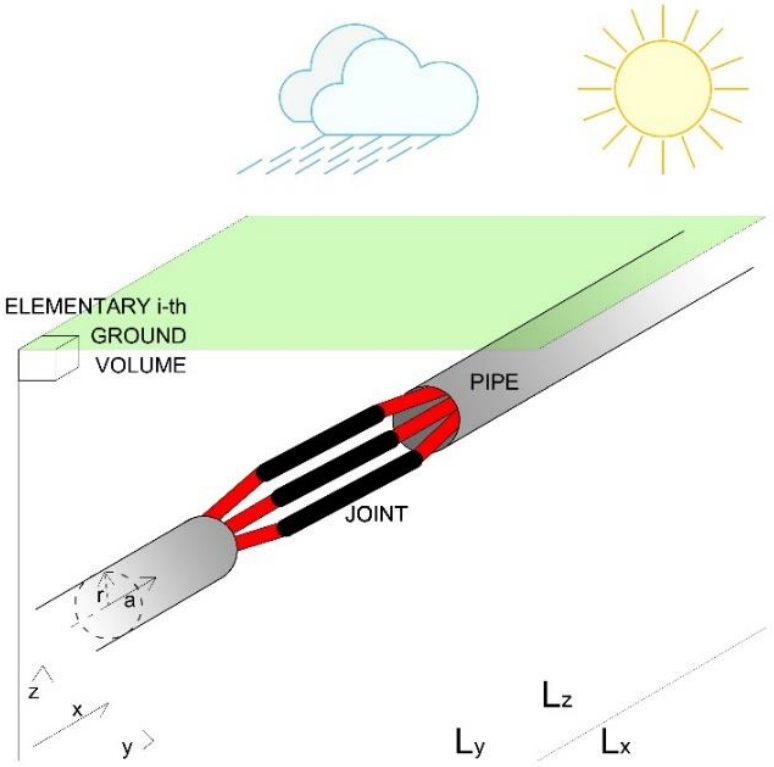


*Figure 41 Elementary cylindrical volume as simulated in the equivalent circuit model.*

The model is based on the following main basic assumptions:

- the geometric dimensions of the parallelepiped volume along the *x* and *y* axes ($L_x$ and $L_y$) are large enough to make the thermal flow through the orthogonal surfaces to these axes negligible; for this reason, the heat flow at both ends of the cable is also negligible;
- the lower surface of the parallelepiped, orthogonal to the *z* axis, has been considered isothermal and this temperature has been considered undisturbed;
- the upper surface of the parallelepiped, orthogonal to the *z* axis, has been considered exposed to weather changes;
- sky has been considered clear, in order to use Berdahl-Fromberg [106] equation to assess the sky temperature;
- soil properties are homogeneous (specific heat, thermal conductivity, granulometry);
- joint is considered directly buried in order to reproduce real operating conditions (joints are normally realized at the end of the pipe where the cable ends in the joint manhole);
- PVC pipe, in which cables are located, is represented as an isothermal surface [107];
- joint sheath surface is supposed isothermal.

The soil volume has been subdivided into smaller volumes (number of subdivisions along *x*, *y* and *z* axes are respectively $n_x$, $n_y$, $n_z$) and each one has been represented by seven lumped electrical elements (6 resistances and 1 capacitor connected to ground, *Figure 42*).

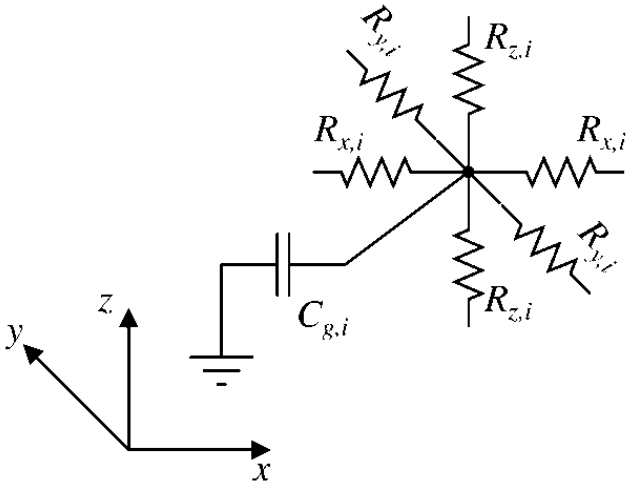


*Figure 42 Elementary i-th soil volume as simulated in the equivalent circuit model.*

Lumped parameters are calculated as:

$$R_{x,i} = \frac{L_x}{2n_x \lambda_g S_{x,i}} \tag{12}$$

$$R_{y,i} = \frac{L_y}{2n_y \lambda_g S_{y,i}} \tag{13}$$

$$R_{z,i} = \frac{L_z}{2n_z \lambda_g S_{z,i}} \tag{14}$$

$$C_{g,i} = c_{g,i} \frac{L_x}{n_x} \frac{L_y}{n_y} \frac{L_z}{n_z} \tag{15}$$

where $S_{x,i}$, $S_{y,i}$ and $S_{z,i}$ are the cross sections of the *i-th* element along the *x*, *y* and *z* axis, respectively, $\lambda_g$ is the soil thermal conductivity and $c_{g,i}$ is the volumetric heat capacity of the *i-th* soil volume.

The thermal conductivity of the soil (usually assumed as a constant by IEC and IEEE approaches), is mainly influenced by the water transport occurring when temperature increases due to the Joule's losses of the cable, thus reducing the liquid water content. Since the thermal conductivity of the vapour phase is up to 20-times lower than the one of liquid phase, the heat transfer deteriorates significantly. Kroener et al. [108] presented a complex and extensive method, which includes liquid-vapour transport in the soil; however, according to Ocłoń et al. [109], a simplified model has been used. The model takes into account the soil thermal conductivity variation with temperature according to the following expression:

$$\lambda_g(T) = \lambda_{g,dry} + (\lambda_{g,wet} - \lambda_{g,dry}) \cdot \exp\left[ - a_1 \left( \frac{T - T_{ref}}{a_2 \cdot T_{\max,p}} \right)^2 \right] \tag{16}$$

where, $\lambda_{g,dry}$ and $\lambda_{g,wet}$ are the soil thermal conductivities in dry and wet conditions, whereas $T_{ref}$ and $T_{\max,p}$ are the reference temperature ($T_{ref}$ = 20 °C) and the maximum allowable operating temperature, respectively. Coefficients $a_1$ and $a_2$ are defined as:

$$a_1 = \frac{T_{\max,p}}{T_{ref}} \tag{17}$$

$$a_2 = 1 - \frac{1}{a_1} \tag{18}$$

In the model, $\lambda_g$ is only dependent on temperature, this entailing that temperature increases give rise to a moisture migration, which consequently deteriorates the heat dissipation process. In the present work, $\lambda_{g,wet}$ and $\lambda_{g,dry}$ have been taken equal to 0.5 $W \cdot K^{-1} \cdot m^{-1}$ and 0.3 $W \cdot K^{-1} \cdot m^{-1}$, respectively. Alternatively, if a stratigraphic analysis were available (for instance, thermal backfill arranged around cable lines), Johansen's method could be implemented in order to determine $\lambda_{g,wet}$ and $\lambda_{g,dry}$ [110].

Along *z* axis, resistances $R_{z,i}$ of the elements belonging to the lower surface are connected to an ideal independent voltage generator representing the undisturbed ground temperature, $T_{und}$ = 293.15 K according to [33]. $T_{und}$ is the temperature of the ground layer (about 8 m deep) below which the temperature remains practically constant throughout the year. $T_{und}$ is calculated according to [111] as:

$$T_{und} = 17.898 + 0.951 \cdot T_{amb} \tag{19}$$

where $T_{amb}$ is the average yearly ambient temperature.

On the other hand, the upper surface is exposed to weather changing conditions: this is represented by means of ideal current generators injecting the heat flux $Q_{injected}$. For each iteration, $Q_{injected}$ is calculated according to the heat flow balance [112]:

$$Q_{injected} = Q_{solar} + Q_{conv} - Q_{sky} - Q_{evap} \tag{20}$$

being $Q_{solar}$ the short-wave global solar radiation absorbed by the soil surface, $Q_{conv}$ the sensible convective heat exchanged between air and the upper surface, $Q_{sky}$ the heat flux due to the long-wave radiation emitted by the soil surface to the sky and $Q_{evap}$ the evaporation heat exchange flux. Heat flow balance is represented in *Figure 43*.

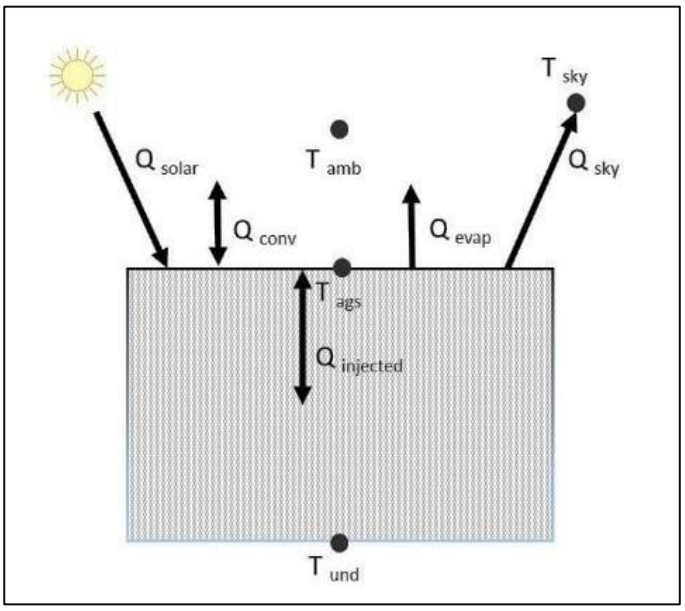


*Figure 43 Heat flow balance on the ground surface.*

$Q_{solar}$ is evaluated with the following expression:

$$Q_{solar} = \alpha_g G \tag{21}$$

where $G$ and $\alpha_g$ are the short-wave global solar radiation and the absorption heat coefficient, respectively. $G$ depends on three parameters (the peak solar irradiance, $S_{max}$, the sunrise time, $t_{rise}$, and the sunset time, $t_{set}$) and varies during the day as follows [113]:

$$G = \begin{cases} 0 & t \le t_{rise} \\ S_{\max} \sin\left( \dfrac{\pi(t - t_{rise})}{t_{set} - t_{rise}} \right) & t_{rise} < t < t_{set} \\ 0 & t \ge t_{set} \end{cases} \tag{22}$$

$S_{max}$ depends on the daily maximum extra-terrestrial irradiance, $I_{ETI,max}$, and the cloudiness, $M$, according to the expression [35]

$$S_{\max} = I_{ETI,\max} M \tag{23}$$

$M$ depends on weather conditions and has been computed according to previous quation in order to get $S_{max}$ equal to 1000 W/m$^2$, whereas $I_{ETI,max}$ may be evaluated by the general formulation of the extra-terrestrial radiance $I_{ETI}$:

$$I_{ETI} = I_0 E_0 \cos\theta_z \tag{24}$$

where $I_0$=1362 W·m$^{-2}$. $\vartheta_z$ is the zenith angle, calculated with

$$\theta_z = \cos^{-1}(\cos L \cos\delta \cos\omega + \sin L \sin\delta) \tag{25}$$

being $\delta$ the declination angle evaluated according to the Spencer's equation [114], $L$ is the Earth heliocentric latitude (rad) and $\omega$ is the hour angle (rad). $E_0$ is the eccentricity correction factor:

$$E_0 = 1 + 0.033\cos\left( \frac{2\pi d_n}{365} \right) \tag{26}$$

which depends on the *n-th* day of the year, $d_n$ (day number one is the 1$^{st}$ of January). $Q_{conv}$ depends both on soil surface temperature and air temperature above the soil surface $T_s$ and $T_{ags}$, respectively, and is assessed by the formula:

$$Q_{conv} = h_{conv} \cdot (T_{ags} - T_s) \tag{27}$$

where $h_{conv}$ is the convective heat transfer coefficient at the soil surface. $Q_{sky}$ is calculated by equation:

$$Q_{sky} = h_{rad} \cdot (T_s - T_{sky}) \tag{24}$$

where

$$h_{rad} = \varepsilon_s \sigma (T_s + T_{sky})(T_s^2 + T_{sky}^2) \tag{28}$$

and $\varepsilon_s$ and $\sigma$ are the emissivity of the soil surface and the Stefan – Boltzmann constant ($\sigma$ = 5.67·10$^{-8}$ W·m$^{-2}$·K$^{-4}$), respectively. The sky temperature $T_{sky}$ is evaluated with:

$$T_{sky} = (0.006 \cdot T_{dp} + 0.74)^{0.25} \cdot T_{ags} \quad (26)$$

where $T_{dp}$ is dew point temperature. In order to calculate $\varepsilon_s$, Berdahl and Fromberg [106] correlation has been used:

$$\varepsilon_s = 0.741 + 0.0062 \cdot T_{dp} \quad (29)$$

being $T_{dp}$ the surface dewpoint temperature (°C).

$Q_{evap}$ is influenced by $T_{ags}$, $T_s$, wind speed, ground cover, soil moisture content and humidity. In order to estimate it, the following equation has been used [115] and [116]:

$$Q_{evap} = b_3 \cdot f \cdot h_{conv} \cdot [(b_1 T_s + b_2) - r_h \cdot (b_1 T_{ags} + b_2)] \quad (30)$$

where $b_1$ = 103 Pa·K$^{-1}$, $b_2$ = 609 Pa and $b_3$ = 0.0168 K·Pa$^{-1}$; $r_h$ is the relative humidity of the air; $f$ is a fraction of evaporate rate, varying between 0 and 1, and depends mainly on the ground cover and moisture. For a bare soil, $f$ can be estimated as follows [34]: for saturated soil, $f$ = 1; for moist soil, $f$ = 0.6 – 0.8; for dry soil, $f$ = 0.4 – 0.5; for arid soil, $f$ = 0.1 – 0.2.

The equivalent electrical network resulting from the cable, joint, PVC pipe and soil modelling is described in transient state by a system of differential equations, due to capacitances $C_i$ and $C_{g,i}$. The system of differential equations is iteratively solved by means of the backward Euler algorithm. From the numerical integration point of view, each capacitance is replaced by a resistance, whose value depends on the integration time step, with a current source in parallel, whose value depends also on the voltage calculated in the previous time step, as described in [117]. In such a way, the equivalent electrical network becomes a purely resistive one and may be solved using the nodal analysis.

The size of the network depends on the chosen discretization. Referring to the analyses reported in the work, the complete circuit model is composed by about 3700 nodes and 11400 branches. A comprehensive and clear representation of the model is impossible to carry out, but an indicative section is shown in *Figure 44*.

A dedicated procedure has been developed by the authors in the Scilab environment. Inputs of the procedure are the geometrical and physical parameters of the whole system (cable, joint, pipe and soil), which define the discretization and the electrical parameters of the equivalent network. Also the highest temperature and the temperature at sunrise time of each day ($T_x$ and $T_n$, respectively), as well as sunrise and sunset times, must be provided as input data in order to simulate the behaviour of the system during a long time span, for instance one year, determining the degree-day values from daily temperature data [40]. The model subdivides the day into three segments: from the sunrise hour, $H_n$, to the time of maximum temperature, $H_x$, from $H_x$ to the sunset hour, $H_o$, and from $H_o$ to the sunrise hour of the next day, $H_p$. The model uses two sine-wave functions in the daylight and a square-root decrease in temperature at night. $H_n$ and $H_o$ are determined as a function of the site latitude and the day of the year. $H_p$ is calculated as $H_p = H_n + 24$. The time of the maximum temperature is set 4 h before sunset ($H_x = H_o - 4$).

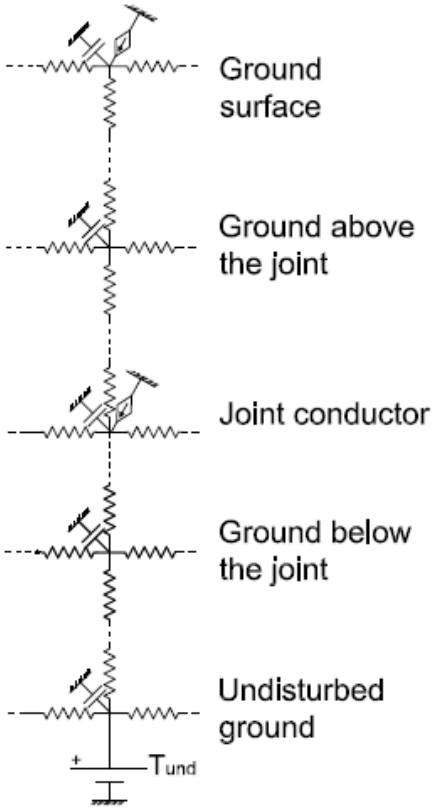


*Figure 44 Elementary portion (including ground and joint) of the equivalent electrical network.*

The temperature at the sunset hour, $T_0$, is estimated by means of $T_x$ and $T_p$ (which is the temperature at $t = H_p$) with the following empirical formula:

$$T_0 = T_x - 0.39 \cdot (T_x - T_p) \tag{31}$$

as suggested by [118]. The ambient temperature trend along the whole day is thus assessed according to the formulation:

$$T(t) = \begin{cases} T_n + (T_x - T_n)\left(\dfrac{t - H_n}{H_x - H_n}\right)\dfrac{\pi}{2} & H_n < t \le H_x \\ T_0 + (T_x - T_0)\sin\left[\dfrac{\pi}{2} + \left(\dfrac{t - H_x}{4}\right)\dfrac{\pi}{2}\right] & H_x < t \le H_0 \\ T_0 + \dfrac{(T_x - T_n)\cdot\sqrt{t - H_0}}{\sqrt{H_p - H_0}} & H_0 < t \le H_p \end{cases} \tag{32}$$

where $t$ is the standard time. The simulated trend of the temperature during one random day of the year, according to previous equation, is shown in the figure below.

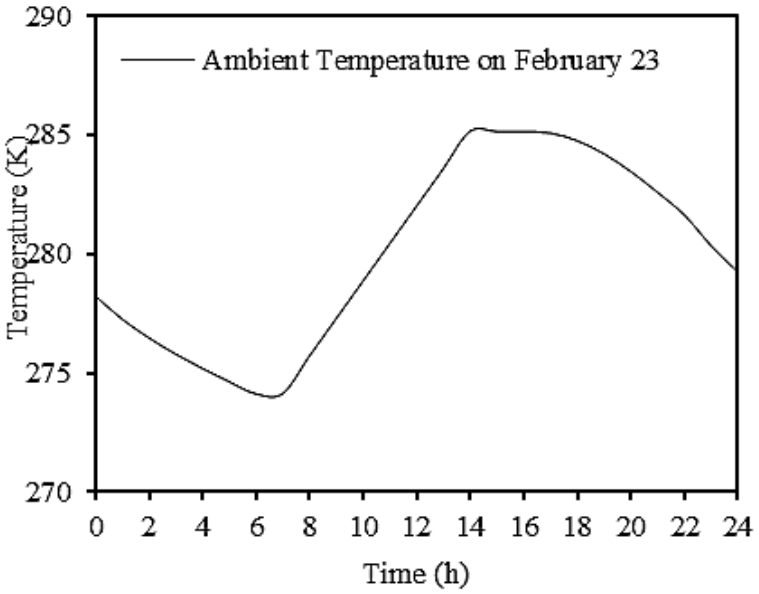


*Figure 45 Ambient temperature trend on 2015 February 23 (Hn = 6:54 a.m.; Tn = 274.15 K; H0 = 5:51 p.m.; Hx = 285.15 K).*

### 4.1.2 *Model validation by means of test in a laboratory*

The joint has been used to connect two single-core cables (ARG7H1R type, insulated with HEPR rubber of G7 quality under PVC sheath, $U_0/U$ 12/20 kV, $L$ = 2.5 m, conductor section $S_{Al}$ = 185 mm$^2$, copper screen section $S_{Cu}$ = 16 mm$^2$) and it has been placed within a PVC pipe ($L$ = 4 m, $S$ = 59040 mm$^2$) laid in open air (*Figure 46*).

*Figure 46 Laboratory test set up*

The temperature has been traced by 11 thermocouples (Type K - L = 2 m - Range -50/750 °C - Class1 - Tolerance=±1,5 °C, Figure 47 a), connected to a portable data logger (Datum-Y 100 Yokogawa - 16 channels, time sampling ranging from 100 ms to 5 h, SD storage up to 2 GB -, Figure

47 b); 7 of them have been placed within the joint (numbered 1, 2, 3, 5, 6, 9 and 10, Figure 48), 2 have been used to measure the external temperatures of the joint and of the cable sheath, respectively (numbered 4, and 7, Figure 48), while the 11th thermocouple measures the ambient temperature. The measure of temperature of PVC pipe (thermocouple numbered 8, *Figure 48)* has been used as a boundary condition into the model. In the real operating conditions, cable and joint are directly buried: experimental test results are thus conservative (i.e., cable and joint reach higher temperatures), since the heat transfer is lower.

a) b)

*Figure 47 Thermocouple and datalogger*

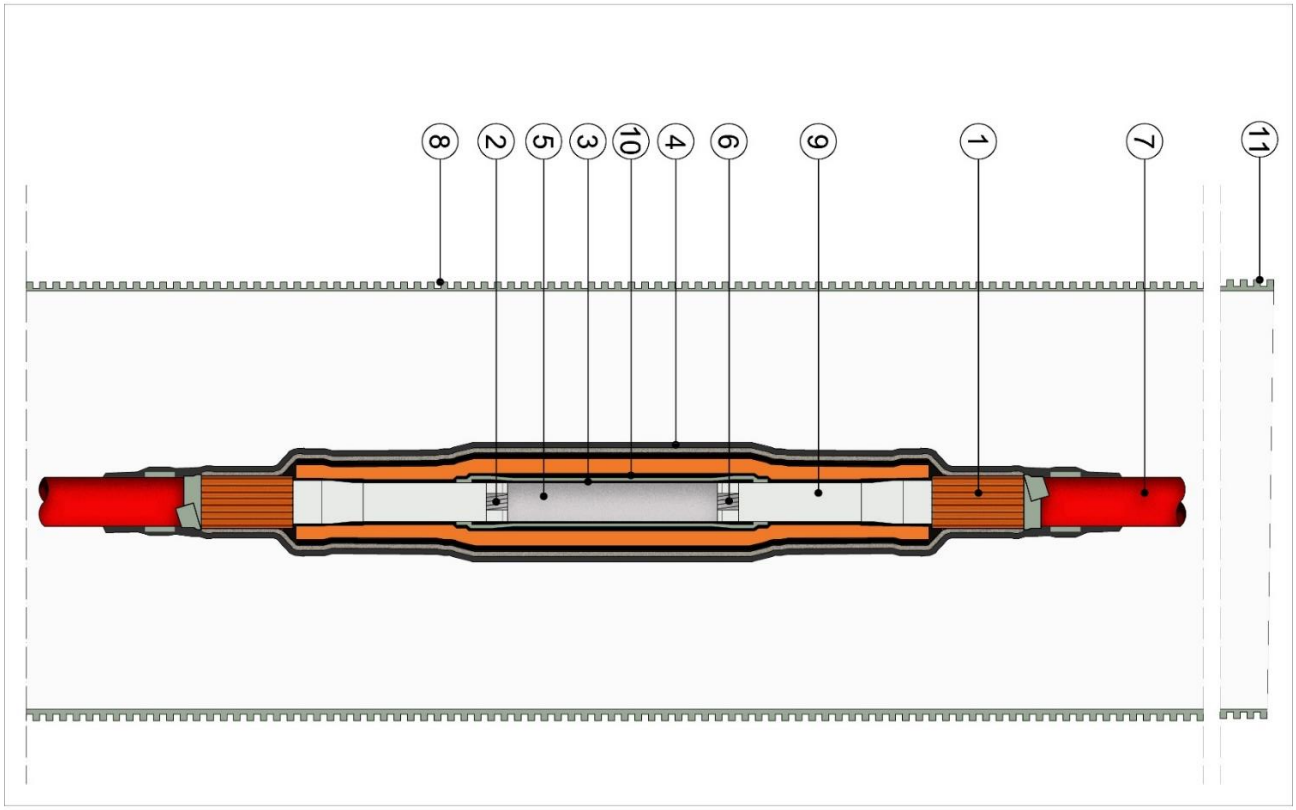


*Figure 48 Position of the thermocouples*

The cable is supplied by a 400 V LV switchgear, where a three-phase variac in series to a three-phase step-down transformer (400 kVA, K = 25, $I_n$ = 577 A) are connected: by varying the variac

output voltage, a current ranging from 0 and the rated 600 A value was supplied by the secondary of the step-down transformer at a very low voltage level (about 16 V).

Two different test arrangements have been set up. In the first one, (*Figure 49*), the cable is supplied by connecting the conductor terminals to two of the three phases of the step-down transformer in order to simulate operational currents (imposing different values of the current flowing through the cable up to the rated value). In the second one (*Figure 50*), instead, one of the cable terminals is short circuited by connecting the conductor to the screen, whereas the other terminal is supplied by connecting conductor and screen to two of the three phases of the step-down transformer in order to simulate fault currents flowing in the sheaths.

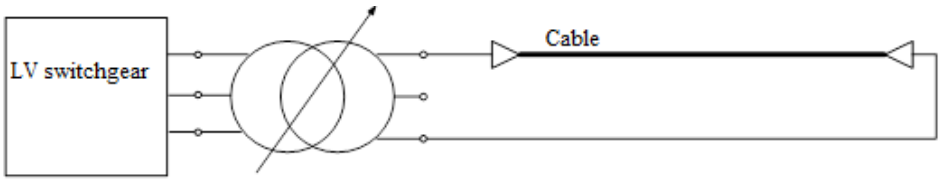


*Figure 49 1st test arrangement*

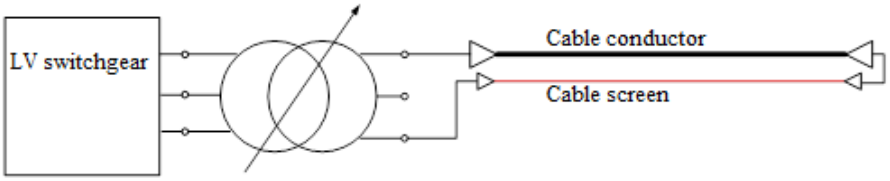


*Figure 50 2nd test arrangement*

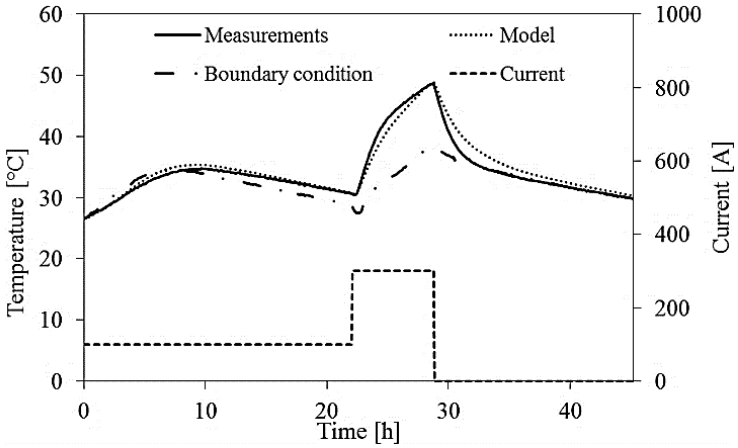


*Figure 51 Temperature trend against time: comparison between thermocouple 4 measurements and simulation results.*

*Figure 51* shows the comparison between measurements collected by thermocouple n° 4, placed above the joint's sheath, and results yielded by the model. The first test arrangement (see Section 2.2) has been used. Data logger's sample time has been chosen equal to 5 minutes. The average and the maximum error between model and measurements are 2.33% and 7.86%, respectively.

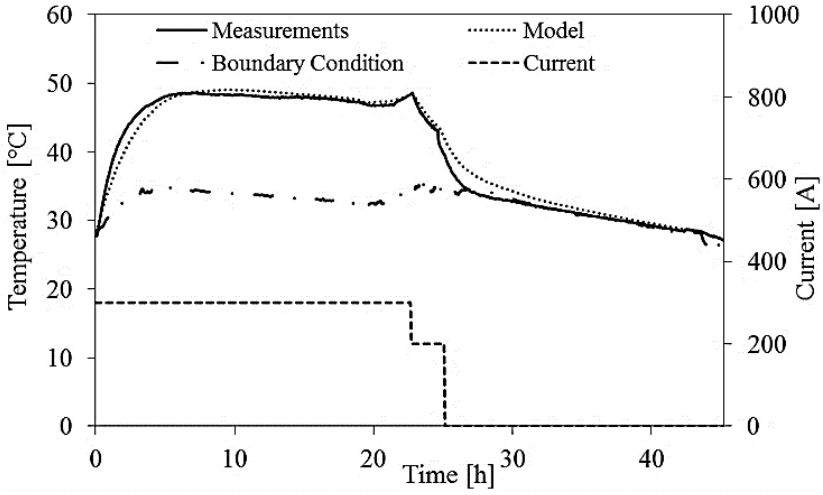


*Figure 52 Temperature trend against time: comparison between thermocouple 1 measurements and simulation results.*

*Figure 52* reports the comparison between measurements collected by thermocouple n° 1, placed close to the connection of the screens within the joint's sheath, and results obtained by the model. The first test arrangement (see Section 2.2) has been used. The average and the maximum error between model and measurements are 2.09% and 7.12%, respectively. Figures 9 and 10 evidence that the proposed model is able to reproduce long transients in order to simulate the standard operation.

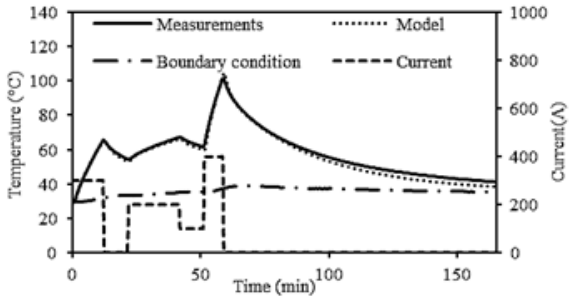


*Figure 53 Temperature trend against time: comparison between thermocouple 7 measurements and simulation results.*

*Figure 53* presents the comparison between measurements collected by thermocouple n° 7, placed above the cable's sheath, and results calculated by the model. The second test arrangement (see Section 2.2) has been used. During this tests, Data logger's sample time has been set up equal to 30 seconds. The average and the maximum error between model and measurements are 3.76% and 7.7%, respectively.

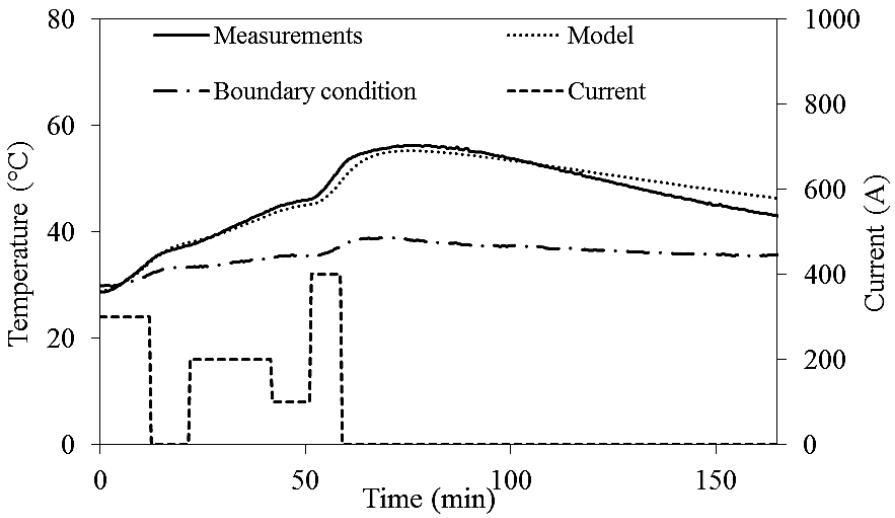


*Figure 54 Temperature trend against time: comparison between thermocouple 10 measurements and simulation results.*

*Figure 54* shows the comparison between measurements collected by thermocouple n° 10, placed above the semi-conductive plate, and model results. The second test arrangement (see Section 2.2) has been used. The average and the maximum error between model and measurements are 2.61% and 7.95%. Figures 11 and 12 indicate that the model is able also to reproduce short transients in order to simulate ground fault effects.

The equivalent electrical circuit model has been validated by comparisons with 27 temperature trends recorded during experimental tests, showing a very good agreement: the average relative errors are always smaller than 1 %, whereas the maximum relative errors never exceed 3 %, as the figures below show.

At first, the proposed 3-D model including joint, cable and pipe (but excluding the soil thermal model described in Section 3.3) has been validated against the experimental tests reported in  (for a detailed description of the experimental set up and the test arrangements see [25]). The aim is to show that the representation of joint, cable and pipe used in the proposed model refines the original model presented in [101].

Among the many comparisons, *Figure 55* reports the one between temperature measurements regarding the joint aluminum connector (collected by thermocouple n° 3 in the experimental set up described in [101] and using the first test arrangement described in [25]), and simulations results obtained by the model. The average and the maximum error between model and measurements are 0.353% and 1.33%, respectively, whereas the average and the maximum error between the original model and measurements are 2.33% and 5.44%, respectively.

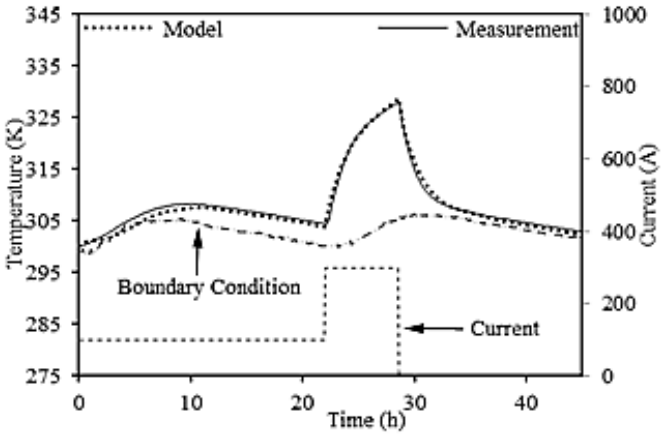


*Figure 55 Temperature trend against time: comparison between measurements and simulation results (joint aluminum connector temperature; boundary condition refers to the measured PVC pipe temperature).*

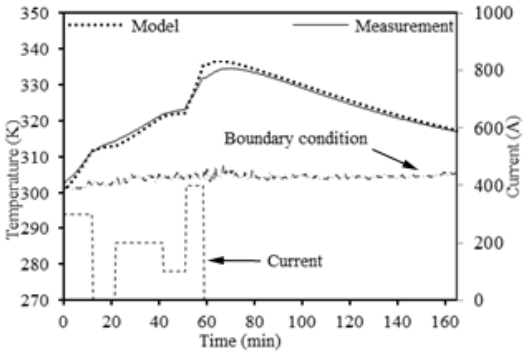


*Figure 56 Temperature trend against time: comparison between thermocouple 6 measurements and simulation results.*

*Figure 56* shows the comparison between measurements collected by thermocouple n° 6, placed above the joint's sheath, and results yielded by the model. The second test arrangement (see Section 2.2) has been used. The average and the maximum error between model and measurements are 0.572% and 2.56%, respectively. Figure 10 shows that the model is also able to reproduce short transients, thus being capable to simulate thermal effects due to single-phase-to-ground faults.

Generally speaking, errors made by the present model are more than halved if compared to the original model presented in [101]: the average relative errors are always smaller than 1 % (against 2.33 % in [101]), whereas the maximum relative errors never exceed 3 % (against 7.86 % in [101]).

### 4.1.3 *Model validation by means of test in a real environment*

This section presents the features of the adopted experimental setup carried out in Terni (a city in the center of Italy) by the local DSO (i.e., Terni Distribuzione Elettrica, productivity unit of ASM Terni S.p.A.). The system consists of three cold shrinkable joints (Nexans 24GAS1.185E) which connect stretches of cables (Prysmian ARG7H1RX with HEPR insulation and 360 A as rated current). One of these joints includes some thermocouples (Type K – L=10m - Range - 50/750 °C - Class1 – Tolerance = ±1.5 °C), placed above different materials during its packaging, as shown in Figure 58. As shown in Figure 57 (a) and (b), thermocouples are arranged for measuring the temperatures of the mastic above the connector inside the joint (Probe 1), the insulation and the sheath of the cable inside the joint (Probes 4 and 3) and the joint external sheath (Probe 2). Thermocouples are connected to a portable data logger (Datum-Y 100 Yokogawa - 16 channels, time sampling ranging from 100 ms to 5 h, SD storage up to 2 GB).

The system of joints and cables has been buried to reproduce real operating conditions, as shown in Figure 59 (a): the depth of burial is 1 m, while the surface area of the hole is 10.35 m2 (length and width are 4.5 m and 2.3 m, respectively). The cable has been carried out following the best practice currently implemented by DSOs in Italy, as shown in Figure 59 (b): namely, covering cables with a first layer of sand aiming at reducing and preventing damages of joints' sheath occurring during cable burial; in a subsequent phase, a second layer of soil has been used to cover the remaining part of the hole. The depths of sand and ground layers are 45 cm and 55 cm respectively, as reported in Figure 57 (a); moreover a thermocouple has been placed in the extreme part of the sand layer.

In order to reproduce realistic thermal conditions, the joints and the cables have been heated by a current flowing through the cable during the day; the arrangement presented in Figure 60 has been implemented: a 400 V low voltage (LV) switchgear supplies the cable by means of a three-phase automatic variac which is connected in series to a three-phase step-down transformer, shown in Figure 61 (400 kVA, K=25 ± 2.5%, 50 ± 2.5%, In=577 A). The variac allows supplying currents ranging from 0 to 400 A, supplying at a very LV level (8–16 V) the secondary of the step-down transformer; it has been also equipped with a timer to turn on and off the switchgear.

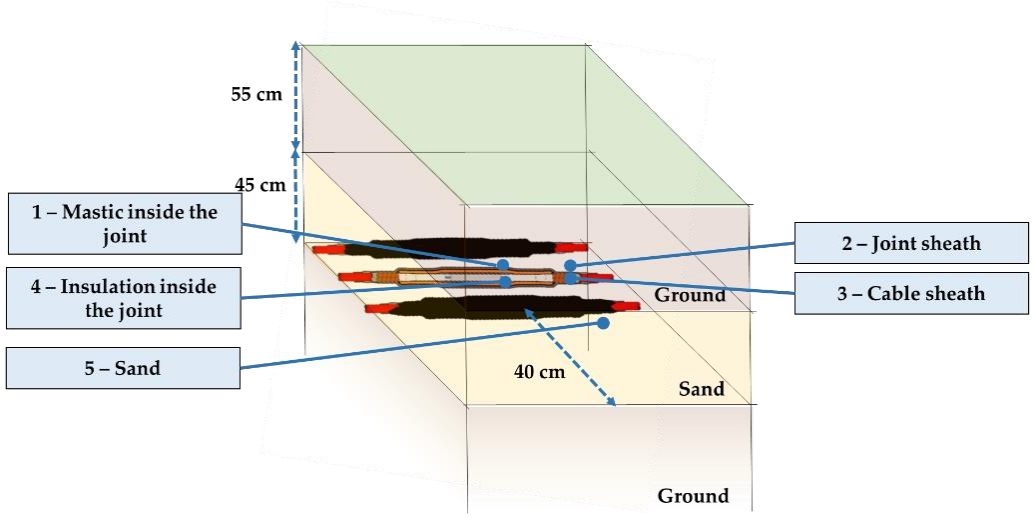


*(a)*

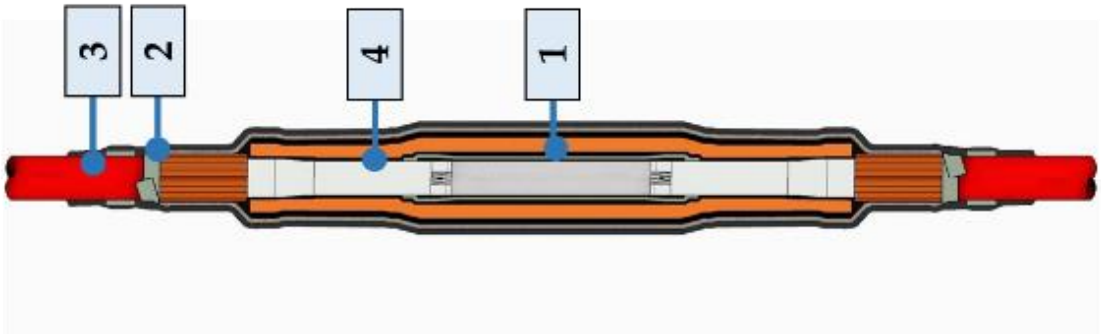


*(b)*

*Figure 57. (a) Outline of the experimental setup for measurements; (b) Thermal probes inside the joint.*

The measurement campaign started on 31/08/2018 and it ended on 01/10/2019 in order to record temperature variation during a year. Different current steps had been applied, from 31/08/2018 to 21/09/2018 four 140 A - 2 hours long current steps were daily applied; from 28/09/2018 to 08/10/2018 a current periodically varying from 285 to 330 A was applied for ten days; finally, three 140 A current steps have been applied in the following days from 09/10/2018 to 01/10/2018.

*Figure 58. Thermocouple placed above joint materials during the packaging.*

*(a)* *(b)*

*Figure 59. Laying conditions for the experimental tests. (a) Cable and joints directly buried at 1 m depth; (b) Hole covered by sand at 0.55 m of depth, the remaining part by soil.*

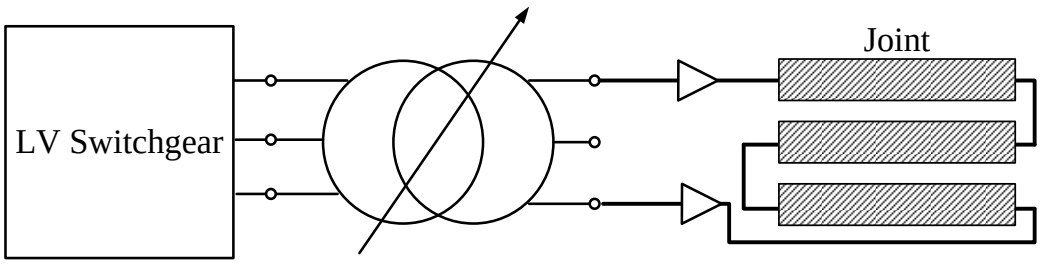


*Figure 60. Test arrangement [14].*

*Figure 61. Three-phase step-down transformer supplying the cable-joint system.*

This section presents the experimental results obtained during the measurement campaign. For the sake of clarity, this section reports only the data collected for 4 weeks, each one referred to a different season. Moreover, all plots show soil temperature (measured by thermal probe 5), air temperature (according to the data gathered by the nearest weather station) and the current flowing through the system (measured by the current probe); finally, for each figure, various trends of temperatures, as measured by thermocouples placed above or within the joint and the cable, are reported.

Figure 62*Figure 62* reports the temperature trend of insulation inside the joint during autumn; Figure 63 shows the temperature variation in correspondence of the joint sheath during winter period; temperature variation of the cable sheath during spring period is reported in Figure 64; temperature of the mastic inside the joint during summer period is shown in Figure 65. Finally, a comparison between temperature trends along different materials is proposed in Figure 66, in which mastic and cable sheath temperatures are reported, measured by probe 1 and 3, respectively.

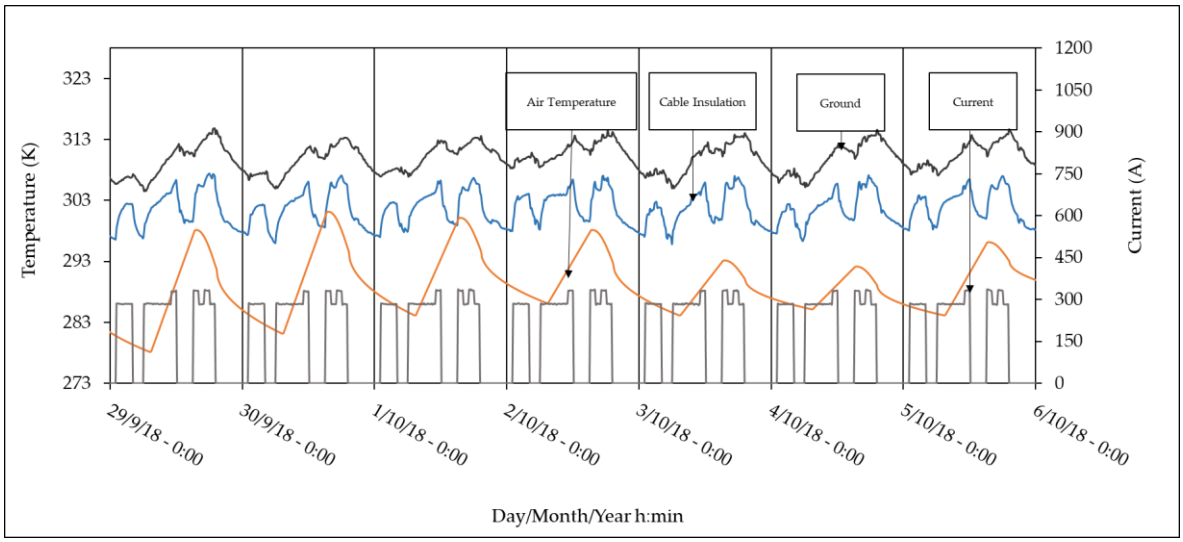


*Figure 62. Temperature variation of the joint during 7 days in autumn (Probe 4).*

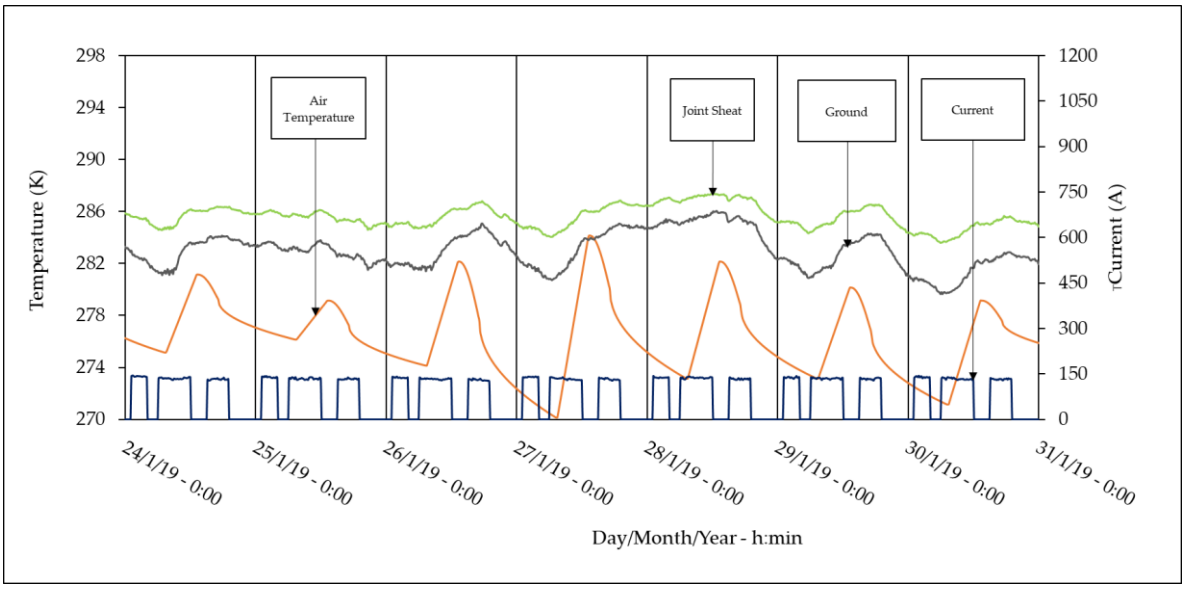


*Figure 63. Temperature variation of the joint during 7 days in winter (Probe 2).*

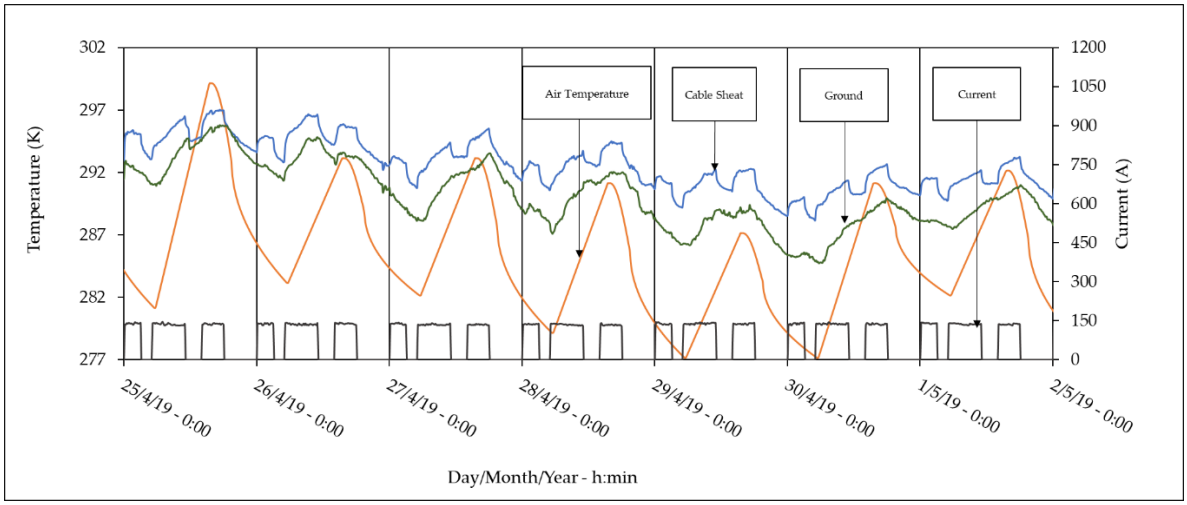


*Figure 64. Temperature variation of the joint during 7 days in spring (Probe 3).*

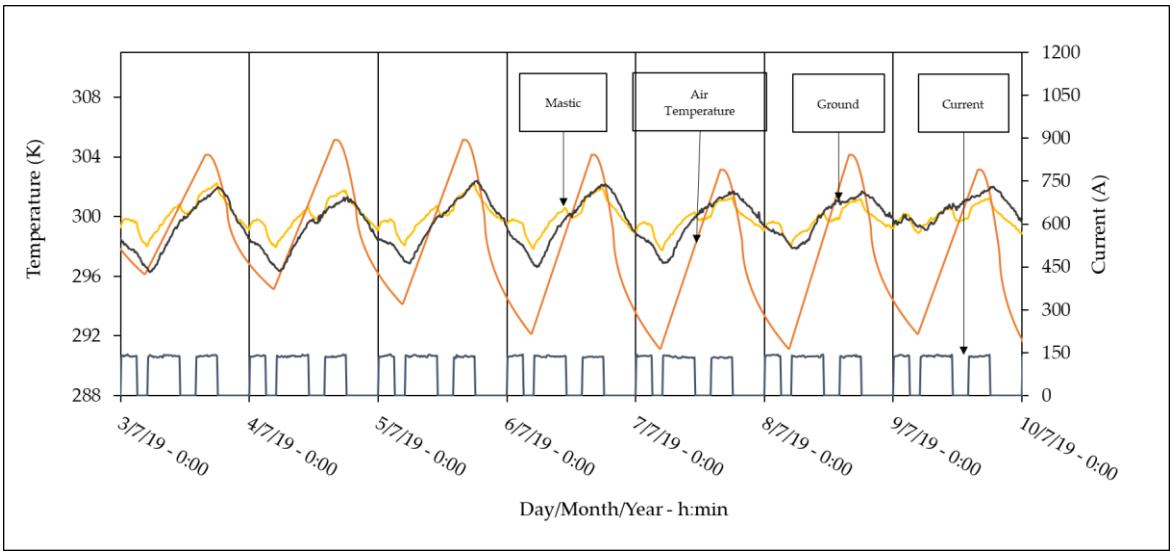


*Figure 65. Temperature variation of the joint during 7 days in summer (Probe 1).*

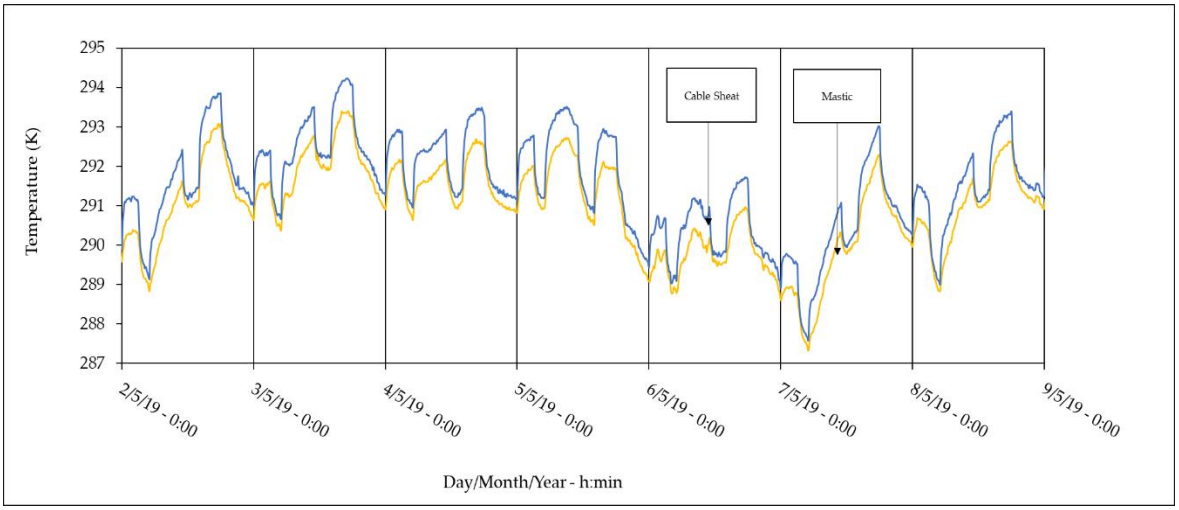


*Figure 66. A comparison between temperature trends inside cable sheath and mastic during 7 days in spring.*

Results of the measurement campaign show that joint heating is not notable during one year, especially considering that the maximum operating temperature of the cable insulation is 90 °C. The most notable temperature variations within the joint have been detected during August and September, when soil temperatures are the highest in the year. This suggests that joint failures are not related to ambient temperature, since most failures are recorded during June and July. In this respect, it is worth noting that the average temperatures of joints' material are mainly influenced by soil temperature variation. Therefore, it can be argued that average temperature of cable and joint during a certain period mainly depends on the soil temperature around the cable (influenced by the soil characteristics); variations of current flowing along the cable have a lesser influence on cable temperature, as shown in Figure 62 and Figure 64.

Daily variation of temperature is influenced by both cable loading and soil temperature which vary during the days; effects produced by the current are more notable in Figure 62, where temperature of cable insulation is reported, as well as in Figure 64, where measured temperatures of cable sheath are shown. Conversely, in Figure 65 trends of soil and mastic temperatures are very similar and differences are negligible, whereas in Figure 63 joint temperature trend is mostly

influenced by the soil temperature and variations of current flowing through the cable during the day seem to cause no significant joint temperature variation.

Experimental tests highlights that temperature trends along joint sections made up of different materials are different, depending on the distance from the cable conductor, which is a heat generator due to Joule losses, and from the soil, which is practically isothermal. Figure 66 shows that mastic is colder than cable sheath; it is worth noting that the former covers the metallic connector of the joint, whilst the latter is a portion of the cable sheath inside the joint. It can be argued that two factors mainly influence the temperature difference: on the one hand, the radial distances from the conductor surface of mastic and sheath are 5 and 4 mm, respectively (i.e., the mastic is further away from Joule losses); on the other hand, mastic is colder than sheath since the Joule losses per unit length are less in its proximity. Indeed, based on measurements presented in this work and simulation results reported in [88], it can be stated that the joint is colder than the cable since Joule losses produced in the connector part are about a quarter of those generated by the cable conductor. In this respect, according to measurements, the effect of CR on metallic connector overheating can be neglected, as argued in [119].

*Figure 67* presents the comparison between measurements collected by the thermocouple placed above the cable's insulation within the joint (data logger sampling time is 10 min) and results calculated by the model. Case 1 arrangement is used. A very good agreement is found between measurements and simulations: average and maximum error between model and field measurements are 0.30% and 0.89%, respectively. In order to highlight the good performance of the model, *Figure 67* B) shows the zoom in the time period from hour 110 to hour 158.

*Figure 68* shows the comparison between measurements collected by the thermocouple placed above joint's mastic (data logger sampling time is 10 min) and results yielded by the model. Case 2 arrangement is used. Also in this case, a very good agreement is found between measurements and simulations: average and maximum error between model and field measurements are 0.54 % and 1.55 %, respectively. In order to highlight the good performance of the model, *Figure 68* shows the zoom in the time period from hour 30 to hour 78.

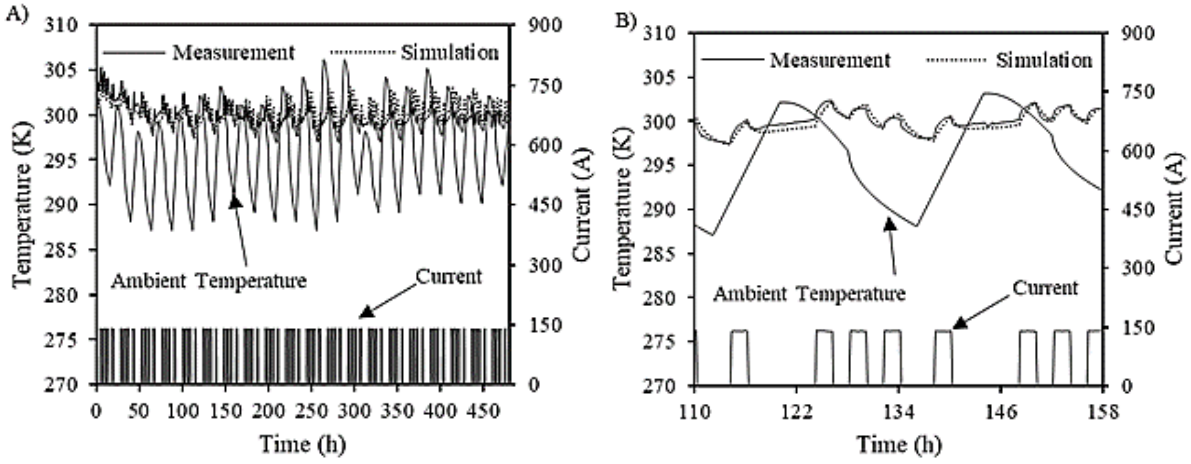


*Figure 67 Case 1 results: comparison between measured (thermocouple placed between cable insulation and mastic in joint Section 2 and calculated temperatures. A) Whole time period; B) zoom from hour 110 to hour 158.*

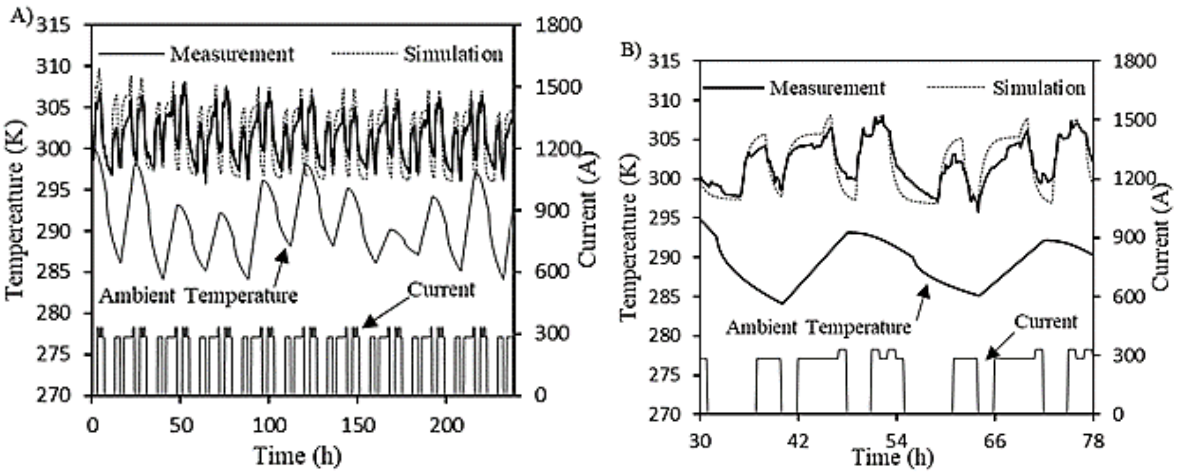


*Figure 68 Case 2 results: comparison between measured (thermocouple placed between mastic and insulation in joint Section 1) and calculated temperatures. A) Whole time period; B) zoom from hour 30 to hour 78.*

*Table 11* reports parameter values used in the model, in addition to joint and cable parameters already detailed in *Table 10*, *Table 9* and *Table 8*, for the simulations reported in previous figures.

*Table 11 Soil parameters and coefficients used in the simulations*

| $L_x$ (m) | $L_y$ (m) | $L_z$ (m) | $h_{conv}$ (W· $K^{-1}$·$m^{-2}$) | f | $\alpha_s$ | $\varepsilon_s$ | $T_{und}$ (K) | $\lambda_g$ (W· $K^{-1}$·$m^{-1}$) | $c_g$ (J·$K^{-1}$· $m^{-3}$) | $\lambda_{g,dry}$ (W· $K^{-1}$ ·$m^{-1}$) | $\lambda_{g,wet}$ (W· $K^{1}$· $m^{-1}$) |
|---|---|---|---|---|---|---|---|---|---|---|---|
| 2.3 | 4.5 | 10 | 1 | 0.6 | 0.8 | 0.9 | 293.15 | 0.666 | 1920000 | 0.3 | 0.5 |

Simulations of the one-year operation of an MV cable have been then carried out, by using the yearly loading profile measured by A.S.M. Terni S.p.A. on a feeder of its MV distribution network, as well as ambient temperature and relative humidity trends recorded by a weather station. Results show that the joint is the coldest element of the MV cable line when it is correctly installed. Simulations have been then repeated by using a modified yearly current profile, in which current values are very close to the cable ampacity, in order to simulate the thermal heating of a high loaded feeder. Also in this case results confirm that joint is always the coldest element; moreover, the maximum operating temperature of the cable (363.15 K) is never exceeded.

Results show that joint temperature strongly depends on the current flowing through the cable, whereas is only partially influenced by the ambient temperature variation during the year. From such remark, it does not seem that the anomalous increase of joint failures, observed by Italian Distribution System Operators (DSOs) during summer 2015, is related to ambient temperature. In order to better investigate such issue, the circuit model will be improved by representing the electrical contact resistance between joint stocking and cable screens (whose value depends either on an unqualified joint installation or on the grip slackening of cold-shrinkable joints during operation). Indeed, the effect due to such contact resistance may significantly influence the thermal behaviour of the joint, especially when cross-country faults occur.

### 4.1.4 *Thermal effects of ground faults on MV joints*

Different arrangements are provided by the joint manufacturers (e.g., copper braid or socks mounted with a ring or a weld) in order to ensure screen continuity between the cable stretches; in all of these cases, a CR is introduced in both terminals of the joint.

In literature, the evaluation of CR is performed by means either of cylindrical volumes, which have their basis as contact sections, or of metallic films, which are overlapped. The density of contact spots is investigated in [120] and a generalized formula is defined in [121]. Other papers studied the influence of pressure and temperature: experimental tests have demonstrated that contact resistance decreases when they are increasing, describing this correlation by means of non-linear relationships with hysteresis characteristics, as in [122]. In the present work, the CR influence has been taken into account by increasing the Joule losses produced locally, as in [123].

The effect of the CR has been evaluated including a specific current generator in the model, which injects a current equal to the heat flow produced by the Joule losses, as shown in *Figure 69*, which is an extract of the whole equivalent network (consisting of about 35,000 nodes) used for the simulation.

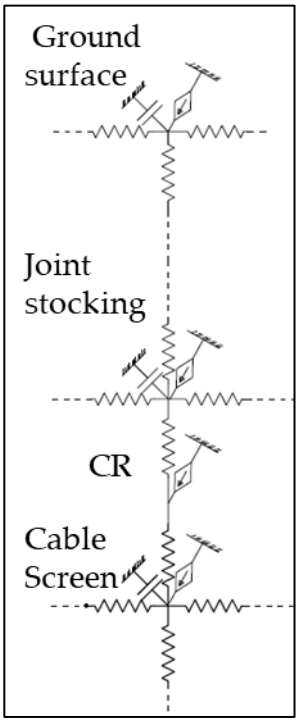


*Figure 69 Detail of the equivalent network representing the CR.*

In this work, in order to quantify the value of CR, measurements have been carried out in [124]. Such measurements on different joints allowed to define a range of CR values, as well as to take into account the different arrangements. Data have been collected by a CHAUVIN ARNOUX C.A. 6547 digital meter, as shown in *Figure 70*; results are reported in *Table 12*.

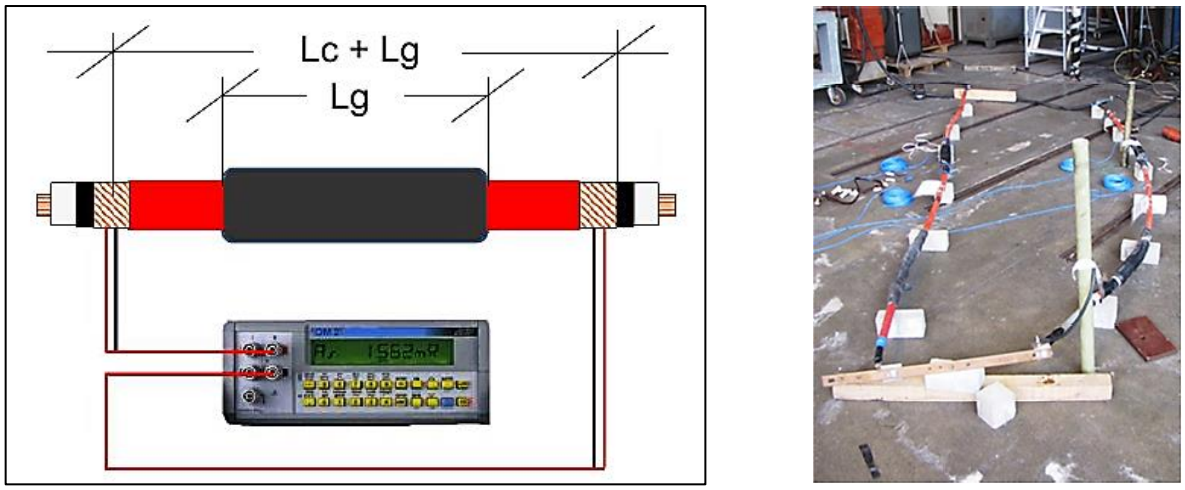


(a) (b)

*Figure 70 (a) Outline of the experimental setup for CR measurements; (b) Laboratory setup for the tests* [124].

In the test, both screen and joint stocking are made of copper, with 16 mm$^2$ and 100 mm$^2$ equivalent cross sections, respectively, whereas the temperature of the screen is 70 °C, leading to a $1.68 \cdot 10^{-8}$ Ω·m resistivity value. Moreover, it is unknown the distribution of the joint CR between the two joint terminals. Starting from measurements in [124], the joint CR has been estimated according to the following equation:

$$CR = R_{s,T} - r_{16} \cdot \left(L_c + 4 \cdot L_{c,g}\right) - r_{100} \cdot L_g \,, \tag{5}$$

where $R_{s,T}$ is the overall screen resistance measured by the digital meter according to Figure 2a configuration, $r_{16}$ is the cable screen resistance per unit length (1.329 mΩ·m$^{-1}$ for the tested cable-joint system), $r_{100}$ is the joint stocking resistance per unit length (0.16 mΩ·m$^{-1}$ for the tested cable-joint system), $L_c$ is the length of the portion of the cable outside the joint, $L_{c,g}$ is the length over which the screen continuity is carried out (corresponding to Section 3 in *Figure 39*) and $L_g$ is the joint length, as shown in *Figure 39*. Measured $R_{s,T}$ values, as well as the corresponding CR values calculated with (5), are reported in *Table 12*.

*Table 12 Measured $R_{s,T}$ and CR evaluation*

| $L_c + L_g$ (m) | $L_g$ (m) | Measured $R_{s,T}$ (mΩ) | CR (mΩ) |
|---|---|---|---|
| 1.08 | 0.75 | 8.693 | 7.743 |
| 1.03 | 0.75 | 3.11 | 2.225 |
| 1.03 | 0.75 | 7.076 | 6.191 |

#### 4.1.4.1 *Input data of the simulations: equipment and ground parameters, fault currents and auto-reclosure schemes.*

The model is applied to simulate the effect of grounded faults occurring in a MV network. Fault current and fault clearing time are inputs of the problem, together with physical and geometrical parameters of the system (i.e. cable, joint, PVC pipe, soil), which are reported in *Table 8*, *Table 9*, *Table 10* and *Table 11*, respectively.

Different CR values are used, corresponding to different simulated case, as reported in Table 6. In accordance with *Table 13* maximum CR value used in simulations is 7.3 mΩ (case 6), corresponding to about 100 times the equivalent resistance of the cable screen in Section 3 (i.e., the section in which the screen continuity in carried out); a nil CR value has also been simulated (case 1, corresponding to a perfectly installed joint). In all simulated cases, CR value has been equally shared among the two joint terminals.

*Table 13 Contact Resistance considered in the simulations*

| **Case** | **1** | **2** | **3** | **4** | **5** | **6** |
|---|---|---|---|---|---|---|
| **CR (mΩ)** | 0 | 0.073 | 0.73 | 1.825 | 3.65 | 7.3 |

As already written in previous section, fault currents corresponding to CCFs have been simulated, since CCFs cause very large currents (comparable to line-to-line fault currents) flowing through screens, especially if screens are connected to the earthing system of the primary substation (PS), as shown in [23,24]. The maximum simulated current value injected through screens was 10 kA, which is anyway very uncommon in MV networks, as evidenced by the authors in [25], reporting a statistical study about fault currents due to CCFs for a typical Italian MV network, owned and managed by e-distribuzione (the most important Italian distribution system operator) and supplied by a 40 MVA transformer. In [25], the maximum calculated CCF current value is about 8.4 kA, whereas the average one is about 3 kA.

Regarding fault clearing times, the reclosing cycles of circuit breakers, CBs, actually adopted by e-distribuzione in its MV distribution networks have been considered. Simulations have been carried out by injecting the fault current, $I_F$, in the core and in the screen of the MV cable. The possible presence along the MV feeder of a secondary substation (SS) equipped with an automatic CB, which is a less common case in Italy (where automatic CBs are normally installed only at the beginning of the feeder), has been taken into account: in this case, different reclosing cycles have been considered, as reported in the following.

Two main UCs have been identified. The first one (named A) involves a MV feeder equipped with a CB at the beginning of the line; it is worth highlighting that this is the most common case since the protection along a MV feeder is installed only in the PS (i.e., all SSs supplied by the MV feeder are equipped with disconnectors instead of a CB). In this UC, MV feeder protection is performed by definite-time overcurrent relay with three tripping thresholds: the first one is set at 120% of the rated ampacity, $I_{rated}$, of the MV cable (extinction time is 0.17 s if zero sequence current, $I_0$, is larger than 150 A, 1.07 s otherwise. Time of extinction is considered adding the time of tripping and time of maneuver of breaker – conventionally assumed 0.07 s); the second one is set at 800 A (extinction time is 0.17 s if $I_0$ is larger than 150 A, 0.32 s otherwise); the third one is set to 1400 A, with a fixed 0.12 s fault clearing time. After the extinction, reclosing cycles are performed until the fault is cleared, according to *Table 14* (C: CB status is closed; O: CB status is open). If the fault is not cleared after the auto-reclosure cycle, a permanent opening of the CB is made (not reported in *Table 14*).

The second UC (named B) regards an MV feeder along which a SS is equipped with a CB (SSS in the following) with network grounded by impedance (Petersen Coil); this CB defines two sections of the feeder (i.e., a section before the SSS and a section after the SSS). In such UC, the time-based overcurrent relaying coordination and the auto-reclosure schemes of the circuit breaker installed in the SSS are described in Table 8, in case the fault is located in the line section before the SSS, and *Table 16*, in case the fault is located in the line section after the SSS. Also in these two cases, if the

fault is not cleared after the auto-reclosure cycle, a permanent opening of the circuit breaker is made.

In this work, $I_{rated}$ has been assumed equal to 295 A, so that the first threshold is 354 A; moreover, thermal transients have been simulated over a 150 s timeframe, in order to show the thermal behaviour of the joint during a complete auto-reclosure cycle.

*Table 14 Auto-reclosure scheme in UC A*

| **Current** | | **Duration of breaker status (s)** | | | | | | | |
|---|---|---|---|---|---|---|---|---|---|
| $I_F$ | $I_0$ | **C** | **O** | **C** | **O** | **C** | **O** | **C** | **UC** |
| **[1.2·$I_{rated}$, 800 A]** | **>150 A** | 0.17 | 0.6 | 0.17 | 30 | 0.17 | 70 | 0.17 | A1 |
| **[1.2·$I_{rated}$, 800 A]** | **<150 A** | 1.07 | 0.6 | 1070 | 30 | 1.07 | 70 | 1.07 | A2 |
| **[800 A, 1400 A]** | **>150 A** | 0.17 | 0.6 | 0.17 | 30 | 0.17 | 70 | 0.17 | A1 |
| **[800 A, 1400 A]** | **<150 A** | 0.32 | 0.6 | 0.32 | 30 | 0.32 | 70 | 0.32 | A2 |
| **>1400 A** | **-** | 0.12 | 0.6 | 0.12 | 30 | 0.12 | 70 | 0.12 | A1 |

*Table 15 Auto-reclosure scheme in UC B, with a fault in the line section before the SSS.*

| **Current** | | **Duration of breaker status (s)** | | | | | | | |
|---|---|---|---|---|---|---|---|---|---|
| $I_F$ | $I_0$ | **C** | **O** | **C** | **O** | **C** | **O** | **C** | **UC** |
| **>800 A** | **<150 A** | 0.32 | 0.6 | 0.32 | 30 | 0.32 | 70 | 0.32 | B1 |

*Table 16 Auto-reclosure scheme in UC B, with a fault in the line section after the SSS*.

| **Current** | | **Duration of breaker status (s)** | | | | | | | |
|---|---|---|---|---|---|---|---|---|---|
| $I_F$ | $I_0$ | **C** | **O** | **C** | **O** | **C** | **O** | **C** | **UC** |
| **[1.2·$I_{rated}$, 500 A]** | **>150 A** | 0.8 | 0.6 | 0.8 | 30 | 0.8 | 70 | 0.8 | B2 |
| **>500 A**[1] | **<150 A** | 0.2 | 0.6 | 0.2 | 30 | 0.2 | 70 | 0.2 | B2 |

#### 4.1.4.2 *Simulation results*

In the simulations reported in this section, the equivalent electrical model has been applied considering a pre-fault cable insulation temperature equal to 90 °C, i.e. the pre-fault current through the MV cable was $I_{rated}$. It is worth highlighting that most results regard the section where the contact between the cable screen and the metal sheath of the joint occurs, referred as screen continuity inside the joint, SCJ, in the following. In addition, even if the model developed would allow, in principle, to obtain, as a result of the parametric analysis, temperatures well above those shown in the next figures (e.g., up to 5000 °C and beyond), the upper limit for temperature represented in all plots has been set to 1000 °C, as this is already far above the maximum tolerable temperature of the cable insulation during a faults (which, for the simulated cable, is 250 °C, as declared by the manufacturer).

According to *Table 14*, *Table 15* and *Table 16* the main difference between tripping thresholds is due to a SSS along the MV feeder. In order to properly compare results, at first UCs A1 and B1 are considered: $I_F$ values ranging from 1400 A and 10 kA have been injected, with a fault clearing time of 120 ms (UC A1) and 320 ms (UC B1), not simulating reclosing cycles.

*Figure 71* reports the trends of maximum temperature calculated at the SCJ over $I_F$; Figure 4a refers to UC A1, whereas Figure 4b to UC B1. According to *Table 13*, six different CR values are simulated for each UC (curves 1 to 6), even if case 2 is not reported since the trend is practically equal to case 1 trend. Results show that, if CR is nil or equal to 0.073 mΩ (case 1 and case 2 of *Table 13*, respectively), the 250 °C maximum allowable temperature is never exceeded in any case, whilst dangerous conditions could occur if a CR value larger than 0.73 mΩ (case 3 of *Table 13*) was considered. If larger CR values are considered (for instance 3.65 mΩ and 7.3 mΩ) temperatures dramatically increase and exceed the maximum allowable value also in case of common $I_F$ values in both the UCs.

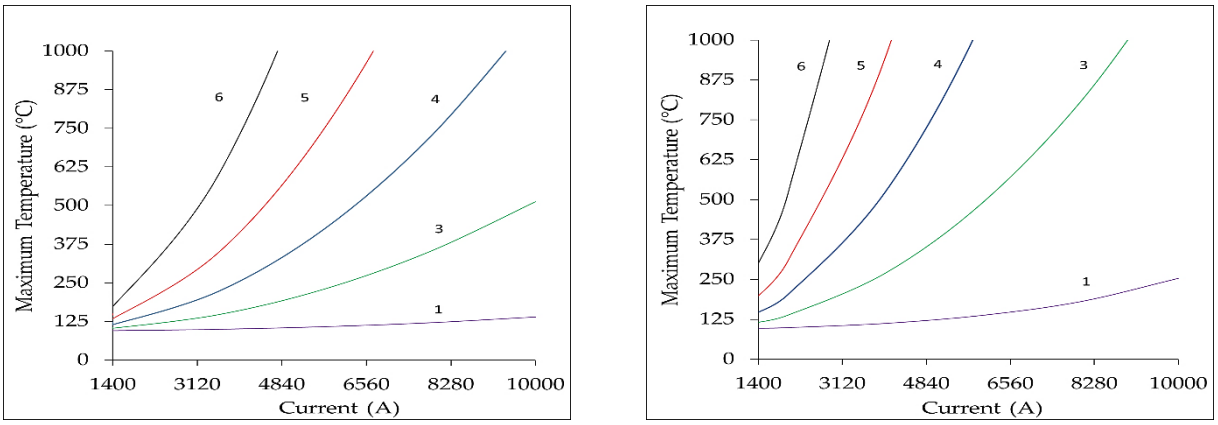


*Figure 71 Maximum Temperature calculated for short circuit currents cleared in 120 ms (a) and 320 ms (b); different CR values are simulated, as defined in Table 6.*

*Figure 72* shows thermal transients simulated in the SCJ and the cable screen when $I_F$=3 kA (the average value of $I_F$ in [125]) and the auto-reclosure scheme of UC A1 in *Table 14*, considering CR values of *Table 13.* The whole thermal transients in SCJ for cases 1, 4, 5 and 6, as well as the thermal transient in cable screen for case 3, are reported in *Figure 72 a*. *Figure 72 b* shows a zoom of the same trends of in the timeframe from 0 to 2 s, in order to show the two temperature peaks corresponding to the 1st and the 2nd opening of the CB, which are not distinguishable in *Figure 72 a*. Also in these cases, simulations show that SCJ does not reach dangerous temperatures if CR is lower than 3.65 mΩ, thus not impairing or breaking the joint. Cable screen temperature trend is reported only for case 3 simulation, since in all cases is very similar to the temperature trend along the SCJ; however, it is worth noting that in case of a perfect screen contact (i.e., CR nil), the screen reaches temperature higher than the joint because of its smaller section (not reported in other simulations). During the most severe simulated thermal transients (as in case 4, case 5 and case 6 of *Figure 72*), the time instant when the maximum temperature is detected corresponds to the 2nd opening of the CB: this result is consistent, since the time period between the first and the 2nd opening of the CB is very short and, consequently, temperature decreases in a negligible way.

*Figure 73* shows the thermal transients in SCJ for cases 1, 2 and 3, as well as the thermal transient in cable screen for case 3, evaluated for $I_F$=3 kA and using the auto-reclosure scheme of UC B2 in *Table 14*. Simulation results show that for CR values greater than or equal to 1.825 mΩ

(case 4), the maximum allowable temperature is always exceeded, thus causing the impairment or the breaking of the joint.

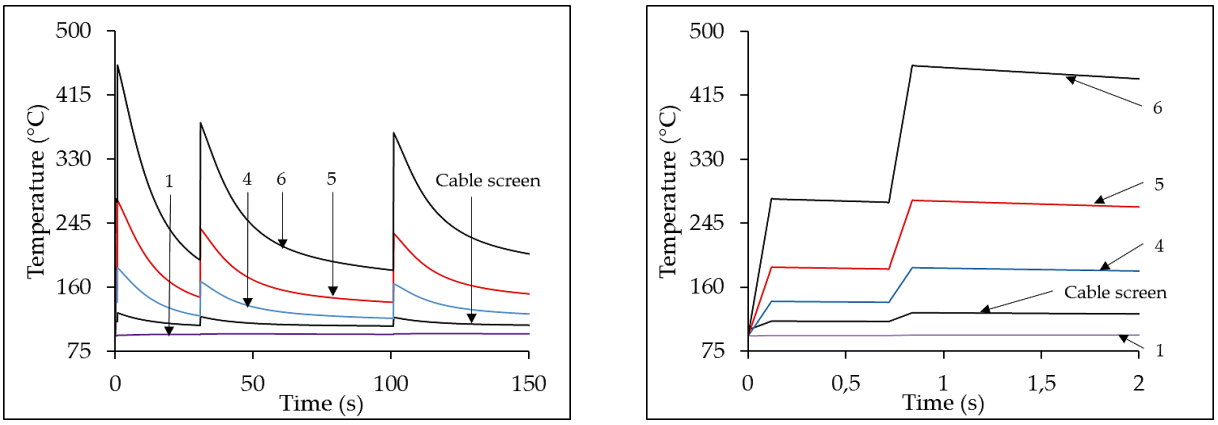


*Figure 72 (a) Thermal transients in SCJ (cases 1, 4, 5 and 6) and in the cable screen (case 3). IF=3 kA, UC A1. (b) Zoom of (a) in the timeframe from 0 s to 2 s.*

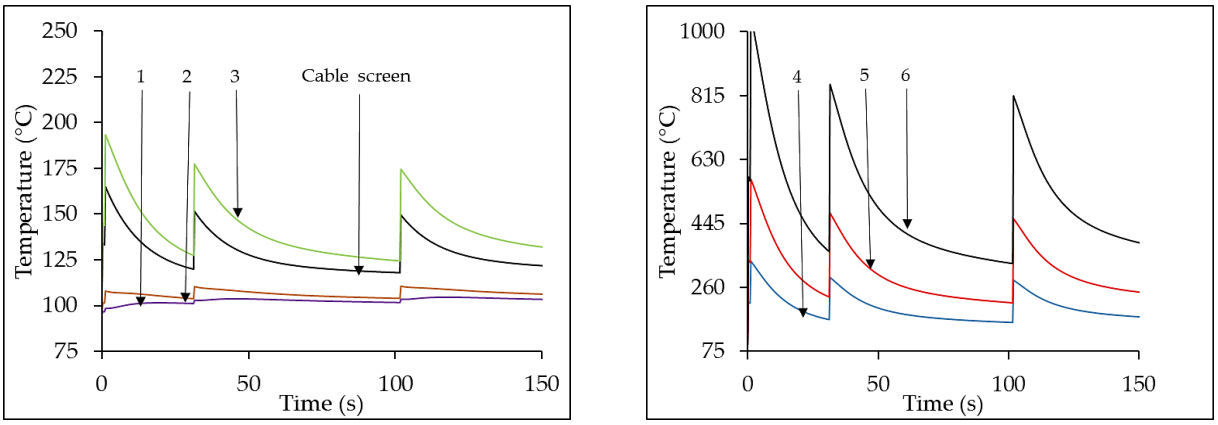


*Figure 73 Thermal transients for IF=3 kA (UC B2). (a) Cases 1, 2 and 3; (b) Cases 4, 5 and 6.*

*Figure 74* reports thermal transients evaluated for $I_F$=800 A, for two different fault clearing times, namely 1070 ms and 320 ms (UC A2 in *Table 14*). Temperature trends are calculated for different CR values: Figure 7a reports trends for cases 1 and 3 of Table 6, whilst *Figure 74 b* shows transients for cases 4 and 6. Thermal transients reported in *Figure 74* are tolerable from the cable and joint; on the other hand, if CR=7.3 mΩ, a fault clearing time of 1070 ms leads to unacceptable temperatures for the cable, with a maximum value equal to 310 °C.

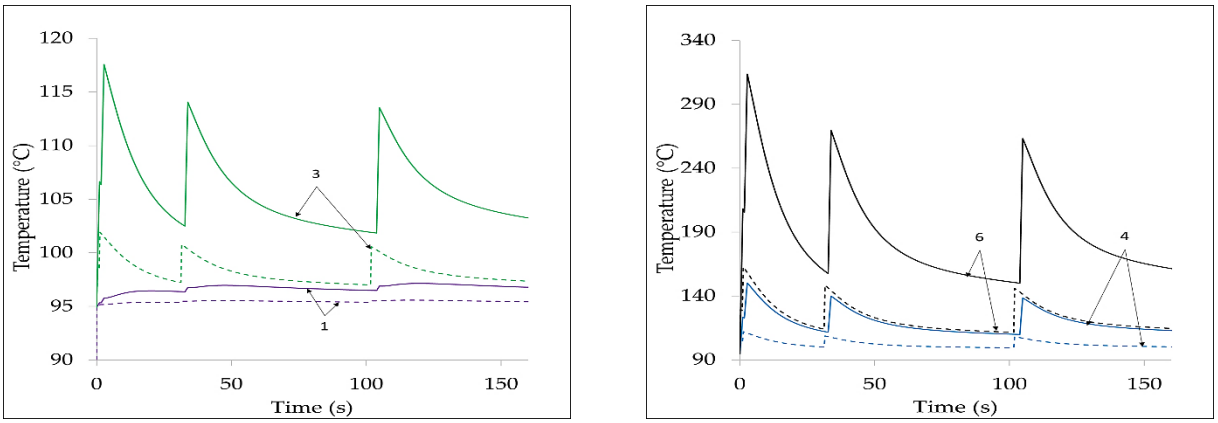


(**a**) (**b**)

*Figure 74 Thermal transient along SCJ, IF=800 A; fault clearing times: 1070 ms (solid line) and 320 ms (dashed line). (a) Cases 1 and 3; (b) Cases 4 and 6.*

*Figure 75* reports thermal transients simulated for $I_F$=1400 A, considering two different clearing times, namely 320 ms and 120ms. Four different CR values are considered: *Figure 75 b* reports temperature trends for case 1 and case 3, whilst *Figure 75 b* for case 4 and case 6. Also in this case, if CR=7.3 mΩ, a fault clearing time of 320 ms leads to unacceptable temperatures for the cable.

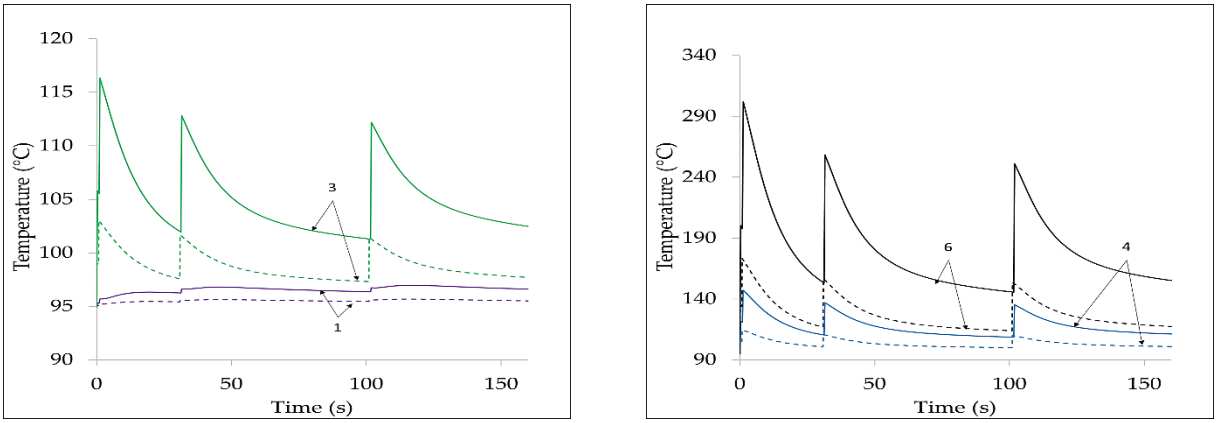


(**a**) (**b**)

*Figure 75 Thermal transient along SCJ, IF=1400 A; fault clearing times: 320 ms (solid line) and 120 ms (dashed line). (a) Cases 1 and 3; (b) Cases 4 and 6.*

In order to summarize the results of the simulations, carried out according to *Table 14*, a correlation is further presented. *Figure 76* shows the short circuit current which causes heating up to a certain limit temperature (i.e., 250 °C, 500 °C, 750 °C and 1000 C°) as a function of CR value. Moreover, different fault clearing times have been considered; notably 120 and 320 ms are reported by *Figure 76 a* and *Figure 76 b*, respectively.

*Figure 76* allows to assess the maximum current flowing through SCJ as a function of joint CR, considering different thermal limits. With respect to the design of MV networks, this would imply that the maximum CCF current defines the maximum admissible value of the joint CR.

From *Figure 76*, very small differences are noticed for the two different clearing times; if different temperature limits are considered, the more the temperature limit increases the more the offset among temperature trends decrease.

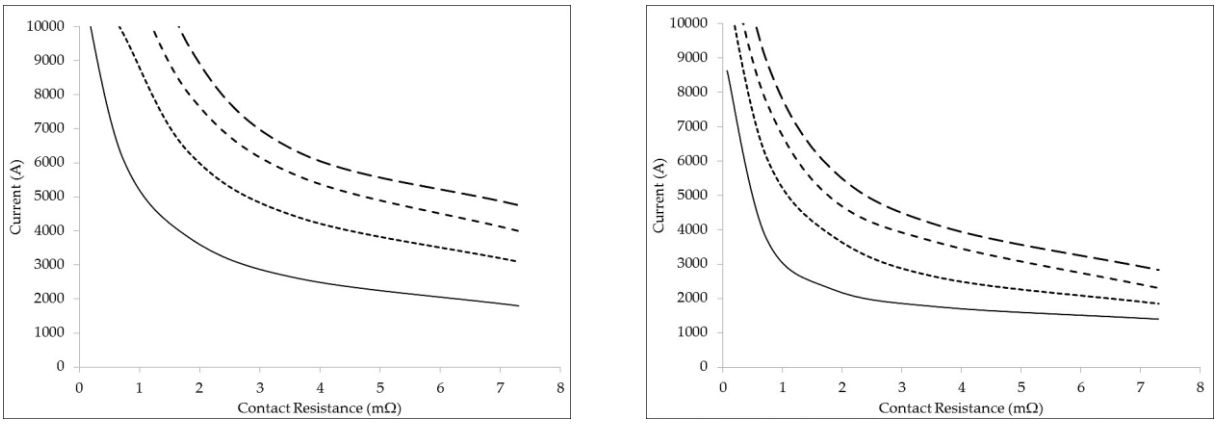


(**a**) (**b**)

*Figure 76 Fault current values causing SCJ heating up to the maximum tolerable temperature, as a function of joint CR. Four different maximum tolerable temperature are considered: 250 °C (solid line), 500 °C (dotted line), 750 °C (short-dashed line) and 1000 °C (long-dashed line). (a) 120 ms fault clearing time (UC A1); (b) 320 ms fault clearing time (UC B1).*

Results presented in this section highlight the pivotal role played by the CR if large short circuit currents flow through the cable screen, as in the case of CCFs. Correct assembly of the joint does not cause appreciable CR, but if the joint is not assembled correctly (for example, the joint and cable are not perfectly centred), or if the pressure applied by the shape memory sheet on both ends of the joint is reduced due to ageing, CR values of up to a few milliohms may occur.

Considering reclosing cycles of circuit breakers actually adopted by e-distribuzione in its MV distribution networks, practically no ground current flowing through cable screens is able to damage joints if CR value is near 0 m□: in fact, for so small value of the CR, only ground fault currents larger than about 10 kA, tripped in 320 ms, would be able to heat the joint up to its maximum tolerable temperature, but such values are unrealistic in real MV distribution networks.

On the contrary, if the CR reaches a value of some milliohms (such values have been measured in healthy joints in operation, as reported in [124]), realistic ground fault current values are able to damage and/or to break the joint, depending on the fault clearing time and the CR value. Parametric analyses, as the ones reported in Figure 4 and Figure 9, show that, for CR values of about 2 mΩ, $I_F$ values of about 4 kA are detrimental even for fast fault clearing times (120 ms); for larger CR values (about 6-7 mΩ), CCFs practically always cause an unacceptable heating of the joint.

## 4.2 Resilience assessment for validating new development plan of the distribution network

In literature, several studies assessing the resilience of MV distribution networks against extreme weather events are available. The general purpose of these studies is to evaluate how the assets vulnerability can have technical, social and economic impacts. Reference [126] focuses on two types of extreme events – floods and heat waves – and assesses two types of adaptation measures – substation flood protections and demand-side management. Reference [127] and [128] report experiences about the approaches adopted by DSOs to evaluate resilience considering

different threats. A resilience assessment framework to measure the resilience of power distribution system was proposed in [129], which focused on the performance of customers. Reference [130] presents a procedure to assess resilience of a distribution network against ice sleeves threats. Reference [131] thoroughly reviewed existing studies on resilience assessment and methods for its improvement, considering a resilient load restoration.

Other studies, related to HV networks, are also available. In particular, [132] proposes a framework for assessing the influence of ice disasters on the resilience of power transmission systems; reference [133] applied their assessment framework on a reduced version of the Great Britain's power network; reference [134] has assessed resilience with respect to typhoons. Reference [135] present an enhancement method to improve resilience of wind power penetrated power systems. Moreover, with respect flooding threats on power systems, some works are also available. Reference [136] addresses the risk management of floods at grid and primary substations in England, Scotland and Wales due to coastal, river and surface water flooding. Reference [137] assess resilience of critical infrastructure to flooding using a response curve approach and it moreover outlines the interdependencies between public service and electric energy availability.

This work presents a procedure able to assess the resilience of a distribution network considering flooding threat. The aim is to validate a workflow, through which a DSO can evaluate the resilience of its own infrastructure as is and it can easily identify the remedial actions that can be adopted to enhance network resilience. The proposed procedure has been applied on a real Distribution Network (DN) located in the center of Italy, owned and operated by TDE.

### 4.2.1 *The Proposed Procedure*

The main methodological elements for identifying and evaluating actions to increase the resilience in the network are described below, focusing on the calculation of the resilience indices and the expected impacts. Therefore, it presents the elements to assess resilience as well as to calculate resilience of the single asset of the distribution network. In this work, an asset may be a substation or a line (i.e., a basic building block of the model described in next subsection).

Methodology approach has its starting point from the collaboration and information exchanges among the main Italian stakeholders, which assess the resilience of electric network as requested by Italian Authority ARERA in [138] and already reported in references [128], [130] and [139]. These references, as well as the present work, aim at assessing resilience considering a risk index defined as follows:

$$\mathrm{R} = \frac{\mathrm{D}}{\mathrm{TR}} \tag{33}$$

In (33), D is defined as the magnitude of the considered damage, for instance the number of users disconnected or the total duration of disconnections. The Return Period of the event (TR) is an average period that occurs between two events caused by the same threat. TR is identified as the inverse of Probability of service Disrupt (PD):

$$\mathrm{PD} = \frac{1}{\mathrm{TR}} \tag{34}$$

In this work, PD is the probability that an extreme meteorological event can occur and lead to a fault on an asset of the network (e.g., a line or a substation). With respect to flooding events, details about assessment of TR are provided in the section 2.4.

In resilience analysis an additional parameter must be introduced, the equivalent $TR_e$, assigned at each substation and defined as the minimum TR of all assets that lead to a disconnection when

they are lost. This parameter allows to evaluate the effect of a threat (i.e., the number of unsupplied customers) on the network independently of the type of the involved asset (substations or lines).

Since the main concern of the work is the distribution network, the extent of the damage D is identified as the Number of LV Users Disconnected (NUD). Therefore the related risk index, IRI, is:

$$\mathrm{IRI} = \frac{\mathrm{NUD}}{\mathrm{TR_e}} \tag{35}$$

The Resilience Index (IRE) is the inverse of the risk index and is therefore equal to the return period of the event divided by the number of low voltage users disconnected:

$$\mathrm{IRE} = \frac{\mathrm{TR_e}}{\mathrm{NUD}} \tag{36}$$

The purpose of the method is to define resilience indices that do not depend on the type of threat; indeed the work proposes a unique model able to provide results having consistency also in case the model is applied on different scenarios. For this reason, the following additional indices may be considered:

- an index to evaluate the network property to allow back-feeding (IGCR), defined as:

$$\mathrm{IGCR} = \frac{\sum_i \mathrm{k} \cdot \mathrm{NUC_i}}{\mathrm{NUT}} \tag{37}$$

  with k = 1 if $TR_{e,i} = \infty$ and k = 0 if $TR_{e,i} \neq \infty$ (this means that the formula does not depend on the type of threat); $TR_{e,i}$ is the return period of the i-th node, $NUC_i$ is the number of LV users connected to the node, while NUT is the number of LV users of the network; the sum is extended to all the nodes of the network. The $TR_{e,i}$ is evaluated considering a generic threat occurring on a branch of the network. This index does not depend on the type of threat, since it is a feature of the network, representing its back-feeding capability.

- the degree of network resilience (IGRR) with respect to the threat considered, defined as

$$\mathrm{IGRR} = \frac{\left[\sum_i \left(1 - \frac{1}{\mathrm{TR_{e,i}}}\right) \cdot \mathrm{NUC_i}\right]}{\mathrm{NUT}} \tag{38}$$

  the index of users' vulnerability (IGVU) from the network, regardless of the threat considered, defined as

$$\mathrm{IGVU} = \frac{\sum_j \mathrm{NUD_j}}{\mathrm{NUT}} \tag{39}$$

where $NUD_j$ is the number of LV users disconnected when the j-th asset of the network has been removed (i.e., a substation or a line); the sum is applied to all the considered scenarios (that are as many as the branches of the network).

These indices can evaluate different actions on the network, as well as they can compare the performance of different networks, due to their generality.

### 4.2.2 *Model of a MV network for resilience assessment*

In order to assess the resilience, a homemade software has been developed by the authors in the Octave environment. Inputs of the procedure are: the topology of the distribution network (i.e. nodes and connections between nodes in the network), the typology of network components (i.e.,

lines, primary substations, secondary substations, switches, and disconnectors), the number of users supplied by each substation. All data are provided by the SCADA (Supervisory Control And Data Acquisition) system installed in the Terni DN and owned by TDE. Other relevant inputs are the TR of each asset, calculated considering both external conditions (i.e., probability of the threat) and asset features (i.e., the asset's ability to resist the specific threat), according to the methodology described in previous subsection. The procedure provides in output all the relevant resilience indexes of the DN, i.e. $TR_e$, IRI, IGCR, IGRR and IGVU. A schematic representation of the whole simulation model is given in *Figure 77*.

The $TR_e$ has been evaluated considering closed all switches and all equipment allowing all possible paths to perform any back-feeding, as well as considering also the full availability of all external interconnections (at HV and MV levels). In addition, the simulation model can simultaneously represent all primary substations feeding the MV network with their $TR_e$ (actual or assumed). Furthermore, the whole MV network has been modelled without introducing any layout reduction, nor making assumptions about aggregations for SSs.

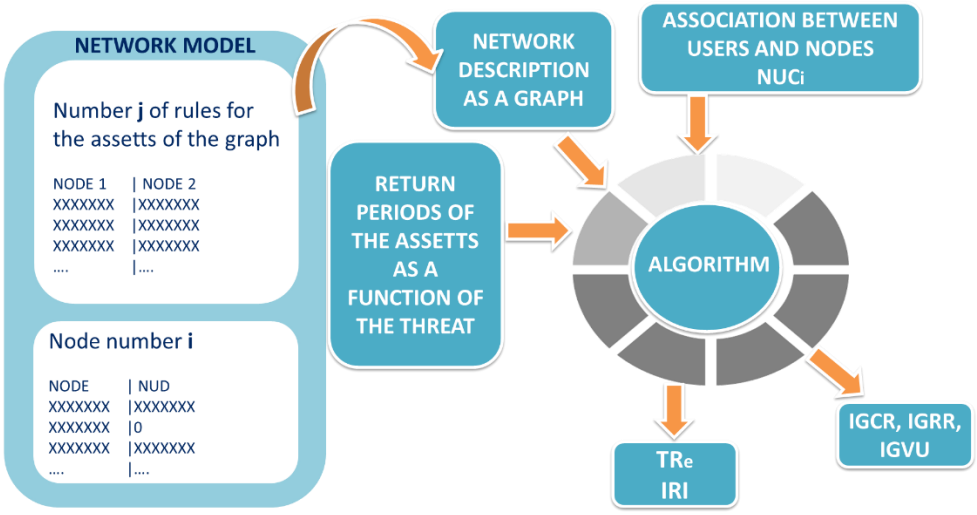


*Figure 77 Representation of simulation model.*

Assuming all switches and disconnectors closed, the simulation program initially generates the graph of the network, in which each node represents a substation (and consequently the number of supplied users) or a stiff connection, while each branch represents the connection line between two substations and / or stiff connections. The graph has been represented using a table in which each line represents a connection, each identified by a from-node and a to-node, as well as by the kind of connection (e.g., cable or overhead line).

The interconnections with other networks (at MV and HV levels), which are the power supply points, have been simulated in order to take into account their potential effects on the resilience assessment (*Figure 78*). The aim is to develop an algorithm able to inspect the graph that has a single starting point. Moreover, the return periods of each single interconnected networks have been taken into account by assigning an appropriate return period to the fictitious interconnection branches.

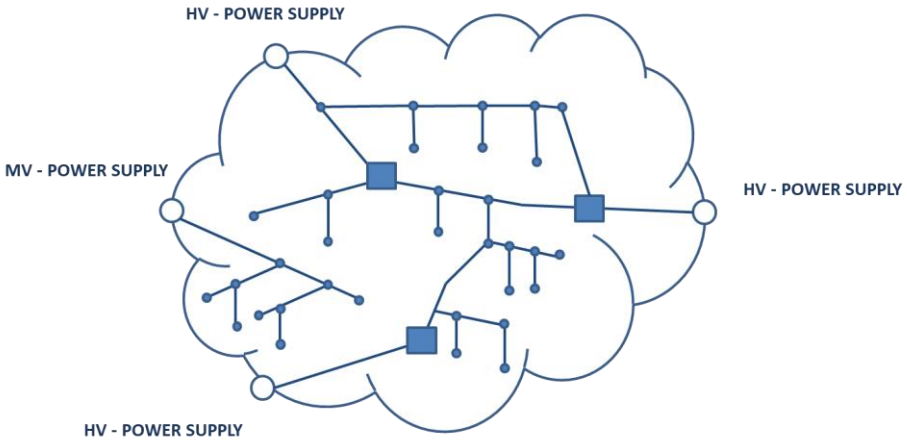


*Figure 78 Fictitious branch representation.*

The exploration of the network graph has been carried out by means of the Dulmage-Mendelsohn decomposition algorithm [140], which also allows identifying all isolated nodes in the network. Indeed, the aim of the simulation model is to identify all the substations (i.e., the number of the users associated with these ones) that will be unsupplied whenever an asset is lost because of a threat event. Then, IRI and all other indices are calculated according to $TR_e$.

The algorithm has been applied to every possible scenario obtained by eliminating an asset at a time, thus simulating the possible faults occurring on the network elements represented by that asset. For each scenario, the algorithm provides the list of nodes and/or NUD that cannot be reached because of the failure.

It is worth pointing out that the proposed simulation model is independent of the type of threat, as well as some indices introduced in this work in order to assess the resilience of the network.

### 4.2.3 *Resilience assessment for different treats*

#### 4.2.3.1 *Prediction of Substation Faults caused by Flooding*

The aim of this subsection is to present the methodology used to identify the return time of fault events caused by floods. According to the previous subsection, it has been assumed that flooding events can affect only the substations, namely a node is eliminated from the graph at each iteration of the simulation model. The probability that a substation is disconnected because of a flooding event consists of two elements, namely the return time of the weather event and the vulnerability of the substation, which is the fault probability of the asset when the event occurs.

Therefore, the probability of the flooding event has been firstly assessed. These data are easily available, since they are provided by the authorities that supervise the hydrogeological basins and evaluate the return time of the floods. With respect to this work, the applied methodology is provided by the authority responsible for the management of the hydrogeological basins that affects the action area (i.e. the Terni basin).

With respect to the return times of flooding events, the hydrogeological risk plan drawn up by the Province of Terni and Tiber River Basin Authority has been used [141]. These data have been provided by the plan of hydrogeological assets [142]. Among the Terni municipality areas, the authority considered only the ones characterized by hydrogeological risk and grouped them into 3 different zones, each one with a specific return time, as in the following:

- Zone A, with 50 years return time (high hydrogeological risk);

- Zone B, with 200 years return time (medium hydrogeological risk);
- Zone C, with 500 years return time (low hydrogeological risk).

As last step, for each substation in the distribution network, the software assigns the following return times:

- TR=50 years for substations in Zone A
- TR=200 years for substations in Zone B
- TR=500 years for substations in Zone C
- TR=999 years for substations not located in any of the above listed zones (i.e., no hydrogeological risk).

With respect to the action area, these zones are reported in *Figure 79*.

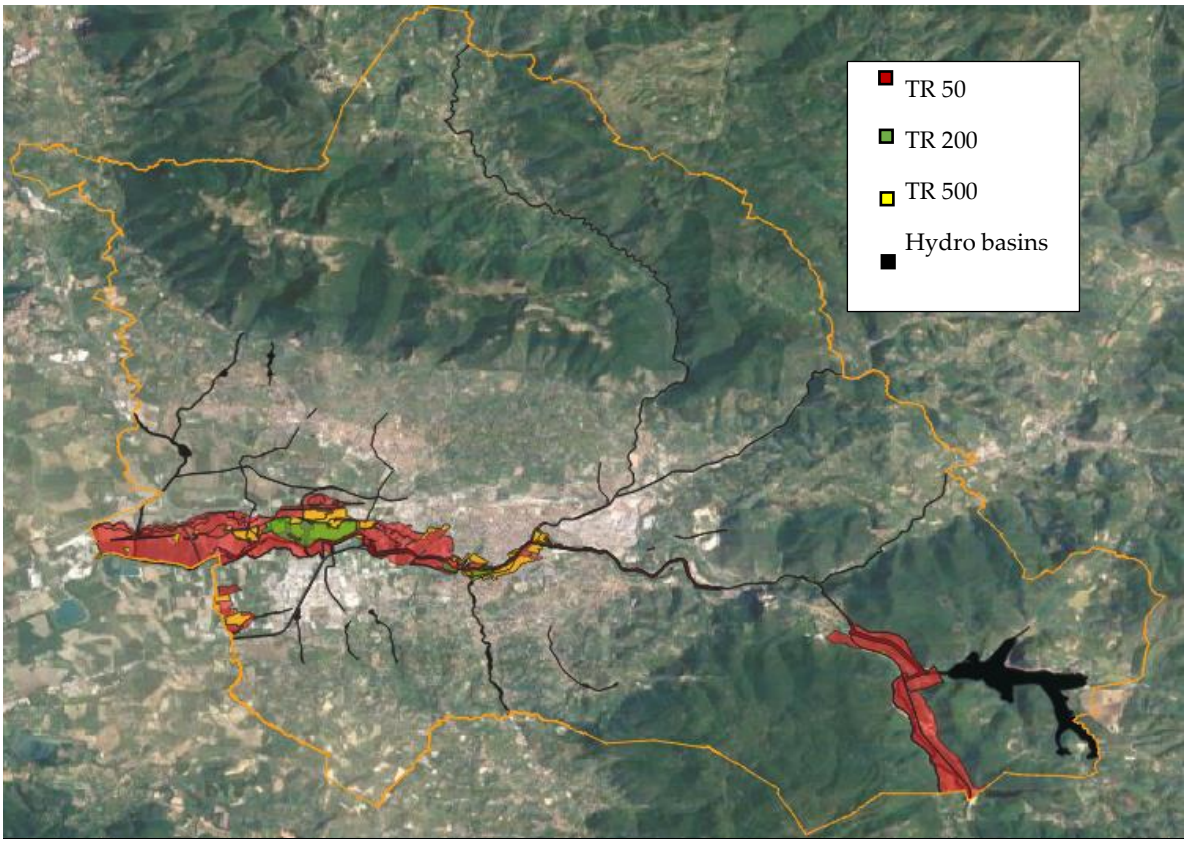


*Figure 79. Flooding risk zones with respect to Terni Municipality (red: Zone A; green: Zone B; yellow: Zone C)*

As already carried out in a previous work [143], by means of the open-source QGIS application, a map with the coordinates of the substations has been overlapped to the map defining the areas with the same probability of a flooding event (*Figure 80* and *Figure 79*). Therefore, a correlation between the floodable areas and the return times in case of such events has been defined.

In order to evaluate the probability that an extreme event actually affects a substation, a vulnerability coefficient has been taken into account. The coefficient can vary in the range between 0 and 1 and corresponds to the probability that a flooding event leads to a fault. For each substation, the vulnerability coefficient has been evaluated by means of an empirical approach, as presented in

[144], because of the absence of proper historical data correlating weather events and substation faults. Coefficient values used in the simulation model are listed below:

- for each underground substation, the coefficient has been considered equal to 1, assuming that a flooding event leads to a disconnection of that asset;
- for each substation that could be affected partially by the floods, an of uncertainty degree has been considered. Substations that can be included in this group are those inside buildings, boxes and prefabricated systems. The vulnerability coefficient has been evaluated equal to 0.75;
- for the secondary substations raised off the ground (e.g. pole-mount transformers), the coefficient has been considered null since a flooding event is not able to cause the disconnection of the asset.

The action area considered in this work is the TDE's MV/LV distribution network. It is connected to the Italian National Transmission Grid (NTG) by means of 3 primary substations and 7 HV/MV transformers. The network also includes 6 MV/MV substations, since there are two different voltage levels, namely 10 kV and 20 kV. LV customers are supplied by means of 588 secondary substations (with an aggregate of 127 MVA installed power), 96 of them are controlled remotely by a SCADA system.

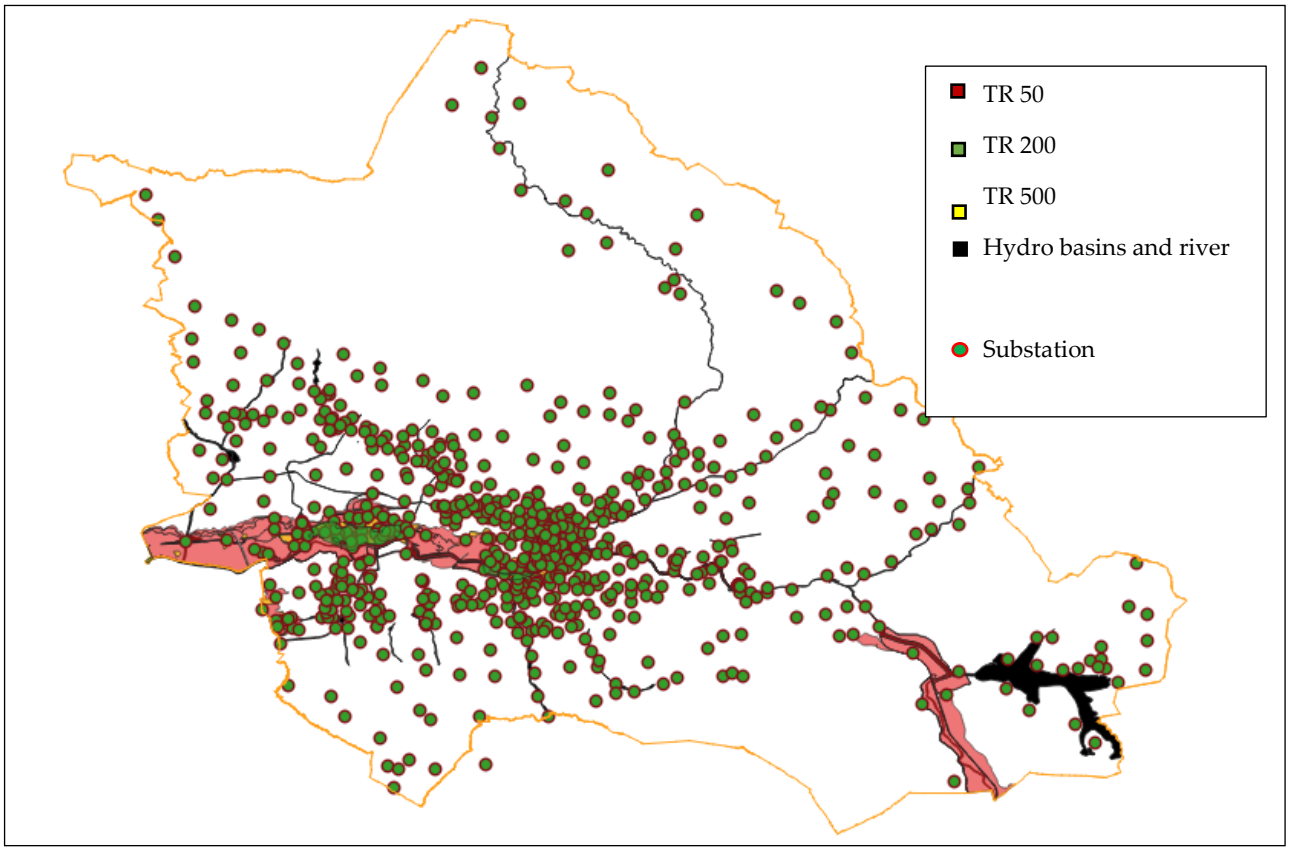


*Figure 80 Flooding risk areas with respect to electric substations in Terni Municipality*

Considering the aim of the resilience assessment, it is worth presenting the main geographical characteristics of the area which is the whole municipality of the city. The surface is 211 km2, the valley climbs from 104 m to 1017 m above sea level, while 52.6% of its territory consists of mountains, 31.6% are hills and 13.4% is lowland. The average maximum temperature is 21.1 °C,

whereas the minimum one is -10°C; lastly, the average amount of rainy days during one year is 86 (852 mm is the average rain level).

#### 4.2.3.2 *Resilience assessment against flooding events [145]*

Simulation results are presented in this subsection. Firstly, the assumptions made in order to carry out the analysis are listed below:

- all external interconnections (at HV and MV levels) are fully available, since this depends on other stakeholder infrastructures (i.e., the NTG and the networks of other DSOs); however, if TR values of these infrastructures are known, the algorithm can easily take them into account;
- vulnerability has been accounted based on the experience of the network operators, because of the absence of proper historical data that correlate weather events to substation faults;
- the algorithm does not take into account current limits that a network reconfiguration could overcome;
- the TR of the substation not comprised in the flooding area has been assumed equal to 999, independently of the vulnerability;
- all remedial actions considered in this study for the improvement of the resilience are at MV level; the LV grid is always assumed radial both in topology and in operation;

*Table 17 Substations sorted by impact (NUD)Table 17* shows the results of the simulations: each substation corresponds to a row and its identifier is reported in column 2. In *Table 17*, substations are sorted by NUD, which does not depend on the TR evaluation since it is the actual number of users that could be disconnected from the grid in case of the node loss.

*Table 17 Substations sorted by impact (NUD)*

| # | ID | TR | Substation Vulnerability | Connected Users | NUD |
|---|---|---|---|---|---|
| 1 | 0011012 | 999 | 0.75 | 0 | 2228 |
| 2 | 1021022 | 999 | 0.75 | 327 | 1952 |
| 3 | 1021372 | 67 | 0.75 | 297 | 1283 |
| 4 | 0011001 | 999 | 0,75 | 0 | 1176 |
| 5 | 1021326 | 999 | 0.75 | 217 | 840 |
| 6 | 1021462 | 999 | 1 | 220 | 785 |
| 7 | 0011003 | 999 | 0.75 | 0 | 776 |
| 8 | 1021585 | 999 | 0.75 | 39 | 760 |
| 9 | 1021341 | 999 | 0.75 | 91 | 741 |
| 10 | 1021147 | 999 | 1 | 41 | 712 |
| … | … | … | … | … | … |
| 597 | 1021001 | 999 | 0 | 1 | 1 |

*Figure 81* shows the possible events of substation disconnection as a function of their impact on the network, represented in terms of number of users disconnected and event probability, represented as return period.

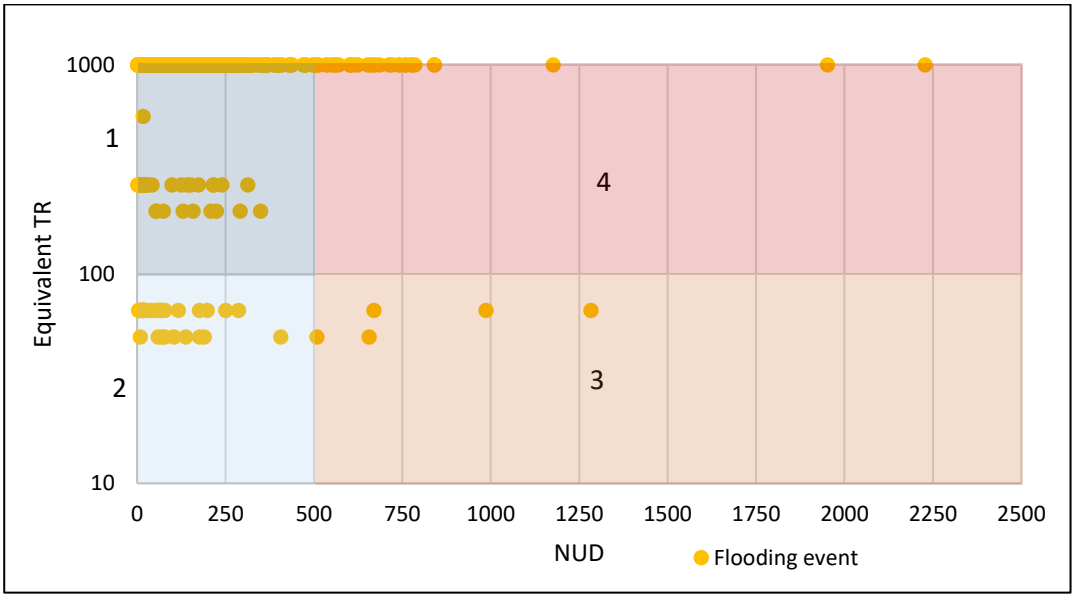


*Figure 81 Flooding events on substation represented as NUD and equivalent return time.*

In order to define if events would have a low or high impact, a benchmark equal to 500 NUD has been used; it is the 95th percentile of the statistical distribution (number of events versus NUD), as shown in *Figure 82*. Moreover, 500 NUD is about 4.5 times the average number of user connected at a substation in the distribution network (i.e., 110 users).

Therefore, four areas can be identified in the diagram:

- at the top left (1), the area collects events having low impact but high return period (i.e. the flooding risk is not foreseen by the hydrogeological authority);
- at the bottom left (2), the area corresponds to events that have both low TRe and low NUD
- at the bottom right (3), an area with high NUD and low TRe has been identified;
- at the top right (4), the area refers to events that have not so high probability to occur but that would cause a high NUD;

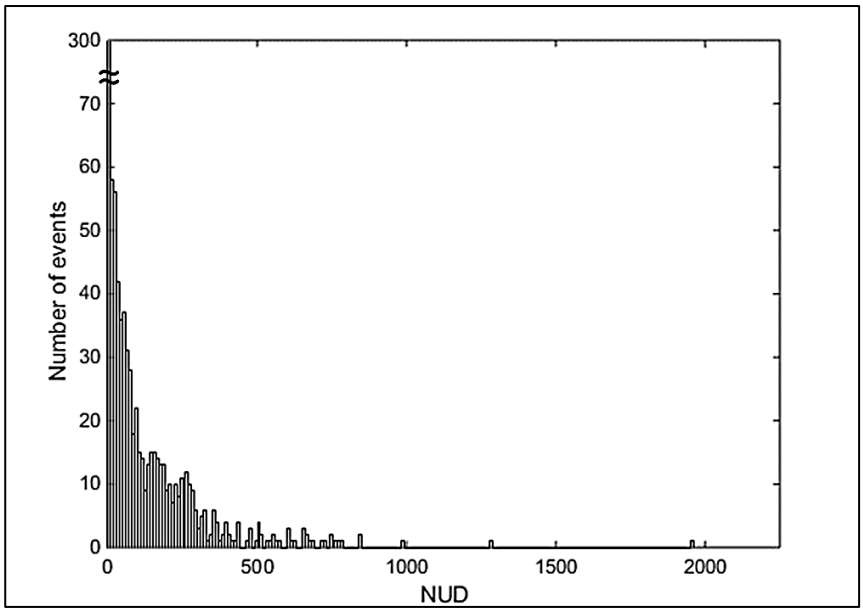


*Figure 82 Statistical distribution of flooding events in terms of NUD.*

In *Table 18*, substations are sorted by IRI (considering only those having NUD greater than 500), evaluated according with equation (3). This table provides the priority of the interventions to increase the grid resilience with respect to floods: substations with higher IRI have a higher priority of interventions. If two substations had the same IRI (which is a very rare case, however), the one with the highest NUD would have higher priority. It is worth pointing out that the case of substations with both same IRI and NUD may occur only to substations with very low IRI and NUD values, corresponding to very low priorities. Finally, column 1 of *Table 18* (the substation progressive number #), which refers to the NUD ranking shown in *Table 17*, is reported in order to compare the two different sorting strategies.

*Table 18 Substations sorted by IRI*

| # | ID | TR_Flood | IRI | Users | NUD |
|---|---|---|---|---|---|
| 3 | 1021372 | 67 | 19.14925 | 297 | 1283 |
| 14 | 1021713 | 50 | 13.12 | 148 | 656 |
| 1 | 0011012 | 999 | 2.23023 | 0 | 2228 |
| 2 | 1021022 | 999 | 1.953954 | 327 | 1952 |
| 4 | 0011001 | 999 | 1.177177 | 0 | 1176 |
| 5 | 1021326 | 999 | 0.840841 | 217 | 840 |
| 6 | 1021462 | 999 | 0.785786 | 220 | 785 |
| 7 | 0011003 | 999 | 0.776777 | 0 | 776 |
| 8 | 1021585 | 999 | 0.760761 | 39 | 760 |
| 9 | 1021341 | 999 | 0.741742 | 91 | 741 |
| … | … | … | … | … | … |
| 597 | 1021001 | 999 | 0.001 | 1 | 1 |

Additional indices, evaluated according with the equations previously described, are reported in *Table 19*. They provide the comparison between ex-ante and ex-post status of network. The ex-post evaluation has been carried out considering all remedial actions on the basis of the priority established by the IRI values in *Table 18*and referring to all substations having a NUD greater than 500.

*Table 19 Resilience indices comparing ex-ante and ex-post status of the network*

| **Additional resilience indices** | **ex-ante** | **ex-post** |
|---|---|---|
| Degree of back-feeding – IGCR | 0.7830 | 0.8637 |
| Degree of vulnerability – IGVU | 1.6254 | 1.2534 |
| Degree of resilience – IGRR (flooding events) | 0.9981 | 0.9984 |

The results are reported in Figure 7, which represents flooding events, using the same approach of Figure 5. Finally, Figure 8 shows the effects of remedial actions comparing ex-ante and ex-post impact in terms of NUD for the first ten substations listed in *Table 17*.

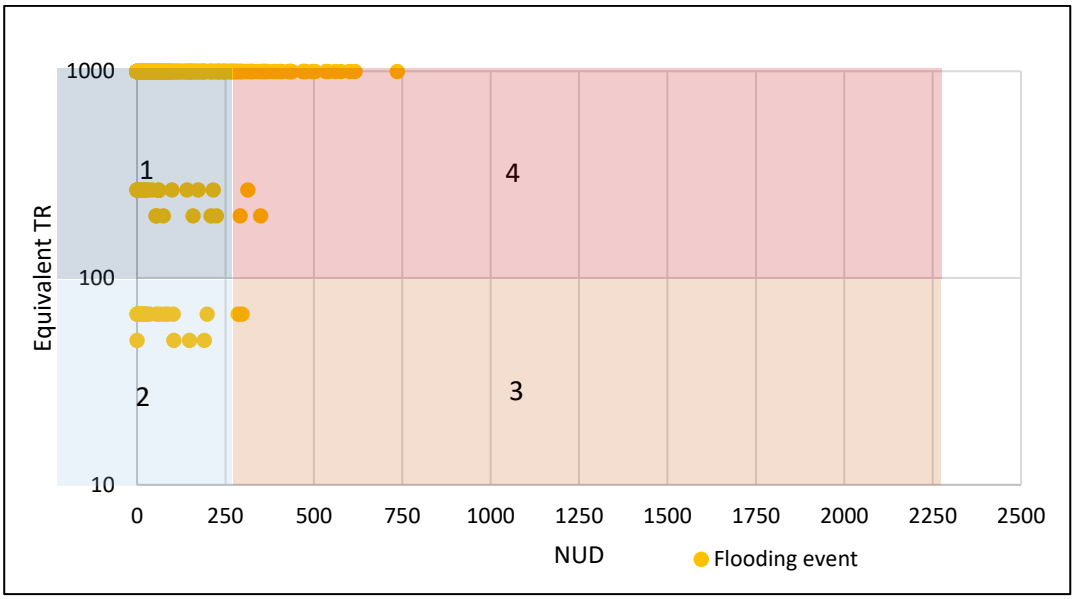


*Figure 83 Flooding events on substations represented in terms of NUD and equivalent return time (ex-post evaluation).*

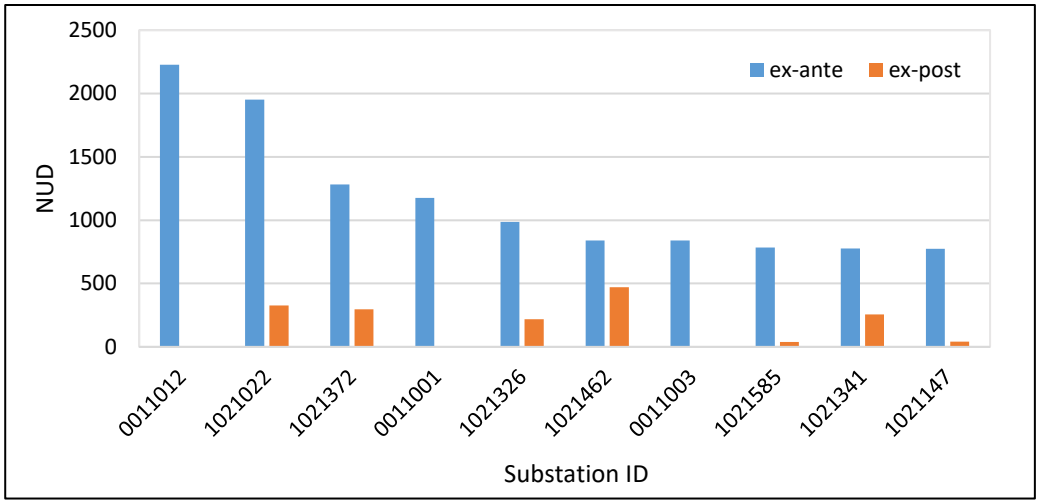


*Figure 84 Comparison between ex-ante and ex-post impact for the first ten substations listed in Table 17.*

*Table 17* shows that the algorithm identifies the weakest sections of the network, that are those for which a substation loss causes an impact higher than the number of users connected. This result does not depend on the type of threat. On the other hand, *Table 17* provides the ranking based on IRI: this could provide a different point of view in order to define the intervention priority on the grid that can improve resilience according with a specific threat.

With respect to *Figure 81*, it is worth pointing out that, if different threats affecting a substation were considered, each event bullet could change its vertical position, because of a $TR_e$ variation with respect to a specific threat (i.e., a higher or lower vulnerability of the asset against the threat). On the other hand, the bullet cannot move horizontally since its abscissa represents the effect on the grid in terms of NUD, whenever that asset is lost.

As shown in *Table 19*, the IGRR ex-ante is very close to 1 and it shows that the network is already resilient with respect to the flooding events. This fact is also supported by the high degree of meshing of the network: in case of a substation loss, a back-feeding of the other substations is normally allowed (more than 78% of the users can be already supplied in MV back-feeding, see IGCR in Table 3), since the case of substations supplied in antenna is very limited.

According to the previous sections, the ex-ante assessment identifies intervention that can be applied in a development plan of the DSO. Then, the model has been applied to simulate the effect of the flooding events on the distribution network in case of full achievement of the selected interventions (the applied remedial actions refer to all substations having a NUD greater than 500).

According with the reported values in *Table 19*, the proposed interventions have not notable effects on the network in terms of its resilience with respect to flooding events (the IGRR rises from 0.9981 to 0.9984, i.e., the increase is only about 0.02%).

Considering the proposed intervention, the improvement of the degree of vulnerability of users is notable (the IGVU index decreases from 1.6254 to 1.2534, i.e., the reduction is more than 22%, see Table 3).

With respect to the network back-feeding index, the remedial actions produce more evident benefits (the IGCR index, which does not depend on the type of threat, rises from 0.7830 to 0.8637, the increase is about 10%, see Table 3), confirming that the network's meshing is increased anyway. With respect to ex-post analysis, *Figure 83* shows that the interventions are going to reduce the

impact of flooding events, as well as they are going to improve the resilience of the network itself. In area 4 of the figure, the reader can still observe some substations which have a NUD more than 500: this is due to the fact that all hypothesized remedial actions at MV level cannot reduce the NUD under the number of LV users supplied by the substation, because the LV network is full radial.

*Figure 84* clearly shows the effectiveness of the remedial actions proposed by the simulation model, outlining the notable reduction of NUD for the most critical assets reported in *Table 17*.

#### 4.2.3.3 *Resilience assessment considering ice sleeves [146]*

This subsection presents the resilience assessment in respect of ice sleeves on overhead lines. The TR index has been calculated in accordance with the standards European standard CEI EN 50341 (EN 50341-2-13), which defines the criteria for sizing overhead electrical lines with nude conductors, based on the stresses resulting from the presence of ice sleeves and the simultaneous action of the wind, and it also defines criteria to assess TR value of lines already in operation based on their mechanical characteristics and geographical location. With respect to the Terni distribution network, an assessment of TR of the existing lines has been carried out and then the procedure has been implemented.

*Figure 85* represents the possible events of disconnection as a function of their impact on the network, evaluated in terms of number of users disconnected and their probability, represented as return period. In the diagram, 4 areas can be identified:

- Events in the area in the upper left part of the graph have both low probability and their impact on the network is low.
- The area in the bottom left is referred to events having low impact but high return period.
- The bottom right area corresponds to events for which both high NUD and high TR have been evaluated. This is the focus area where works on the network are prioritized based on the threat (i.e. ice sleeves).
- The upper right area is referred to events that are not so much probable but for which a high NUD is expected. These events could define a focus area based of new threats.

Processing the results of the simulations, the additional indices proposed by TDE have been calculated, thus obtaining the following values:

- IGCR = 0,7830
- IGRR = 0,9979
- IGVU = 0,471

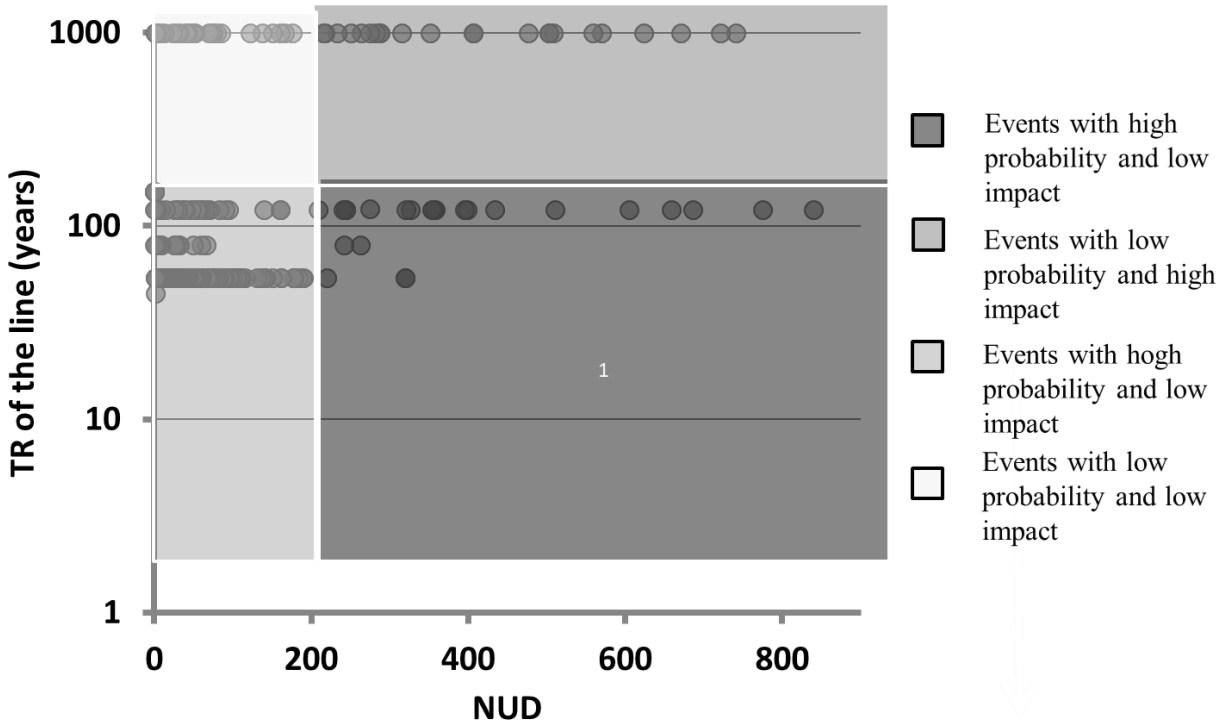


*Figure 85 Return period of events on the network as a function of number of users disconnected (ex-ante results).*

Based on the results obtained from simulations, 5 possible lines of action were identified. It should be noted that the results of the simulations, also show that it is one of the most important actions for improving the grid resilience, as shown in this study and envisaged in the DSO's Network Development Plan.

Once the actions have been identified on the basis of the results described in the previous section, the rules representing the network connection were modified accordingly, and the simulation model for the evaluation of the IRISS and IRESS relating to the post-intervention scenarios was applied again.

The expected impact, i.e. the improvement of the risk index, was also assessed as the difference between the risk index under post-intervention conditions and the risk index under pre-intervention conditions, referring to each node in the network. The same procedure is applied to evaluate the resilience index.

In particular, with respect of post-intervention scenarios, simulation results are reported in tables not shown here for the sake of brevity. Table I is shown as example.

The first table shows the list of SSs ordered by decreasing IRISS values, together with the NUD, TR and IRE values. SSs that fall within the 10ì% threshold set in the previous section are at the top of the table. The secondary substations and their return times are listed in the second table. The third table lists the all branches and their corresponding return times with resilience values, depending on the disconnected users and the reference territorial area.

A comparison between the values of IRISS and IRESS is instead shown in the fourth table for the SSs and in particular for those that exceed the threshold referred to in the table (IRISS,EX-ANTE > 0.4296, corresponding to the value that identifies 10% of the SSs that are more critical with respect to the threat considered.

The analysis of the results shows that, as expected, the proposed actions improve the risk and resilience indices. The impact is prevalent on 10% of the most critical SSs, but there are also positive effects in some of the remaining 90% SSs.

*Table 20 Indices For The 5 Most Critical SS Evaluated For One Interconnection Point.*

| SS | NUD | TR | IRI (MV) | IRE (LV) |
|---|---|---|---|---|
| #1 | 190 | 54 | 3,5185 | 0,2842 |
| #2 | 151 | 54 | 2,7963 | 0,3576 |
| #3 | 142 | 54 | 2,6296 | 0,3803 |
| #4 | 131 | 54 | 2,4259 | 0,4122 |
| #5 | 274 | 122 | 2,4259 | 0,4453 |

*Table 21 Intervention Values Of The Additional Indices Introduced by this work*

| Indices | | ex-post | ex-ante |
|---|---|---|---|
| Degree of back-feeding | IGCR | 0.8068 | 0.7830 |
| Degree of resilience | IGRR | 0.9981 | 0.9979 |
| Degree of vulnerability | IGVU | 0.2859 | 0.4711 |

With respect to the additional indices introduced by TDE, the analysis of the results obtained produced the result summarised in *Table 21*. Based on the values considered, it is worth pointing out that the proposed actions have a low impact on the network in terms of its resilience, since the network is already adequately resilient with respect to the threat considered. The value of the degree of pre-intervention resilience is already very close to the unit, it is in fact 0.9979 due to the low probability of ice sleeves occurring with the combined action of wind in the geographical area of action; the percentage increase is in fact only 0.02%.

Considering the network back-feeding index (which is independent of the threat considered), the proposed actions have produced a more evident benefit, in fact the percentage increasing of this index was 3.04%, confirming that the network's meshing was increased.

Considering the proposed intervention, it is even more valuable the improvement of the degree of vulnerability of users, which does not depend on the threat. In fact, this index has decreased by 39.31%, confirming the effectiveness of the proposed actions regardless of the occurrence of ice sleeves with the action of wind in the municipality of Terni. *Figure 86* reports a drastic reduction of the events that affect a wide number of users, compared to *Figure 85*. Furthermore, Figure 5 shows that the magnitude of the most critical event is reduced by 61%. In conclusion, the proposed actions do not increase the resilience of the network with respect to this specific threat, since it is already immune (the index is in fact close to unity).

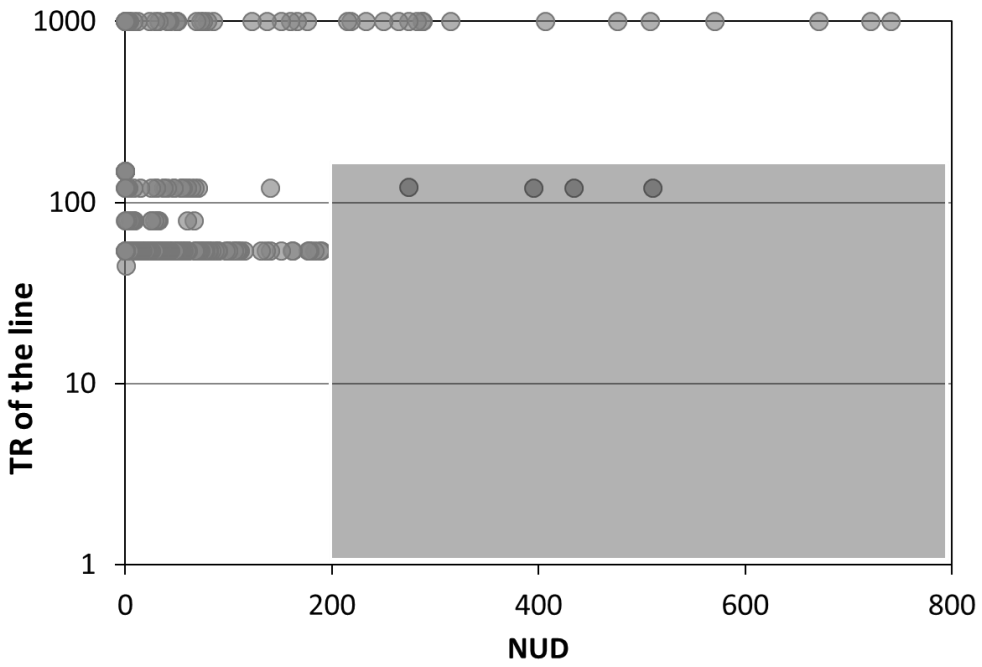


*Figure 86. Return period of events on the network as a function of number of users disconnected (ex-post results)*

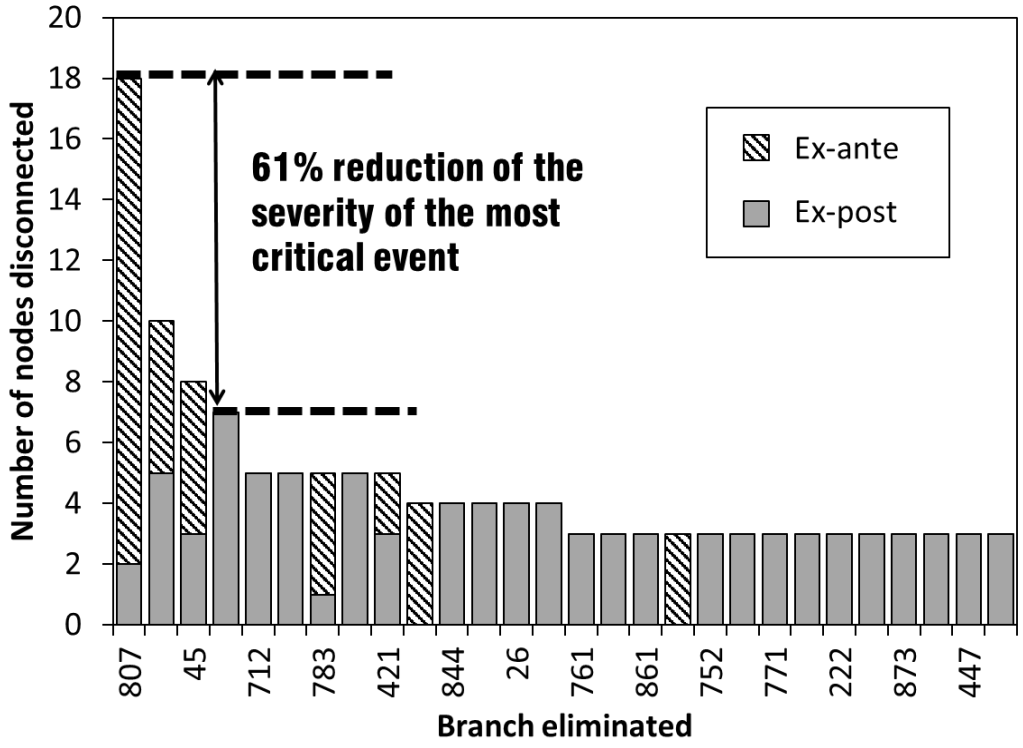


.

*Figure 87 Reduction of the severity of the most critical event.*

Otherwise, the same improvements on the network allow to increase network meshing (as evidenced by the modest increase in the index related to back-feeding), and drastically reduce the number of disconnected users if events of any nature occur in the areas covered by the intervention itself. This approach does not take in account the recovery time of the system after the event, which

depends on the fault location along the distribution grid. Further indexes, able to evaluate how fast the normal operation is restored, could be considered to refine the resilience assessment.

#### 4.2.3.4 *Resilience assessment considering heat waves [147]*

This Section presents the methodology used to evaluate the TR of fault events caused by HWs. According to Section II, the assumption that HWs affect only the substations (i.e., at each cycle of the algorithm, a node is eliminated from the graph) is made. The probability that a substation is disconnected because of a HW depends on two quantities, namely the return time of the weather event and the vulnerability of the substation (i.e., the fault probability of the asset when the event occurs).

HWs can be defined as a period of consecutive days where temperatures are excessively higher than normal, as in [148]. According with [149], a 3-day period is suitable for defining these events that have tremendous impact; in order to understand if a HW occurs, the annual maxima of 3-day-mean area-averaged daily maximum temperatures (TX3X) is analysed. Moreover, it is worth noting that the TR of HW is going to increase year by year, as reported in [150] and [149]. With respect of the frequency of fault events, it has been assumed that a HW with a TX3X of 34 °C can be a severe condition for the heat transfer in the SS. In the analysis presented in this work, the TR of such extreme weather conditions has been assumed equal to 17.7 years, as in [149].

Following an empirical approach based on DSO's experience and know-how [151] and [152], a vulnerability coefficient has been defined for each substation. Vulnerability, as the opposite of robustness, can be defined as the uncertainty and severity of the consequences for an asset, given the occurrence of the initiating event [153]. Such coefficient, varying in the range between 0 and 1, corresponds to the probability that a HW event leads to a fault and depends on the substation typology, as well as on the typology of the medium voltage panel (MVP) installed in the substation.

Regarding substation typology, all existing substations in the action area (i.e., the distribution network in the city of Terni) have been subdivided as in the following:

- Tower Substation (Type 1)
- Undergrounded Substation (Type 2)
- Pole Mounted Distribution Transformer (Type 3)
- Prefabricated Substation (Type 4)
- Building Undergrounded Substation (Type 5)
- Box Substation (Type 6)
- Raised Prefabricated Substation (Type 7),

Different vulnerability coefficients have to be assigned to each substation type: for instance, an undergrounded substation is expected to be more vulnerable to HWs than a tower substation. Moreover, substations of the same typology may respond differently depending on the MVP installed. In this regard, three different MPV types have been considered:

- SF6 insulated MVP (Type 1)
- Protected MVP (Type 2)
- Air insulated MVP (Type 3)

where protected MVPs consist of modular blocks designed for protecting lines and transformers, widely used in the distribution networks. In the study reported in the work, it is

assumed that air insulated MVPs are less efficient and more vulnerable to severe thermal transients; therefore, a higher vulnerability coefficient is assigned to Type 3 MVPs. The overall vulnerability coefficients assigned to the substations in the action area are reported in *Table 22. Table 23* reports the substation TRs used in this study for HW threat, also in this case considering both the substation and the MVP typologies, as well as considering a 17.7 years TR of a HW in the territory of Terni. In Terni, the average maximum temperature is 21.1 °C, whereas the minimum one is -10°C. All data regarding weather conditions used in this study are gathered by the "Federico Cesi" observatory of Terni [154].

*Table 22 Substation Vulnerability Coefficients*

| **Substation Type** | **Vulnerability coefficients for different types of MVP** | | |
|---|---|---|---|
| | **MVP 1** | **MVP 2** | **MVP 3** |
| **1** | 0.1 | 0.175 | 0.225 |
| **2** | 0.3 | 0.525 | 0.675 |
| **3** | 0.1 | 0.175 | 0.225 |
| **4** | 0.2 | 0.35 | 0.45 |
| **5** | 0.1 | 0.175 | 0.225 |
| **6** | 0.2 | 0.35 | 0.45 |
| **7** | 0.1 | 0.175 | 0.225 |

*TABLE 23 TR (Years) for the Substation Outage due to Heat Wave Event*

| **Substation Type** | **TR for different types of MVP** | | |
|---|---|---|---|
| | **MVP 1** | **MVP 2** | **MVP 3** |
| **1** | 177.99 | 101.71 | 79.11 |
| **2** | 59.33 | 33.91 | 26.36 |
| **3** | 71.19 | 71.19 | 71.19 |
| **4** | 88.99 | 50.85 | 39.55 |
| **5** | 177.99 | 101.71 | 79.11 |
| **6** | 88.99 | 50.85 | 39.55 |
| **7** | 177.99 | 101.71 | 79.11 |

Numerical results presented in this Section have been calculated according to the following assumptions:

- interconnections with other networks are fully available, although this depends also on other stakeholder infrastructures (i.e., the NTG and the networks owned by other DSOs);
- substation vulnerability has been evaluated according to the DSO's experience, since historical data that can correlating HWs and substation faults are not available;
- network nodes are stiff derivations with a 999 years TR;

- line capabilities are not considered by the algorithm (i.e., any network reconfiguration is implemented disregarding current limits);
- the software takes into account some network peculiarities, such as different voltage levels and different transformers hourly indices at the primary substation, in order to reduce the execution time for implementing network reconfiguration;
- the LV network is both radially structured and radially operated;
- remedial actions aimed at improving the resilience of the network are at MV level.

Table III reports the substations in the network sorted by NUD in decreasing order; for each substation, the IRI index referred to HWs (IRI_HW) is also reported.

*Table 24 Substations sorted by impact (NUD)*

| N° | NUD | Users | IRI_HW |
|---|---|---|---|
| 1 | 1952 | 327 | 38.27451 |
| 2 | 1283 | 297 | 16.24051 |
| 3 | 986 | 317 | 12.48101 |
| 4 | 840 | 217 | 16.47059 |
| 5 | 785 | 220 | 30.19231 |
| 6 | 760 | 39 | 9.620253 |
| 7 | 741 | 91 | 9.379747 |
| 8 | 712 | 41 | 20.94118 |
| 9 | 671 | 576 | 25.80769 |
| 10 | 669 | 419 | 19.67647 |
| … | | | |
| 935 | 0 | 0 | 0 |

*Figure 88* plots the possible events of substation disconnection as a function of their impact on the network, considering both: the substation equivalent TR (i.e., the event probability) and NUD (i.e., the impact of the event).

A NUD threshold value equal to 500 has been considered in order to classify the impact of each HW event: NUD values higher than 500 correspond to high impact events, whereas NUD values lower than 500 correspond to low impact events. Such threshold value is about 4.5 times the average number of user supplied by a substation in the distribution network (i.e., 110 users). According to the threshold, four areas can be identified:

- area 1: events with low impact (i.e., low NUD) and low probability (i.e., high TR);
- area 2: events with low probability and high impact;
- area 3: events with high impact and high probability;
- area 4: events with low probability and high impact.

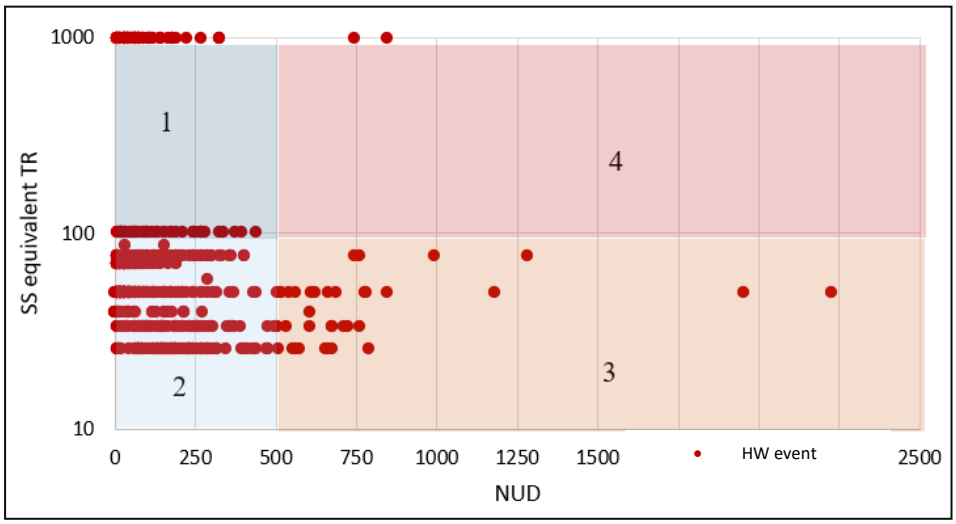


*Figure 88 HW events on substations represented in terms of NUD and equivalent TR (ex-ante evaluation, see text for details).*

*Table 25 Substations sorted by IRI*

| N° | NUD | Users | IRI_HW |
|---|---|---|---|
| 1 | 1952 | 327 | 38.27451 |
| 5 | 785 | 220 | 30.19231 |
| 9 | 671 | 576 | 25.80769 |
| 11 | 656 | 148 | 25.23077 |
| 12 | 652 | 176 | 25.07692 |
| 16 | 560 | 286 | 21.53846 |
| 8 | 712 | 41 | 20.94118 |
| 17 | 553 | 0 | 21.26923 |
| 10 | 669 | 419 | 19.67647 |
| … | | | |
| 927 | 0 | 0 | 0 |

*Table 26 Resilience indices comparing ex-ante and ex-post status of the network*

| Additional resilience indices | ex-ante | ex-post | Additional ex-post |
|---|---|---|---|
| **Degree of back-feeding – IGCR** | 0.7830 | 0.8637 | 0.8367 |
| **Degree of resilience – IGRR (HW events)** | 0.9742 | 0.9747 | 0.9768 |
| **Degree of vulnerability – IGVU** | 1.6254 | 1.2534 | 1.2534 |

*Table 25* reports the substations in the network sorted by IRI_HW in decreasing order (numbers in the first column refer to the NUD ranking reported in *Table 24*). Such sorting establishes the hierarchical order for the interventions required to increase resilience to HWs: higher priority of intervention is required for the substations with the highest IRI_HW values.

The IGCR, IGRR and IGVU indices are reported in *Table 26* which provides the comparison between ex-ante and ex-post status of network, evaluated considering all remedial actions based on the priority established by the IRI values in *Table 25*, considering only secondary substations with a NUD higher than 500. An additional ex-post analysis has also been carried out, considering the possibility to change the asset vulnerability (i.e., changing the MVP or the type of substation).

*Figure 89* and *Figure 90* reports the effects of the remedial actions of the ex-post and additional ex-post analysis, respectively.

As shown in Section 4.2.2, the developed procedure allows identifying which substation loss could cause an impact higher than the number of users connected, namely, the most vulnerable part of the grid independently from the type of threat. These results are summarized in Table III. With respect to HWs, *Table 25* shows the IRI of the substations: it is worth noting that the ranking is different from the one in *Table 26*, since in this case also the probability of fault is taken into account. Therefore, a development plan of a DSO has to take into account these vulnerabilities, considering also the impact of each specific threat.

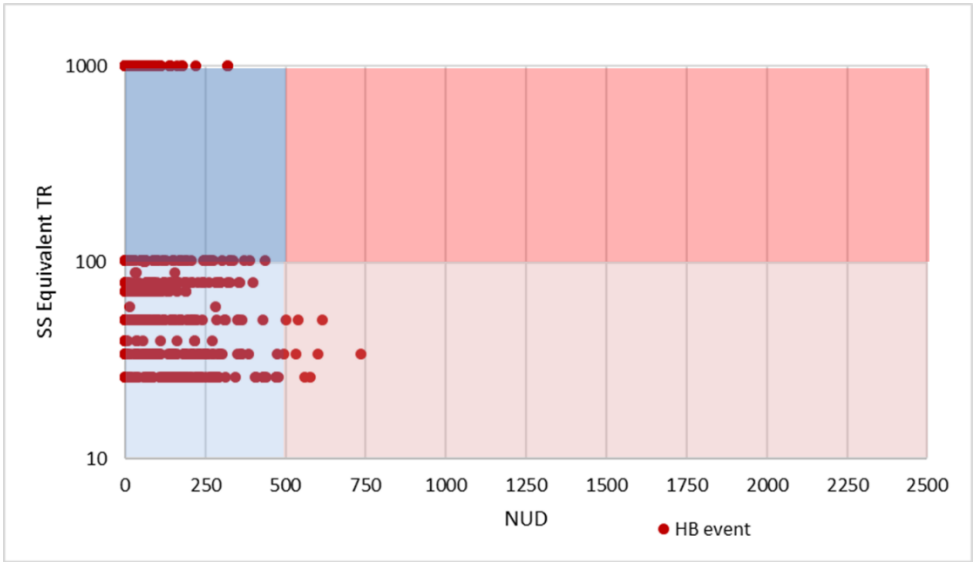


*Figure 89 HW events on substations represented in terms of NUD and equivalent TR (ex-post evaluation, see text for details).*

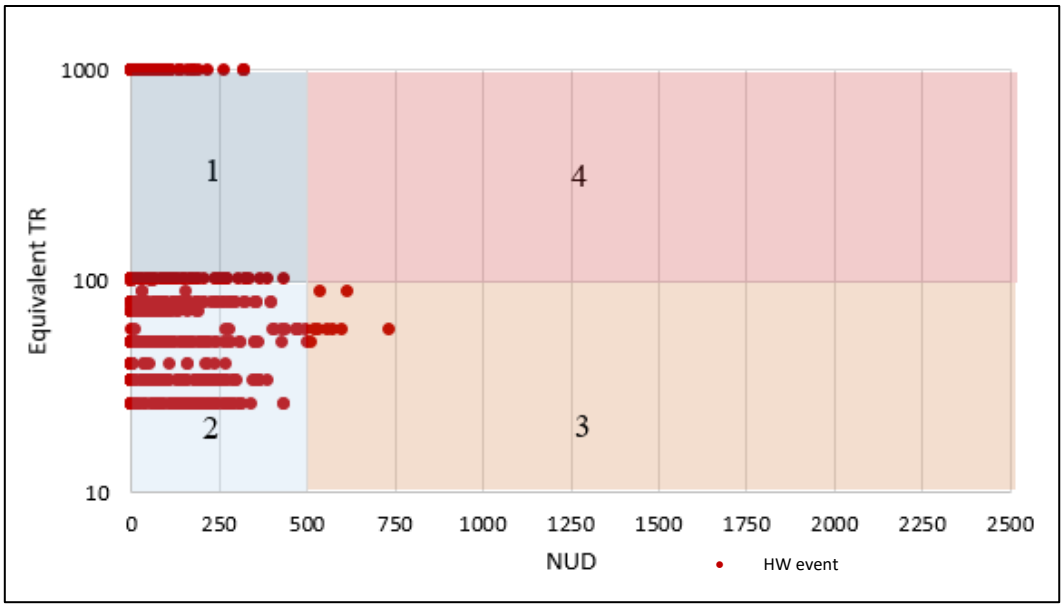


*Figure 90 HW events on substations represented in terms of NUD and equivalent TR (additional ex-post evaluation, see text for details).*

Moreover, starting from the present status of the network, *Figure 88* shows also an intervention ranking; notably, area 4 shows the interventions that would not increase resilience against HW but that could be meaningful if other threats were considered. On the other hand, area 3 reports the most significant events in respect of HW events.

The algorithm may be used to define and evaluate a development plan; in the study reported in the work, two types of remedial actions are considered. The first bunch of interventions consist of increasing the meshing degree of the network, by adding new lines and by reducing the number of substations whose outage would lead to a NUD significantly higher than the number of connected users. The second bunch of interventions (defined as additional ex-post analysis) assumes that the type of substations and the type of MVP can be changed, improving the resilience of the single asset. These scenarios have been simulated by the procedure applying remedial actions only to substation having a NUD greater than 500.

From results reported in last table, the proposed interventions strongly improve the degree of vulnerability of users, since IGVU index decreases from 1.6254 to 1.2534, with a reduction of about 22%. On the other hand, they have not notable effects on the network in terms of resilience to HW events: the IGRR rises from 0.9742, to 0.9747 in the first ex-post analysis and to 0.9768 in the additional ex-post analysis. This is because the value of IGRR ex-ante is very close to one, indicating that the grid is already resilient to HWs The implementation of the development plan would produce more evident benefits in terms of network back-feeding. In this respect, the IGCR index increases from 0.7830 to 0.8637, with a 10.3% improvement of the meshing degree of the network, despite the meshing degree of the network ex-ante is high, since about 78% of the grid customers can be already back-fed at MV level. Lastly, it has been shown that both the proposed development plans are able to strongly reduce the most severe HW events, corresponding to area 3.

### 4.2.4 *A summary of the resilience assessment*

In the last decade, extreme natural events, such as floods, ice and windstorms, hurricanes, tsunamis and earthquakes, have had a tremendous impact on countries' public security and economic prosperity. Stakeholders are considering climate-related risk management of critical

infrastructure as a dominant theme, because of the intensification of magnitude and frequency of disruptive weather events and natural disasters that have caused notable damage of the infrastructures.

From this perspective, electrical networks can be considered more critical in comparison with all other infrastructures (e.g., heating, water, mobility, telecommunications, etc.), being the main pillar of these ones. Therefore, on the one hand, making networks more resilient leads to a reduction of the global impact on essential and interdependent services due to natural exceptional events; on the other hand, the improvement of resilience requires new tools for planning and design of future distribution networks.

In this work, it has been proposed a tool able to evaluate the resilience of a distribution network against flooding threats. The starting point is the network graph, obtained by closing all the switches and all the equipment needed to perform back-feeding. Every possible scenario, representative of all threats and obtained by eliminating one asset at a time (i.e. a substation or a line), is then analyzed by Dulmage-Mendelsohn decomposition carrying out the list of disconnected nodes. On the basis of this table, all relevant indices are computed. All possible remedial actions have been identified and rated by their effectiveness. *Figure 91* reports resilience assessment of different treats in the same graph considering the network as is. It is worth noting that some SS are vulnerable only to one treat whilst others are vulnerable to two of them. In respect of ice sleeves, their impact is less than flooding or HW since it affect only lines.

The improvement of index values due to the implementation of the identified remedial actions have been also evaluated, quantifying the possible benefits. Finally, these countermeasures are consistent with those foreseen in the DSO development plan.

The generality of the proposed procedure and indices, as well as the robustness of the methodology implemented for the evaluation of the remedial actions make this tool applicable for the assessment of resilience of distribution networks with respect to flooding and more threats.

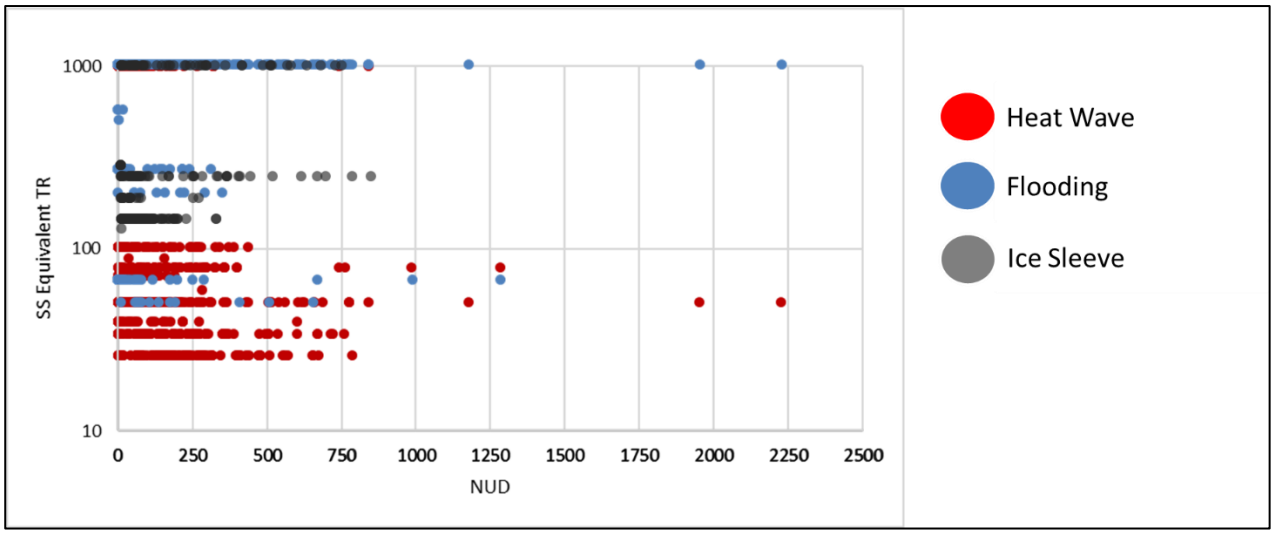


*Figure 91 Resilience assessment of different treats in the same graph.*

# 5 Real – time operations for Power Quality Improvement: Flexibility Sources and their management

The notable amount of energy produced by RES by a DGs, connected at the DN leads to new challenge for the stakeholders and notably for the DSO, in charge to ensure and enhance power quality to consumers and producers.

As already explained in Section 2.1, new technologies are going to be at the disposal of DSO in order to manage in real – time the network in a more efficient way; in this upcoming scenario, DSO could use different levers for the management of the distribution network for better fulfilling the current and future requirements. With respect to the traditional tasks such as the power quality (i.e., outages reduction and voltage within the limits) and the energy efficiency, they would be further enhanced but in addition DSO would be able to participate in a more active way in the management of the grid providing network observability, foreseeing the load profiles at the Primary Substation and the others Transmission/Distribution connection points leveraging on an Advanced Metering Infrastructure (AMI) and exploitation of Energy Flexibility Resources, controlling them DSO is able to manage possible deviation caused by external and unforeseen sources.

These two pillars (i.e., AMI and Flexibility) have been addressed by this work and this chapter is going to present enabling tools and their exploitation that have been demonstrated in the Terni Pilot Site, namely the headquarters of ASM Terni S.p.A. and the distribution network own and managed by its business unit, Terni Electrical Distribution. Enabling technologies that have been actually used in the demonstration activities are described in Section 5.1, whilst Sections 5.2 and 5.3 report their application on energy efficiency and adequacy of electrical parameters, respectively.

In respect of Advanced Metering Infrastructure, Terni has participated in Horizon 2020 project Nobel GRID, [3], which has enriched the distribution network with a notable amount of innovative AMI that are going to dramatically change paradigms of metering infrastructures. The aim of this new framework, presented in Section 5.1.1, is to provide, from the meter side, an alignment of the different standards that the electronic Smart Meters currently implement, making data available over a proper Virtual Private Network in which DSO and stakeholders can work to provide their services. The biggest innovation is that these data can be collected integrating the existing Smart Meters including a IoT device (e.g., Raspberry pie, Banana pie or Beaglebone), this do not affect the billing purpose still in charge of the traditional electronic Smart Meters as well as the IoT module will manage the rapid changes in HW & SW technology without involving the meter part which at the moment become obsolescent in more year than IoT devices and Sotware components. Moreover, data are provided near real time; namely, adopting 1 – 5 s as sampling time and configuring that update measurement is automatically sent to the servers that acquire them through MQTT protocol or the most desired de facto standard since the Smart Meter has a multi-protocol capability.

Section 5.1.1 provides also details about the deployment of these devices, pointing out the new challenges that a DSO is going to face in the future as well as highlighting “data gathering” as a renewed business model, significantly different from what is currently asked to the DSO by the actual standards and Authority resolutions. In this respect, DSO is going to become a central actor enabling new opportunities for stakeholders which ask for data with different sampling time, availability degree and accuracy (e.g., RESCO, ESCO, Aggregators, microgrid and VPP Manager, Authority, TSOs and other DSOs).

Leveraging on the aforementioned metering infrastructures, during the demonstration activities, the Flexibility Resources have been exploited, notably, Section 5.1 reports details about how flexibility resources have been managed in this work, which has mainly investigated on the explicit Demand Response managed by an Aggregator or a Microgrid, Electrochemical Storage and Electric Vehicles recharging sessions; other Flexibility Resources (e.g., Not electrochemical storages) have been not taken into account as well as the explicit contribution on energy balance from RES and their curtailment have not been evaluated.

In sections 5.2 and 5.3 the report of the activities is presented, notably, two main paths have been identified; on the one hand, the flexibility can be used for balancing resources of a district when it is needed, namely for the energy balance of a district and for enabling islanding operation of a microgrid after the disconnection from the main network. On the other hand, it has been assessed how smart grid technologies can increase the adequacy of electrical parameters, notably, in this work the usage of storage is presented as well as the frequency control and the Demand Response campaigns for congestion reduction.

## 5.1 Enabling technologies for demonstration activities

### 5.1.1 *Real-time Smart Meters*

In order to carry out DR campaigns in real environment, innovative tools developed over Nobel GRID project [11], have been deployed in the pilot site. According to general architecture (*Figure 92*), the main pillars of the DR campaigns are the near real-time Smart Meters (SMs), which leverage USM concept, and software tools that perform data analysis and bidirectional communications.

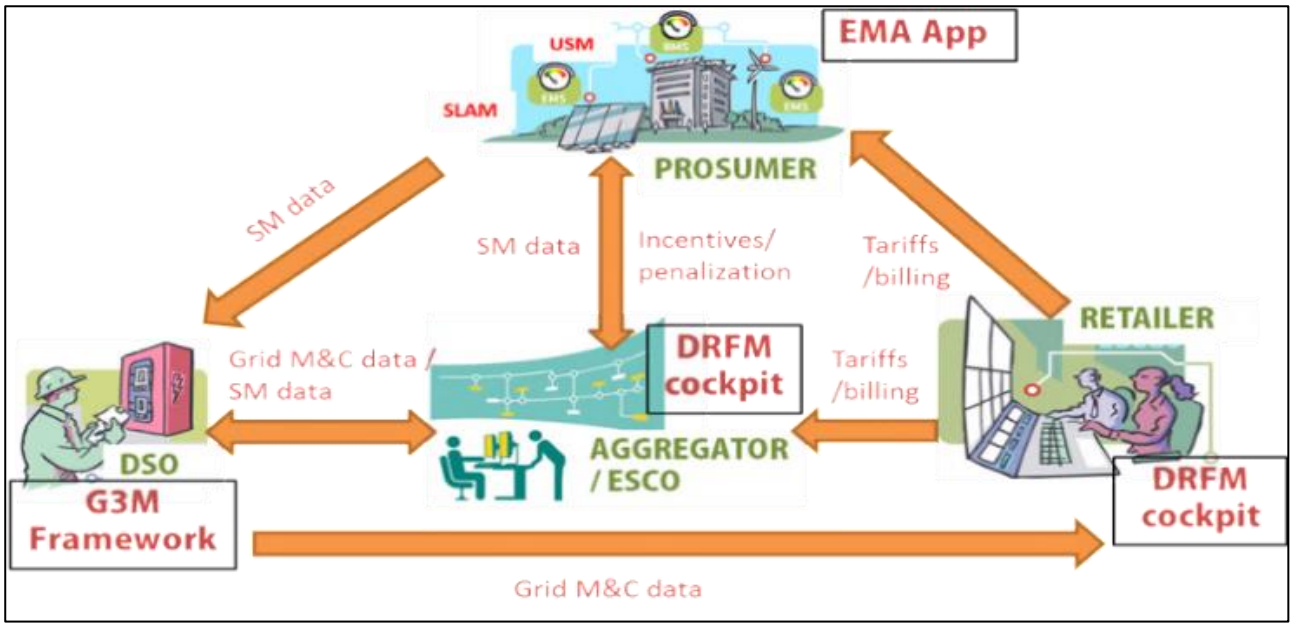


*Figure 92 Nobel GRID general architecture,* [11]

Near real-time Smart Meters: the Unbundled Smart Meter (USM) is a systematic framework in which Smart Meter (SM) functionalities are properly grouped in two separate (unbundled) components (*Figure 3* and *Figure 4* reported below). It was developed over the Nobel GRID project.

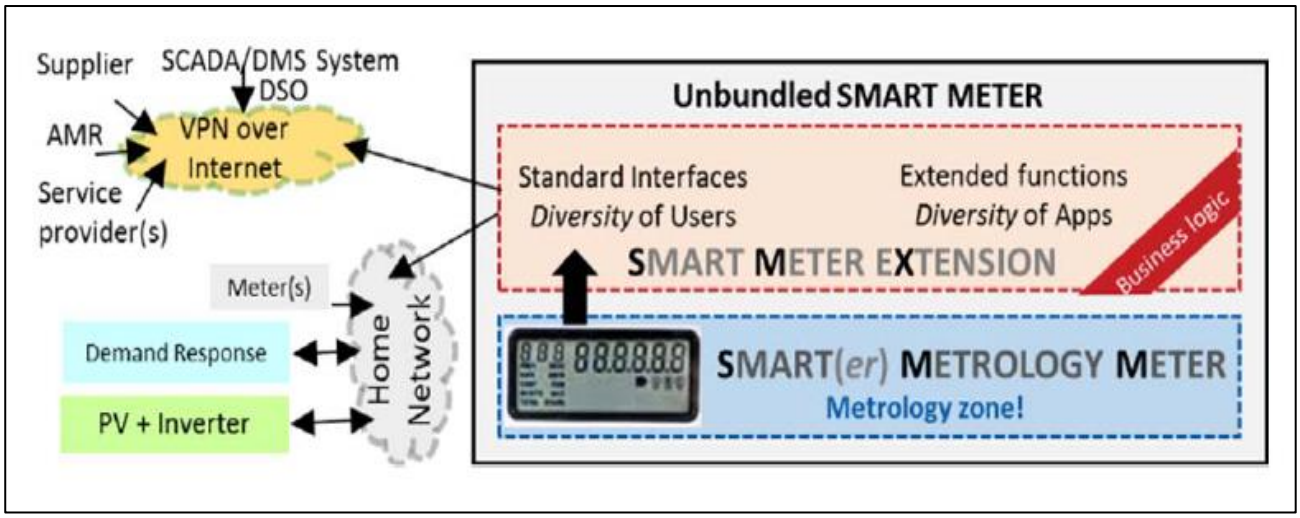


*Figure 93 Unbundled Smart Meter Architecture,* [11]

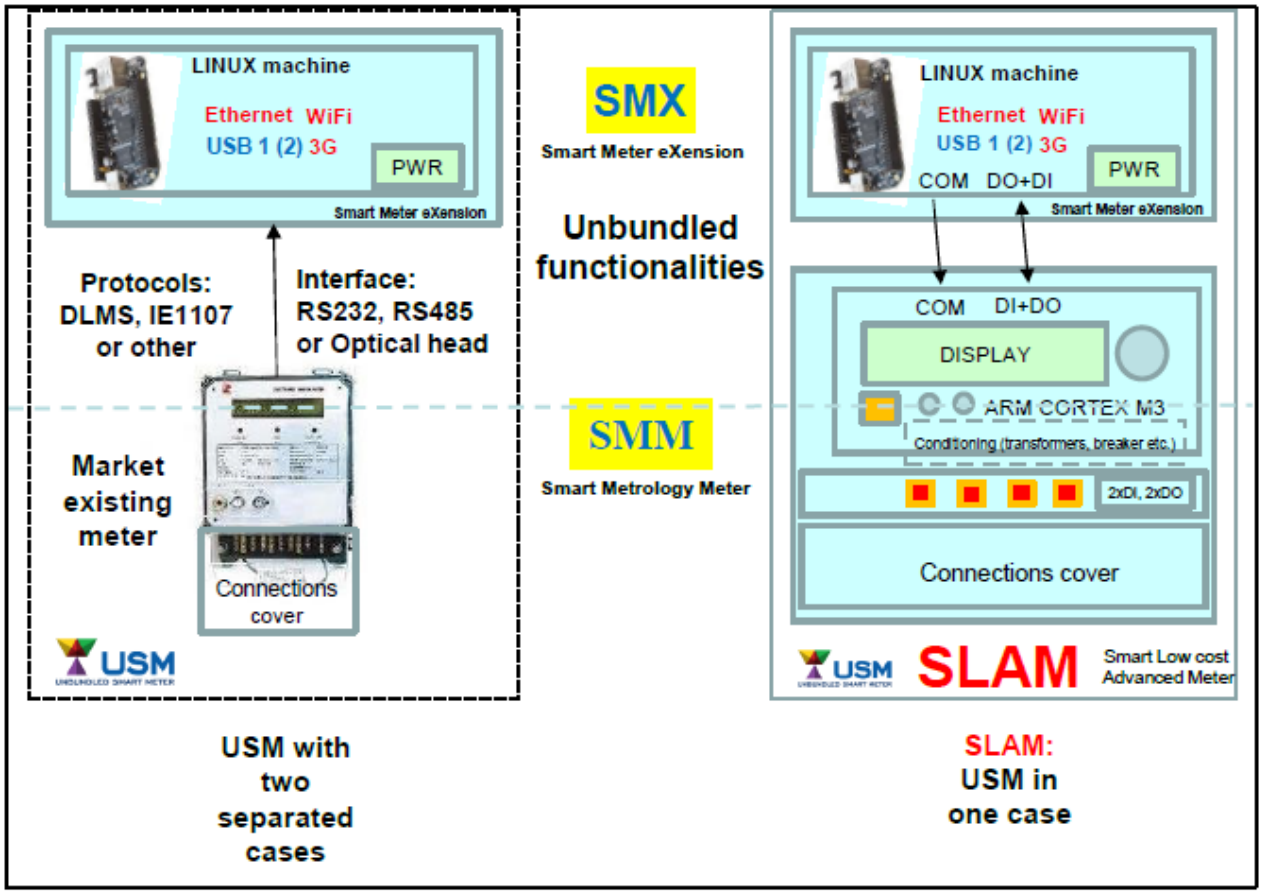


*Figure 94 Unbundled Smart Meter in the Nobel GRID project,* [11]

USM was initially thought to support the future evolution of the Smart Grid and energy services; it is comprised of a metrological part, named Smart Metrology Meter (SMM), devoted to handle "hard real-time" functions, and a Smart Meter eXtension (SMX), a gateway able to provide the flexibility required by the new functionalities deployed during the meter lifetime. The concept was first introduced in [155] and also presented in [156], but it has been subsequently refined; notably, reference [157] presents an alternative Power Quality (PQ) framed aggregation algorithm to be implemented on USM; reference [158] shows different Smart Grid services and functionalities

enabled by USM. In addition, it can implement high data security (e.g., digital signatures) and accommodate local agents; in this respect, SMX is able control the intelligent local appliances and sub-metering devices, as well as the energy transfer from generating units and other energy services, [159].

With respect to the equipment used in this work, SMX part is a full quad-core Linux machine on a Beagle Bone black, implementing a multi-protocol communication (e.g., DLMS, COSEM, IEC1107) as well it allows communication with different interfaces (e.g., RS-232, USB) and channels (e.g., Wi-Fi, Ethernet, mobile network). At the Terni demo site, both the Smart Meter Extension (SMX) and the Smart Low-cost Advanced Meter (SLAM) have been deployed [3] as summarized in the table below. The SLAM is a systematisation where smart meter functionalities are adequately grouped in two separate (unbundled) components: A Smart Metrology Meter (SMM) and a Smart Meter eXtension (SMX). In the pilot site, 100 SMX and 100 SLAM were installed.

*Figure 95. SLAM installation in an apartment building*


*Figure 96. SLAM installation in an apartment building (details)*

*Figure 97. SMX+ZMD installation*

*Figure 98. SMX+Wally-A installation*

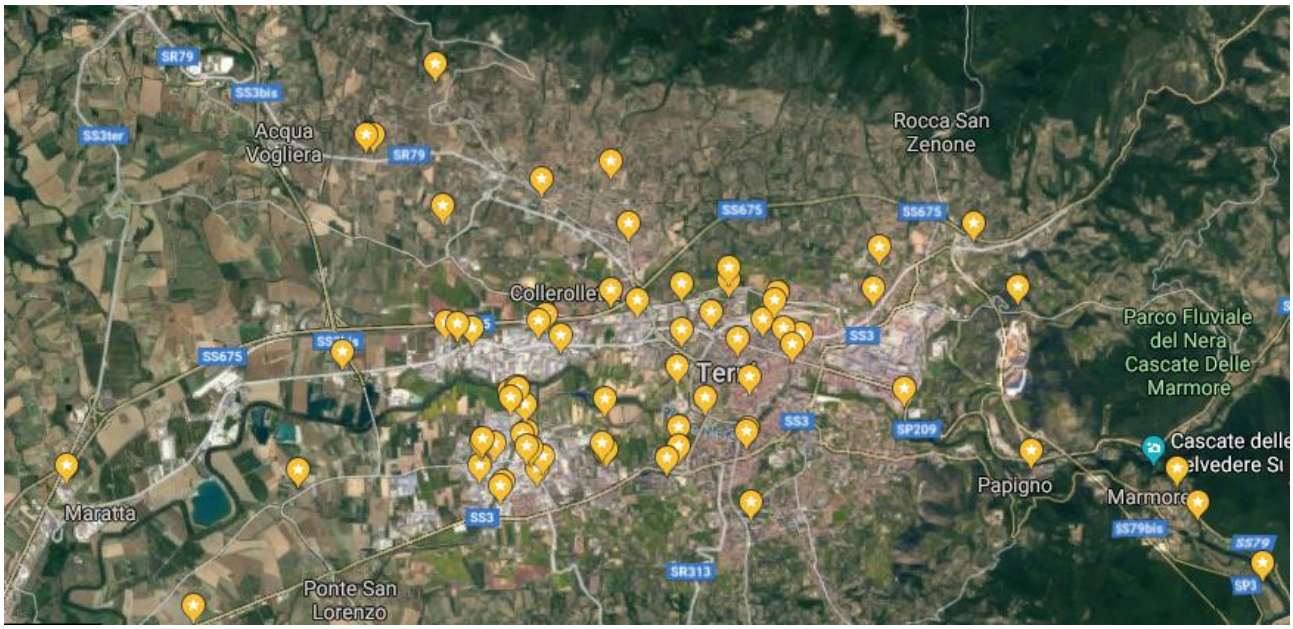


*Figure 99 Location of 3-phase ZMD SMs in the city of Terni*

Two devices, already used to perform metering operations, are available at the pilot site to communicate with the SMX:

- The Landys+Gyr ZMD electronic smart meter (SM)
- A 3-phase high-precision power quality analyser (PQA). The device is named Wally-a produced by Teamware.

The SMs able to communicate with the SMX are currently working for their everyday use in the distribution power network. Actually, they are already used by ASM to measure energy transfer (absorption / consumption) for billing purposes. Due to the existing conditions of operation, the SMX installation (and further their integration in several applications) must not limit or interfere with the already deployed communication between the SMs and ASM server.

The framework foresees that the communication between the electronic smart meter and a GSM modem is done using a dedicated RS-232 channel. Through the GSM communication, the data collected every day is sent at midnight to a dedicated server.

For these reasons, some adjustments have been requested by the company. The SM will be connected to the SMX using the RS-232 cable (DLMS protocol), and the SMX will communicate to the GSM modem through the USB port. The arrangement of USB/RS-232 adaptors has been requested for the installation of the SMX. This implied that the measurement, collected by the SMX from the RS-232 interface, had to be exactly duplicated at USB port in order to maintain the same efficiency of the previous framework.

To complete the description of the framework, it is worth pointing out that the SMX is able to communicate with the project server using both LAN and mobile network, whose details are outlined Figure below shows the interconnection between the SMX-SM-GSM modem-server.

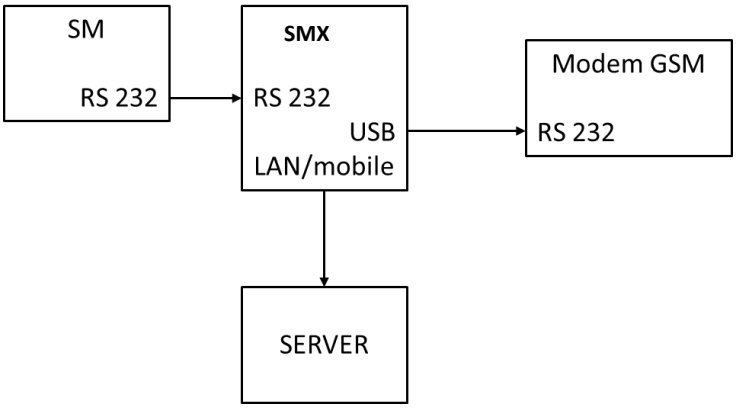


*Figure 100. Simplified architecture for the communication between SM and SMX*

The SMXs have also been connected to the power quality analyzers [3]. The PQA is a device already connected to LAN. These are typically installed at the primary substations in order to measure voltage waveforms, frequency and detailed recording of fault events. The SMX have been connected through Internet protocol, hence by means of configuration, each SMX acquires the IP address of the PQA.

At the same time, an additional SMX has been connected to a power quality analyser (PQA) and tests were performed in order to verify the communication between the PQA and the SMX, completed successfully in mid-September. After about fifteen days of continuous working, the SMX communication failed; after investigating this issue, it was discovered that the monthly data transmission capacity of 2 GB is not sufficient for SMX's normal operation. Hence, the capacity has been increased to 4 GB and the problem has not appeared anymore.

The PQA is able to communicate through both Ethernet port and SIM card. At the beginning of the deployment, PQAs were using SIM cards to send data for their scope, so that connecting SMX and PQAs appeared as the unique way to collect data from that apparatus. Meanwhile, for some of these PQAs, the communication channel has been changed moving from the mobile network to ASM LAN. This new set-up required the change of the installation of the SMX. This solution led to a simpler way to deploy SMX+PQA. First of all, the SMXcore was modified accordingly, so that the device was able to collect data only knowing the IP address of the PQA. Thus, due to the fact that the SMXs belong to the same LAN, the installation of SMXs for the PQA (i.e. for the PS) could be done in the headquarters. These installations, showed in the previous figure below, are very easy to configure and do not require any physical adjustment; furthermore connectivity issues or maintenance caused less effort during test and deployment.

Following the same approach, all the PQAs already connected in ASM LAN were integrated. It is worth pointing out that 6 PQA installations were done at ASM headquarters in order to make it an eligible test site for a DR campaign, having a full comprehension and monitoring of energy flows of ASM facility. The communication between PQA and SMX proved always stable.

Deployment activities were started in May 2017. From June 2017 to April 2018, all the adjustments pointed out in the previous part of this paragraph were handled; furthermore, some installations have been done in order to test if the setup was working properly.

Software tools for DR management: in order to organize DR campaigns (choose the goal, select potential final users, get forecasts, see results), the DRFM cockpit developed under Nobel GRID was

used (see *Figure 92*). DRFM cockpit is a tool that bridges Demand-Side Resources and their flexibility with distribution grid actors to improve the operation of the processes under their control and more specifically to maximize profit and manage planning deviations for aggregators and retailers, while supporting grid operators to ensure network stability and security.

Grid Management and Maintenance Master Framework (G3M) has been deployed at the Terni demo site by the technical partner ETRA. G3M is a tool for DSO actors providing an interface for micro-grid management, monitoring and fault detection. The G3M framework is not a single module but a set of tools and technologies that altogether provide DSO the capability to better maintain the distribution grid [160].

The DSO utilizes the dashboard to acquire a general idea of the current status of the grid by collecting different pieces of relevant information. These pieces of information include:

- The list of current alarms, with the details and status.
- The list of work currently in progress or scheduled.
- Evolution on the consumed and produced energy in real time.
- Indicators on the status of the different meters in the system.
- Active DR Campaigns.
- The following figure is a screenshot made at the end of May 2018.

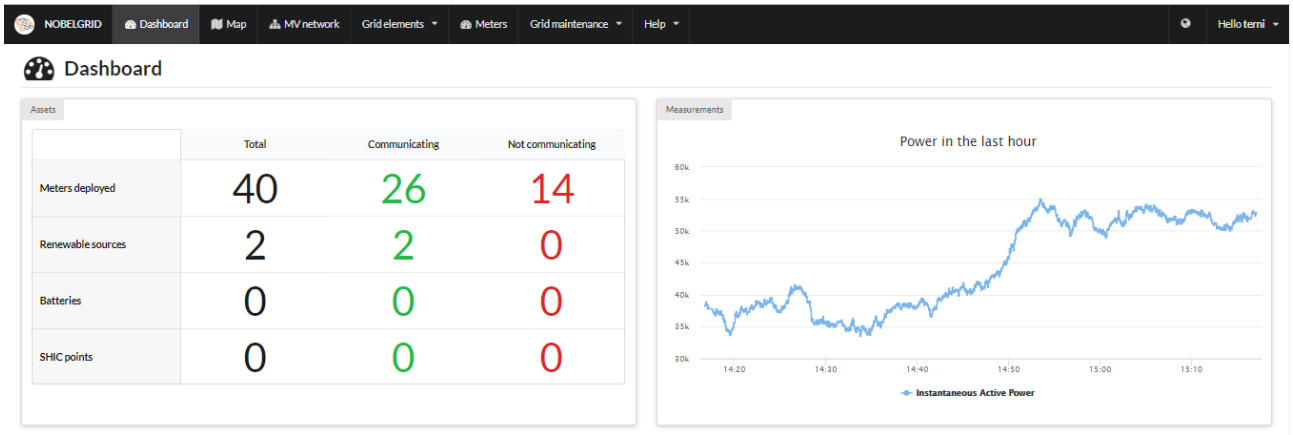


*Figure 101 G3M Dashboard*

DSO can also collect other information and make some actions by means of useful and efficient tools, already included in the framework. It can collect a generic geographical view of the different assets in the infrastructure providing details and maintenance status. The map provides general controls for in/out zooming, geographical searching, and layer selection. An additional map view is available for the DSO with extended topology functionalities. Specifically, a tree list with the hierarchy of all elements in the grid is available on the left. The DSO operator navigates the tree in search of the elements to display at any topology level. Besides the geographical views, there is a MV general view with the schematics connection and the MV lines.

Furthermore, a specific list of usage points is available in the application. The list is provided with a simultaneous geographical view that allows the user to locate the points that are currently being shown in the list. Additionally, the list is paginated and can be filtered using different criteria. All the information available for the selected usage point is shown on a detail page. This information

includes location, technical characteristics, billing and contact information, among others. In the same fashion of the previous section, an inventory of the meters in the system and their features is available in a separate section. This information is extended when selecting one of them.

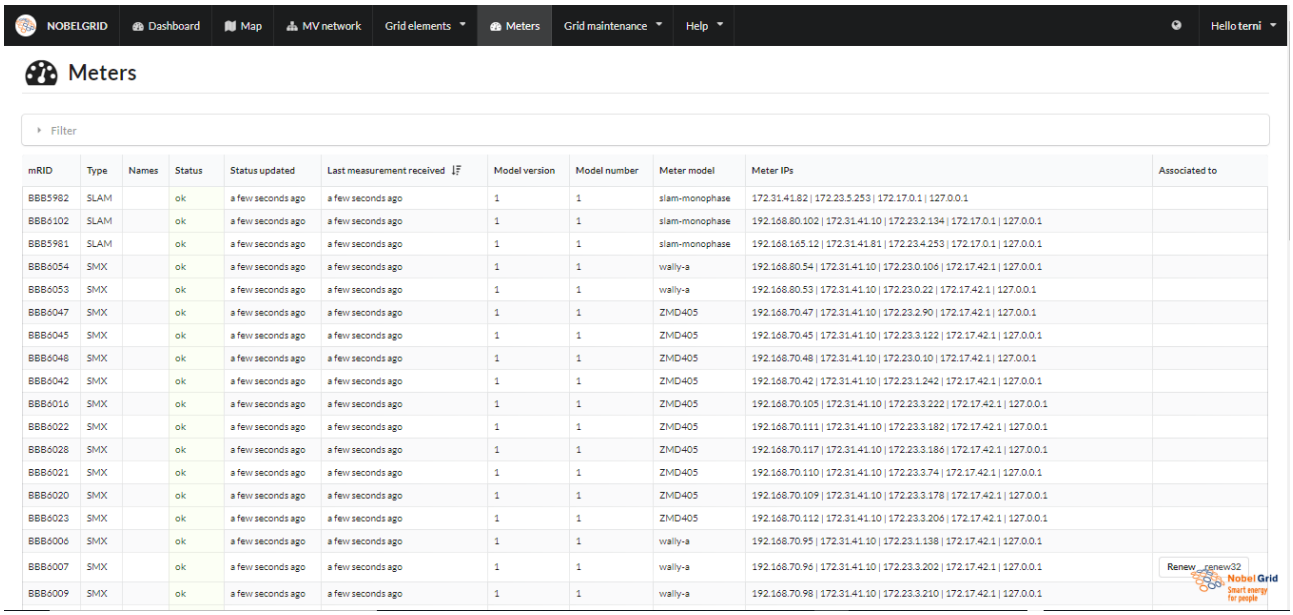


| mRID | Type | Names | Status | Status updated | Last measurement received | Model version | Model number | Meter model | Meter IPs | Associated to |
|---|---|---|---|---|---|---|---|---|---|---|
| BBB5982 | SLAM | | ok | a few seconds ago | a few seconds ago | 1 | 1 | slam-monophase | 172.31.41.82 \| 172.23.5.253 \| 172.17.0.1 \| 127.0.0.1 | |
| BBB6102 | SLAM | | ok | a few seconds ago | a few seconds ago | 1 | 1 | slam-monophase | 192.168.80.102 \| 172.31.41.10 \| 172.23.2.134 \| 172.17.0.1 \| 127.0.0.1 | |
| BBB5981 | SLAM | | ok | a few seconds ago | a few seconds ago | 1 | 1 | slam-monophase | 192.168.165.12 \| 172.31.41.81 \| 172.23.4.253 \| 172.17.0.1 \| 127.0.0.1 | |
| BBB6054 | SMX | | ok | a few seconds ago | a few seconds ago | 1 | 1 | wally-a | 192.168.80.54 \| 172.31.41.10 \| 172.23.0.106 \| 172.17.42.1 \| 127.0.0.1 | |
| BBB6053 | SMX | | ok | a few seconds ago | a few seconds ago | 1 | 1 | wally-a | 192.168.80.53 \| 172.31.41.10 \| 172.23.0.22 \| 172.17.42.1 \| 127.0.0.1 | |
| BBB6047 | SMX | | ok | a few seconds ago | a few seconds ago | 1 | 1 | ZMD405 | 192.168.70.47 \| 172.31.41.10 \| 172.23.2.90 \| 172.17.42.1 \| 127.0.0.1 | |
| BBB6045 | SMX | | ok | a few seconds ago | a few seconds ago | 1 | 1 | ZMD405 | 192.168.70.45 \| 172.31.41.10 \| 172.23.3.122 \| 172.17.42.1 \| 127.0.0.1 | |
| BBB6048 | SMX | | ok | a few seconds ago | a few seconds ago | 1 | 1 | ZMD405 | 192.168.70.48 \| 172.31.41.10 \| 172.23.0.10 \| 172.17.42.1 \| 127.0.0.1 | |
| BBB6042 | SMX | | ok | a few seconds ago | a few seconds ago | 1 | 1 | ZMD405 | 192.168.70.42 \| 172.31.41.10 \| 172.23.1.242 \| 172.17.42.1 \| 127.0.0.1 | |
| BBB6016 | SMX | | ok | a few seconds ago | a few seconds ago | 1 | 1 | ZMD405 | 192.168.70.105 \| 172.31.41.10 \| 172.23.3.222 \| 172.17.42.1 \| 127.0.0.1 | |
| BBB6022 | SMX | | ok | a few seconds ago | a few seconds ago | 1 | 1 | ZMD405 | 192.168.70.111 \| 172.31.41.10 \| 172.23.3.182 \| 172.17.42.1 \| 127.0.0.1 | |
| BBB6028 | SMX | | ok | a few seconds ago | a few seconds ago | 1 | 1 | ZMD405 | 192.168.70.117 \| 172.31.41.10 \| 172.23.3.186 \| 172.17.42.1 \| 127.0.0.1 | |
| BBB6021 | SMX | | ok | a few seconds ago | a few seconds ago | 1 | 1 | ZMD405 | 192.168.70.110 \| 172.31.41.10 \| 172.23.3.74 \| 172.17.42.1 \| 127.0.0.1 | |
| BBB6020 | SMX | | ok | a few seconds ago | a few seconds ago | 1 | 1 | ZMD405 | 192.168.70.109 \| 172.31.41.10 \| 172.23.3.178 \| 172.17.42.1 \| 127.0.0.1 | |
| BBB6023 | SMX | | ok | a few seconds ago | a few seconds ago | 1 | 1 | ZMD405 | 192.168.70.112 \| 172.31.41.10 \| 172.23.3.206 \| 172.17.42.1 \| 127.0.0.1 | |
| BBB6006 | SMX | | ok | a few seconds ago | a few seconds ago | 1 | 1 | wally-a | 192.168.70.95 \| 172.31.41.10 \| 172.23.1.138 \| 172.17.42.1 \| 127.0.0.1 | |
| BBB6007 | SMX | | ok | a few seconds ago | a few seconds ago | 1 | 1 | wally-a | 192.168.70.96 \| 172.31.41.10 \| 172.23.3.202 \| 172.17.42.1 \| 127.0.0.1 | Renew_renew32 |
| BBB6009 | SMX | | ok | a few seconds ago | a few seconds ago | 1 | 1 | wally-a | 192.168.70.98 \| 172.31.41.10 \| 172.23.3.210 \| 172.17.42.1 \| 127.0.0.1 | |

*Figure 102 Meter list*


*Figure 103 Meter details*

The DRFM (Demand Response Flexible Market) cockpit is an additional tool that bridges Demand-Side Resources and their flexibility with distribution grid actors to improve the operation of the processes under their control and more specifically to maximize profit and manage planning deviations for aggregators and retailers, while supporting grid operators to ensure network stability and security. The tool allows for the optimization of aggregators', retailers' and ESCOs' consumer portfolio performance and facilitates demand response strategy optimization in technical, operational and financial terms.

Hence, the DRFM cockpit is a Decision Support System (DSS) supporting different business stakeholders (aggregator/retailer/ESCOs) in portfolio management. Each role has a list of enabled functionalities summarized in the following table.

| | Aggregator | Esco | Retailer |
|---|---|---|---|
| **Monitor prosumers** | V | V | V |
| **Billing management** | | | V |
| **Tariff management** | | V | V |
| **Compare tariff** | | V | V |
| **Data mining process** | V | V | |
| **Business strategy simulation** | V | V | |
| **Trigger manual demand response strategies** | V | | |
| **Trigger automated demand response strategies** | V | | |

*Table 27 List of DRFM Cockpit functionalities*

All the features that are provided via external tools have been integrated in the cockpit interface. The following picture shows the basic architecture of the cockpit and the main integration features.

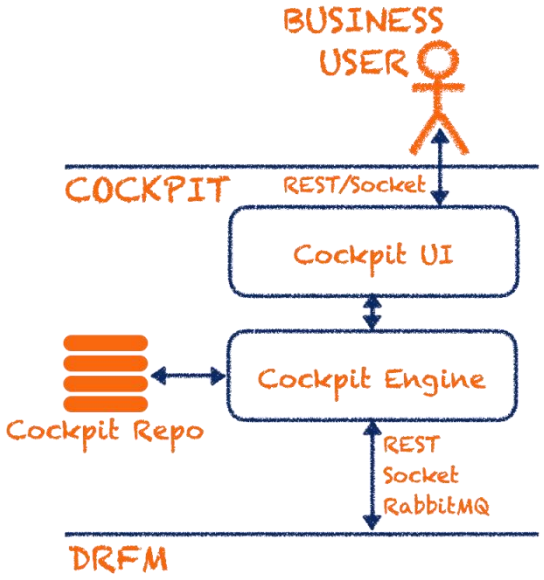


*Figure 104 DRFM Cockpit Architecture Environment*

*Figure 105* and *Figure 106* show basic webviews for an aggregator-type user. This webview is a basic view to monitor the current situation of a set of prosumers.

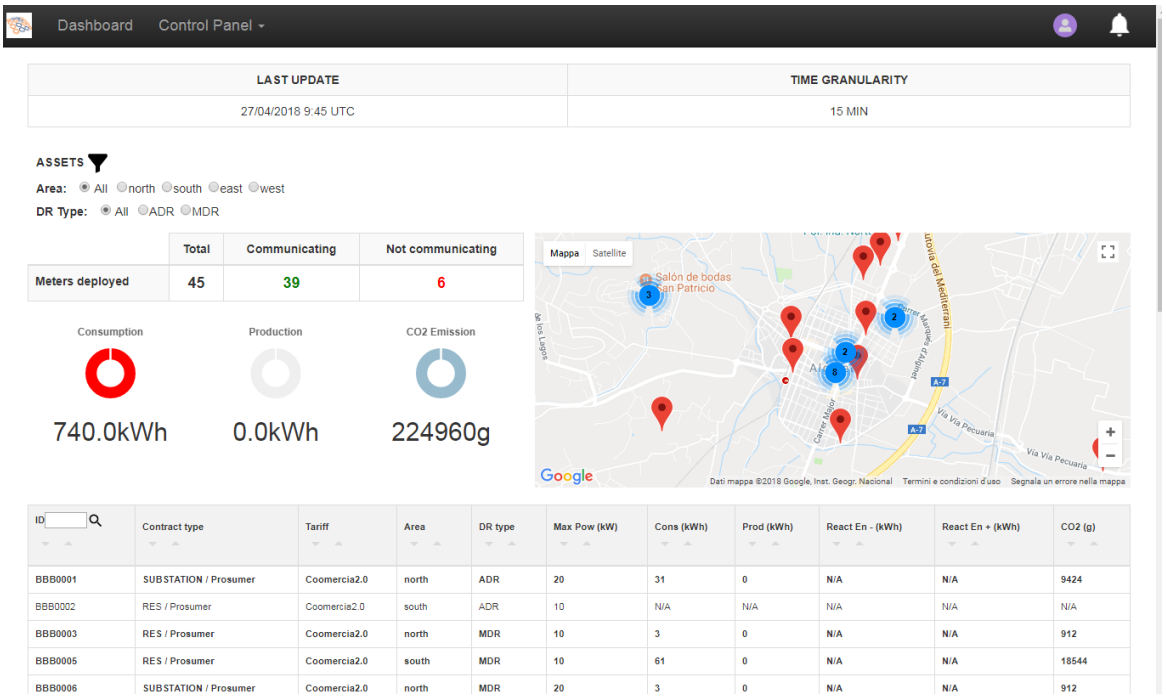


*Figure 105 DRFM Cockpit Homepage for an aggregator*

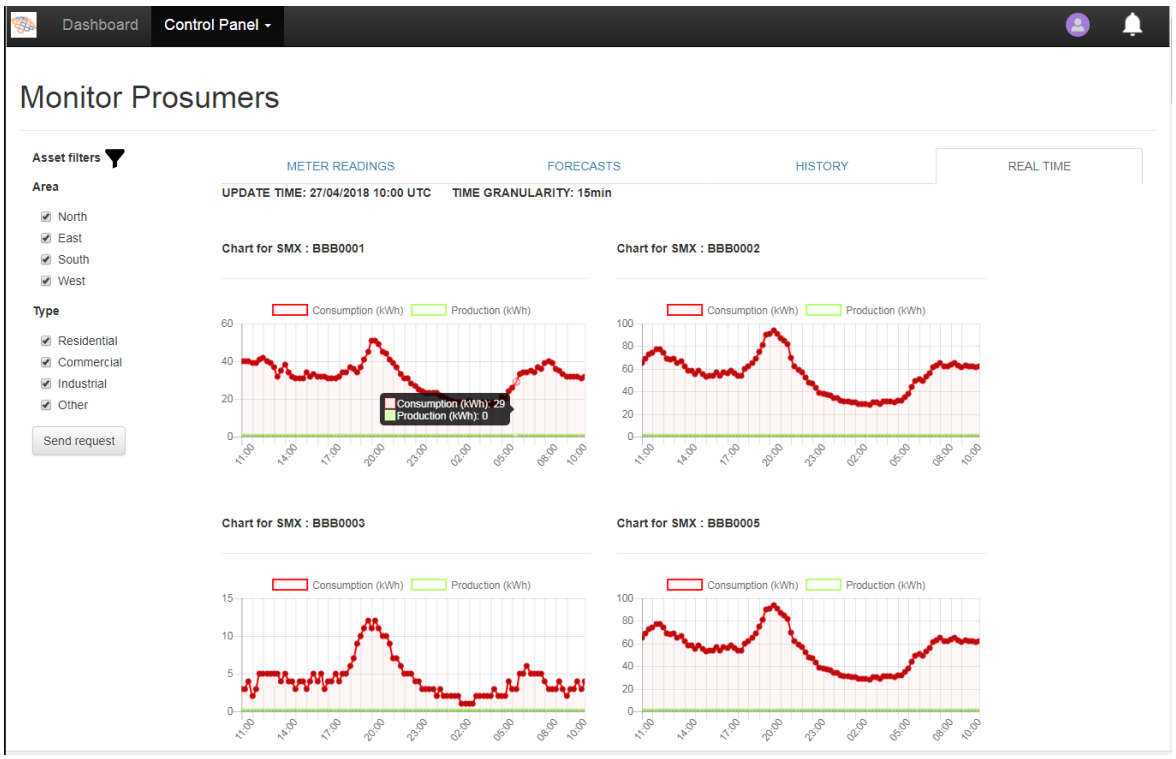


*Figure 106 DRFM Cockpit real time monitor features*

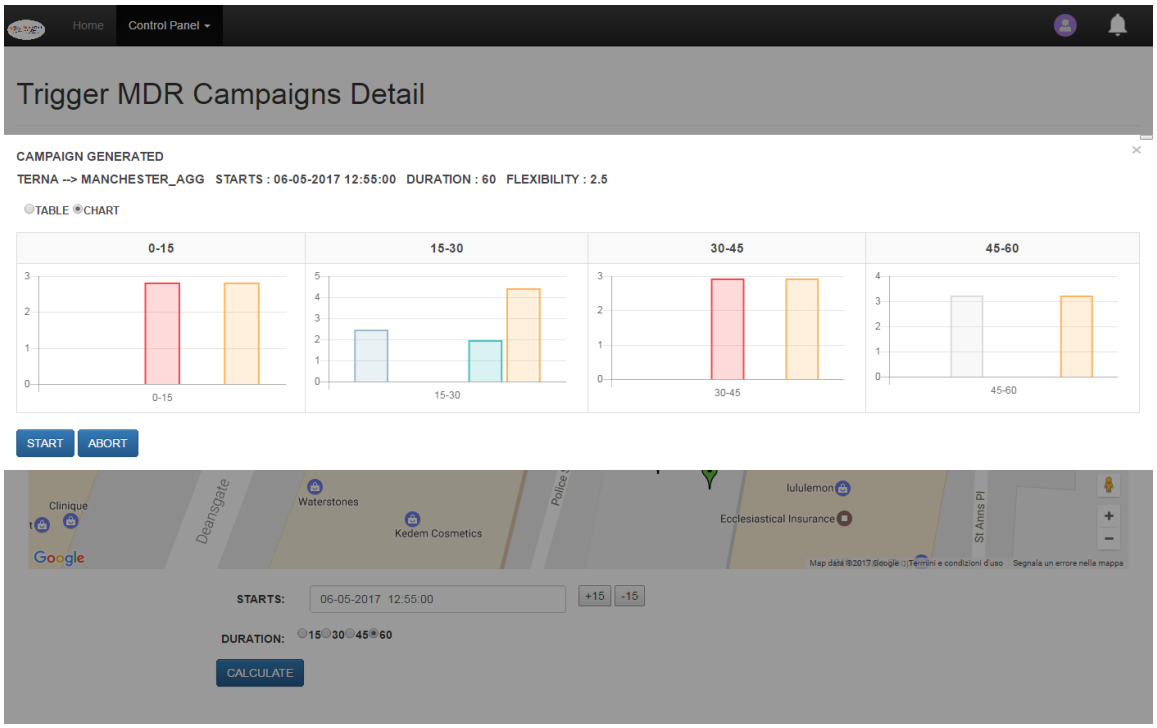


*Figure 107 DRFM Cockpit Demand Response features*

In the Terni test scenarios, DRFM has been used for the following tasks:

- To create and monitor groups of users to be involved in DR campaigns
- To calculate DR campaigns
- To signal the EMA app to execute manual DR campaigns.

The Italian version of the application was released in 2018 and spread among the people involved in the trial. Every participant at the pilot site can use the EMA-app for the following tasks:

- Users can monitor their own electricity consumption and see real-time data.
- Users receive notifications about upcoming demand response campaigns.
- View results of past demand response campaigns
- View details about the dynamic pricing schemes
- View the current carbon intensity of the Italian electricity grid

Because the main view of the app is the real-time data from the own SMX or SLAM, it is not useful to provide the app to people that don't have an SMX or SLAM.

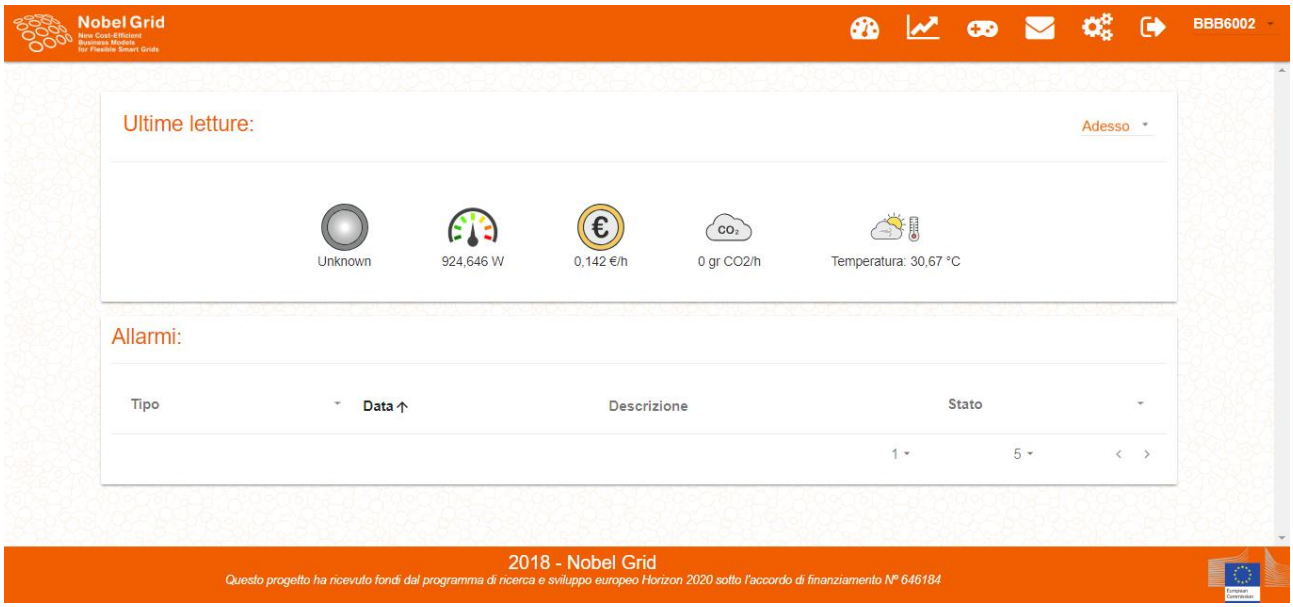


*Figure 108 A screenshot of the EMA app*

### 5.1.2 *Second Life Batteries in Real Enviroment*

At these premises of ASM headquarters, it has been installed the ESS (*Figure 109* and *Figure 110*), made up by six SLB, that were used in six full electric vehicles, namely a Renault Kangoo Lithium-Ion batteries. Although these batteries have finished their respective lifecycles for the mobility purpose, they have still a capacity equal to 11 kWh each one, guaranteed by the manufacturer. In addition, the system is able to provide active power up to 72 kW since rated power of each module is 12 kW and they are connected in parallel; DC voltage of each battery is 360 V (range 240 – 398 V). This was a result of ELSA H2020 project, [76].


*Figure 109. Storage system at ASM presimses*

*Figure 110. 2nd life Li-ion batteries*

The ESS is connected to the Low Voltage (LV) distribution network through six inverters and one transformer. In order to enable the system to provide ancillary services, a proper interface between the battery control module and the Supervisory Control And Data Acquisition (SCADA) system has been implemented. In order to allow the communication between the two systems, a gateway converts the MODBUS messages sent by the control module to IEC61850 protocol, (i.e, already implemented by the SCADA and widely used in Smart Grid applications). By means of this adjustment, the SCADA system collects the main electrical parameters of the ESS (e.g, Active Power, State Of Charge); therefore, a specific interface has been deployed, as shown in Figure 3. In particular, five window interfaces have been implemented to allow Human Machine Interface (HMI), which monitors the Secondary Substation at MV level, getting alarms from ESS, managing and getting measurement from the ESS. With respect to the communication channels, the connection between the SCADA system and the ESS is leveraging an existing HYPERLAN connection.


*Figure 111. SCADA HMI interface during a (P,Q) request*

### 5.1.3 *An overview of cutting-edge technologies for boosting Smart Grids*

#### 5.1.3.1 *Secure Open Federation of IoT Platforms Through Interledger Technologies - The SOFIE Approach [161]*

Distributed Ledger Technologies (DLTs) such as blockchains offer decentralized solutions for collaboration and interoperability. One of the main features of DLTs is the immutability of data: ledgers are append-only databases where existing data cannot be modified and only new data can be added. Another major feature of DLTs is a distributed consensus mechanism [162], which controls what and how data is added to the ledger. Finally, DLTs also replicate data to participating nodes thus improving availability. Because of these three properties, DLTs lack a central point of failure and offer resilience against many attacks. It is easy to determine if any of the participating nodes in the DLT are misbehaving, and even if the attacker manages to take over the majority of the DLT's resources, the attacker still cannot modify the existing data, only control the addition of new data. Technically, DLTs can be implemented with different levels of openness. They can be fully open (permissionless), which means that anyone can join the DLT and propose transactions; most well-known DLTs such as Bitcoin and Ethereum are based on this principle. However, DLTs can also be permissioned such as semi-open, in which case read access is open to everyone but write access is restricted, or closed, in which case both read and write access are restricted.

The main practical innovation of DLTs is the enablement of distributed trust. While there have been multiple proposals for distributed databases in the past, they have mostly concentrated on

the distributed implementation, while the trust model has remained centralized. In contrast, DLTs allow various entities, such as individuals, organizations, and companies, which may not fully trust each other, to collaborate in a safe and transparent manner, with only a low risk of being cheated by others. This makes DLTs a natural approach for solving the interoperability problem between IoT platforms.

There exists a large number of DLTs each offering different trade-offs in terms of latency, throughput, consensus algorithm, etc. thus rendering them suitable for different types of applications. In complex systems it is therefore often not feasible to use only a single DLT for everything, hence the interledger approach that allows different DLTs to exchange data with each other is required in most situations. Using multiple ledgers is also beneficial for privacy reasons, which affect both individuals and companies. Participants within a DLT need to be able to independently verify its integrity, therefore they can access all the data stored in that DLT. This in turn encourages the participants to use private ledgers, and store only a subset of the data to the main ledger used for collaboration with others. Multiple ledgers are also necessary to enable crypto-agility as cryptographic algorithms used by DLTs (such as SHA-256) will not stay safe forever, thus it is necessary to have a mechanism to transfer data from one ledger to another.

Previously, various interledger approaches have been used, and while there are no established standards for interconnecting DLTs, a few repeating patterns have been observed: a shared motivation for the interledger solutions is to move away from the 'one chain to rule them all' model to one that allows the interconnection of multiple ledgers. Interledger approaches include: 1) atomic cross-chain transactions, 2) sidechains, 3) bridging, 4) transactions across a network of payment channels, 5) ledger-of-ledgers, and 6) the W3C Interledger Protocol (ILP). Voulgaris et al. compare the approaches according to whether they support the transfer or the exchange of value, their interconnection trust mechanism, complexity, scalability, and cost, [163].

There exists various proposals for solving the IoT interoperability problem. Some approaches rely on creating a new common interoperability layer, which is not feasible in most cases, since it requires making changes to the existing IoT platforms. Other approaches include BIG IoT [164] that aims to allow interoperability between IoT systems through a common API and Marketplace; however the proposed marketplace is designed to be centralized, limiting its uses. WAVE [165] provides decentralized authorization solution for IoT devices using private Ethereum blockchain and smart contracts, but it assumes that IoT devices are able to interact with the blockchain directly, which is not a feasible approach for many constrained devices.

There are also application specific approaches utilizing DLTs for, e.g. energy trading [166], [167] and [168]. Often they use cryptotokens issued by a single party as currency, which can lead to speculation. Such an approach distracts the solution from its actual use case, and while the cryptocurrency was the original use case of blockchains, it is important to use separate DLTs for performing payments and for other uses, such as asset tracking, logging, etc.

Therefore, the existing work does not fully address the need for an open, decentralized solution for the IoT interoperability problem, which supports existing IoT platforms and enables new open business models.

The main aim of SOFIE is to federate existing IoT platforms in an open and secure manner, without making internal changes to the platforms themselves. Here, openness refers both to technical aspects (interfaces, implementation, etc.) and to flexible and administratively open business models. The approach also aims to preserve users' privacy and be compliant with the EU General Data Protection Regulation (GDPR), which requires the minimisation of personal data collection. One promising technology utilized by SOFIE for improving privacy are decentralized

identifiers (DIDs) [169] and [170] that allow users to create and control short-lived digital identifiers in a flexible manner.

An overview of the SOFIE architecture is depicted in *Figure 112.* At the core of SOFIE Federation is the interledger transactions layer, which allows transactions between multiple ledgers such as Ethereum, Hyperledger Fabric, Guardtime KSI, etc. Federation Adapters are used to allow the interaction between the existing IoT platforms (both open-source and commercial ones) and SOFIE federation framework without making changes to IoT platforms themselves. SOFIE will also utilize existing work in this area, such as W3C Web of Things (W3C) and FIWARE IoT platform. As an example, DLTs and smart contracts can be used for managing access control and performing automatic payments even with constrained and disconnected IoT devices [171] and [172]. The first version of the SOFIE federation framework will be released under open source license during autumn 2019.

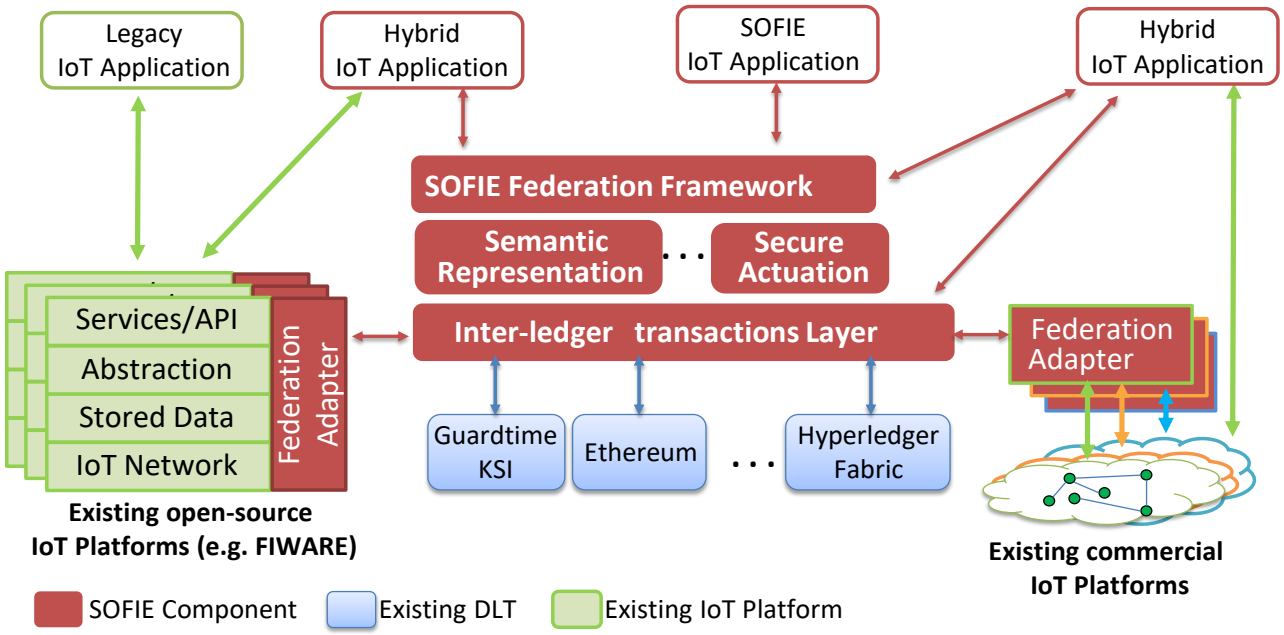


*Figure 112 The SOFIE architecture*

The SOFIE approach will be demonstrated in four real-life pilots within three different topic areas: agricultural supply chain where the produce's growth and transportation conditions are tracked from field to fork, power balancing of the electrical grid by offering incentives to EV owners to charge their cars at the certain time, mixed reality mobile gaming where gamers can interact with real world through IoT devices, and utilizing data from electricity smart meters to develop applications for them. First two pilots will be described in more details in the subsequent sections.

In Terni pilot, the SOFIE platform is utilised to balance the energy chain of a real energy network, namely the distribution grid of the city of Terni located in the central Italy. There, a notable amount of energy is produced locally by distributed photovoltaic plants, which on occasion can cause Reverse Power Flow, when unbalances between produced and consumed energy occur. To avoid this abnormal operation, electrical vehicles (EVs) will be offered significant incentives to match their EV charging needs with the distribution network's requirements.

The actors in the pilot, as depicted in *Figure 113*, are the *Distribution System Operator (DSO)*, who is responsible for the grid management, *fleet manager*, who is the manager of charging stations

and represents EVs in energy price negotiations, and the *EV users*, who receive information and requests about the optimal scheduling of the charge of their vehicle. The SOFIE platform is then utilised to run a decentralised marketplace enabling a peer to peer exchange mechanism between DSO and fleet manager, thus forming an end-to-end scenario from production via distribution to storage and consumption.

The DSO and the fleet manager interact with the system through their dedicated dashboards that show near-real time data collected from the two IoT subsystems (i.e. smart meters for the DSO and EV/EVS sensors for the fleet manager) and the actors create market requests and offers accordingly. The business logic for the request and offers collection and for the winning offer selection algorithm is coded inside smart contracts, ensuring transparency and auditability of the whole process.

The current version of the smart contract implements an auction mechanism, in which the best offer is selected following the "lowest bidder" rule. In the future, the upgraded version of the smart contract will consider a different matchmaking algorithm, based on the clearing price algorithm, used in commodity trades. In addition, the smart meter readings are stored on blockchain to ensure transparency, and the blockchain will also contain data of electric vehicles, charging stations, and charging events. Such data will be used for payments by the DSO to the fleet manager and for rewarding the users (through tokens or discounts) in an automated manner.

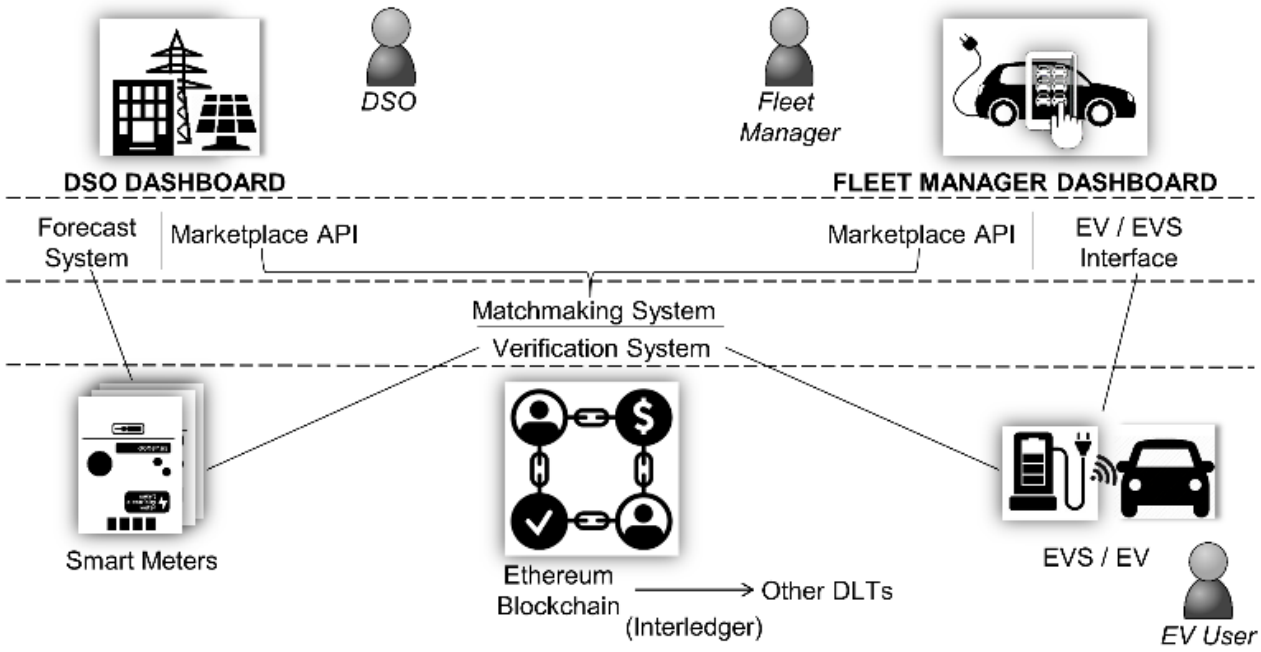


*Figure 113 An overview of the SOFIE energy pilot*

Two main scenarios will be studied in the pilot, called *day ahead planning* and i*ntraday contingency planning* scenario, respectively. In the *day ahead planning* scenario DSO needs to shave peaks of locally produced energy, so it will put a flexibility request in the day-ahead market asking for an amount of energy to be drawn at specific time interval and location and provides incentives (e.g. tokens or discounts). Meanwhile, the fleet manager matches fleet needs with offers in the platform to achieve the maximum bonus available in terms of incentives, placing the corresponding offers in the marketplace. On the other hand, in the *intraday contingency planning* scenario the DSO puts out a flexibility request asking for an amount of energy (kWh), a timeslot, and a location (GPS

coordinates) while providing an incentive (tokens) in order to shave peaks of locally produced power in the same day. The marketplace will then automatically identify potential candidates to fulfil the request based on user type, current location, residual autonomy, and EVs' current status. The selected EV users will receive a direct notification, offering a token incentive if they agree to charge the vehicle using an assigned charging station in a specific time interval.

In future experiments, SOFIE's interledger capabilities will be leveraged by utilising multiple ledgers so that a private DLT acts as a "first layer", granting privacy (i.e. data cannot be read by external parties) and reducing transactions costs and times (i.e. mining is not required), and a public DLT then acts as a "second layer", where the status of the private blockchain is periodically synchronized, granting security and auditability, thus protecting the data stored in the first layer DLT from any alterations.

Compared to the existing solutions, a key benefit of SOFIE is the federation of existing platforms (i.e. the EV platform in charge of the EV manager and the Advanced Metering Infrastructure managed by the DSO). Thanks to the technology-agnostic SOFIE federation framework, DSO and fleet manager can interoperate in the same decentralized marketplace, keeping intact their own internal IoT platforms. SOFIE implementation is going to produce benefits for both sides, on the one hand, services are temporally synchronized and benefits of the actors are optimized, on the other hand, new services can be investigated in the future and provided to third parties, opening new business models for the actors themselves (e.g. a stable prediction of the active power exchanges with the Transmission System Operator (TSO), carried out by balancing the loads of the charging points, can be subject to monetary incentives).

### 5.1.4 *Enabling Flexibility Services of microgrids [173]*

The capability of modifying the energy consumption and/or generation pattern is modelled by the concept of flexibility. It is defined as follows: "On an individual level, flexibility is the modification of generation injection and/or consumption patterns in reaction to an external signal (price signal or activation) in order to provide a service within the energy system. The parameters used to characterize flexibility include the amount of power modulation, the duration, the rate of change, the response time, the location, etc." [174].

In the context of a typical microgrid, the energy behavior of many actors can be modelled by means of flexibility actions to be structured within a flexibility-as-a-service view. A flexibility service is generally classified by the time response of the energy resources involved [175] real-time flexibility, short term one, mid-term one, and long term/seasonal one. As such, according to the responsiveness and the dynamics of the flexibility provider, different areas of grid management can benefit from flexibility exploitation: supply and demand balancing; grid operation; user participation; emission reduction. Moreover, the innovative techniques brought by the flexibility open new perspectives for the introduction of tailored flexibility service market places where to trade and give economic values to flexibility. In this view, the figure of the aggregator, in charge of collecting and managing different flexibility contributions in order to give them relevance and effectiveness to the grid, is gaining more and more momentum.

#### 5.1.4.1 *Smart control of flexibilty services*

As discussed above, the flexibility can be arranged properly in order to provide tailored services to a power system stakeholder, such as a grid operator. The strategies for the control and management of these processes are therefore designed in order to exploit flexibility services at their bests. Firstly, the economic benefit maximization of the actors providing the flexibility is the main driver of almost all the management approaches. Subsequently, the technical aspect related to the

control of distributed generation, as well as the storage system, are essential aspects taken into account for establishing a management strategy, along with the improvement of power quality indicators. Some other techniques are directly linked to the service requests of a stakeholder, for instance in terms of power profile or price trend following. Finally, these strategies can be also driven by environmental aspects, such as energy losses reduction, polluting emissions control, energy efficiency, etc.

Due to the high inherent complexity of these management tasks, the platforms in charge of the flexibility management are often based upon dedicated solution methods that allow to take into account several aspects and different trends of the phenomena under study. Some of the most innovative and promising techniques among those employed today are: heuristic optimisation, machine learning, multi-agent systems, etc. In this work, an optimisation framework based upon a heuristic algorithm, in particular a genetic one, is proposed.

#### 5.1.4.2 *Cross-functional Modular Platform Solution for Flexibilty Management*

In this section, the ICT platform solution proposed by the inteGRIDy project is presented and discussed.

The main goal of the inteGRIDy project is to provide a complete ICT platform aimed at integrating all the new actors involved in the operations of modern smart microgrids. The integration addresses both new technologies, components, and devices, such as RES, storages, etc., and communication and computational means, such as metering and sensing devices, smart algorithm, and control techniques, etc. In this view, many software and hardware components are going to be integrated in a unique Cross-functional Modular Platform (CMP), an innovative and powerful set of synergetic components relying on openness and interoperability functionalities.

#### 5.1.4.3 *Architecture*

The architecture of the CMP is structured in three main layers, grouping the main components envisioned for the provision of the different system functionalities. It consists of the different tools, models and mechanisms conceived to support the smartening of distribution services. The CMP consists of the following, hierarchically connected layers of subcomponents:

- Modelling and profiling of grid, Demand Response (DR)/Demand Side Management (DSM) & storage layer: this layer aims at integrating existing models/modelling tools in order to have a wide base of models and profiles characterization able to deliver to the other layers an accurate assessment of the behavior of involved entities.
- Operation analysis framework/simulation layer: this layer produces intermediate results or alternative scenarios, in order to support the decision making and optimisation mechanisms. It integrates current contexts, e.g. current grid conditions or monitoring data, with previously extracted models/profiles in order to use forecasting and prediction techniques.
- Decision making & optimization mechanisms/toolset layer: this layer is in charge of performing all the smart management techniques envisioned for the inteGRIDy system. As a matter of fact, all the information gathered and computed by the other layers of the architecture are conveyed to the Decision making & optimization mechanisms/toolset layer that implements all the functionalities related to the smart control of the energy resources of the system. The adopted approach relies upon several techniques able to optimize, take decisions, and schedule strategies taking into account different sets of criteria or goals to be achieved in particular energy context.

The architecture is enriched with an Integrated Visualization Platform (IVP) that comprises of a set of Human Machine Interfaces (HMIs), tools and services, responsible for enabling access to information of the underlying layers. Moreover, the field middleware modules allow the integration with the physical equipment, enabling access to real-time monitored information, historical data and notifications, suggestions for actuation, as well as the exchange of information with the grid operators. It consist of all the sensors, energy meters, actuators, controllers, etc., that will provide data to the CMP. Finally, the Reference Knowledge Warehouse is responsible for storing the different models, profiles, schemas, indicators, created and maintained by the different CMP components, acting as a common space for sharing and updating information.

#### 5.1.4.4 *CMP implementation*

The solution proposed in this work allows to manage a rural microgrid described in the next section. The main goal is optimizing the operation of the microgrid taking into account the internal economic benefits of the microgrid and the service request form the DSO.

The envisioned system consists of several components and tools properly mapped over the architecture described above:

- a dashboard put at disposal of the DSO for selecting the typology of service requested;
- a DSO and a microgrid monitoring tool in charge of retrieving real-time data from the field, both regarding grid connection point and internal devices;
- a set of forecasting modules responsible of evaluating the forecasted power profiles of the energy units inside the microgrid;
- a set of modelling modules in charge of simulating the behavior of the energy units inside the microgrids;
- a load flow module aiming at simulating the electrical parameters of the microgrid physical infrastructure;
- an optimization engine responsible of the evaluation regarding all the power profiles, as well as set-points of the system that implements the management criteria;
- a communication module based on openADR, [176] in charge of handling the information exchange between all the involved actors.

In *Figure 114*, a diagram of the proposed architecture is shown.

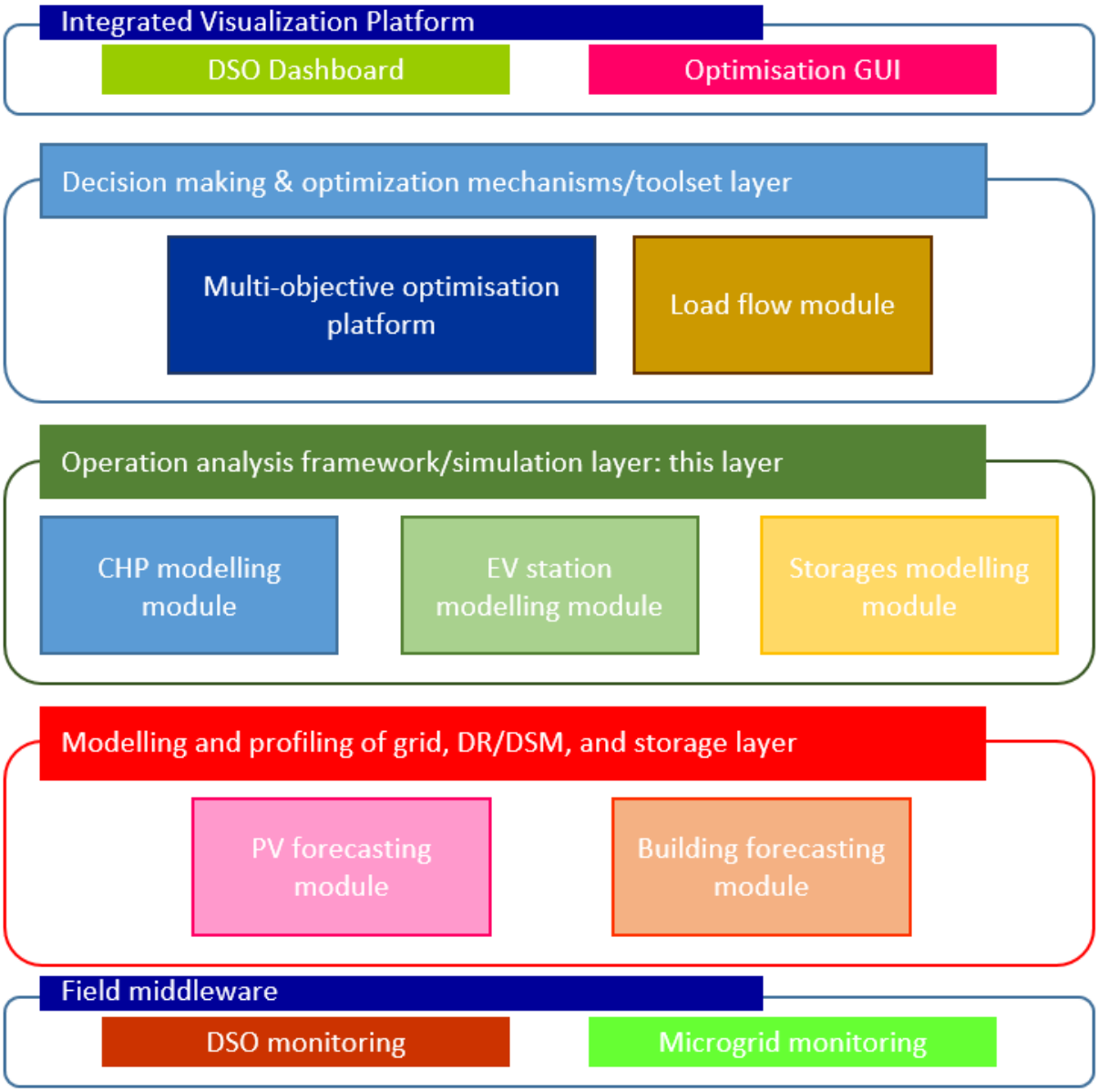


*Figure 114 inteGRIDy Terni implementation ICT architecture.*

## 5.2 Active role of the DSO for power balancing

### 5.2.1 *Microgrid supporting DSO during abnormal operation [177]*

#### 5.2.1.1 *Microgrid Components*

Terni Pilot is going to be developed on the border between Terni and Rieti municipalities. The pilot site comprises the already existing farm "Il Moggio", which is at present a stand-alone microgrid, and the local energy infrastructures managed by ASM. An MV/LV secondary substation is going to be deployed and the necessary hardware and software equipment will be set up in order to monitor and control the microgrid resources. The farm covers an area of 14 hectares, in which 9 buildings are devoted to agricultural and commercial activities (basically primary and tertiary sectors).

"Il Moggio" microgrid comprises a significant amount of distributed generation: a 30 kWp rated PV plant, two 31 kVA – 25 kWt biomass CHP generators and a 60 kWh battery energy storage system (BESS). In detail, apart from internal loads due to the agricultural and commercial activities, the available generation and energy storage units, as well as load units, are as follows:

- The PV power plant is composed of 7 strings; each one has 14 modules (300 W), for an overall 29.4 kWp. The PV plant can feed simultaneously both the microgrid load and the battery storage system through a static inverter made up of a DC/AC converter, a series-connected transformer and a DC/DC converter.
- 2 CHP generators, each 31 kVA – 25 kWt, connected without a static converter, whose fuel is supplied by two gasifiers. They are able to supply fuel for both electrical and thermal uses and require only dry organic materials (as wood chips, walnut shells, agricultural waste) to provide their services.
- The battery energy storage system consists of 50 series-connected 12 V - 100 Ah rated lead batteries, for an overall 60 kWh rated energy, responsible for the management of distributed generators without curtailments.
- A 50 kVA rated three-phase load bank, composed by a 40 kW – 400 V resistive load and a 30 kVAR inductive load, needed in order to operate the microgrid which is currently a stand-alone grid:

The connection of the "Il Moggio" stand-alone microgrid to the MV distribution network is under deployment. A 250 kVA SS will be built by ASM and connected to an existing overhead MV feeder. The SS will be connected to the SCADA system, whereas the technical-economic management of the microgrid flexibility will be carried out by a dedicated calculation platform, as presented in Subsection 5.1.4.2.

At present, "Il Moggio" is an islanded microgrid and will be connected to an MV feeder by means of a 250 kVA SS currently under construction. Moreover, the SS will be connected to the already existent DSO monitoring tool (i.e., the SCADA system already deployed in the ASM MV grid) by means of a Power Quality Analyzer (PQA), which is in charge to forward voltage, current and active/reactive power measurements from the field to the SCADA and vice versa. The possibility to supply an islanded portion of the ASM MV network by using the microgrid resources has been investigated.

This case is of interest for the DSO, since the islanded operation of a portion of the MV grid could allow the DSO to avoid penalties due to the lack of supply; moreover, the microgrid could gain economic benefits for this service. In the work, however, only the feasibility of such task is investigated in terms of energy balances and so the inteGRIDy CMP reference architecture presented in [178] is not used, i.e. only the use of components actually installed on the field is considered and no optimization procedure among the ones considered in the inteGRIDy project is employed.

The considered islanded system is located in a rural area and consists of the microgrid itself, the SS connecting the microgrid to an ASM MV feeder, the 12 kilometers long MV feeder (nominal voltage 20 kV) and two aggregate loads. A simple 4-bus model, shown in *Figure 115*, has been developed and implemented in the MATPOWER environment.

The microgrid (bus 1 in the figure, nominal voltage 400 V) has been simulated in the load flow as an equivalent generator and a load; the 250 kVA MV/LV transformer is connected between bus 1 and bus 2. Bus 3 and bus 4 represent two aggregate loads supplied by two small-sized SSs, which have not been simulated in this study. More specifically, bus 3 is a load bus (35 kW contractual

power) representing three telecommunication antennas, whereas bus 4 is a load bus representing an aggregate civil load (4 users, 24 kW contractual power). A six-month period, from January 1st to June 30th 2017, has been considered: both measured and simulated load and generation profiles are with a time rate of fifteen minutes (17280 quarter hours in total). Bus 3 and bus 4 load profiles have been taken from ASM measurements, collected every quarter hour. About bus 1 load profile (3.3 kW contractual power), no information was available from ASM, since microgrid is at present disconnected from the grid, so a six-month load profile of a similar ASM customer has been used.

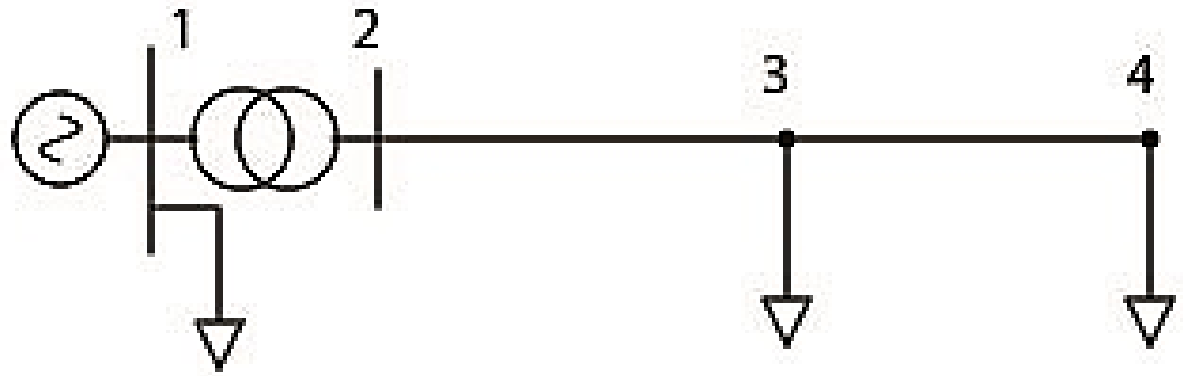


*Figure 115. Microgrid schema*

Microgrid PV generation profile has been obtained by averaging measurements of 33 PVs installed in Terni and scaling according to the rated power. *Figure 115* depicts the PV generation profile along the simulated six-month period. Lastly, the MV feeder is a three-phase, single circuit overhead line equipped with 70 $mm^2$ aluminum conductors: resistance, reactance and capacitance per unit length are 0.423 Ω/km, 0.37 Ω/km and 10 nF/km, respectively.

#### 5.2.1.2 *Microgrid Resource Control Strategy*

During the islanding operation of the microgrid, two main circumstances are considered: the PV production is greater than zero (case 1) or the PV production is nil (case 2). In both cases, CHPs (named CHP1 and CHP2 in the following) may be in operation or not. During islanding, if not strictly necessary, the balancing between generation (PV production, which depends on weather conditions, and CHP1 and CHP2 productions, which depend on the microgrid owner's choices) and load is performed only by charging or discharging the BESS.

At first, let us consider the case that generation exceeds load, so that the BESS must be charged. When the state of charge (SOC) of the BESS exceeds a threshold value close to the maximum SOC, and the load is lesser than the generation, CHP1 or CHP2 or CHP1+CHP2 generation is reduced in order to match the load. If such reduction is not feasible (for instance, in case CHPs are off), the load bank is operated. With this strategy, in one case the islanding operation is not feasible, i.e. if the generation exceeds the load more than the maximum active power of the load bank (40 kW).

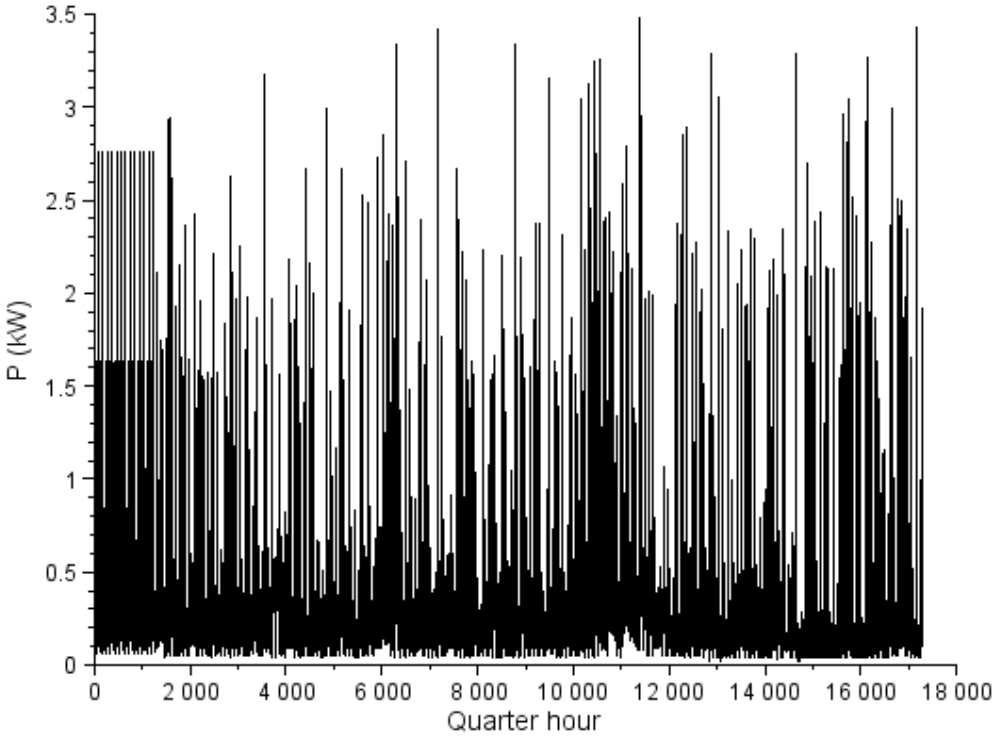


*Figure 116. Simulated microgrid load during the considered six-month period.*

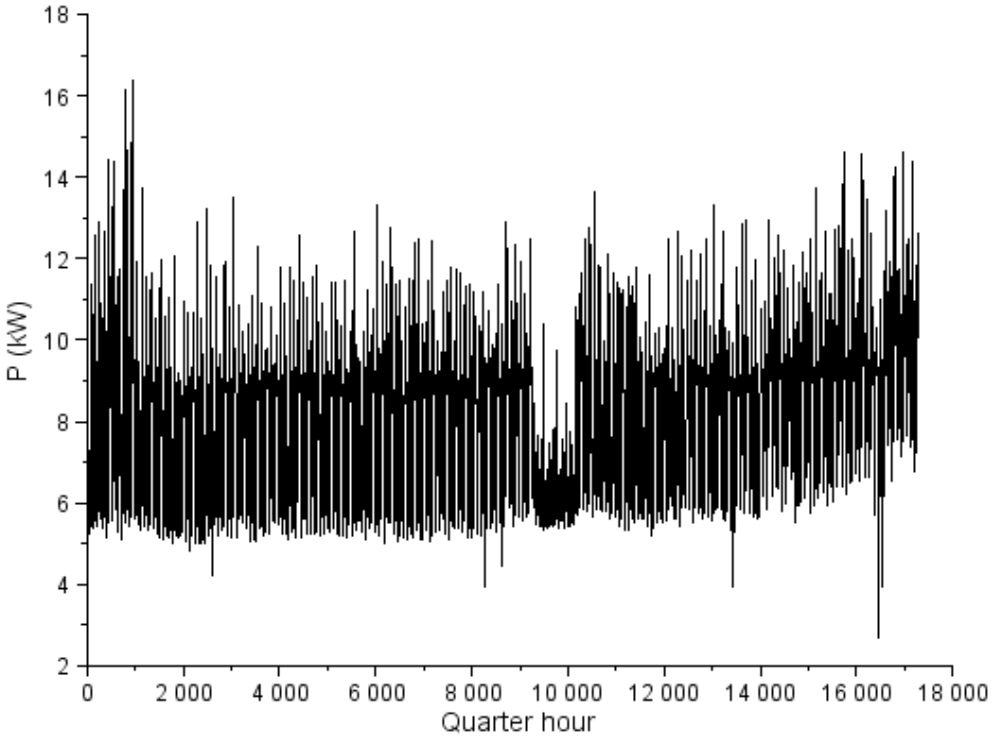


*Figure 117. Measured load (bus 3 and bus 4) during the considered six-month period.*

Let us now consider the case that load exceeds generation, so that the BESS must be discharged. When the SOC of the BESS decreases at under a threshold value, and the generation is lesser than load, CHP1 or CHP2 or CHP1+CHP2 generation is increased in order to match the load. If this increase

is not feasible (for instance, CHPs are off or are generating the maximum power), the islanding operation is not possible.

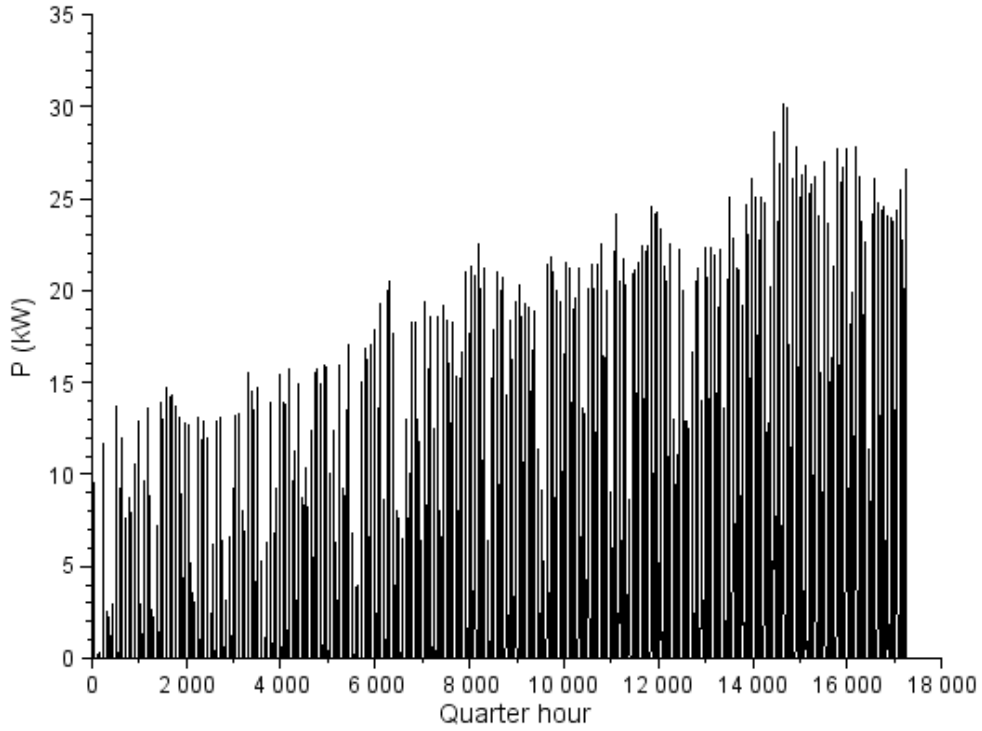


*Figure 118. PV generation profile during the considered six-month period.*

During islanding, if not strictly necessary, the balancing between generation (i.e. CHP1 and CHP2 productions, which depend on the microgrid owner's choices) and load is performed only by charging or discharging the BESS.

At first, let us consider the case that also CHPs are off at the beginning of the islanding operation. CHPs then must be activated and the initial operation of the microgrid depends only on the SOC of the BESS until CHPs are on. If load is not nil and SOC=0 kWh, the operation is not feasible. If the initial SOC of the BESS allows discharging, the operation is feasible.

Let us now consider the case that CHPs are on at the beginning of the islanding operation. CHP generations are not altered, unless SOC exceeds a threshold value (when load is greater than generation) or decrease under a threshold value (when generation is greater than load). In the first case, CHP outputs are increased in order to match the load and the islanding operation is not feasible if the load exceeds the maximum output power of both the CHPs. In the second case, CHP outputs are decreased in order to match the load (alternatively, the load bank may be activated), whereas if the load is lesser than the minimum output power (4.72 kW for each CHP, decreased by the auxiliary consumptions equal to 1.1 kW for each CHP) the load bank must be activated.

#### 5.2.1.3 *Results*

A statistical analysis is presented in this Section, in which during the six-month period 100,000 different islanding operation cases are generated, by randomly varying the following quantities:

- The quarter hour when islanded operation begins: a uniform distribution between 1 and 17280 has been generated.

- The duration of the islanded operation: a normal distribution, with average 3 and standard deviation 1 has been generated; moreover, for the i-th case study the end of the islanded operation is limited to 17280.
- The CHPs output power: for each CHP, a uniform distribution between 0 and the maximum output power, which is 29.9 kW considering the auxiliary consumptions, has been generated; moreover, if the CHP output power is lesser than the minimum output power (3.62 kW), the generation is set to nil.
- The BESS initial SOC: a uniform distribution between 0 and 60 kWh has been generated.

*Figure 119* reports the probability distribution for the 100,000 generated initial SOCs, showing that each initial SOC value has approximatively the same occurrence (about 1.65 %). *Table 28* reports the simulated durations (in quarter hours) of the islanded operation, showing that only eight different durations have been extracted (from one quarter hour to two hours) and the more probable values are three quarter hours and one hour. The generated 100,000 cases have been solved in steady state by means of the power flow available in MATPOWER, taking bus 1 in *Figure 115* as slack bus. Power flow results have been then elaborated in the light of the control strategies described previously. The charge and discharge efficiency of the BESS has been considered and taken equal to 75 %.

Main results of the statistical analysis are the following:

- For the 76,259 % of all simulated cases the islanding operation is feasible by only using the BESS in order to balance load and generation in the microgrid, without changing PV and CHPs outputs.
- For the 3.622 % of all simulated cases the islanding operation is not feasible since, at the beginning of the islanding operation, the output of both CHPs is nil and the BESS is not able to balance the load in excess due to its too low initial SOC.
- For the remaining 20.119 % of all simulated cases the islanding operation is feasible by changing the output generation of CHPs and, when necessary, by activating the load bank.

*Figure 120* reports the probability distribution of the SOC of the BESS at the end of the islanding operation. Only when SOC=0 kWh (about 7 % of all simulated cases) and SOC=60 kWh (about 17 % of all simulated cases) the islanding operation required to vary the CHP output or, when strictly necessary, to activate the load bank. *Figure 121* and *Figure 122* show the probability distributions of the output variations (in terms of active energy) of CHPs for the 20,119 simulated cases that required such variations in order to perform islanding.

Results show that “Il Moggio” microgrid is capable to supply the considered islanded system for the vast majority of the considered cases (96.378 %). Steady state simulations have been carried out in the work with the aim to investigate only the feasibility of such task; however, transient simulations are required in order to check the voltage stability of the system during off-grid operation.

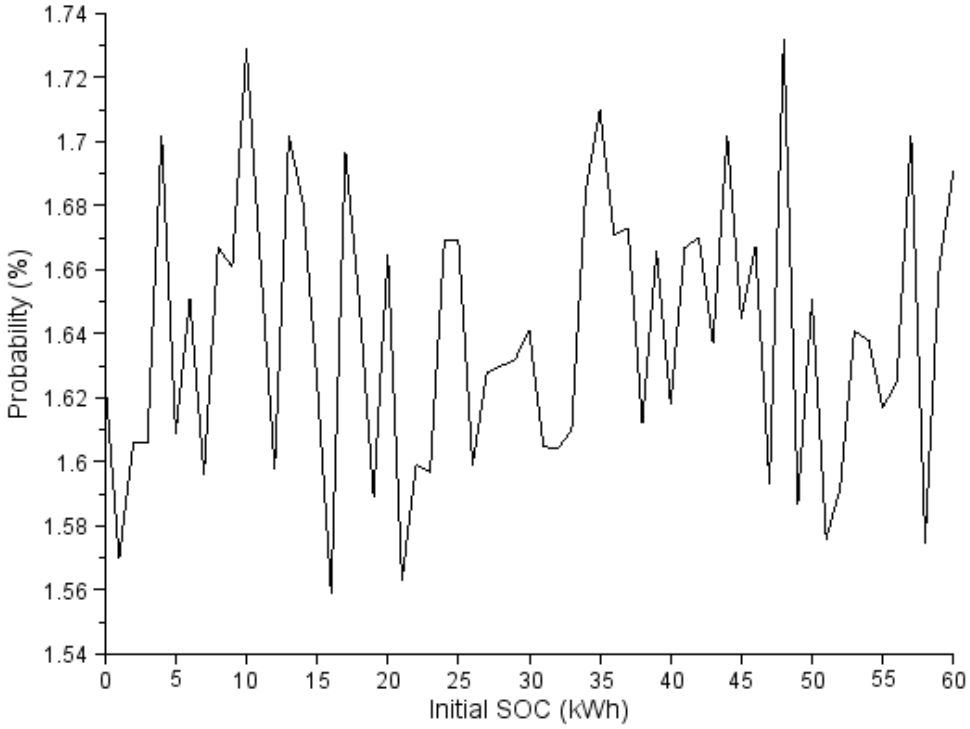


*Figure 119 Probability distribution for the simulated initial SOCs.*

| Islanding duration (quarter hours) | Probability (%) |
|---|---|
| 1 | 2.177 |
| 2 | 13.746 |
| 3 | 34.019 |
| 4 | 34.119 |
| 5 | 13.616 |
| 6 | 2.191 |
| 7 | 0.130 |
| 8 | 0.002 |

*Table 28 Probability values for the simulated durations of the islanding operation.*

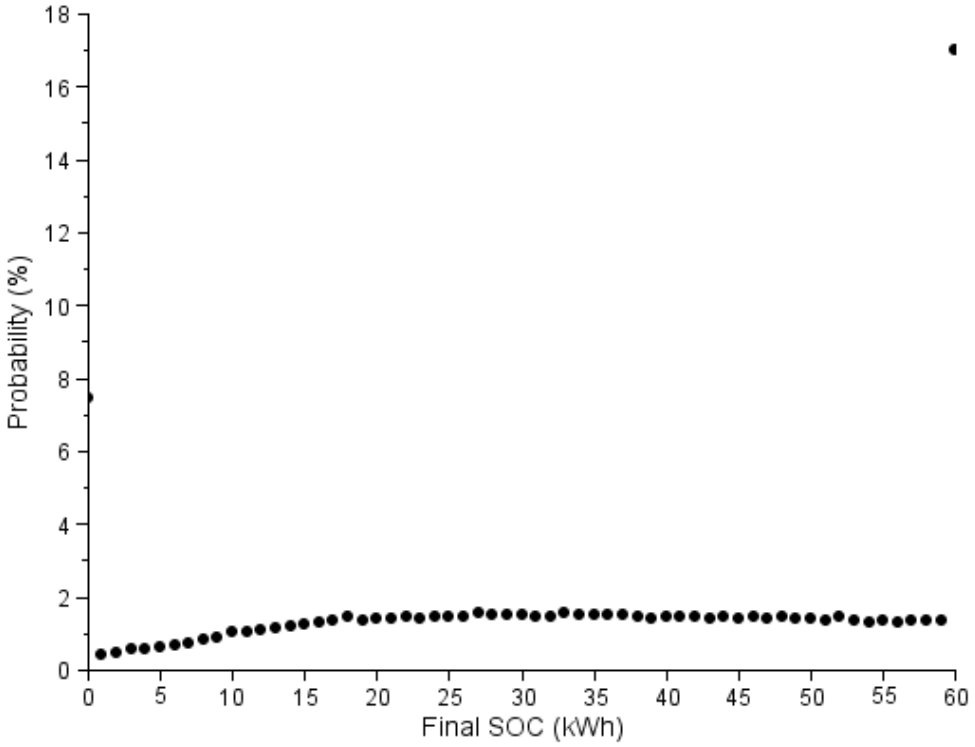


*Figure 120 Probability distribution for the calculated final SOC.*

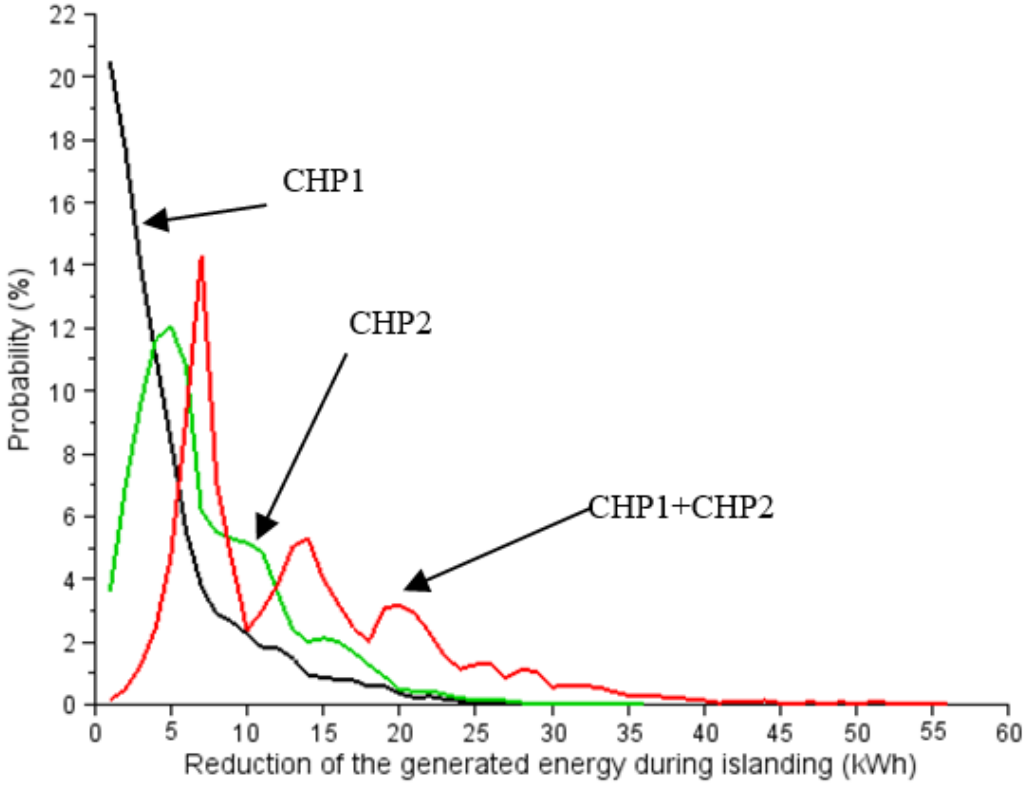


*Figure 121. Probability distribution of the reduction of the energy generated by the CHPs during islanding operation: black line – only CHP1 reduces output; green line – only CHP2 reduces output; red line – both CHP1 and CHP2 reduce output.*

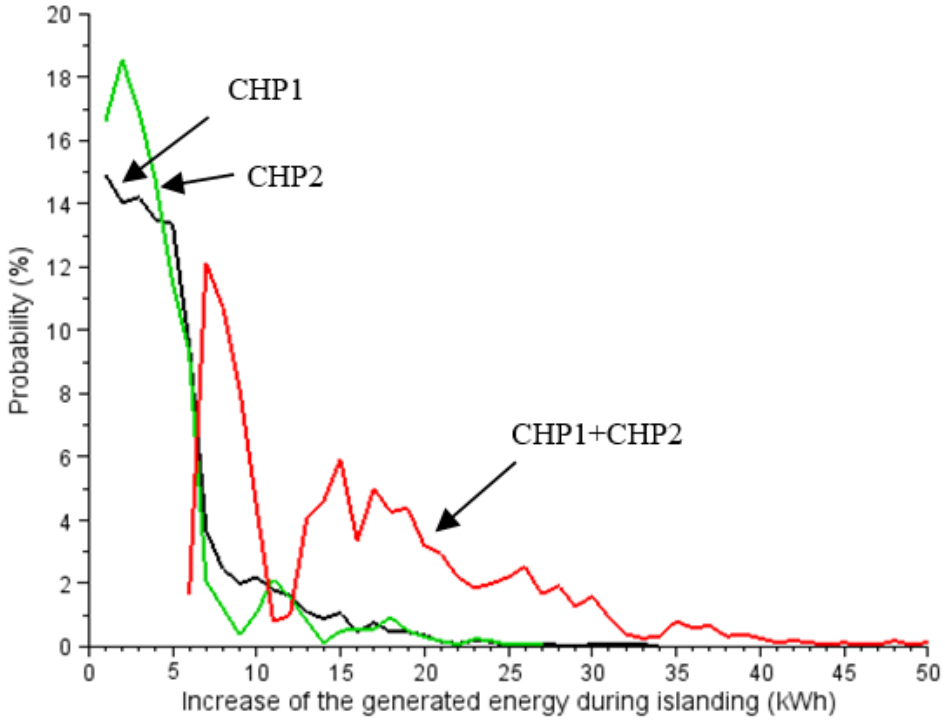


*Figure 122 Probability distribution of the increase of the energy generated by the CHPs during islanding operation: black line – only CHP1 increases output; green line – only CHP2 increases output; red line – both CHP1 and CHP2 increase output.*

Results show that the microgrid is able to operate the system in islanded mode for the vast majority of the 100,000 simulated cases. In a considerable share of cases (about 76 %), the islanded operation did not require to modify CHP generation output, since the BESS was able to balance the mismatch between aggregate load and generation. Only for the 3.622 % share of cases the islanding operation was not possible, since at the beginning of the islanding operation the output of both CHPs was nil and the BESS was not able to balance the load in excess due to its too low initial SOC. Further studies will address transient simulations in order to check the voltage stability of the system when off-grid.

### 5.2.2 *2nd Life batteries for energy management of a district [179]*

This section provides the evaluation of the KPIs for the energy services related to the District Management, notably peak shaving and power smoothing of local production.

The centralized ELSA District Energy Management System (EDEMS) is the software tool developed during the project and designed with the purpose of coordinating - in negotiation way - the district Blocks of Energy Unit (BoEUs). Its aim is to achieve the optimal solution responding to district power profiles requests from the DSO. Optimal solution consists of the exploitation of BoEU flexibilities to achieve the requested power profile, maintaining a sustainable usage of renewable resources. Algorithm implements a multi-objective framework based on the Non-dominated Sorting Genetic Algorithm II, high flexibility on constraints as well as a better modelling of the economic, technical and operational behaviour.

#### 5.2.2.1 *Peak shaving*

Peak shaving consists of reducing the amount of energy consumption at district level during peak demand hours. The service is requested by the DSO and managed at district level following a combined coordination of load shifting EV charging stations and discharging of SLB. In order to evaluate the reduction of peak consumption service the Minimum power Gap ($P_{MinGap}$) KPI is used:

$$P_{MinGap} = \frac{\min(P_{Dis}(t_i) - P_{DSOr}(t_i))}{\left|P_{DSOr}(t_y)\right|} 100, i \in [1, T] \quad (40)$$

- $P_{Dis}$ ($t_i$) is the average power consumed or injected by the district during every time slot $t_i$;
- $P_{DSOr}$ ($t_i$) is the reference value of the power profile requested by the DSO during every time slot $t_i$;
- *T* is the number of intervals in the time horizon of the optimization process;
- *y* is the value of *i* for which the minimum value occurs.

Equation calculates the minimum of all deviations between the power profile achieved by the district and that requested by the DSO. With respect to the signs, Active Power flows are assumed positive in case of power generation; then meaningful results are collected only for negative values, since positive values means that the system had not consumption peaks over the DSO power request (i.e., the minimum among these negative values represents the maximum absolute value of consumption peak). A target value is also provided and it is estimated referring to simulations performed with the system according to the DSO needs. Smaller is the absolute value, better is the optimization performed.

The EDEMS was able to perform long lasting experiments, notably an example of Peak shaving service over three days is analysed. *Table 29* shows the Minimum power Gap KPI values achieved for the test period, the target value for this KPI is - 17.5%. In the first day the Minimum power Gap is near the target reaching the value of -18.33%, the obtained result is suitable for the DSO since the peak power consumption is effectively reduced. During the second and the third day the system achieved the target KPI.

*Table 29 PMinGap over three test days*

| | **October 3rd** | **October 4th** | **October 5th** | **Target value** |
|---|---|---|---|---|
| **PMinGap** | -18.3% | -17.2% | -16.3% | -17.5% |

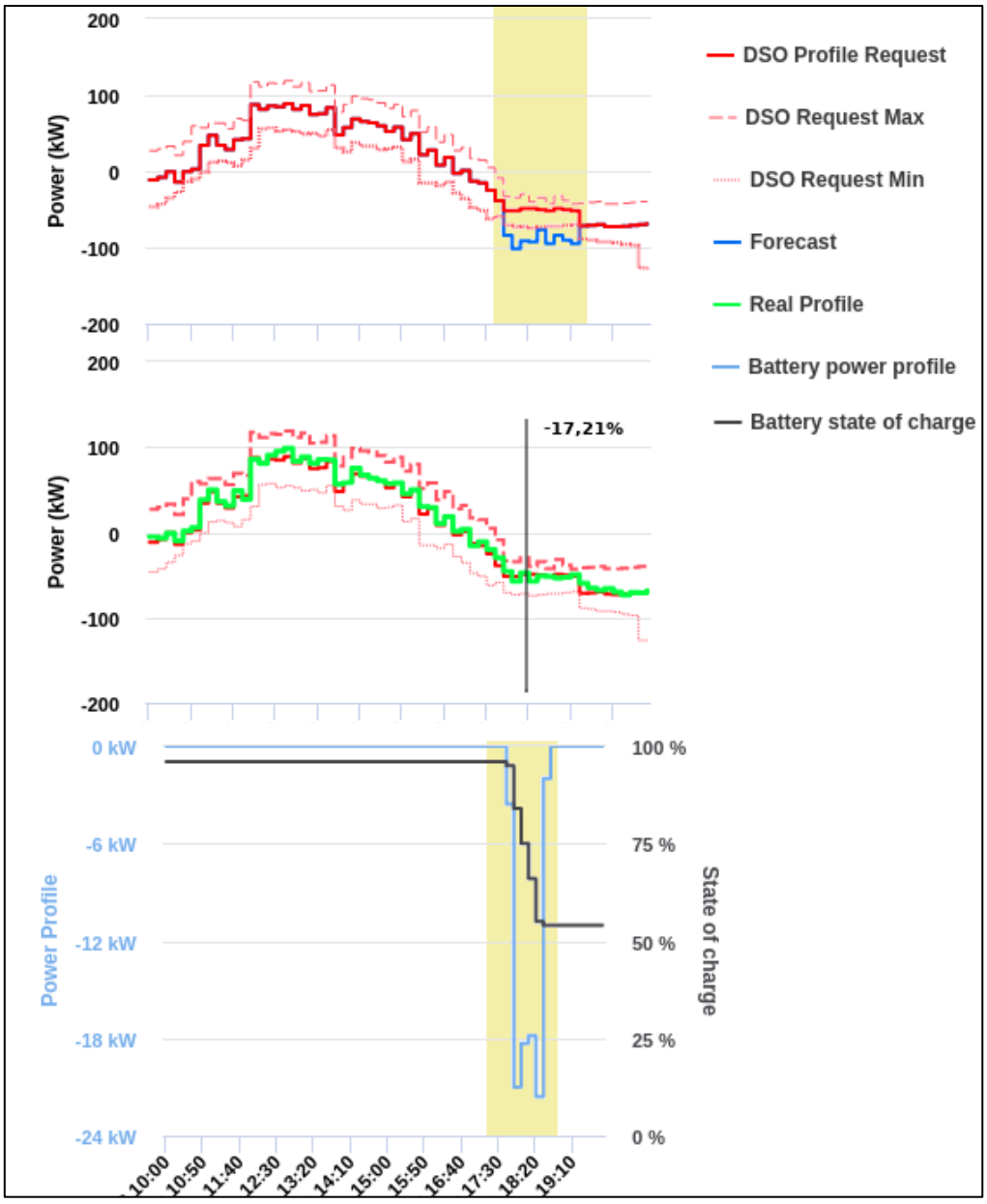


*Figure 123: Test of peak shaving service in October 4th,2018*

*Figure 123* shows a graphical representation of a test performance on 4th October 2018. The area marked in yellow represents the interval, during which peak shaving was requested (17:00 to 18:30); notably, the battery system started discharging at 17:40. In the upper part, the power profile requested by the DSO (red line) and the forecasting of district load profile (blue line) is represented. Then, a power profile is provided to the EDEMS as triplet, one for each time interval, including the expected profile (red continuous line) and a tolerance region (red dotted lines) around this value. In the middle of picture, the graph represents the actual power profile achieved by the district (green line) after the optimization process compared to the power profile requested by the DSO (red lines).

The power KPI reached the value of -17.21% at 17:30. At the bottom of *Figure 123*, the power profile of the batteries is represented by the blue line, in this case, positive values are referred to battery charging; black line represents the State of Charge (SoC).

In a demand and supply setting, it is worth measuring the overall deviation between DSO request and actual power provision of the district. Then, a proper KPI is used:

$$TpD = \sqrt{\frac{(P_{Dis}(t_i) - P_{DSOr}(t_i))^2}{T}} \quad (41)$$

The performed optimization is more effective when the deviation decreases. *Table 30* shows *TpD* values for the tests evaluated according to the equation. It is worth pointing out that all results are aligned with the target value (11 kW).

*Table 30 TpD over a three test days*

| | **October 3rd** | **October 4th** | **October 5th** | **Target value** |
|---|---|---|---|---|
| **TpD** | 6.1 kW | 5.3 kW | 7.2 kW | 11 kW |

The district output should be much as close as possible to the requested power; however, other values are considered acceptable in case they remain inside the acceptance area. Therefore, for each interval, an acceptance area is defined by $P_{DSOr,DOWN,}$ and $P_{DSOr,UP}$, which represent the lowest and the highest value of acceptable power provided by the district respectively. The following KPI represents the number of intervals in which the $P_{Dis}$ exceeded the $P_{DSOr,DOWN}$ with respect to the total number of intervals, expressed in percentage.

$$N_{DOWN} = \frac{Card(Downward)}{T} 100 \quad (42)$$

*Downward* is the set of intervals for which $P_{Dis}$ is lower than $P_{DSOr,DOWN,}$ whilst *Card* is the cardinality function. Following the same approach of previous KPI,

$$N_{UP} = \frac{Card(Upward)}{T} 100 \quad (43)$$

*Table 31 Nup and Ndown over three test days*

| | **October 3rd** | **October 4th** | **October 5th** | **Target value** |
|---|---|---|---|---|
| **NUP** | 1.4% | 0% | 0% | 2.8% |
| **NDOWN** | 0% | 0% | 1.7% | 2% |

*Upward* is the set of intervals for which $P_{Dis}$ is higher than $P_{DSOr,UP}$. *Table 31* shows the results of the two KPIs for the period test. For peak shaving service the Number of power downward KPI is more relevant. Indeed, it represents the number of intervals in which the district exceeded the lower value delimiting the acceptance area on respect of the total number of intervals, evaluated as a percentage. For this KPI the target value is 2%. In all of test cases, the achieved values are smaller than the established target value.

#### 5.2.2.2 *PV power smoothing*

The PV Power smoothing service represents the possibility to smooth the PV production peak storing the energy or consuming it to charge EV with re-arranged scheduling (load shifting). All in order to mitigate fluctuating power injection from the district to the grid. The service is requested by the DSO as part of the overall power profile request and handled at district level increasing the load or activating the battery charging. In order to evaluate the PV power smoothing service the Maximum Power Gap ($P_{MaxGap}$) KPI is evaluated as follows:

$$P_{MaxGap} = \frac{\max(P_{Dis}(t_i) - P_{DSOr}(t_i))}{|P_{DSOr}(t_k)|} 100, i \in [1, T] \quad (44)$$

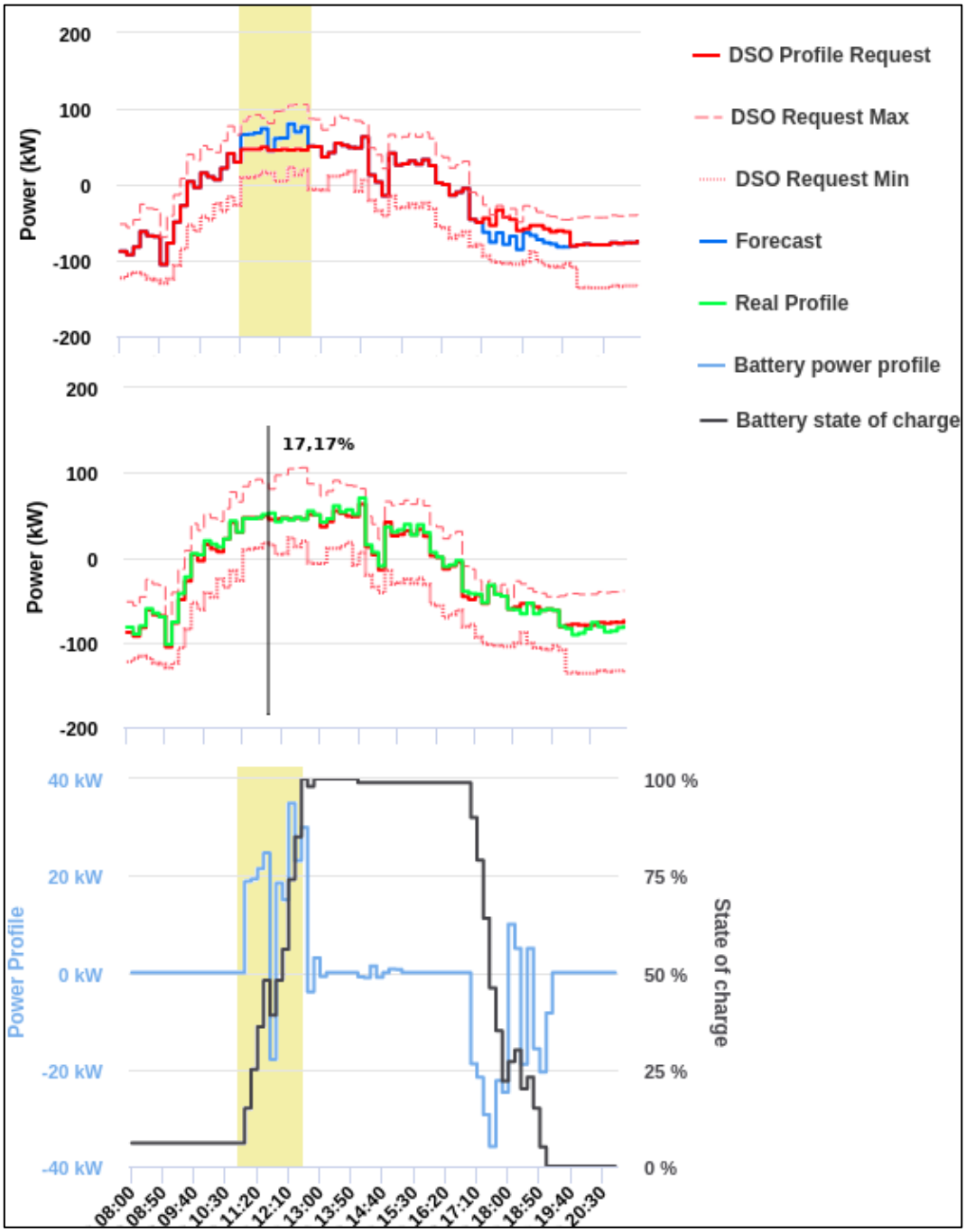


*Figure 124: A test of PV power smoothing service in September 26th, 2018*

In equation, $t_k$ is the time interval during which the maximum occurs. It calculates the maximum of all deviations between the power profile achieved from the district and power profile requested from the DSO. Results are relevant only for positive values otherwise it means that the system had not PV production peaks on respect of the DSO power request. In this respect, lower values correspond to better performances.

As already presented for peak shaving, power smoothing over three days is analysed. During three days, the PV power smoothing service was requested during the time frame 11:00-13:30 (i.e., when the PV power production is high). *Table 32* shows the Maximum power Gap KPI values achieved for the test period. The target (18.5%) is estimated referring to simulations performed with the system according to DSO needs; it is worth pointing out that the target were reached every time.

*Table 32 $P_{maxGap}$ over three test days (PV power smoothing)*

| | **September 26th** | **September 27th** | **September 28th** | **Target value** |
|---|---|---|---|---|
| **PMaxGap** | 17.2% | 17.6% | 15.6% | 18.5% |

A test has been carried out on 26th September 2018 and its results are shown in *Figure 124*. Figure description have been already provided for *Figure 123*. In this example, the Maximum power Gap reached the value of 17.2% at 11:40. The batteries are charged from 11:00 to 12:30 reaching the 98% of total capacity in order to smooth the PV power peak. *TpD*, calculated according to (5), is reported in *Table 33*. Results over three day period of test are lower than the target value.

*Table 33 TpD over three test days (PV power smoothing)*

| | **September 26th** | **September 27th** | **September 28th** | **Target value** |
|---|---|---|---|---|
| **TpD** | 4.8 kW | 9.7 kW | 7.2 kW | 11 W |

*Table 34* shows the results of $N_{UP}$ and $N_{DOWN}$ (evaluated according to (6) and (7) respectively). With respect to power smoothing, $N_{UP}$ is more relevant, since it represents the number of intervals in which the district exceeded the higher value delimiting the acceptance area on respect of the total number of intervals (in percentage). For this KPI the target value is 2.8%. In all tests, the power profile achieved by the district does not violate the tolerance region requested by the DSO.

*Table 34 $N_{up}$ and $N_{down}$ over three test days (PV power smoothing)*

| | **September 26th** | **September 27th** | **September 28th** | **Target value** |
|---|---|---|---|---|
| **NUP** | 0% | 0% | 0% | 2.8% |
| **NDOWN** | 0% | 0% | 0% | 2% |

## 5.3 Adequacy of electrical parameters during normal operation

### 5.3.1 *Storage for ancillary services [179]*

This section reports and discusses the ancillary services provided by SLB to the DSO. It has been planned to evaluate the following services:

- Power Quality and Power Balance,
- Dynamic Control and Compensation of Reactive Power (Q),
- Power intensive application

A test of ancillary service has be carried out during September 2018, by means of only one inverter. In order to perform a closed loop regulation and to acquire feedbacks about power quality, Current transformers (CTs) have been installed in a node that belongs to the same LV network.

#### 5.3.1.1 *Power Quality and Power Balance*

The Power Balance Regulation, aims at reducing unbalancing between phase currents through the inverter which provides the current injection to compensate any difference between phases. The current single phase A, B and C have actually different values, as reported in *Figure 125*. During this test, 83% of the capability of the SLB was used for the active power injection whilst 17% to compensate the unbalance between the phases. With respect to the evaluation of power balance, the related KPI highlights the power flexibility that the ESS offers between the phases. The KPI formula is as follows:

$$\Delta P\% = \Delta P/P1*100 \quad (45)$$

Where $\Delta P$ is defined as follows:

$$\Delta P = (P1-P2) + (P1- P3) \quad (46)$$

$P1$, $P2$, $P3$ correspond to the active power consumed or produced by the phase 1, 2 and 3, respectively. It is worth pointing out that a phase (e.g., phase 1) has been taken as a reference for the KPI calculation.

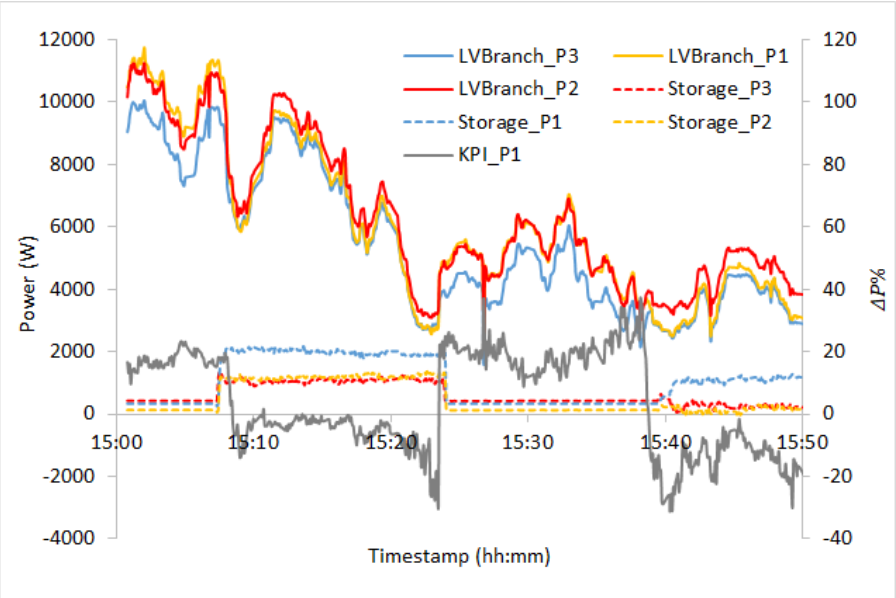


*Figure 125. Power profiles for each lines and KPI variation over time, in case of Power balance*

*Figure 125* shows that from 15:10 to 15:20 the average KPI is less than 3%; when power balance is not implemented, the average KPI increases up to 18 %, showing that SLB can effectively reduce unbalances in DN (i.e., the obtained value is adequate for a DSO).

#### 5.3.1.2 *Dynamic Control and Compensation of Reactive Power*

With respect to the Dynamic Reactive Power Control, DSO sends a (P,Q) request to the SLB and it follows this set point. Figure 3 shows the operational point provided by SLB. The inverter has charged and discharged the system to maintain stable this point; notably relevant differences were not detected by the SCADA interface.

When reactive power is compensated by the ESS, DSO has to reduce the amount of the reactive energy that flows in the line, in order to decrease Joule losses and increase distribution efficiency. In this scenario, the amount of reactive power has been monitored at the point of delivery (i.e., connection node between network and ESS) by means of $\Delta$Q%, defined by the equation 3:

$$\Delta Q\% = (Q_{REF} - QSS)/Q_{REF} \quad (47)$$

where $Q_{REF}$ is the reactive power on the point of the CTs installation, QSS is the reactive power of the ESS and $\Delta$Q% is the difference between the need and the providing of reactive power in percentage. *Figure 126* shows the variation of the KPI over time (considering average values collected every 10 minutes); notably, when this functionality is applied, the KPI is practically 0% (i.e., period from 14:40:00 to 14:50:00). Before the activation, the value is 32% whilst the value decreases to 23% after the deactivation.

#### 5.3.1.3 *Tests for power intensive applications*

A set of tests have been carried out to evaluate if the deployed SLBs are suitable for the application on power intensive field. In this respect, a proof of concept about the Primary Reserve contribution is reported. When DSO asks for this kind of service, the ESS changes its set point of P according to the frequency value contributing to frequency stability of global network. The request of the P injection or absorption should be provided by a TSO parameterization in a local device. Test has been done by a simulation of a TSO request for power injection and power absorption as shown in the Figure 127.

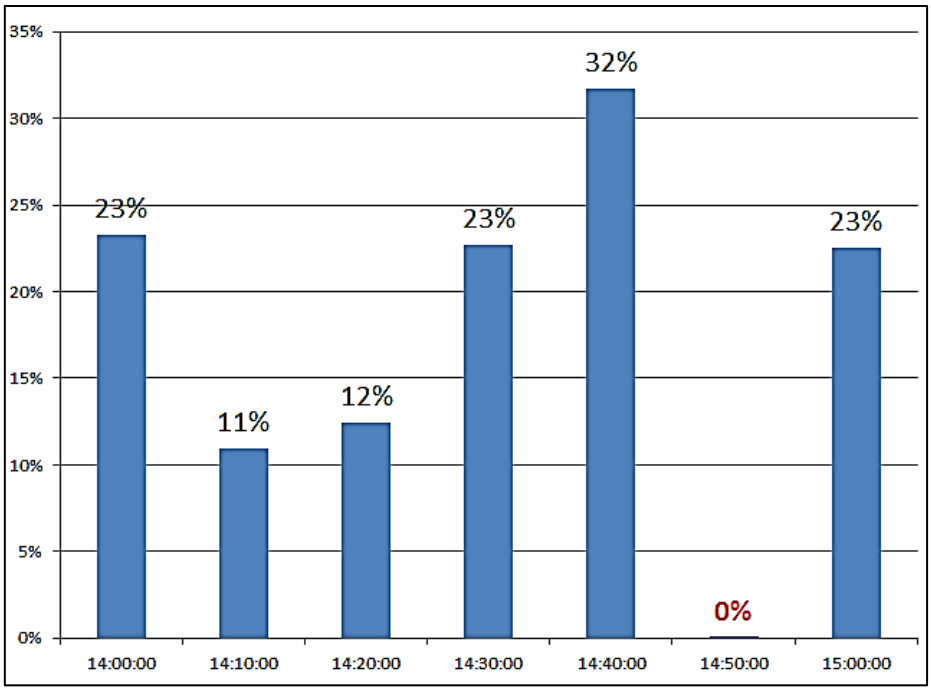


*Figure 126. Reactive Power Compensation: KPI variation over time*

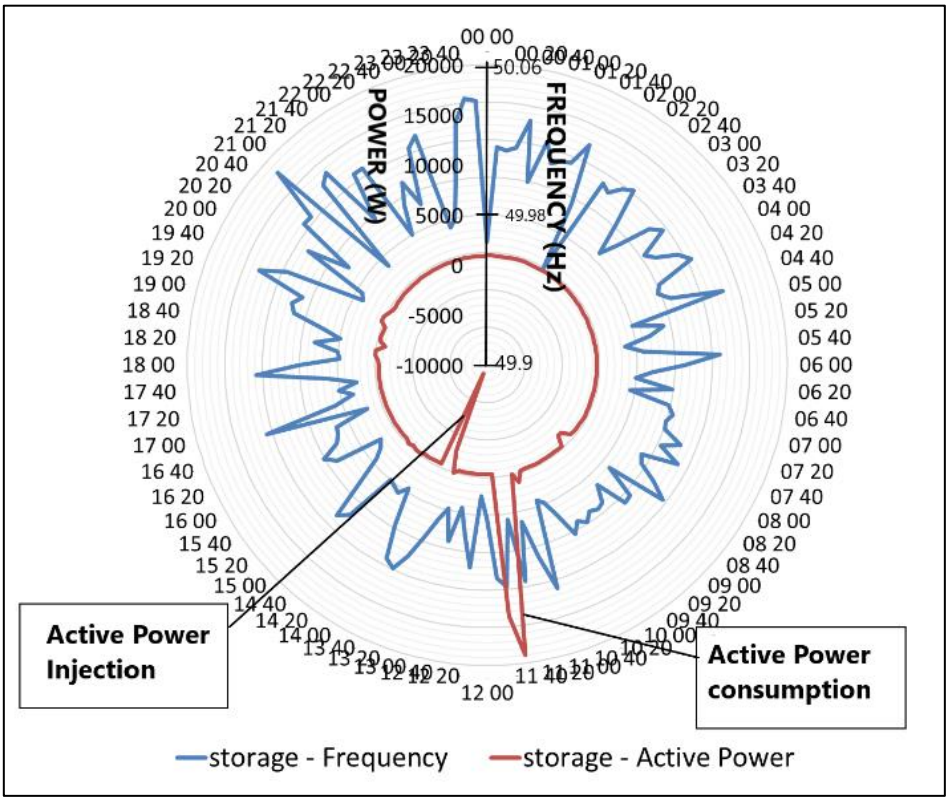


*Figure 127. Primary Reserve Service: Frequency and P variation over time*

In addition, the time response of the whole system has been evaluated by means of a waveform recorder. Figure 128 shows the current transient after a step request of Power Injection performed by DSO. The system (i.e., batteries and inverters) has taken 0.4 seconds to reach the requested Set Point (i.e., 20 times the period since the network is 50 Hz). It is worth pointing out that these

performances are suitable for the previously described energy services (e.g, Power Balance and Reactive Power Compensation). In order to obtain better performance of Dynamic Reactive Power and Primary Reserve an update of inverter ramp is required and other tests should be carried out.

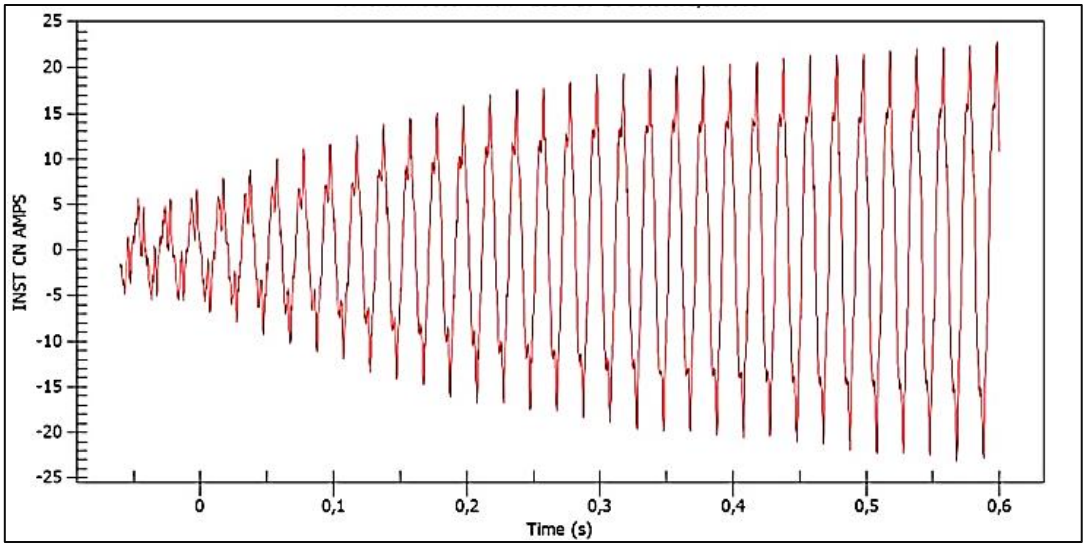


*Figure 128. Current transient after a step request of P injection/absorption*

Therefore, based on the results, it can be argued that the system currently implemented in the Terni trial site achieved adequate performances. However, based on the tests carried out, the most meaningful results have been collected when power intensive is not requested. With respect to the ancillary services, notable results have been achieved in case of unbalancing of current phases. On the other hand, valuable services can be provided to shave its load peak and to smooth local generation that have been presented in previous subsection.

### 5.3.2 *Frequency control [180]*

Frequency is considered to be a common parameter in the synchronous power systems. However, this situation occurs only in theoretical steady-state situations, and in practice there are small differences between the measurement points, due to the fact that the stable situation is always disturbed by changes, producing differences between different grid points to have only some millihertz values.

In addition, the measurements made with Phasor Measurement Units (PMUs) and more recently also based on real-time data from smart meters, give additional differences, due to their specific measurement errors. These meter-based frequency measurement differences may be higher than the ones from PMUs, based on the method of measurement.

Finding information to be processed in order to assess grid data inconsistency is a challenge. To get cross-grid data consistency in local, regional and pan-European areas, it is needed also that the data has no private content, such that it can fulfil the General Data Protection Regulation (GDPR) requirements. Power data from grid users may be in this situation, as it can show behavior of persons, thus being under the GDPR requirements. Grid only related data can be considered as being the grid frequency, voltage level and even rate of change of frequency (rocof). From these parameters, frequency and voltage can be easily measured but voltage is also regionally dependent, thus being not adequate for a general approach. It remains the grid frequency as a proper parameter candidate, both easy to calculate – while in many cases also necessary to be calculated because of

the need to synchronize samples of data needed for other purposes, and completely non-private in its nature (it can be measured by anybody, in any plug, if the right equipment is used).

Frequency can be measured at any level and thus the data consistency can be assessed bot at local grid level as well as at pan-European level, in the usual situation when the grid is in normal state, with no islanding situations.

One solution is developed by using the Unbundled Smart Meter architecture, already presented in chapter 5.1 of this work. In this setup, frequency can be obtained each one to 10 seconds from the Smart Meter, as real-time value synchronously acquired over the network, and the data can be sent from each metering point to a central station which can make real-time comparison of the frequency values over the local network.

An improved solution, shown in *Figure 129*, is based on additional incorporation of a low cost PMU, which can bring not only frequency and voltages, as being redundant at the local level, but also derivate of frequency (rate of change of frequency, or rocof). The additional information may be processed also as grid data, however in a different way, as it is showing practically disturbances rather than current status (observability of steady-state) of the grid. Measurement of frequency and rocof have been used also for different functionalities in the grids. Figure 2 shows the extension of previous materialized in the equipment named NORM (Next generation Open Real time Meter), where a low cost PMU and a higher data security using physical unclonable function (PUF) [181], [182] and [183] are added. The setup has been developed as proof of concept in SUCCESS project, [184].

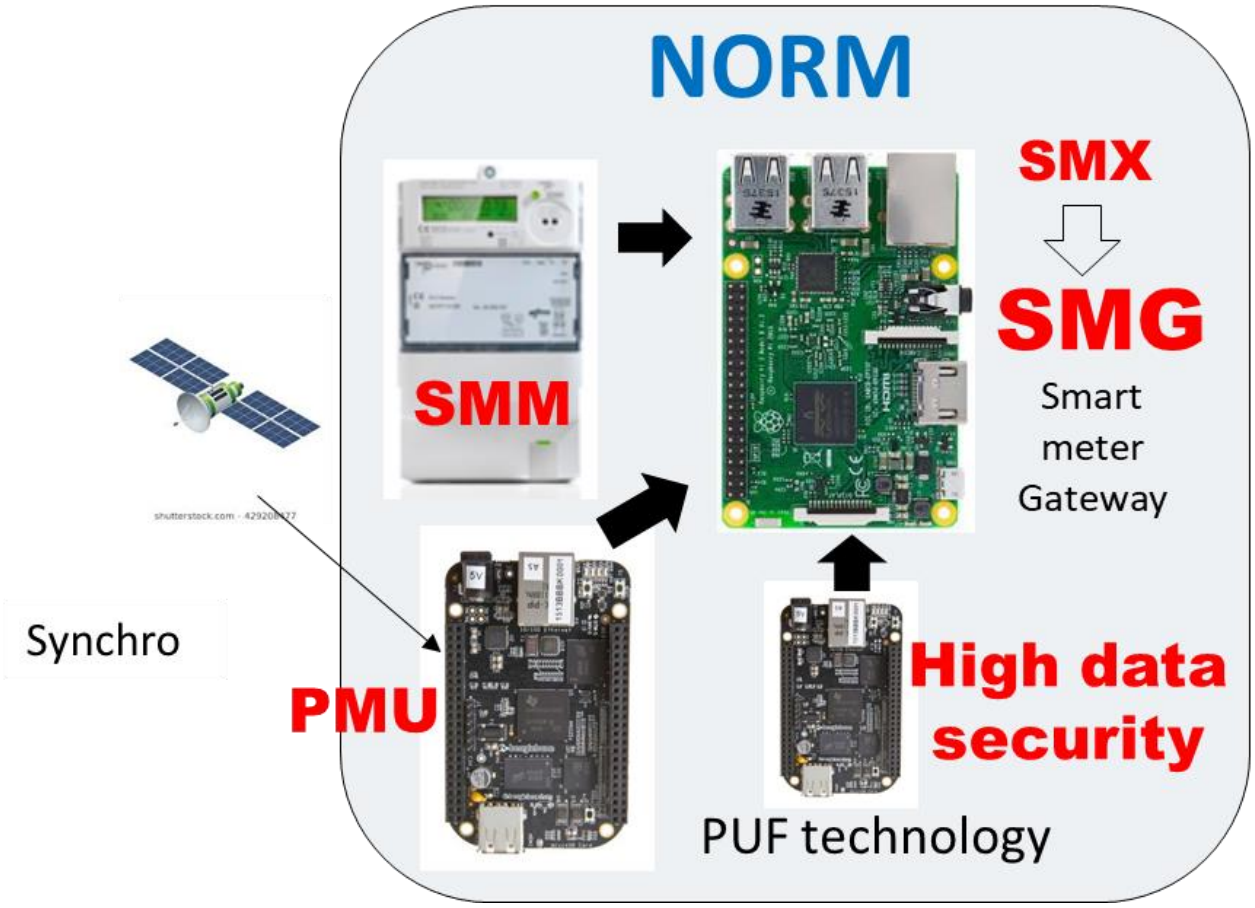


*Figure 129 NORM architecture, extending USM with PMU and PUF*

The Smart Meter eXtension integrates data from both sources – meter and PMU and thus has a redundancy for voltage level and frequency measurements. The reporting rate for both SMM and PMU is at one second, bridging in a practical way smart meter real-time data and phasor measurements.

*Figure 130* shows that data from NORM can be sent through a wide area network to the traditional distribution system operator (DSO) actor, to its control platform considered as a critical infrastructure system, to the different energy business actors, such as aggregators, energy service companies (ESCOs) or markets, but also to a Critical Infrastructures Security Operation Center (CI-SOC) for analyzing at high level cyber security threats. The communication between NORM and various end-point is made through secure remote connections using Virtual Private Network (VPN) technology. A different VPNs is considered for each actor, such that compromised zones from cyber-security point of view are not expanded to all the participants which communicate through the wide area network with NORM. The solution is particularly applicable in real-time applications (on-line), however it can be also applied for off-line analysis.

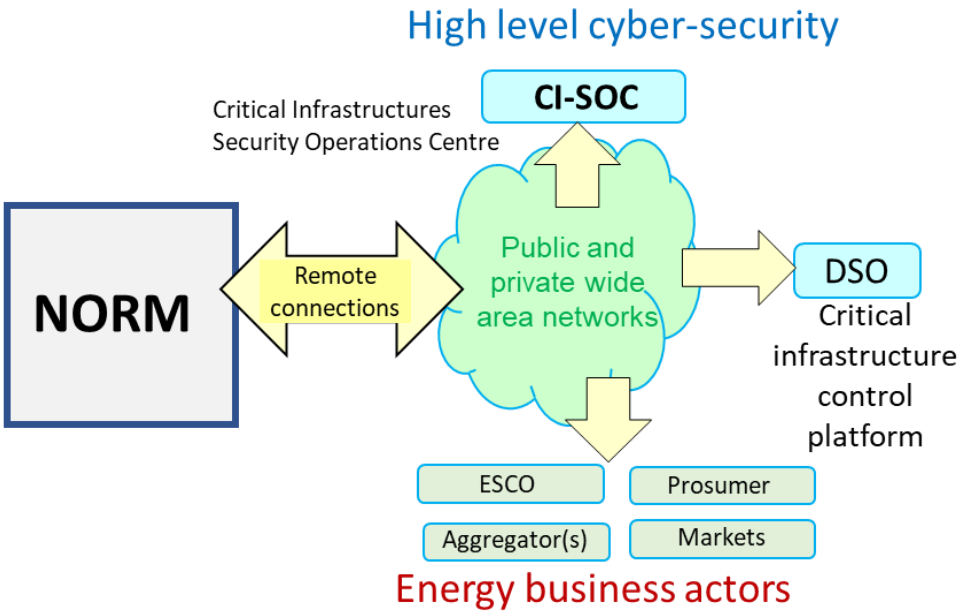


*Figure 130. NORM data flow towards energy actors and to a security infrastructure*

By using setups based on classic USM and on its extended mode NORM, several measurements and their assessment and interpretation are given below.

Figure 130 shows how is evolving the measured frequency in a NORM equipment, using simultaneous data from the meter and from the PMU section. Measurement are recorded over a selected widow of one hour and the frequency vales are obtained with a reporting period of one second for each source (meter and PMU).

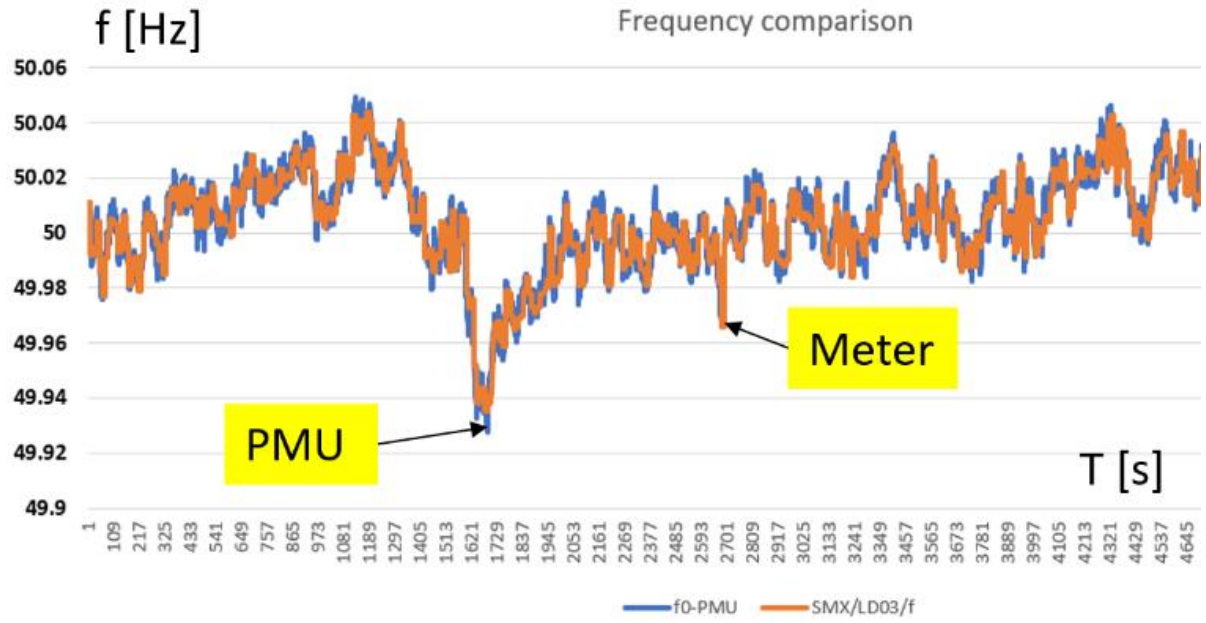


*Figure 131. PMU and Meter frequency measurements and comparison in NORM*

Using data analytics, the deviation between the measurements taken in different grid points can be monitored with statistical means and anomalies can be detected, based on the patterns of frequency deviation evolution.

*Figure 132* shows a similar evolution, but the superposition is now between three different points in distant places in the main grid. It can be seen that it is as well a nearly perfect match, as the frequency has very small differences over the grid, as specified above.

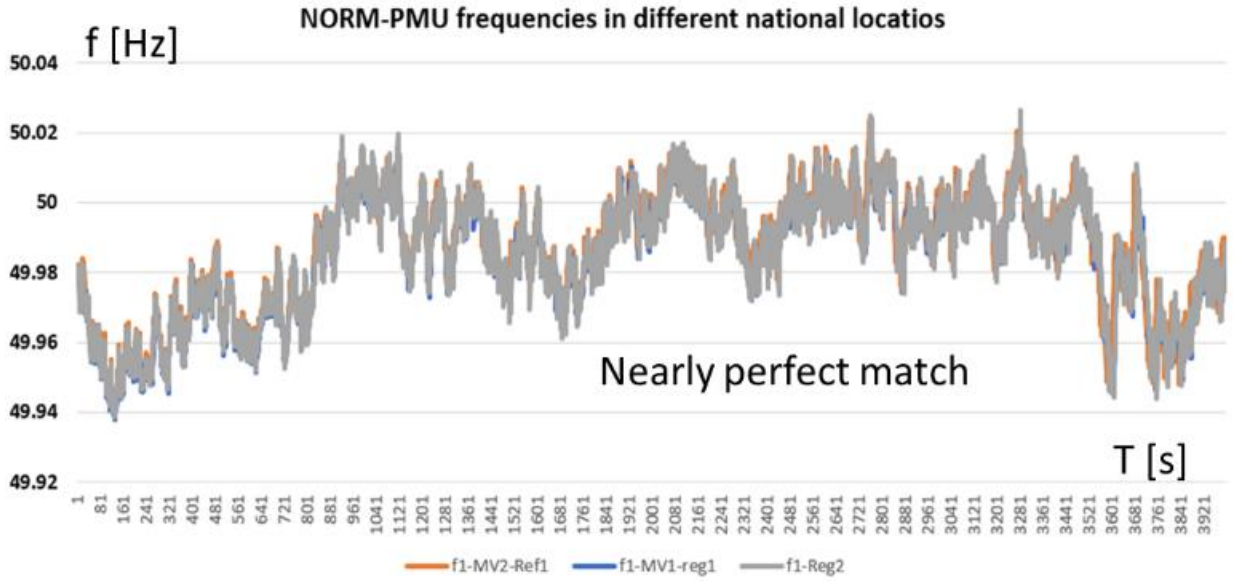


*Figure 132. NORM frequency measurements and comparison in three different grid points*

The real-time differences, considered as frequency deviation, can be calculated with one of the following formulas:

*Error1 = max(abs(f1-f2), abs(f1-f3),abs(f2-f3))* (1)

*Error2 = max(abs(f1-fMED), abs(f1-fMED),abs(f2-fMED))* (2)

where f1, f2 and f3 are the frequencies measured in three points, fMED is the average frequency between the three values and abs means the absolute value.

The evolution of such deviation can be represented in a synthetic graph showing "circles" of healthy values, as per *Figure 133*. In this figure, a trigger of 0.03 or 0.035 Hz can be used to detect an inconsistent situation, triggering a possible malicious attack.

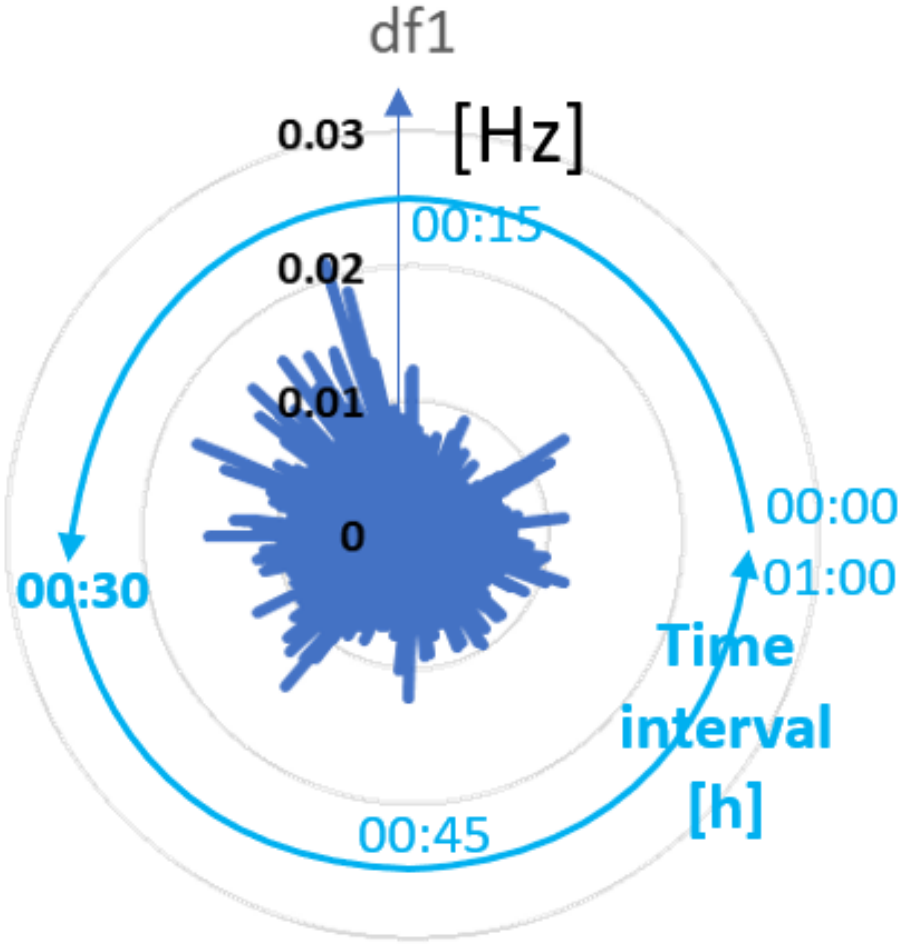


*Figure 133 Cross network frequency match*

In *Figure 134* is presented a situation in which a disturbance occurs in the grid. In this particular situation, there is a perfect match between frequencies in the two metering points in the normal steady state situation, but in a specific moment a certain grid disturbance occurs, namely a short-circuit which is cleared in short time.

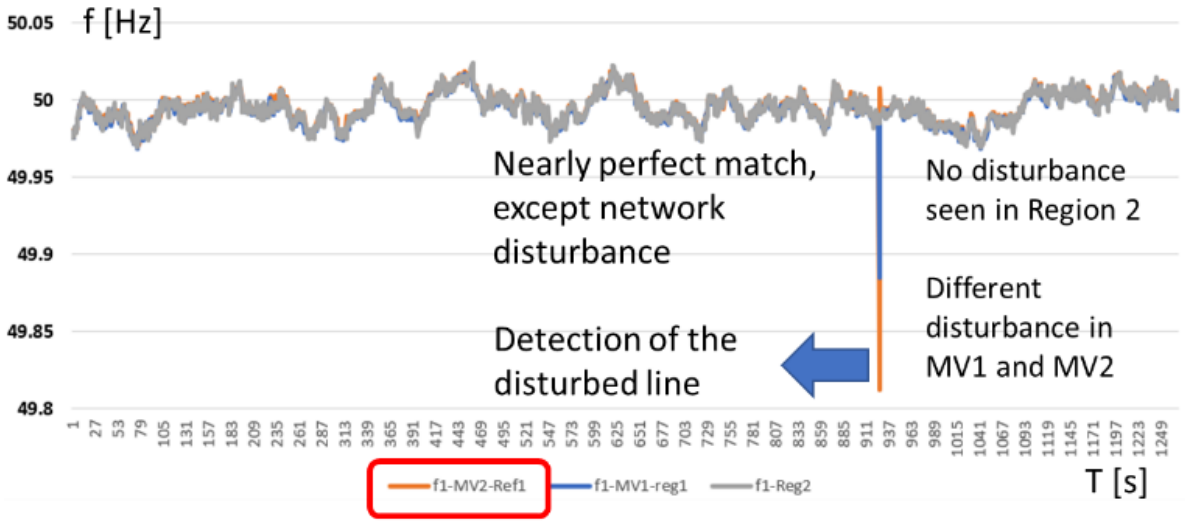


*Figure 134. Cross network frequency match in a medium voltage grid with a disturbance record*

As the two measuring points are in the same medium voltage network but on different lines, the disturbance is "seen" through frequency measurements in a different way in each metering point. The temporary grid disturbance gives wrong measurements on frequency also on temporary basis, but the frequency deviation is higher on the line more near to the real grid disturbance. *Figure 135* shows such a situation, with a far short-circuit on feeder 3, which is recorded in PMU1 and PMU2 with a different degree of disturbance on the PMU measured frequency.

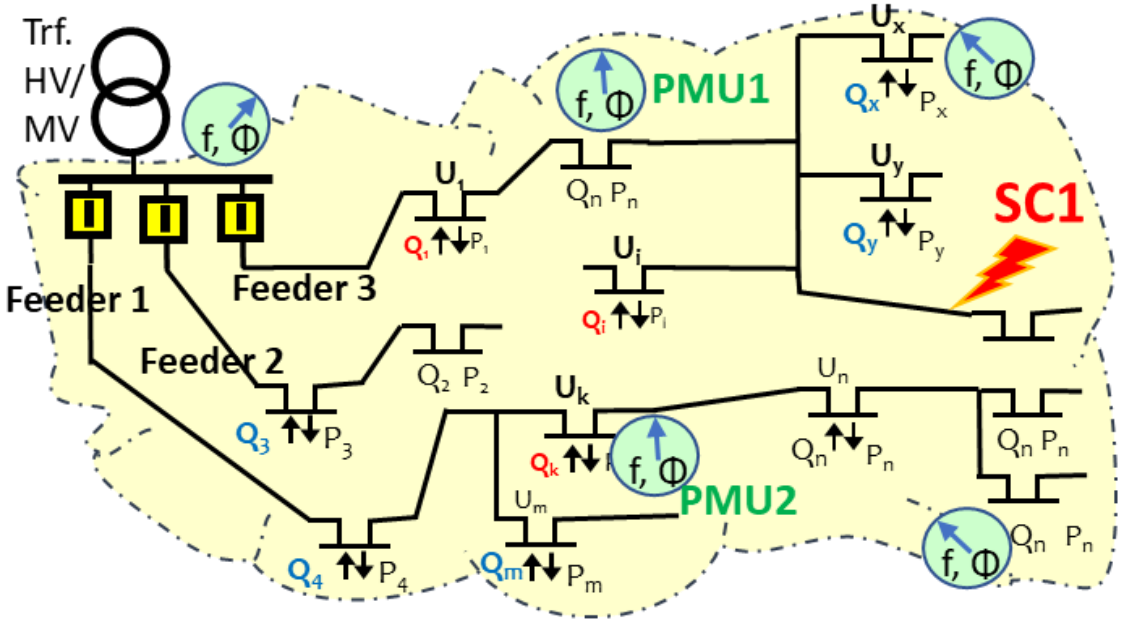


*Figure 135. Short-circuit in a medium voltage network with three feeders*

This practical finding shows that frequency measurement and comparison on grid level can be a complementary way to detect a place of physical disturbance in the grid.

The way how the situation can be seen at CI-SOC level can be observed in *Figure 136*, where a similar representation as in is given. The two higher than normal deviations suggest that the

temporary frequency deviation is related to a grid event situation, and not to a cyber-security issue, which normally CI-SOC system is trying to detect.

The deviations are shown as being synchronous (same short period of one or two seconds in recording PMU data reported each one second) and un-equal in magnitude, suggesting that the disturbance has been differently recorded in different places of the grid. This situation occurs because the frequency measurement during a disturbance is affected by the level of disturbance, which is also dependent on its grid electrical distance from the measuring point.

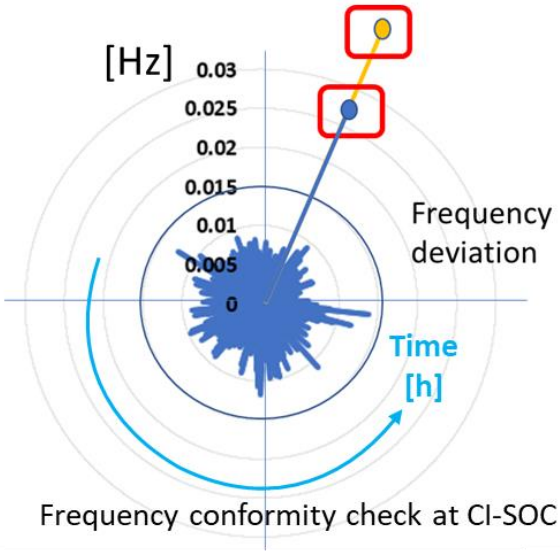


*Figure 136. Frequency disturbance as it is detected at higher level*

Different statistical methods can be applied in order to value possible cyber-attacks as well as grid disturbances, however this analysis used the previous presented formulas (1) and (2).

*Figure 137* shows the simulated situation of a cyber-attack. In this setup, most of the frequencies have a small deviation, which is depicted with blue color on the rotational evolution of the frequency deviation. In the Figure, a suspicious frequency deviation, shown in green color, associated to a specific metering point, is shown as being much higher than all other deviations. This inconsistency may show a possible cyber-threat, and counter-measures can be taken, such as neglecting all the NORM values in the central control system and considering a quarantine and/or labeling the end-device as a non-trustable source.

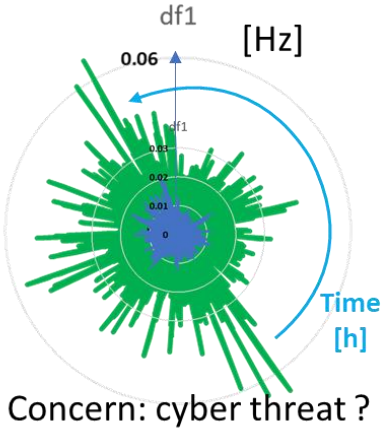


*Figure 137. Possible cyber-threat due to high statistical deviation of measured frequency*

Specific additional algorithms may even better dissociate suspicious metering points bringing frequency values with high statistical deviations, compared with the most of other grid points. Based on the basic algorithm and visual awareness described in this work, a security operation center may use such information to assess consistency at grid level and to detect abnormal situations.

However, grid frequency is a nearly constant value only to fully connected synchronous grids. In real networks functionality, it is possible that some grid areas which support microgrid functionality may be temporary disconnected from main grid and start working in islanded mode. In such zones the frequency are locally synchronous but may have different average values compared with the main grid, thus bringing a systematic frequency difference compared with the frequencies from metering points still connected to the main grid. *Figure 138* shows in a similar way as in the previous situations how frequency deviations from an islanded microgrid can appear at the security operation center level, using the same visual representation with time intervals during a complete rotation of the grid frequency deviations (radar-like view).

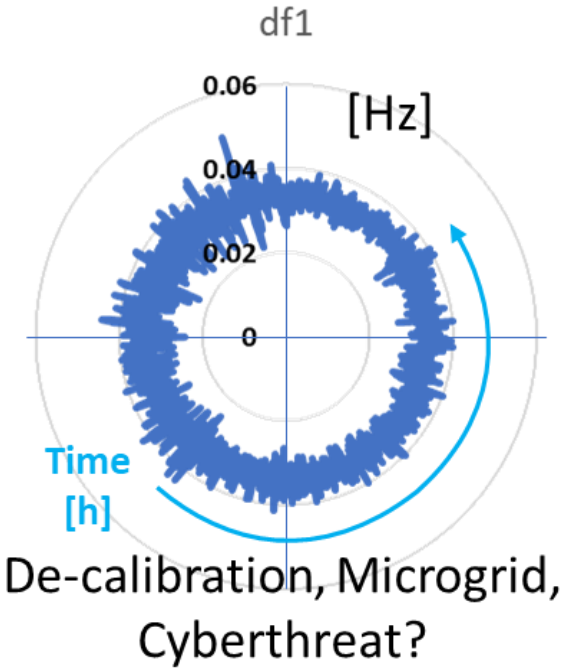


*Figure 138. Systematic deviations of a metering point or of a group of such points in the grid*

The situation occurs in grids such as in *Figure 139*, where PMUs numbered 1.x are coherent but different from the data from PMU numbered 2.1 and 2.2, as the right part of the grid is in island mode after opening in point K. This can be a method of detecting islanding, situation which is already approached in different ways in other works [185].

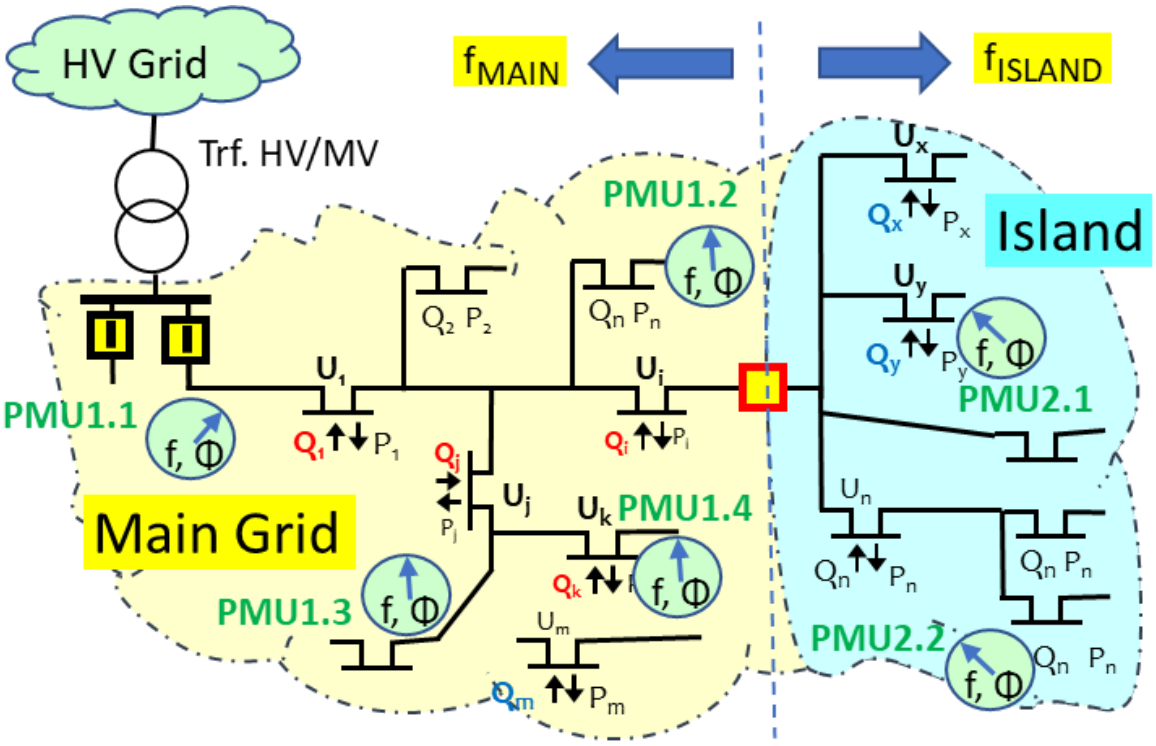


*Figure 139. Main and islanded grid. Clustering PMU data with different f*

The situation may occur also in the situation that one (or some) point is de-calibrated (but not too many at a time) or if a cyber-threat shows signs of occurrence. Real situation can be deducted by using additional data and rules.

Finally, pan-European consistency of the frequency can be assessed by comparing specific measurements from distant point in European grid. *Figure 140* shows real measurements from different points in the European grid, one from Italy (in Terni) and two in Romania, on the points of common coupling of a hydro plant and of a PV plant, in different medium voltage networks not directly connected.

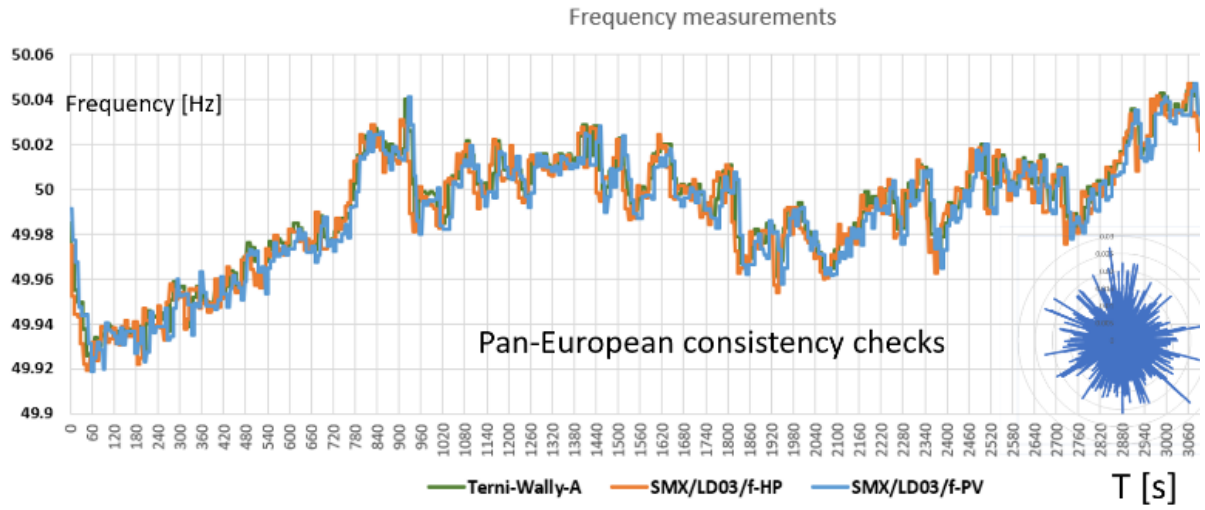


*Figure 140. Frequency measurements over European grid*

It can be seen that even the measurements are from two different countries, there is a high consistency between the measurements, as basic situation which can be used to trigger abnormal situations.

The above assessment on frequency measurements has been proven to be applicable at the three levels, using redundancy available in each situation:

- At local level, due to redundancy of frequency measurement at NORM level (meter and PMU measurements)
- At local grid level, by analyzing frequency measurements from different metering points in the local grid;
- At national and pan-European grid, by selecting some measurements placed at different points in the European main grid.

The different analysis show that frequency is a good choice for performing data consistency analysis over a large interconnected grid, as a prerequisite for detecting false data injection and consequent cyber-attacks. By choosing proper analytical tools such as statistical analysis and rule-based decisions, cyber threats have additional ways of being detected in order to trigger counter-measures. The real-time analysis of these data may ask also for high computability features at the level of CI-SOC, however statistical algorithms may be adapted for parallel computing, thus allowing modern computer architecture to be used for accelerating the on-line analysis and detection of process data inconsistencies.

Similar developments can be used to assess grid data consistency based on derivate of frequency (rocof), as additional tool to detect abnormal situations, to be assessed as usual grid disturbances or suspicious to be analyzed against other possible reasons, such as measurement decalibration, cyber threat or islanding of microgrids.

The presented analysis shows how frequency, as a common parameter in the synchronous power systems, can be used to assess data consistency over the grid, thus being able to detect eventual intrusions through cyber-attacks. The method is based on the analysis of the frequency evolution at different levels in the grid, namely local – at the metering point level, regional, at the local grid level and national / pan-European, by using selected metering point over the main European grid.

Specific examples, based on real measurements from NORM equipment, as well as their interpretations, are given in the section, to show the effectiveness of the presented method.

It is also shown that, by choosing appropriate analytical tools such as statistical analysis on synchronized frequency measurements as well as rule-based decisions, there are additional ways to detect cyber threats, in order to trigger specific counter-measures.

Moreover, it is shown that monitoring frequency deviations over a local grid can enhance the observability of grid disturbances and to allow a better localization of the fault, as a new method not used in previous works.

### 5.3.3 *A Real Life demonstration of DR campaign [186]*

Considering the huge amount of distributed generators, the Distribution System Operator (DSO) has to manage a huge number of small distributed generators that have not programmable power injection. In this respect, many solutions (e.g., storage systems, Demand Response, Demand Side Management) have been widely evaluated both theoretically and in real case situation to increase the efficiency of the system (e.g., increasing self-consumption, reducing of imbalance, etc.),

and to build smart grids and smart cities. In literature, many experiences with Demand Response (DR) have been collected in the reviews [187] and [188]. Whilst the reference [187] points out that DR requires an Advanced Metering Infrastructure (AMI), the reference [188] focused on DR applications in industrial sector, arguing that up to now its potential has not been evaluated. The authors in [189] pointed out that the flexibility from large consumers (e.g., commercial activities, industrial entities and services sector) remains untapped and thus it is worth focusing on consumers with high electricity demand who can change their consumption temporarily.

In order to identify in which hours of the day energy injected from DSO to TSO is highest, a statistical analysis has been carried out by means of DRFM. The aim is to identify the proper timeslot to have more meaningful campaigns in terms of RPF reduction.

*Figure 141* shows the results of the statistical analysis carried out for each T/D interconnection point. For each day of 2017, it has been identified the period of 15 minutes during which the RPF energy is at its daily maximum, then it is shown the distribution of 365 days. It is clear that the RPF is usually maximum at night (for substations with hydro power plants) or during the lunch break (in which the low consumption is combined with the maximum production from PV plants).

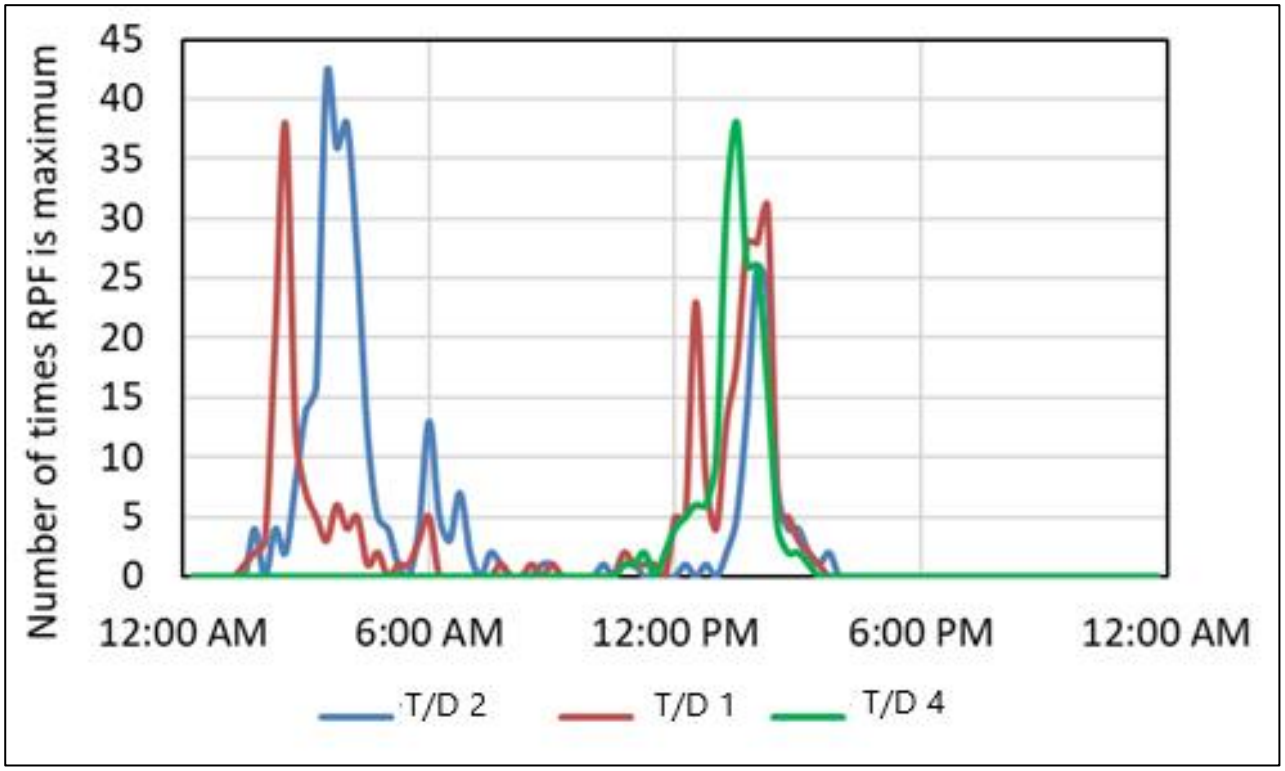


*Figure 141. Statistical distribution of RPF during the day (evaluated for each T/D connection point in 2017).*

As shown in *Figure 141*, in the most part of the days, RPF peak hour can be foreseen easily. Focus of such DR campaign was commercial and service sector consumers, equipped with a near real-time SM. After the timeslot identification, a group of users, equipped with near real-time SM, was involved in the DR campaign. This group of customers consists of 12 customers, having a total contractual power equal to 400 kW (commercial consumers or tertiary services).

As a third step, a campaign was scheduled and carried out in June 2018; these campaigns have been scheduled from 1.00 PM to 2.00 PM in working days. The users were encouraged to increase their consumption in order to maximize green energy consumption and self-consumption at DSO level. Data gathering and analysis were carried out by means of near real-time SM, as well as they

provide historical data about customer behaviour in order to compare Business as Usual (BaU) conditions and DR results.

Data during DR campaign were collected by near real-time smart meters with a sample time equal to 5 s (i.e., sample time of USM can be up to 1 s), with near real-time availability for the DSO and other stakeholders to download and visualize them.

In order to provide a representative example of customer's response, two daily load profiles are reported in *Figure 142* and *Figure 143*, showing a load profile without and with DR respectively. This load profile belongs to a company of tertiary sector (contractual power, 150 kW, yearly energy absorbed 150 kWh), with a PV plant (peak power, 185 kWp). It is worth pointing out that about 100 people work currently in this building; they were informed about the DR some days before its start, and therefore its energy manager had time to identify most suitable load shifting (i.e., its Heat Ventilation Air Conditioning, HVAC) to increase consumption when it was requested.

*Figure 142*, corresponding to the power profile without a DR campaign, clearly shows that there is not matching with the PV production, namely the profile is quite flat. Otherwise, *Figure 143* shows a different behaviour.

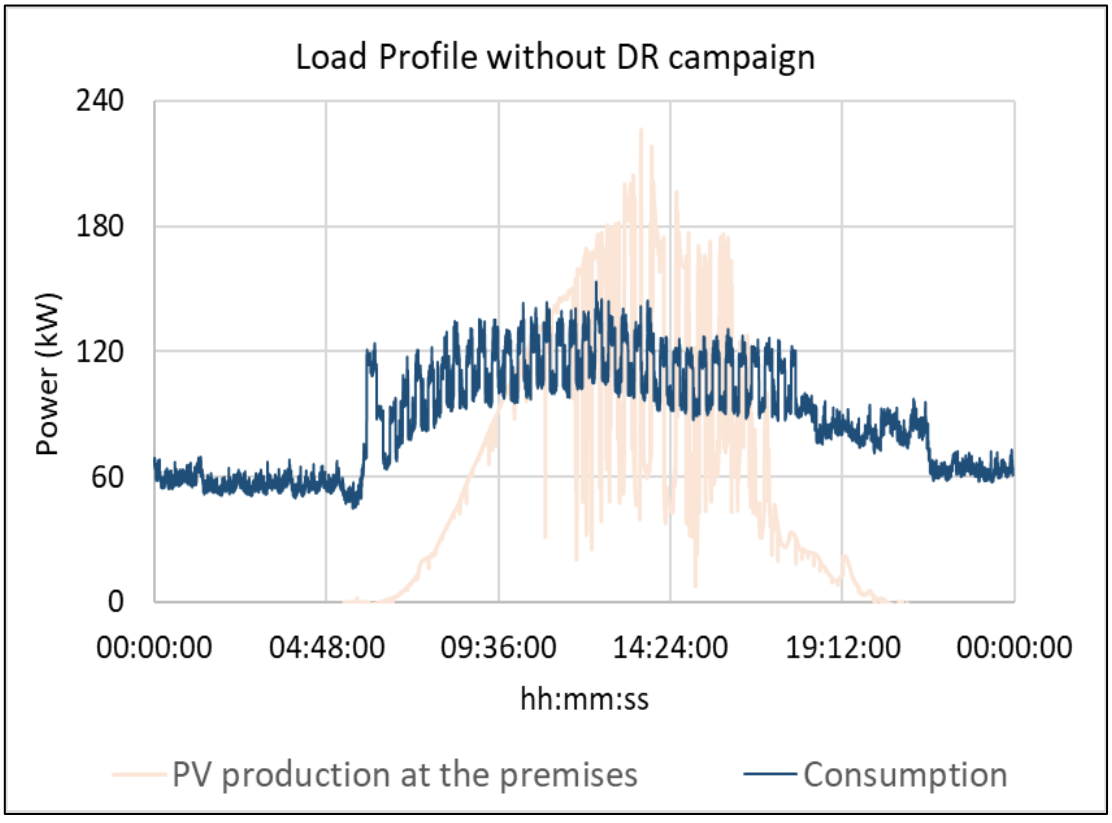


*Figure 142 Load profiles without DR campaign*

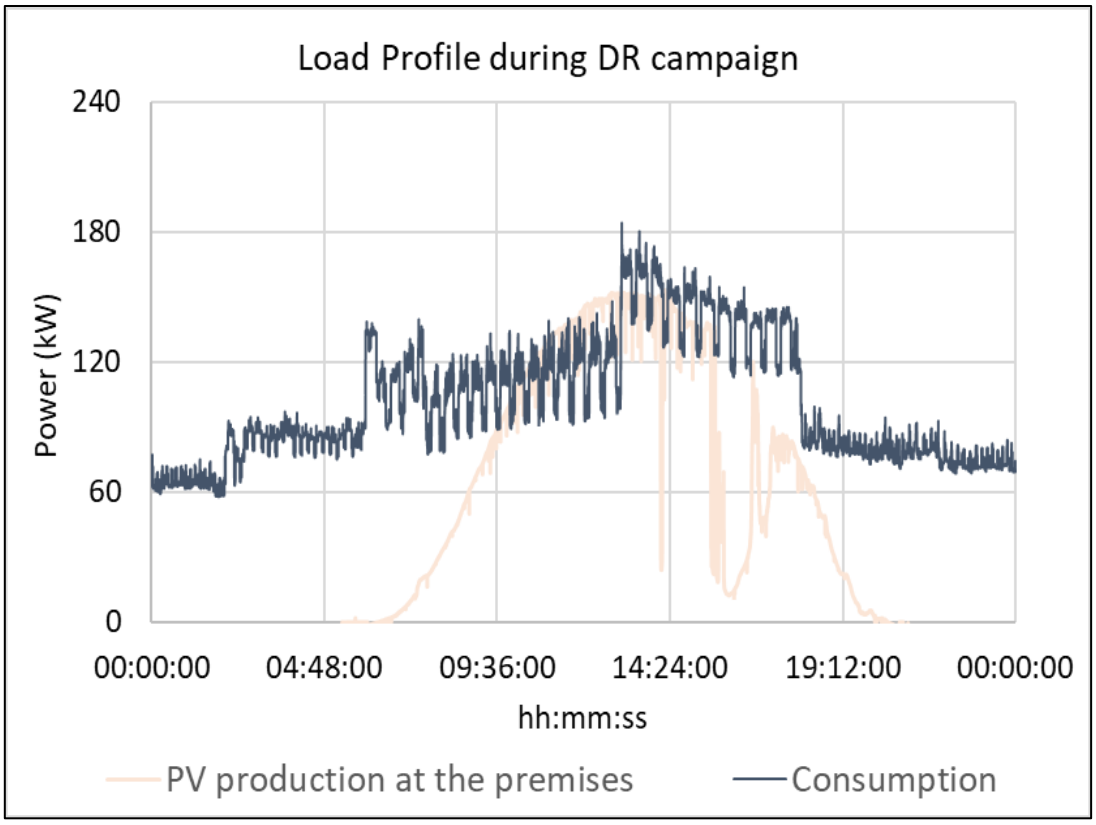


*Figure 143 Load profiles with DR campaign*

This behaviour, assumed by the company, can be considered paradigmatic because it represents how daily load profile of big electricity consumers (e.g. companies, small industries, commercial) should change. On the one hand, it expresses clearly that these could absorb high amount energy during maximum period of RPF (i.e., working hours of the day) and then they provide a service to the DSO. On the other hand, shifting their consumption and not affecting their activities, they can increase self-consumption at prosumer level, through an actual matching between not-programmable production and consumption habits. With respect to the representative customer, its daily self-consumption rate (ratio between energy consumed and produced by the prosumer in a day) is increased by 12.5%.

#### 5.3.3.1 *Key Performance Indicators (KPIs)*

The following Key Performance Indicators (KPIs) have been defined for evaluating the effectiveness of the DR campaigns:

- Customer Responsiveness (CR) is an indicator of how many customers have responded to a DR program following a DR signal sent to them, like a change in price, its formulas is

$$CR = (successful\ DR\ signals)/(DR\ signals\ sent) \quad (48)$$

It can be measured as the total number of DR signals that resulted in at least X% (e.g., 70%) of the target flexibility

- Peak Hour Change (PHC) is an indicator of how much has peak-hour consumption changed due to DR schemes (in kWh)

$$PHC = \sum NPC - BPC \quad (49)$$

New Peak Consumption (NPC) is measured via smart metering techniques while the Baseline Peak Consumption (BPC) has always to be estimated because it reflects the demand that should have been occurred if no DR event has been settled.

- Off-Peak Hour Change (OHC) is an indicator of how much has off-peak-hour consumption changed due to DR schemes.

$$OHC = \sum NOC - BOC \tag{50}$$

The New Actual Off-Peak Consumption (NOC) is measured via smart metering techniques but the baseline off-peak consumption has to be estimated (similarly to baseline peak consumption).

- DR scheme Impact on Load is an indicator of the intensity of customer's response to DR signals.

$$DRI = \sum DRC - BPC \tag{51}$$

DRI is the difference between the actual DR-enabled Consumption (DRC) and the Baseline Peak Hour Consumption (BPC); it can be measured as the change in load during a period where a DR scheme is enforced for a group of endpoints.

- Relative peak hour change is an indicator of how much has peak-hour consumption changed due to DR schemes (in %) and given by

$$RPHC = PHC / \sum BPC \tag{52}$$

- Relative off-peak hour change is an indicator of how much has off-peak-hour consumption changed due to DR schemes (in %) and given by

$$ROHC = OHC / \sum BOC \tag{53}$$

- Relative DR scheme Impact on Load is an indicator of the intensity of customer's response to DR signals (in %) and given by

$$RDRI = DRI / \sum BPC \tag{54}$$

Table reports KPIs obtained during such tests and evaluated with equations; DRFM calculated these values by means of near real-time SM. A positive value means an increase in the load while a negative one refers to a reduction. Considering collected KPIs in Table II, DR campaigns have obtained a good customer responsiveness (~75%) and a good impact on load. A significant decrease in consumption after the campaign in the off peak period has been also registered (compared to BaU). This implies that consumption has been shifted from the timeslot, when it normally happens, to the period of the day suggested by the DSO.

| KPI | Unit | Value |
|---|---|---|
| **Customer Responsiveness** | % | 75 |
| **Peak hour change** | kWh | 29.4 |
| **Relative peak hour change** | % | 21.7 |
| **Off-peak hour change** | kWh | -14.94 |
| **Relative off-peak hour change** | % | -2.7 |
| **DR scheme Impact on Load** | kWh | 34 |
| **Relative DR scheme Impact on Load** | % | 25 |

*Table 35 calculated KPIs during DR Campaigns*

#### 5.3.3.2 *Simulating The Effect of DR Campaigns on the RPF*

In order to scale up results of DR campaigns, a simulator of a LV/MV grid has been developed, capable of emulating network events such as Demand Response campaigns. In order to understand the potential of such demand-side management techniques in avoiding/mitigating the consequences of RPF at the primary substation level on an annual basis, the simulator has been configured so that it reflects the T/D connection point 4, which, as discussed, hosts a large number of prosumers. More specifically, the following real data have been used:

- the actual, quarter-hour load profiles for the complete year 2016 (i.e., same patterns of 2017) as well as the number of consumers belonging to the residential, commercial and industrial customer segments (counting 4623, 58 and 502 members respectively) in the standard configuration of ASM network;
- the actual RPF values for the primary substation for 2016 in order to identify the timing of the DR campaigns and the flexibility requirements that would cancel the excess load injected to the TSO;

Furthermore, the following assumptions were made on the key factors determining the simulated obtained flexibility:

- 30% of ASM Terni customers, regardless of their segment, have a contract with Aggregators who manage DR campaigns on behalf of the DSO;
- Each customer segment is expected to contribute a certain share of the requested flexibility. In this case, it has been assumed that the portfolio management policy instructs that 25% should come from industrial members, another 25% from commercial members and the rest 50% by residential consumers. The latter share is equally split between houses where activities take place throughout the day (named “Residential all-day”) and those that are empty most of the day (named “Residential evening”). Nevertheless, members of the same segment are asked to contribute equally.
- Each member, upon receipt of a DR request by its Aggregator, decides whether to accept it (or not) as follows. First of all, and since the focus has been on “manual” DR campaigns, that member needs to be available (i.e., present at their premises). Different customer segments have their own activity cycles (e.g., some commercial customers are closed on Sunday). Furthermore, it has been assumed that 50% of the available members will find it convenient to increase their load consumption at any timeslot (instead of the observed responsiveness of 75%, which would not be sustainable on the long term without a

reward). In order to counterbalance these restrictions an Aggregator can increase the requested flexibility; for this reason it has been assumed 100% redundancy.

- The flexibility obtained from each member cannot be higher than 25% of its actual load, as it has been found during the actual DR schemes that took place in Terni (see Table II).
- Using data for 2016, 10 simulations have been carried out and the results have been averaged. *Figure 144* shows that the number of RPF events during 2016 would be reduced by 39% on average if DR campaigns were realized. Note that the number of events is slightly lower for 2016 (6.5% compared to 6.8%, measured in 2017).

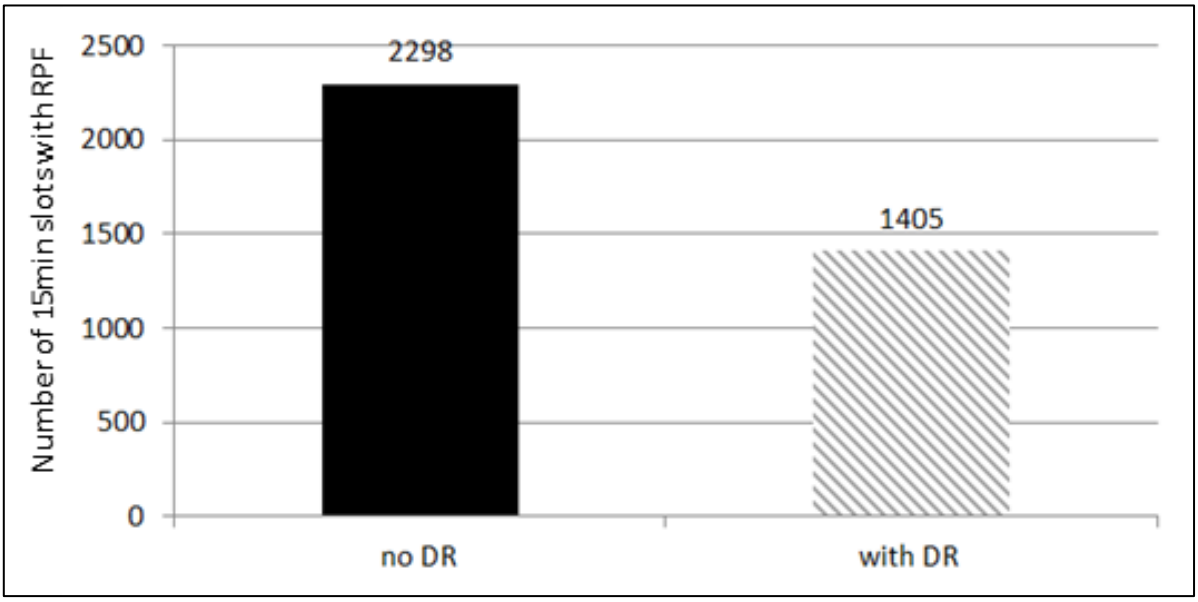


*Figure 144 The number of 15min slots with RPF*

As shown in *Figure 125*, the flexibility obtained according to simulations accounted to 27.6% of the total annual RPF for the primary substation under study, reaching 96883 kWh on average.

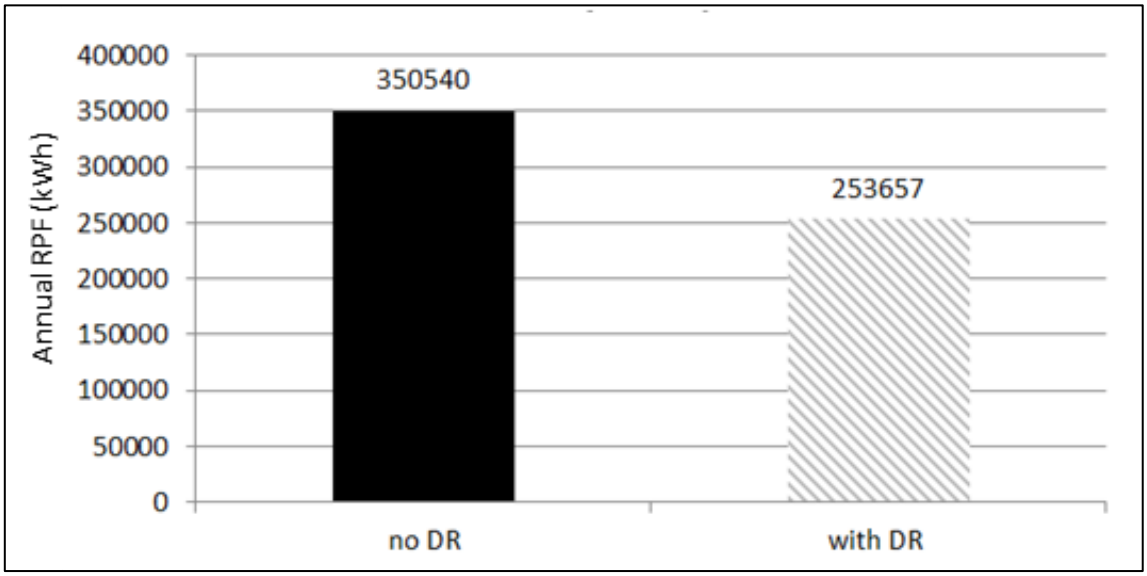


*Figure 145 The annual RPF for T/D n° 4 (in kWh)*

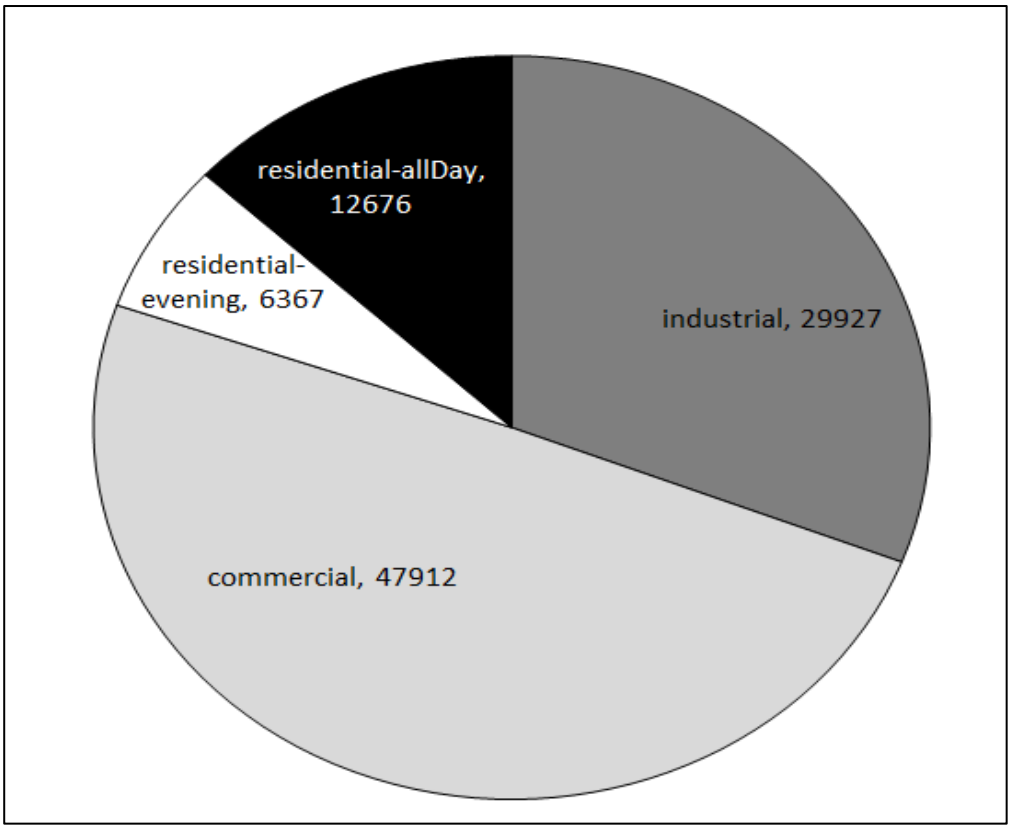


*Figure 146 A breakdown of the flexibility obtained by each customer segment (in kWh)*

Finally, *Figure 146* suggests that almost 50% of the flexibility came from commercial consumers due to their significant number and high average load.

Summarizing results, this section presents a real experience on a DR campaign, carried out by a DSO in Italy. Based on the analysis of the pilot site, the increasing RES penetration is raising topics about Smart Grid as new drivers for development plans of the DSOs. In this respect, RPF can be a meaningful and straightforward parameter for evaluating the effects of the DG on the DN; moreover, its reduction can lead to technical benefits as well as to economic savings, especially in case penalties were established.

The real-life implementation requires near real-time availability of consumption data and proper tools to perform analysis and to allow online observability of the network, as well as historical data to define baselines. In this respect, USM has a key role as platform enabling Smart Grid; these functionalities will be further tested and improved in other projects that are going to involve a higher number of customers.

Finally, the DR campaign has involved large energy consumers (e.g., commercial activities, public services, industries) that, according to literature, have potentialities in DR still not fully investigated and exploited. In this respect, the results obtained from the actual campaigns and simulations have shown that these consumer segments can provide an effective contribution to the DSO management of power flows, since they normally have several levers to modify consumptions, without habits changes.

This section presents a real experience on a DR campaign, carried out by a DSO in Italy. Based on the analysis of the pilot site, the increasing RES penetration is raising topics about Smart Grid as new drivers for development plans of the DSOs. In this respect, RPF can be a meaningful and

straightforward parameter for evaluating the effects of the DG on the DN; moreover, its reduction can lead to technical benefits as well as to economic savings, especially in case penalties were established.

The real-life implementation requires near real-time availability of consumption data and proper tools to perform analysis and to allow online observability of the network, as well as historical data to define baselines. In this respect, USM has a key role as platform enabling Smart Grid; these functionalities will be further tested and improved in other projects that are going to involve a higher number of customers.

In this work, the DR campaign has involved large energy consumers (e.g., commercial activities, public services, industries) that, according to literature, have potentialities in DR still not fully investigated and exploited. In this respect, the results obtained from the actual campaigns and simulations have shown that these consumer segments can provide an effective contribution to the DSO management of power flows, since they normally have several levers to modify consumptions, without habits changes.

### 5.3.4 *Techno economic analysis of DSO using Demand-Side Management techniques for minimizing Reverse Power Flows and reducing congestion issues that can lead to power outages [190]*

In this subsection a business model is presented assuming that a DSO asks for flexibility from an Aggregator in order to deal with technical issues; in particular Reverse Power Flows (RPF) and congestions on LV/MV network. Two scenario will be compared, the first one has been identified as Business as usual (i.e., the DSO will not act any particular change in its policy and new levers are not available) the second one corresponds to the scenario enabled by the full availability of the Nobel GRID technologies, notably the DR campaigns.

#### 5.3.4.1 *Minimizing Reverse Power Flows*

In the case of Minimizing Reverse Power Flows the following effects of high PV penetration in rural areas have been investigated:

- Increased (technical) network losses
- Increased voltage at the end of rural lines and thus PV disconnection

However, the simulator does not consider voltages or network losses, thus the business model evaluation task will be based on estimations regarding the costs involved. This means that the following simulations will focus only on the congestion issues due to RPF and the implications of RPF to the financial relationship with the TSO. In particular, the following effects have been identified:

- RPF reduce the energy-related costs to TSO, because injected energy during a certain period (e.g., a month) is subtracted from the energy absorbed during the same period. These costs are given by the following equation:

$$\max((energy\_received - energy\_injected * 1.023) * rate, 0) \quad (55)$$

Note that according to the current regime the energy injected is increased by 2.3% and thus cost savings are further magnified. Moreover, in the extreme scenario where more energy was injected than delivered during a period, the TSO does not pay ASM Terni.

- On the other hand, it has been assumed that RPF can create congestion issues at MV feeders in case of high PV penetration rates, which can lead to higher maintenance costs, power outages, higher penalties and customer dissatisfaction. In such a scenario, RPF could reach feeder capacity limits whenever RES production is significantly higher

than demand. Here it has been assumed that capacitors are already installed (or reactive power management has taken place) and thus the far away PV plants in rural areas (connected to secondary by means of long LV lines) will not be disconnected because voltage along the line does not overcome maximum limit, before overload issues occur. Furthermore, such outages lead to higher maintenance costs (both planned and reactive ones), higher replacement costs due to shorter life span of equipment and increased personnel.

Thus, there is a trade-off between reduced transmission costs (i.e., a benefit) and costs due to high RPF.

In order to identify the market conditions that render Demand Side Management services attractive to such a DSO a set of what-if scenarios (simulations) have been carried out. Such market conditions are the PV penetration rate which affects the frequency of congestion events that could be dealt with DR campaigns, the Aggregator's portfolio size, member's availability for participating and response rate, presence of controllable loads such as Electric Vehicles, remuneration asked etc.).

The details of the simulations performed are the following:

1. The focus was on a certain LV/MV loop that is serviced by the Terni Ovest (TO) primary substation, where as described in D16.1 significant reverse power flows exist. More specifically it has been simulated the feeders fed by a bus of TO (Green Bus) TO_GB LUZI and TO_GB SALIT where 1000 points of delivery exist. Being a loop, there is the possibility to change the length of the feeder, reducing one and increasing the other, by switching the status of some disconnectors, which are remotely controllable. This is a rather conservative decision as outages are harder to take place compared to a tree-like topology. The reason is that customers will likely be served even if a technical failure takes place along one of the lines. Eventually, in Section YYY, in order to scale up results to the rest ASM Terni network, it has been assumed that increased PV penetration is expected in up to 10-12 similar feeders.
2. The probability of a technical failure occurring on any feeder is a random variable following the Bernoulli distribution with p=0.5%. Thus about 160 failure/maintenance events happen per year on each feeder.
3. The effective bottleneck capacity of each line (after considering the technical losses involved) is 5.518313873 MW.
4. An outage occurs if
    - both feeders experience a technical problem, or
    - there is topology reconfiguration and the effective capacity of the only feeder in use cannot cope with the production (or demand as it will be described in the following). In respect of this, the worst case is that a single feeder has to feed all the secondary substations in case of maximum production/consumption, or
    - the total surplus production (or demand) exceeds the combined capacity of the feeders
5. It has been assumed that whenever the (perfectly forecasted) load exceeds a threshold (set at the 90% of the effective line capacity) a DR campaign will be triggered, where the flexibility asked is given by the formula

$$\max(surplus\ production - capacity\ threshold, 0)$$

This applies to the case where a topology reconfiguration has taken place due to a technical failure, or maintenance, on the other feeder. When both feeders are unexpectedly off, all served endpoints get disconnected and no flexibility can be procured.

6. A complete year is simulated in quarter-hourly (15min) slots.
7. Loads for consumers depend on the location and are those for a typical residential family, based on synthetic load profiles. These customers are assumed to be charged with a (country-specific) fixed rate.
8. Similarly, production is location-specific and is based on profiles generated using the PVsol commercial software for a rooftop PV system of 3.6 kWp. The exact production is then scaled up/down according to the average peak capacity installed in that area by residential, commercial or industrial prosumers (no generator-only entities have been considered). More specifically, the average peak capacity for:
    - residential prosumers is 4.29 kWp
    - commercial prosumers is 23.351 kWp
    - industrial prosumers is 41.9 kWp

    where considered according to input from ASM Terni.
9. The number of prosumers depends on the PV penetration rate, i.e., the percentage of prosumers in that area. As explained this is one of the core simulation parameters in the sense that it determines the maximum production that can be injected.
10. An additional load that can greatly affect the capability of Aggregators (and its members eventually) to deliver the promised flexibility is EV charging. It has been assumed that the EV owner has a charger that can be remotely controlled by the Aggregator of its choice; a form of Automated DR campaign. EV charging depends on the travel patterns of its owner. Two EV owner types have been defined:
    - those that charge it in the afternoon (e.g., when returning home after work or after the driver's shift in case of a company fleet) in order to use it next morning. This user type is named "night chargers" hereafter;
    - the ones that charge it around noon (e.g., when shopping or commute has finished) called "day chargers".

    This is an important assumption because it allows Aggregators to manage their portfolio of EV owners so that they can offer both negative (peak shaving) and positive (valley filling) flexibility to DSOs. Thus, EV charging can be delayed or expedited compared to the slot that its owner would start the process if left alone.
11. In order to model the charging process and the associated loads at any slot the owners of each type into at least two bins have been grouped (the actual number depends on the population of EV owners with minimum 2 and maximum 30). Users belonging to the same bin are assumed to start and stop the charging simultaneously. The exact delay of each bin is a random variable that is normally distributed. In that way it has been introduced randomness into the charging process, which is important for cases of congestion caused by high loads (see next subsection). Obviously, the worst-case scenario for a grid operator would be all owners to start charging the EV batteries at the same time (i.e., having a single bin).
12. Similarly, to PV penetration rate, the number of EVs present (the EV penetration rate), is the second key parameter for this analysis. It determines the percentage of EVs compared to all

vehicles in that area and thus the potential controllable load. Even though the adoption of EVs in European countries is low nowadays, this is expected to change soon as the manufacturers move away from conventional vehicles and costs go down, or authorities provide the appropriate incentives. Furthermore, there has been a focus on individual LV feeders and in upper class neighbourhoods, or in touristic places with EV fleets high adoption rates will be achieved significantly sooner.

13. Furthermore, it has been assumed that there are three types of EVs, each one with a certain battery capacity and associated charger type. In particular:
    - "Small EVs" that are owned by residential users and equipped with a 30kWh battery, which is charged using a level-2 charger of 20kW maximum rate. It has been assumed that each residential end point owns a single "Small EV" with a probability equal to EV penetration rate.
    - "Medium EVs", owned by commercial users and equipped with a 50kWh battery, which is charged using a level-3 charger of 50kW maximum rate. It has been assumed that each commercial end point owns four (4) "Medium EV" with a probability equal to EV penetration rate.
    - "Large EVs", owned by industrial users and equipped with a 80kWh battery, which is charged using a level-3 charger of 50kW maximum rate. It has been assumed that each commercial end point owns four (4) "Large EV" with a probability equal to EV penetration rate.
14. The average EV battery daily charging load of each EV type is assumed to be 20% of the battery capacity; a rather conservative assumption (which was nevertheless determined by simulating the charging process as mentioned above).
15. Furthermore, it has been assumed that the population of EV owners is evenly split between "night chargers" and "day chargers".
16. The DSO asks flexibility from an Aggregator before a severe congestion issue. This means that either flexibility needs are perfectly known, which means 100% accurate production and demand forecasting, or that DSOs have systems with advanced monitoring capabilities.
17. The Aggregator pool size is set to 30%. The rest 70% (700 in this case) are assumed not to provide flexibility of any form. On the other hand, the EV penetration rate is also used for defining the share of 300 users that participate in Automated Demand Response (ADR) campaigns, where flexibility offered comes from cooling, heating, lighting, etc. The rest users (1000*30%*70%=210 in this case) participate in Manual Demand Response (MDR) campaigns. Furthermore, no users with dynamic pricing schemes are in place. It is important to note the importance of locality when addressing congestion issues; no aggregator members from other parts of the distribution network can offer their flexibility. Thus, locality is an important criterion for Aggregators when managing their portfolio (together with load types and usage patterns).
18. Electric Vehicle (EV) owners are assumed not to override/disturb the charging plan as set by the Aggregator. On the other hand, the aggregator's members providing MDR and (non-EV) ADR flexibility do this in a best-effort way. This means that there are no contracts for guaranteeing that the asked flexibility will be delivered upon request, or otherwise a penalty will be paid. More specifically, participants' behaviour is governed by the following parameters
    - Availability, which refers to the probability that a certain user type will be at its premises (during the day) or awake (during the night). This affects the (non-EV) ADR flexibility as

being away is assumed to restrict the controllable load (thus no preheating/precooling takes place).

- Willingness to participate, which refers to the probability that a user (who is available) will accept the DR activation signal. This probability is linked to the monetary reward for each kWh of flexibility delivered. In case of (non-EV) ADR it refers to the case where a user overrides the Aggregator's control action (e.g., temperature set point).

19. The Aggregator defines the monetary reward in such a way that a certain percentage of contacted members and being available will accept the invitation. In particular, if $c$ is the user compensation then a probability density function for the willingness to participate is given by $p = \min(\exp\left(-\frac{0.1}{c}\right), 1)$. This probability tends to $0$ when $c = 0$. Since the probability can be also expressed as $p = target/(\mathrm{N} * \mathrm{x})$ , then the aggregator can select the compensation by using the following formula

$$c = -a/ln(p) \tag{56}$$

, where $target$ is the total flexibility asked by the DSO (in kWh), $N$ is the number of users to be invited (e.g., the complete portfolio or a specially selected subgroup) and $x$ is the individual flexibility asked, which is assumed to be the average hourly load of a residential/commercial/industrial consumer. In this case it has been used used $p = 0.9$, so that the compensation (and consequently the cost to DSO) is not extremely high. Obviously, these parameter values will determine whether the total flexibility asked can be achieved or not. In the latter case, it has been assumed that the DSO accepts the flexibility that can be offered in order to minimize the consequences of RPF. Thus, a simple negotiation phase exists between the DSO and the Aggregator.

20. When a request for flexibility arrives from the DSO, the Aggregator is assumed to determine how much to ask from each member type in the following way:

    - The flexibility asked is increased by 10% (or any other value) in order to account for uncertainty in user behavior.
    - The maximum expected flexibility provided from EVs is calculated first (by considering the flexibility reserved for on-going campaigns).
    - If the flexibility from EVs alone cannot meet the target set in step a), then rest ADR member and MDR ones are involved on an equal basis. The possibility for aggregating the missing flexibility by splitting in halves the contribution from rest ADR loads and MDR members is investigated. This is done by following the approach described in (19) for MDR members and asking the same amount of flexibility from rest (non EV) ADR . If this is not technically feasible (e.g., their number is low), or the maximum amount per kWh that a DSO is willing to pay has been exceeded then they agree on the maximum flexibility that can be achieved.

21. Flexibility provided is load that is shifted in advance or delayed and affects not only the offtake energy, but also surplus production injected to the grid. Furthermore, the load to be shifted is evenly shared amongst a number of slots, which are randomly selected from those slots where the user is available. Note, however, that loads supposed to take place during an outage are not shifted. This is the only form of "efficiency" achieved.

22. Technical losses are not considered.

23. An outage is assumed to last 10 slots, while the duration of the last slot is normally distributed. Thus, the maximum duration of an outage is 150 min.
24. No battery systems are installed, which can reduce RES production surpluses.

Two candidate options for ASM Terni avoiding sustained outages:

- Option1 (Business-as-Usual scenario): upgrade network by installing a new line and assume that congestion issues are definitely avoided. However, it takes 1-2 years until the new line is fully operational.
- Option2 (implementing the solution of Nobel GRID project): ask flexibility from Aggregator (assuming that flexibility needs are perfectly known, which means 100% accurate production and demand forecasting).

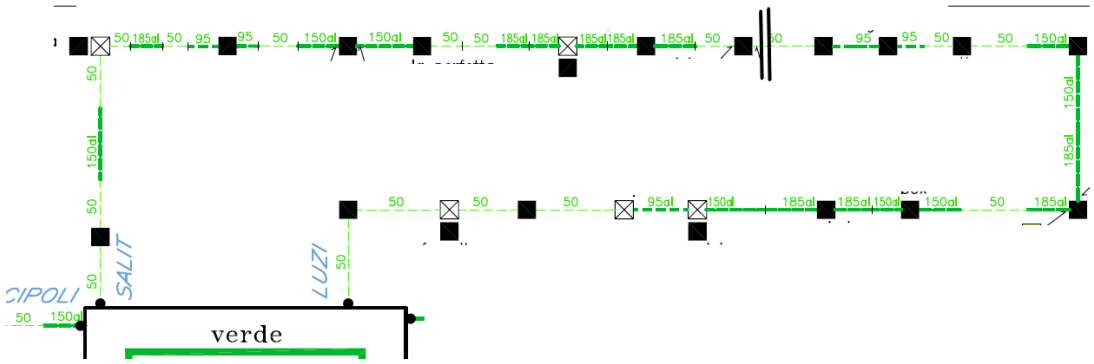


*Figure 147: The topology of the benchmark MV feeder loop in Terni as of today*

In the figure above there is a diagram of the Terni Ovest LUZI and SALIT loop as of today, while the next one presents the new topology after a new line is introduced.

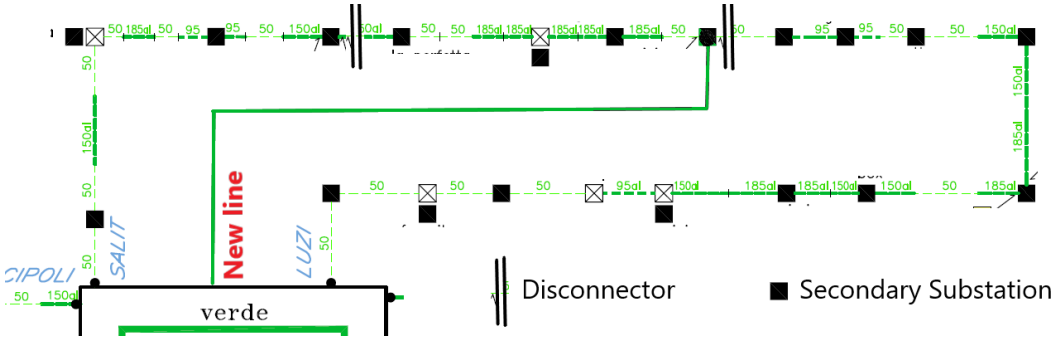


*Figure 148: The new topology of the benchmark MV feeder loop in Terni following the traditional approach of upgrading capacity by adding a new feeder*

The next plot gives us the number of outages per year that are expected, for the parameter values explained above, to be caused by Reverse Power Flows in the Business-as-Usual scenario, when the PV penetration rate varies from 10% to 80% (horizontal axis) and for different EV penetration rates (curves blue, red, green and purple). It has been observed that regardless of the EV penetration rate, which affects the surplus production to be injected, outages start taking place when more than half of the endpoints become prosumers. In particular, 8 outages were found to

be happening every year due to high surplus production if PV penetration reaches 70%, growing to 17 when 80% of endpoints are prosumers.

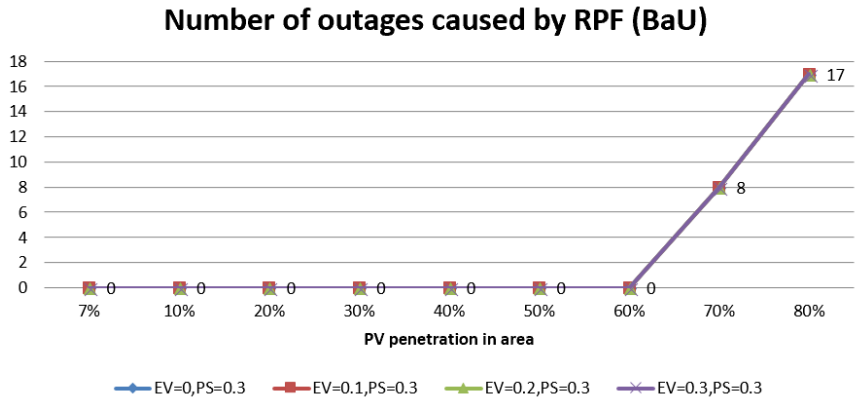


*Figure 149: The expected number of outages caused annually by Reverse Power Flows in Business-as-Usual scenario for the benchmark feeder loop in Terni*

The total number of outages, that is including those originating from unexpected hardware failures, human error or proactive maintenance, is shown in the figure below, notably 1 outage on average will be taking place every year on top of those attributed to high local RES production. Since it has been assumed that the probability of a technical problem is independent of the EV penetration rate, similar graphs were witnessed for the rest cases regarding EV acceptance.

One of the main reasons for performing the simulation study is to see what the effect of Demand Response campaigns would be on the number of outages caused by RPF (excluding those appearing for technical reasons). This is shown in the figure below. It has been observed that for the particular assumptions made and parameter values selected Demand Side management techniques can greatly reduce power interruptions.

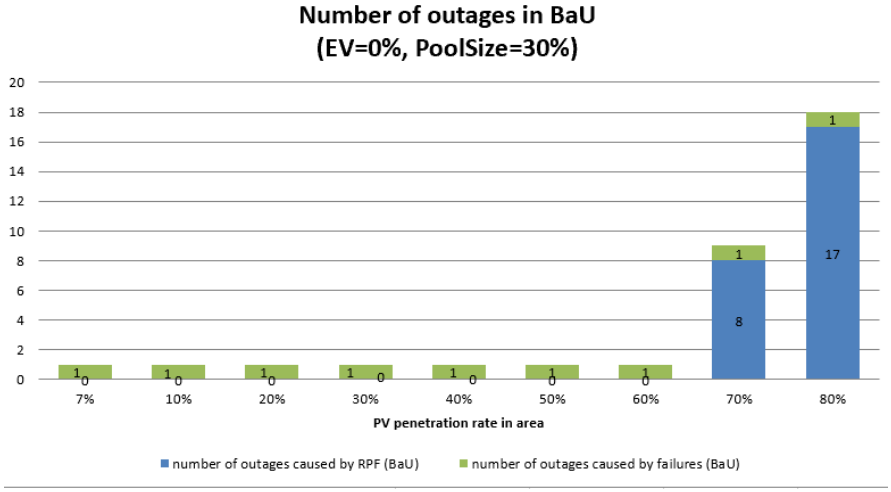


*Figure 150 : The total expected annual number of outages (RPF and technical aspects) in Business-as-Usual scenario for the benchmark feeder loop in Terni*

For example, at 70% PV penetration the number of outages were found to be reduced by 87% (1 instead of 8 events) for EV penetration 10% or more. Thus, the potential of controlled EV charging on dealing with congestion issues is clear. When prosumers reach 80% the outages can be reduced by 62% (2 events instead of 17 in the BaU) for EV market share higher than 10%.

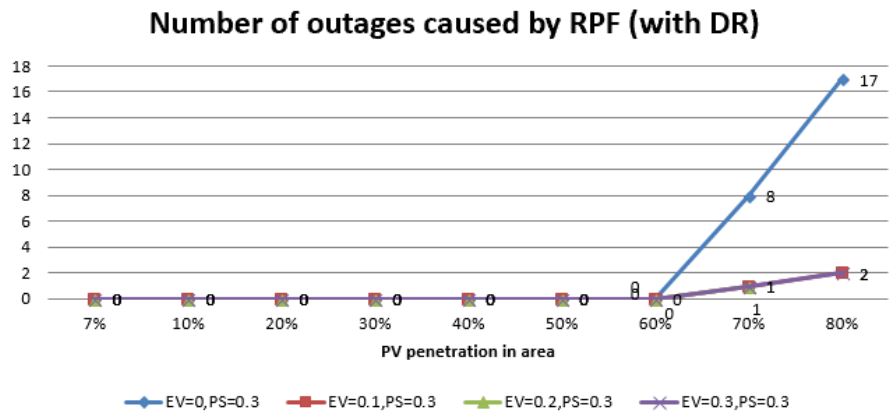


*Figure 151: The expected number of outages caused annually by Reverse Power Flows in the NOBEL GRID-enabled scenario (with DR) for the benchmark feeder loop in Terni*

A breakdown of the flexibility obtained per member type (EV, rest ADR, MDR) is shown in the figure below; EVs contribute the highest share of flexibility in all combinations of PV and EV penetration rates.

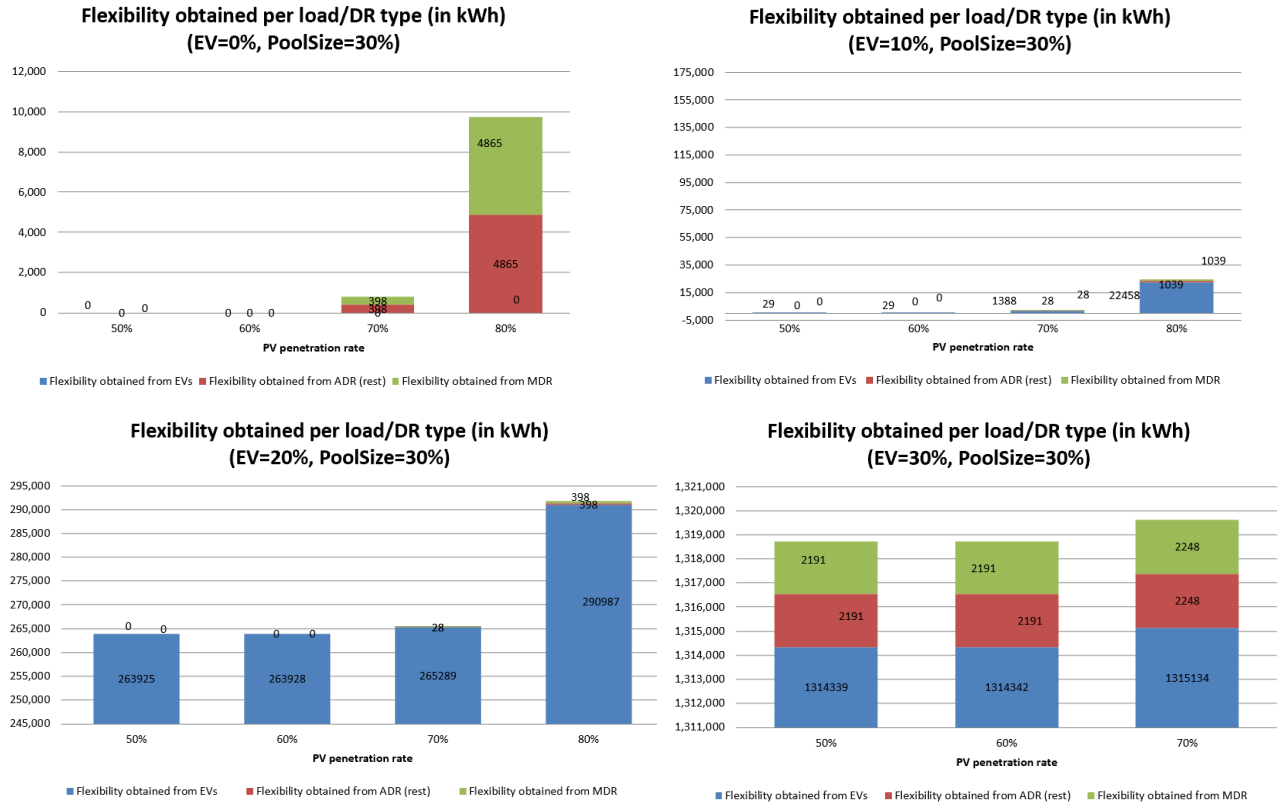


*Figure 152: A breakdown of the flexibility obtained per member type for different combinations of PV and EV penetration rates for the benchmark feeder loop in Terni (low PV penetration rates have been omitted for better readability)*

The following figure compares the estimated minutes of annual outages in the Business-as-Usual and NOBEL GRID-enabled scenarios for 20% EV penetration and varying PV penetration levels. Given the assumption (23) these minutes are analogous to *Figure 149* and *Figure 151*, while these may slightly differ as the duration of the last outage slot is a random variable (e.g., outputs for 20%

and 30% PV penetration rates differ by 4 minutes). Similar figures are obtained for 10%vand 30% EV penetration and thus are omitted.

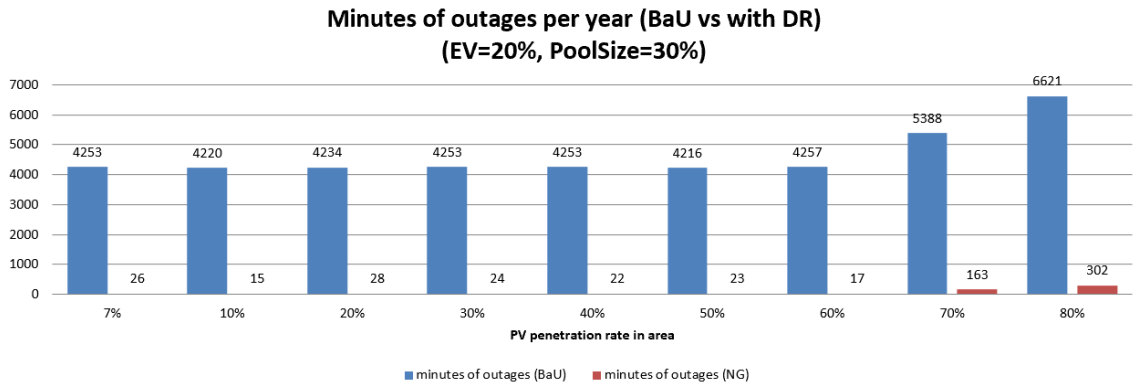


*Figure 153: Comparing the estimated minutes of annual outages due to Reverse Power Flows in the Business-as-Usual and NOBEL GRID-enabled scenarios for EV penetration rate 20% for the benchmark feeder loop in Terni*

The following tables provide a summary of the key technoeconomic metrics that will be used as input in the business model evaluation task. The first one refers to the case where EV penetration is 0%, while the second for EV penetration equal to 10%.

| EV=0,PS=0.3 | PV penetration | | | | | | | | | |
|---|---|---|---|---|---|---|---|---|---|---|
| | 7% | 10% | 20% | 30% | 40% | 50% | 60% | 70% | 80% | 90% |
| number of outages caused by RPF (BaU) | 0 | 0 | 0 | 0 | 0 | 0 | 0 | 8 | 17 | |
| number of outages caused by Loads (BaU) | 0 | 0 | 0 | 0 | 0 | 0 | 0 | 0 | 0 | |
| number of outages caused by failures (BaU) | 1 | 1 | 1 | 1 | 1 | 1 | 1 | 1 | 1 | |
| number of outages caused by RPF (NG) | 0 | 0 | 0 | 0 | 0 | 0 | 0 | 8 | 17 | |
| number of outages caused by Loads (NG) | 0 | 0 | 0 | 0 | 0 | 0 | 0 | 0 | 0 | |
| number of outages caused by failures (NG) | 1 | 1 | 1 | 1 | 1 | 1 | 1 | 1 | 1 | |
| minutes of outages (BaU) | 21 | 25 | 25 | 21 | 25 | 22 | 26 | 1157 | 2441 | |
| minutes of outages (NG) | 21 | 25 | 25 | 21 | 25 | 22 | 26 | 1157 | 2441 | |
| DR requests due to RPF | 0 | 0 | 0 | 0 | 0 | 0 | 0 | 28 | 350 | |
| DR requests due to Loads | 0 | 0 | 0 | 0 | 0 | 0 | 0 | 0 | 0 | |
| TO_GB total energy (from TSO) | 13,570,284 | 13,074,023 | 11,528,310 | 10502269 | 9864042 | 9435622 | 9121684 | 8878655 | 8686202 | |
| TO_GB total energy (to TSO) | - | - | 96,131 | 711933 | 1715549 | 2928972 | 4256878 | 5560191 | 6884581 | |
| lost energy consumed due to outages | 703 | 703 | 703 | 703 | 703 | 703 | 703 | 1126 | 1053 | |
| lost excess energy produced due to outages | - | - | - | 0 | 0 | 0 | 0 | 27704 | 70309 | |
| Flexibility obtained from EVs | - | - | - | 0 | 0 | 0 | 0 | 0 | 0 | |
| Flexibility obtained from ADR (rest) | - | - | - | 0 | 0 | 0 | 0 | 398 | 4865 | |
| Flexibility obtained from MDR | - | - | - | 0 | 0 | 0 | 0 | 398 | 4865 | |
| flexibility from Evs that was not effective | 0 | 0 | 0 | 0 | 0 | 0 | 0 | 0 | 0 | |
| flexibility from non-EVs that was not effective | 0 | 0 | 0 | 0 | 0 | 0 | 0 | 201 | 484 | |
| % of flexibility from Evs that was not effective | #DIV/0! | #DIV/0! | #DIV/0! | #DIV/0! | #DIV/0! | #DIV/0! | #DIV/0! | #DIV/0! | #DIV/0! | |
| % of flexibility from non-EVs that was not effective | #DIV/0! | #DIV/0! | #DIV/0! | #DIV/0! | #DIV/0! | #DIV/0! | #DIV/0! | 0 | 0 | |
| flexibility cost per kwh from EVs | 0.100000 | 0.100000 | 0.100000 | 0.100000 | 0.100000 | 0.100000 | 0.100000 | 0.100000 | 0.100000 | |
| flexibility cost per kwh from ADR | 0.000000 | 0.000000 | 0.000000 | 0.000000 | 0.000000 | 0.000000 | 0.000000 | 0.383292 | 0.307320 | |
| flexibility cost per kwh from MDR | 0.000000 | 0.000000 | 0.000000 | 0.000000 | 0.000000 | 0.000000 | 0.000000 | 0.383292 | 0.307320 | |
| MAX TO_GB power (from TSO) | 4095 | 4043 | 3904 | 3894 | 3894 | 3894 | 3894 | 3894 | 3894 | |
| MAX TO_GB power (to TSO) | 0 | 0 | 975 | 2085 | 3194 | 4303 | 5412 | 6521 | 7631 | |
| DR events for avoiding congestion | 0 | 0 | 0 | 0 | 0 | 0 | 0 | 19 | 332 | |
| DR events for avoiding outages | 0 | 0 | 0 | 0 | 0 | 0 | 0 | 9 | 18 | |
| lost energy consumed due to outages (NG) | 703 | 703 | 703 | 703 | 703 | 703 | 703 | 1,126 | 1052.577258 | |
| lost excess energy produced due to outages (NG) | - | - | - | - | - | - | - | 27,491 | 68581.20295 | |

*Table 36 Useful technoeconomic metrics regarding congestion issues for EV penetration rate 0% and varying PV penetration rates*

| EV=0.1,PS=0.3 | PV penetration | | | | | | | | |
|---|---|---|---|---|---|---|---|---|---|
| | 7% | 10% | 20% | 30% | 40% | 50% | 60% | 70% | 80% |
| number of outages caused by RPF (BaU) | 0 | 0 | 0 | 0 | 0 | 0 | 0 | 8 | 17 |
| number of outages caused by Loads (BaU) | 1 | 1 | 1 | 1 | 1 | 1 | 1 | 1 | 1 |
| number of outages caused by failures (BaU) | 1 | 1 | 1 | 1 | 1 | 1 | 1 | 1 | 1 |
| number of outages caused by RPF (NG) | 0 | 0 | 0 | 0 | 0 | 0 | 0 | 1 | 2 |
| number of outages caused by Loads (NG) | 0 | 0 | 0 | 0 | 0 | 0 | 0 | 0 | 0 |
| number of outages caused by failures (NG) | 1 | 1 | 1 | 1 | 1 | 1 | 1 | 1 | 1 |
| minutes of outages (BaU) | 154 | 167 | 169 | 160 | 165 | 163 | 162 | 1308 | 2584 |
| minutes of outages (NG) | 17 | 29 | 25 | 19 | 27 | 21 | 21 | 166 | 308 |
| DR requests due to RPF | 0 | 0 | 0 | 0 | 0 | 0 | 0 | 28 | 350 |
| DR requests due to Loads | 0 | 0 | 0 | 1 | 0 | 0 | 0 | 0 | 0 |
| TO_GB total energy (from TSO) | 16,313,090 | 15,816,832 | 14,271,120 | 13244647 | 12602507 | 12169173 | 11853263 | 11607031 | 11409009 |
| TO_GB total energy (to TSO) | - | - | 96,131 | 711501 | 1711205 | 2919714 | 4245647 | 5545758 | 6864957 |
| lost energy consumed due to outages | 8,948 | 8,944 | 8,944 | 8944 | 8944 | 8944 | 8944 | 9367 | 9452 |
| lost excess energy produced due to outages | - | - | - | 0 | 0 | 0 | 0 | 27704 | 70089 |
| Flexibility obtained from EVs | 29.4 | 29.1 | 29.1 | 29 | 29 | 29 | 29 | 1388 | 22458 |
| Flexibility obtained from ADR (rest) | - | - | - | 0 | 0 | 0 | 0 | 28 | 1039 |
| Flexibility obtained from MDR | - | - | - | 0 | 0 | 0 | 0 | 28 | 1039 |
| flexibility from Evs that was not effective | 0 | 0 | 0 | 0 | 0 | 0 | 0 | 0 | 0 |
| flexibility from non-EVs that was not effective | 0 | 0 | 0 | 0 | 0 | 0 | 0 | 28 | 57 |
| % of flexibility from Evs that was not effective | 0 | 0 | 0 | 0 | 0 | 0 | 0 | 0 | 0 |
| % of flexibility from non-EVs that was not effective | #DIV/0! | #DIV/0! | #DIV/0! | #DIV/0! | #DIV/0! | #DIV/0! | #DIV/0! | 1 | 0 |
| flexibility cost per kwh from EVs | 0.100000 | 0.100000 | 0.100000 | 0.100000 | 0.100000 | 0.100000 | 0.100000 | 0.100000 | 0.100000 |
| flexibility cost per kwh from ADR | 0.000000 | 0.000000 | 0.000000 | 0.000000 | 0.000000 | 0.000000 | 0.000000 | 0.161802 | 0.334874 |
| flexibility cost per kwh from MDR | 0.000000 | 0.000000 | 0.000000 | 0.000000 | 0.000000 | 0.000000 | 0.000000 | 0.161802 | 0.334874 |
| MAX TO_GB power (from TSO) | 6348 | 6347 | 6347 | 6347 | 6347 | 6347 | 6347 | 6347 | 6347 |
| MAX TO_GB power (to TSO) | 0 | 0 | 975 | 2085 | 3194 | 4303 | 5412 | 6521 | 7631 |
| DR events for avoiding congestion | 0 | 0 | 0 | 0 | 0 | 0 | 0 | 27 | 348 |
| DR events for avoiding outages | 0 | 0 | 0 | 1 | 0 | 0 | 0 | 1 | 2 |
| lost energy consumed due to outages (NG) | 1,101 | 1,100 | 1,100 | 1,100 | 1,100 | 1,100 | 1,100 | 1,100 | 1099.852007 |
| lost excess energy produced due to outages (NG) | - | - | - | - | - | - | - | 3,970 | 8331.539509 |

*Table 37 Useful technoeconomic metrics regarding congestion issues for EV penetration rate 10% and varying PV penetration rates*

The third one refers to the case where EV penetration is 20%, while the forth for EV penetration equal to 40%. Notice that these two tables include the combined effect of reverse power flows and high loads on congestion issues, which in some cases turn into outages. This is evident, for example, in the grey-colored rows for PV penetration higher than 70%.

| EV=0.2,PS=0.3 | PV penetration | | | | | | | | |
|---|---|---|---|---|---|---|---|---|---|
| | 7% | 10% | 20% | 30% | 40% | 50% | 60% | 70% | 80% |
| number of outages caused by RPF (BaU) | 0 | 0 | 0 | 0 | 0 | 0 | 0 | 8 | 17 |
| number of outages caused by Loads (BaU) | 30 | 30 | 30 | 30 | 30 | 30 | 30 | 30 | 30 |
| number of outages caused by failures (BaU) | 1 | 1 | 1 | 1 | 1 | 1 | 1 | 1 | 1 |
| number of outages caused by RPF (NG) | 0 | 0 | 0 | 0 | 0 | 0 | 0 | 1 | 2 |
| number of outages caused by Loads (NG) | 0 | 0 | 0 | 0 | 0 | 0 | 0 | 0 | 0 |
| number of outages caused by failures (NG) | 1 | 1 | 1 | 1 | 1 | 1 | 1 | 1 | 1 |
| minutes of outages (BaU) | 4253 | 4220 | 4234 | 4253 | 4253 | 4216 | 4257 | 5388 | 6621 |
| minutes of outages (NG) | 26 | 15 | 28 | 24 | 22 | 23 | 17 | 163 | 302 |
| DR requests due to RPF | 0 | 0 | 0 | 0 | 0 | 0 | 0 | 28 | 350 |
| DR requests due to Loads | 1361 | 1361 | 1361 | 1362 | 1361 | 1361 | 1361 | 1361 | 1361 |
| TO_GB total energy (from TSO) | 18,766,251 | 18,270,108 | 16,724,395 | 15697878 | 15053576 | 14616328 | 14297706 | 14050383 | 13850370 |
| TO_GB total energy (to TSO) | - | - | 96,131 | 711457 | 1708999 | 2913593 | 4236815 | 5535835 | 6853077 |
| lost energy consumed due to outages | 297,815 | 297,697 | 297,697 | 297697 | 297697 | 297697 | 297697 | 298121 | 298276 |
| lost excess energy produced due to outages | - | - | - | 0 | 0 | 0 | 0 | 27704 | 70125 |
| Flexibility obtained from EVs | 263,925.4 | 263,914.2 | 263,916.9 | 263920 | 263922 | 263925 | 263928 | 265289 | 290987 |
| Flexibility obtained from ADR (rest) | - | - | - | 0 | 0 | 0 | 0 | 28 | 398 |
| Flexibility obtained from MDR | - | - | - | 0 | 0 | 0 | 0 | 28 | 398 |
| flexibility from Evs that was not effective | 0 | 0 | 0 | 0 | 0 | 0 | 0 | 0 | 0 |
| flexibility from non-EVs that was not effective | 0 | 0 | 0 | 0 | 0 | 0 | 0 | 28 | 57 |
| % of flexibility from Evs that was not effective | 0 | 0 | 0 | 0 | 0 | 0 | 0 | 0 | 0 |
| % of flexibility from non-EVs that was not effective | #DIV/0! | #DIV/0! | #DIV/0! | #DIV/0! | #DIV/0! | #DIV/0! | #DIV/0! | 1 | 0 |
| flexibility cost per kwh from EVs | 0.100000 | 0.100000 | 0.100000 | 0.100000 | 0.100000 | 0.100000 | 0.100000 | 0.100000 | 0.100000 |
| flexibility cost per kwh from ADR | 0.000000 | 0.000000 | 0.000000 | 0.000000 | 0.000000 | 0.000000 | 0.000000 | 0.161802 | 0.243276 |
| flexibility cost per kwh from MDR | 0.000000 | 0.000000 | 0.000000 | 0.000000 | 0.000000 | 0.000000 | 0.000000 | 0.161802 | 0.243276 |
| MAX TO_GB power (from TSO) | 10970 | 10968 | 10968 | 10968 | 10968 | 10968 | 10968 | 10968 | 10968 |
| MAX TO_GB power (to TSO) | 0 | 0 | 975 | 2085 | 3194 | 4303 | 5412 | 6521 | 7631 |
| DR events for avoiding congestion | 1361 | 1361 | 1361 | 1361 | 1361 | 1361 | 1361 | 1388 | 1709 |
| DR events for avoiding outages | 0 | 0 | 0 | 1 | 0 | 0 | 0 | 1 | 2 |
| lost energy consumed due to outages (NG) | 1,160 | 1,160 | 1,160 | 1,160 | 1,160 | 1,160 | 1,160 | 1,160 | 1159.667156 |
| lost excess energy produced due to outages (NG) | - | - | - | - | - | - | - | 3,970 | 8331.539509 |

*Table 38 Useful technoeconomic metrics regarding congestion issues for EV penetration rate 20% and varying PV penetration rates*

| EV=0.3,PS=0.3 | PV penetration | | | | | | | | |
|---|---|---|---|---|---|---|---|---|---|
| | 7% | 10% | 20% | 30% | 40% | 50% | 60% | 70% | 80% |
| number of outages caused by RPF (BaU) | 0 | 0 | 0 | 0 | 0 | 0 | 0 | 8 | 17 |
| number of outages caused by Loads (BaU) | 654 | 652 | 652 | 652 | 652 | 652 | 653 | 653 | 653 |
| number of outages caused by failures (BaU) | 1 | 1 | 1 | 1 | 1 | 1 | 1 | 1 | 1 |
| number of outages caused by RPF (NG) | 0 | 0 | 0 | 0 | 0 | 0 | 0 | 1 | 2 |
| number of outages caused by Loads (NG) | 35 | 35 | 35 | 35 | 35 | 35 | 35 | 35 | 42 |
| number of outages caused by failures (NG) | 1 | 1 | 1 | 1 | 1 | 1 | 1 | 1 | 1 |
| minutes of outages (BaU) | 42586 | 42460 | 42591 | 42632 | 42566 | 42556 | 42599 | 43758 | 45005 |
| minutes of outages (NG) | 3615 | 3593 | 3631 | 3643 | 3582 | 3627 | 3630 | 3742 | 4503 |
| DR requests due to RPF | 0 | 0 | 0 | 0 | 0 | 0 | 0 | 28 | 350 |
| DR requests due to Loads | 2582 | 2582 | 2582 | 2583 | 2582 | 2582 | 2582 | 2582 | 2582 |
| TO_GB total energy (from TSO) | 17,249,988 | 16,757,414 | 15,211,700 | 14185005 | 13539189 | 13098107 | 12773355 | 12523489 | 12322180 |
| TO_GB total energy (to TSO) | - | - | 96,131 | 711281 | 1707310 | 2908074 | 4227650 | 5524128 | 6841095 |
| lost energy consumed due to outages | 4,531,918 | 4,528,230 | 4,528,232 | 4528234 | 4528236 | 4528238 | 4530723 | 4531148 | 4531858 |
| lost excess energy produced due to outages | - | - | - | 0 | 0 | 0 | 0 | 27704 | 69660 |
| Flexibility obtained from EVs | 1,314,339.7 | 1,314,329.5 | 1,314,331.9 | 1314334 | 1314337 | 1314339 | 1314342 | 1315134 | 1334252 |
| Flexibility obtained from ADR (rest) | 2,190.9 | 2,190.9 | 2,190.9 | 2191 | 2191 | 2191 | 2191 | 2248 | 2860 |
| Flexibility obtained from MDR | 2,190.9 | 2,190.9 | 2,190.9 | 2191 | 2191 | 2191 | 2191 | 2248 | 2860 |
| flexibility from Evs that was not effective | 13971 | 13973 | 13972 | 13972 | 13972 | 13972 | 13971 | 13745 | 16532 |
| flexibility from non-EVs that was not effective | 996 | 996 | 996 | 996 | 996 | 996 | 996 | 1024 | 1252 |
| % of flexibility from Evs that was not effective | 0 | 0 | 0 | 0 | 0 | 0 | 0 | 0 | 0 |
| % of flexibility from non-EVs that was not effective | 0 | 0 | 0 | 0 | 0 | 0 | 0 | 0 | 0 |
| flexibility cost per kwh from EVs | 0.100000 | 0.100000 | 0.100000 | 0.100000 | 0.100000 | 0.100000 | 0.100000 | 0.100000 | 0.100000 |
| flexibility cost per kwh from ADR | 0.310540 | 0.310609 | 0.310841 | 0.311080 | 0.311328 | 0.311583 | 0.311847 | 0.296410 | 0.292612 |
| flexibility cost per kwh from MDR | 0.310540 | 0.310609 | 0.310841 | 0.311080 | 0.311328 | 0.311583 | 0.311847 | 0.296410 | 0.292612 |
| MAX TO_GB power (from TSO) | 16772 | 16770 | 16770 | 16770 | 16770 | 16770 | 16770 | 16770 | 16770 |
| MAX TO_GB power (to TSO) | 0 | 0 | 975 | 2085 | 3194 | 4303 | 5412 | 6521 | 7631 |
| DR events for avoiding congestion | 2547 | 2547 | 2547 | 2547 | 2547 | 2547 | 2547 | 2574 | 2888 |
| DR events for avoiding outages | 35 | 35 | 35 | 36 | 35 | 35 | 35 | 36 | 44 |
| lost energy consumed due to outages (NG) | 303,347 | 303,228 | 303,228 | 303,228 | 303,228 | 303,228 | 303,228 | 303,228 | 360,129 |
| lost excess energy produced due to outages (NG) | - | - | - | - | - | - | - | 3,970 | 8,332 |

*Table 39 Useful technoeconomic metrics regarding congestion issues for EV penetration rate 30% and varying PV penetration rates*

### 5.3.4.2 *Minimizing congestion issues due to high loads*

This subsection presents a focus on congestion issues as a result of high demand, instead of high production. Such cases can occur after power outage restoration happens, as demand is increased, and this can pose significant grid challenges. To make things worse, local PV production is disconnected due to security reasons and thus along a feeder there is no more internal balance between production and consumption because all the consumptions are supplied by the network; so that the starting branch of the feeder could supply all the loads during their maximum absorption although they are normally supplied by DER. This branch would be a bottleneck and its overload could be not allowed by the breaker and another outage would occur, if this occurs the technician will reduce the number of secondary substation (i.e. the number of users) connected before restarting power by means of remote control.

Furthermore, this is true especially in case of high EV penetration where several customers could start the charging process simultaneously. A focus on the latter case is evaluated, to take advantage of the complementarities with other cases (e.g., similar simulation setup with the minimizing RPF scenario analyzed before).

Congestion issues due to high loads result in higher maintenance costs (both planned and reactive ones), higher replacement costs due to shorter life span of equipment, increased personnel, lost revenues due to power outages, higher penalties and customer dissatisfaction for the DSO in question.

In order to identify the market conditions that render Demand Side Management services attractive to such a DSO a set of what-if scenarios (simulations) have been carried out. Such market conditions are the EV penetration rate which affects the frequency of congestion events that could be dealt with DR campaigns, the Aggregator's portfolio size, member's availability for participating and response rate, presence of self-consumption from PV, remuneration asked etc.).

The details of the simulations performed are the same as in the minimizing RPF scenario, except from the following:

1. The main driver for congestion events considered is the adoption of Electric Vehicles by residential/commercial and industrial consumers. As mentioned in the previous case, the number of EVs present (the EV penetration rate) determines the percentage of EVs compared to all vehicles in that area and thus the potential controllable load. Even though the adoption of EVs in European countries is low nowadays, this is expected to change soon as the manufacturers move away from conventional vehicles and costs go down, or authorities provide the appropriate incentives. Furthermore, it has been focused on individual LV feeders and in upper class neighborhoods, or in touristic places with EV fleets high adoption rates will be achieved significantly sooner.
2. An outage occurs if:
    - both feeders experience a technical problem, or
    - there is topology reconfiguration and the effective capacity of the only feeder in use cannot cope with the demand, or
    - the total demand exceeds the combined capacity of the feeders even when no technical anomaly is present.
3. It has been assumed assume that whenever the (perfectly forecasted) load exceeds a threshold (set at the 90% of the effective line capacity) a DR campaign will be triggered, where the flexibility asked is given by the formula

$$\max(load - capacity\ threshold, 0)$$

    This applies to the case where a topology reconfiguration has taken place due to a technical failure, or maintenance, on the other feeder. When both feeders are unexpectedly off, all served endpoints get disconnected and no flexibility can be procured.
4. Aggregator's members provide negative flexibility, i.e., load that is delayed and thus affects mostly the offtake energy after the campaign period. This is the most important difference compared to the previous case where positive flexibility was sought. Again, the only form of "efficiency" is the lost load during an outage.
5. In contrast to the previous case, the number of prosumers in the area considered is not important. This is mainly due to the assumption that no rebound effects exist after an outage. Nevertheless, to verify this claim simulations with various PV penetration rates were performed.

Thus, as in the case of minimizing RPF, two candidate options for a DSO such as ASM Terni in avoiding a new outage are defined:

- Option1 (Business-as-Usual scenario): upgrade network by installing a new line and assume that congestion issues are definitely avoided.
- Option2 (Nobel GRID): ask flexibility from Aggregator.

The next figure presents the expected number of outages per year in the Business-as-Usual scenario due to high loads. It has been observed that the outages are insensitive to PV penetration rate (horizontal axis) for both EV penetration rates (red, green curves). Furthermore, outages due to high loads start taking place when 10% of the endpoints buy EVs. In particular, 1 outage was found to be happening every year due to high loads if EV penetration reaches 10%.

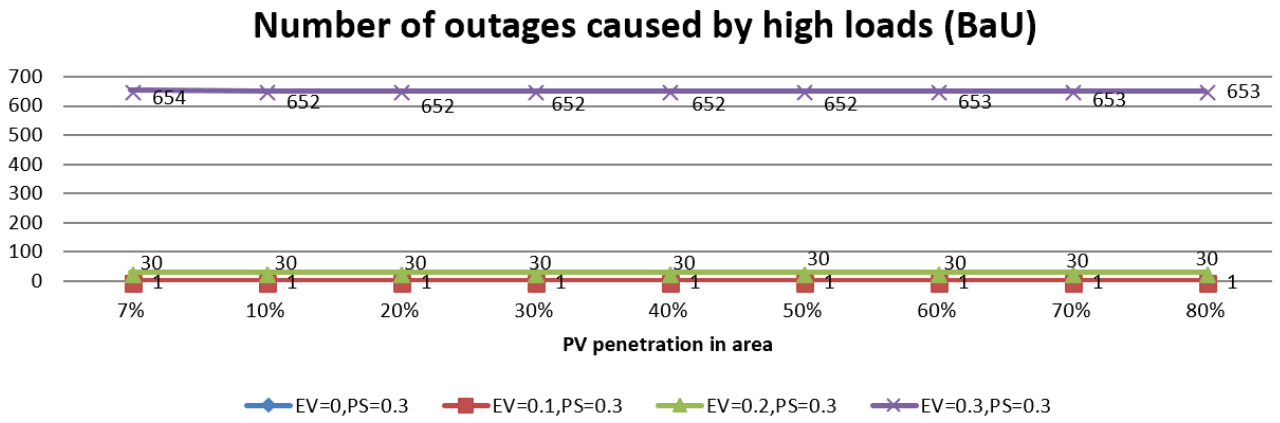


*Figure 154: The expected number of outages caused annually by high loads in Business-as-Usual scenario for the benchmark feeder loop in Terni*

The total number of outages, that is including those originating from unexpected hardware failures, human error or proactive maintenance, is shown in the figure below. As in the case of minimize RPF, results show that 1 outage on average will be taking place every year on top of those attributed to high local RES production.

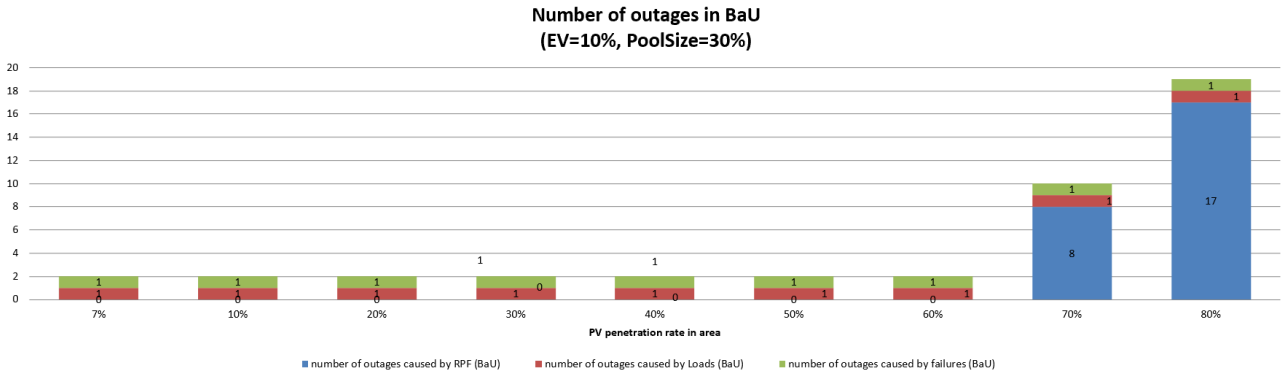


*Figure 155: The total expected annual number of outages (high loads and technical aspects) in Business-as-Usual scenario for the benchmark feeder loop in Terni*

According to the following figure, Demand Side Management techniques succeed in eliminating outages caused by high loads alone or as the combined effect on technical issues on one feeder and failure of the remaining one to handle all loads for EV penetration up to 20%, while significantly reducing those events for higher EV shares.

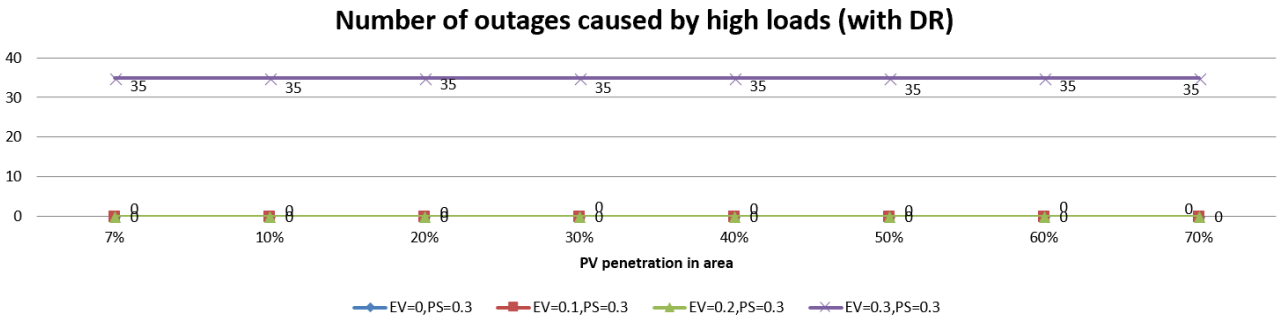


*Figure 156: The expected number of outages caused annually by increased loads in the NOBEL GRID-enabled scenario (with DR) for the benchmark feeder loop in Terni*

The main purpose of Subsections 5.3.4.1 and 5.3.4.2 is to propose innovative business models for individual actors and evaluate the attractiveness of each one when these are combined into value networks for dealing with a challenge or an opportunity that exists in the context of the NOBEL GRID pilot sites. This is important in order to understand the market potential of the NOBEL GRID technologies and the resulting interactions among the market players, namely DSOs, ESCOs/Aggregators, Retailers and Consumers/Prosumers.

In particular the focus has been on the following innovative, as well as, more straightforward business models: DSOs evolved into SmartGrid-enabled DSOs. Under this business model DSOs perform advanced network management by using tools and processes that treat Demand-Side Management techniques on par with traditional ones when performing their tasks, e.g. maintaining the power quality by minimizing Reverse Power Flows or reducing congestion issues that can lead to power outages. It was found that DSOs are allowed to have a low, but positive, IRR in the BaU scenario which is increased in most of the cases with NOBEL GRID technologies. This positive effect of Smart grid solutions can reduce the electricity bills of the end-users.

# 6 Conclusions

The electricity distribution network is the basis of the services provided to citizens, and it is also the backbone of future smart cities. Therefore, increasing attention has been especially focused on the electric power quality that is under the responsibility of the DSO. Moreover the share of connected EV charging stations and Distribute Generators are going to dramatically reduce the residual hosting capacity of the distribution networks.

As for the power quality, this work points out that the DSO is currently focused on the continuity of supply; moreover, the availability of electrical energy will be its first concern also in the future. This work deals with different smart strategies and techniques for Power Quality improvement, which have their own features as well as a common approach which is the following: the increasing of DSO awareness about the network status both with off – line analysis and on – line monitoring. Indeed, the DSO awareness enables the network observability and the control of power flows during real time management of the network. In this respect, different levers have been evaluated in this work.

Off – line analysis provide outcomes for the development plans of the DSO, including resilience as a new driver. In this respect, the results of the resilience assessment point out the most critical branches and nodes of a distribution network and the algorithm provides a hierarchy of the interventions, validating the DSO development plans. In addition, the thermal analysis of a MV joint highlights that joint temperatures are only partially influenced by the ambient temperature variation, whereas temperature variations during a day are mainly due by the cable current profiles: it does not seem that the abnormal number of joint faults may be caused by abnormally high values of ambient temperature, whilst, based on the outcomes of the simulation on CR, it seems that the CR introduced by an incorrect packaging of the joint could increase the vulnerability during faults.

With respect to the monitoring, the USM, developed over Nobel GRID project, has been used for data gathering in a near – real – time mode, allowing observability of hundreds of Points of Delivery in the distribution network. It is worth noting that the cost of this solution is very limited in terms of HW installation since it does not affect the traditional electronic affect, on the other hand the operational expenditure would increase because of the huge amount of data daily gathered. The data management and storage are going to become a challenge for the DSO; indeed, data are resources to be sold to new and old actors but DSOs should acquire new expertise on Big data management and, in addition, data management is going to arise new privacy issues.

On the basis of an increased data availability, this work has evaluated different actions leaded by the DSO; notably, energy storage systems, Demand Response campaigns and a cooperation with a microgrid. The results have been calculated by means of both demonstration activities and simulations. From the technical point of view, interesting outcomes have been evaluated; in particular, DR campaigns which involve commercial and big energy consumer can increase the energy savings as well as energy storage systems enable some services for voltage control.

According to the results of this work, considering the case study of electrical distribution network of Terni, the DSO is already compliant with the high standards required by the Authority in terms of continuity of supply. However, in this context, the DSO is going to face an increasing number of natural hazards as well as the distribution network is going to connect new distributed generators, EV charging stations and new loads because of electrification of the consumptions; therefore, in an upcoming scenario DSO will be an actor which could actively select different flexibility sources, according to the technical – economical instances not only for the power quality

improvement and efficiency of power flows but they can be also leveraged for innovative development plans.

# 7 Published material

*Publications - Journals*

[1] T. Bragatto, M. Cresta, F. M. Gatta, A. Geri, M. Maccioni, M. Paulucci, “Underground MV power cable joints: a nonlinear thermal circuit model and its experimental validation,” Electric Power System Research, vol. 149, pp. 190–197, Aug. 2017.

[2] Bragatto, T.; Cresta, M.; Cortesi, F.; Gatta, F.M.; Geri, A.; Maccioni, M.; Paulucci, M. Assessment and Possible Solution to Increase Resilience: Flooding Threats in Terni Distribution Grid. *Energies* 2019, *12*, 744.

[3] T. Bragatto, M. Cresta, F. M. Gatta, A. Geri, M. Maccioni, M. Paulucci, “A 3-D nonlinear thermal circuit model of underground MT power cables and their joints” Electric Power System Research, vol. 173, pp. 112–121, Aug. 2019

[4] Bragatto, T.; Cerretti, A.; D’Orazio, L.; Gatta, F.M.; Geri, A.; Maccioni, M. Thermal Effects of Ground Faults on MV Joints and Cables. Energies 2019, 12, 3496.

[5] Bragatto, T.; Cresta, M.; Gatta, F.M.; Geri, A.; Maccioni, M.; Paulucci, M. “Measuring yearly variation of temperature of medium voltage cable joints” *Energies* 2019, ***submitted***.

*Publications - Conferences*

[1] T. Bragatto, F. M. Gatta, S. Lauria, M. Lazzaro, A. Geri, M. Maccioni, M. Paulucci, G. Paternò “Flexibility services to power systems from smart rural microgrid prosumers” 2018 IEEE 18th EEEIC, Palermo, 2018,

[2] T. Bragatto, M. Cresta, F. M. Gatta, A. Geri, R. Lamedica, M. Maccioni, M. Paulucci, A. Ruvio “Statistical Analysis of Prosumer Behaviour in a Real Distribution Network over Two Years” 2018 IEEE 18th EEEIC, Palermo, 2018,

[3] T. Bragatto, F. Carere, M. Cresta, F. M. Gatta, A. Geri, S. Lauria, M. Maccioni, M. Paulucci, “Smart Grid and Microgrid Cooperation in a Real Distibution Network under Emergency Conditions” 2018 IEEE 18th EEEIC, Palermo, 2018,

[4] T. Bragatto, M. Cresta, F. M. Gatta, A. Geri, M. Maccioni, M. Paulucci, “Assessment and possible solution to increase the resilience of Terni distribution Grid: the ice sleeves formation threat” AEIT 2018, 110th International Conference, Bari, 2018.

[5] M. Sănduleac, A. Corsi, T. Bragatto, D. Stanescu, C. Stanescu, A. Sbarcea, C. Bulac "Using Frequency measurements for data consistency assessment related to malicious data injection in distribution related ICT systems" ISFEE 2018, Bucarest, 2018

[6] D. Lagutin, F. Bellesini, T. Bragatto, A. Cavadenti, V. Croce, Y. Kortesniemi, H. C. Leligou, Y. Oikonomidis, G. C. Polyzos, G. Raveduto, F. Santori, P. Trakadas, M. Verber "Secure Open Federation of IoT Platforms through Interledger Technologies - the SOFIE approach" EuCNC 2019, Valencia, 2019.

[7] T. Bragatto; V.Croce; M. Cresta; M. Paulucci; F. Santori; D. Ziu “A real-life experience on 2nd life batteries services for Distribution System Operator” 2019 IEEE EEEIC / I&CPS Europe.

[8] T. Bragatto; M. Cresta; C. Kalogiros; M. Paulucci; M. Sanduleac; F. Santori; V. Scotto di Carlo “Innovative Tools for Demand Response Strategies: a Real-Life Experience” 2019 IEEE EEEIC / I&CPS Europe.

[9] F. Bellesini, T. Bragatto, D. Cabagnols, A. Corsi, G. Fiorentino, J. M. Lalueza, F. Rebecchi, "How 5G Enables Smart Energy: Setup and First Experiences from the NRG-5 Pilots" EuCNC 2019, Valencia, 2019 *(Not in Scopus)*

[10] T. Bragatto, M. Paulucci, G. Thanos, M. Minou, C. Kalogiros "DSOs Using Demand-Side Management Techniques For Reducing Congestion Issues: The Case of ASM Terni" HAEE 2019, Athens, 2019 *(Not in Scopus)*

[11] Bragatto, T.; Cresta, M.; Cortesi, F.; Gatta, F.M.; Geri, A.; Maccioni, M.; Paulucci, M. Assessment and Possible Solution to Increase Resilience: Flooding Threats in Terni Distribution Grid. AEIT 2019, 111th International Conference, Firenze, 2019.

[12] N.Bezas, A.Noula, D.Ioannidis, D.Tzovaras, T.Bragatto, F.Santori, "Dynamic clustering mechanism using forecasted input data" The International Conference on Energy and Sustainable Futures (ICESF), Nottingham, 2019. *(Not in Scopus)*

*Publications - Deliverables*

I have also co-authored the deliverables of the European projects in which ASM Terni has participated (a description of the project is provided in subsection 3.2) and which are properly cited in this work.

# References


[1] M. Shabanzadeh et M. P. Moghaddam, "What is the smart grid? definitions, perspectives, and ultimate».

[2] Department of Energy, United States (DOE), “The Smart Grid: An Introduction”, Washington, DC., 2003».

[3] NOBEL GRID Project, «D. 16.2 Local deployment of project results in Terni demo site».

[4] Consortium, WiseGRID, «D12.1 Analysis of Grid Management Technologies for the distribution grid,» 2017.

[5] World Economic Forum, “The Future of Electricity -New Technologies Transforming the Grid Edge”, 2017. [Online]. Available: http://www3.weforum.org/docs/WEF_Future_of_Electricity_2017.pdf».

[6] A. Ipakchi, “Implementing the Smart Grid: Enterprise Information Integration”, 2007. in Grid-Interop Forum 2007, Paper 121.122-1».

[7] N. Rezaee, M Nayeripour, A. Roosta, T. Niknam, 2009, “Role of GIS in Distribution Power Systems”, World Academy of Science, Engineering and Technology 60 2009».

[8] A. Elsayed, 2013, “Integrated GIS and SCADA system model for Alexandria electricity distribution compa-ny”, CIRED 22nd International Conference on Electricity Distribution Stockholm, 10-13 June 2013.

[9] A. Holmlund, R. Sjöberg, 2011, “Information exchange with CIM for the Energy Industry”, Master The-sis, Stockholm, Sweden 2011.

[10] T. Agarwal, “What is SCADA System and Its Applications in Power Systems”, 2017. [online] Available at: https://www.edgefx.in/scada-applications-in-power-system/ [Accessed 6 Nov. 2017].

[11] «The Nobel GRID consortium, Nobel GRID – Nex cost efficient businness models for flexible smart grids . URL ⟨https://nobelgrid.eu/).».

[12] Mihai Sanduleac, Gianluca Lipari, Antonello Monti, Artemis Voulkidis, Gianluca Zanetto, Antonello Corsi , Lucian Toma, Giampaolo Fiorentino, Dumitru Federenciuc. “Next Generation Real-Time Smart Meters for ICT Based Assessment of Grid Data Inconsist».

[13] «Chu, T.; Qin, J.; Wei, J. Distributed storage operation in distribution network with stochastic renewable generation. In Proceedings of the IEEE PES General Meeting Conference & Exposition, National Harbor, MD, USA, 27–31 July 2014.».

[14] «Wu, K.; Jiang, Y.; Marinakis, D. A stochastic calculus for network systems with renewable energy sources. In Proceedings of the IEEE Conference on Computer Communications Workshops, Orlando, FL, USA, 25–30 March 2012.».

[15] «Zoeller, H.; Reischboeck, M.; Henselmeyer, S. Managing volatility in distribution networks with active network management. In Proceedings of the CIREDWorkshop 2016, Helsinki, Finland, 14–15 June 2016.».

[16] «Parvez, I.; Sarwat, A.I.; Wei, L.; Sundararajan, A. Securing metering infrastructure of smart grid: A ma-chine learning and localization based key management approach. Energies 2016, 9, 691.».

[17] «Saxena, N.; Choi, B.J. State of the art authentication, access control, and secure integration in smart grid. Energies 2015, 8, 11883–11915.».

[18] «EG3 First Year Report: Options on Handling Smart Grids Data. Available online: https://ec.europa.eu/ energy/sites/ener/files/documents/xpert_group3_first_year_report.pdf (access on 24 June 2017).».

[19] «Patti, E.; Pons, E.; Martellacci, D.; Castagnetti, F.B.; Acquaviva, A.; Macii, E. "MultiFLEX: Flexible multi-utility, multi-service smart metering architecture for energy vectors with active prosumers", in Proceedings of the 2015 International Confe».

[20] «Pitì, A.; Verticale, G.; Rottondi, C.; Capone, A.; Schiavo, L.L. "The role of smart meters in enabling real-time energy services for households: The Italian case". Energies 2017, 10, 199.».

[21] «NobelGrid Consortium, "Smart Low-cost Advanced Meter (SLAM)", 2017. [Online]. Available: http://nobelgrid.eu/products/».

[22] SUCCESS, H2020 project, http://success-energy.eu/.

[23] W. Consortium, «D6.1 Analysis of storage technologies for the distribution grid,» 2017.

[24] E. IFC, «Energy Storage Trends and Opportunities in Emerging Markets,» 2017.

[25] L. V. C. N. T. Marcus Müller, «Evaluation of grid-level adaptability for stationary battery energy storage system applications in Europe,» 2016.

[26] I. R. E. Agency, «Battery storage for renewables,» 2015.

[27] European comission, «Energy Local Storage Advanced System,» 2014.

[28] ADEME, «Etude sur le potentiel du stockage d'énergies,» 2013.

[29] Consortium, WiseGRID, «D10.1 DR Technologies Outlook and Flexibility Sources Clustering and Classification,» 2017.

[30] EPRS | European Parliamentary Research Service, «Smart appliances and the electrical system,» European Parliament, 2016.

[31] European Commission, «Delivering a New Deal for Energy Consumers - COM(2015) 339 final,» 2015.

[32] Rainer Stamminger, Verena Anstett, «The Effect of Variable Electricity Tariffs in the Household on Usage of Household Appliances,» *Smart Grid and Renewable Energy,* vol. 4, pp. 353-365, 2013.

[33] J. LaMarche, K. Cheney, K. Roth, O. Sachs e M. Pritoni, «Home Energy Management: Products & Trends.,» in *Proceedings of 17th Biennial ACEEE Summer Study on Energy Efficiency in Buildings*, 2012.

[34] Joint Research Center, «Demand Response status in EU,» 2016.

[35] SEDC, «Explicit Demand Response in Europe: Mapping the Markets 2017,» 2017. [Online]. Available: http://www.smartenergydemand.eu/wp-content/uploads/2017/04/SEDC-Explicit-Demand-Response-in-Europe-Mapping-the-Markets-2017.pdf.

[36] Consortium, WiseGRID, «D8.1 Analysis of the electric Transportation sector,» 2017.

[37] E. Commission, «Europe 2020. A European strategy for smart, sustainable and inclusive growth,» 03 March 2010. [Online]. Available: http://ec.europa.eu/eu2020/pdf/COMPLET%20EN%20BARROSO%20%20%20007%20-%20Europe%202020%20-%20EN%20version.pdf.

[38] «EU Crude Oil Imports and supply cost - Energy - European Commission,» [Online]. Available: https://ec.europa.eu/energy/en/data-analysis/eu-crude-oil-imports.

[39] «GlobalPetrolPrices.com,» [Online]. Available: http://www.globalpetrolprices.com/articles/39/.

[40] «Alternative fuels for sustainable mobility in Europe - Mobility and Transport - European Commission,» [Online]. Available: https://ec.europa.eu/transport/themes/urban/cpt_en.

[41] «CLIMATE ACTION - European Comission,» [Online]. Available: ec.europa.eu/clima/news/articles/news_2013062501_en.

[42] «DIRECTIVE 2009/33/EC OF THE EUROPEAN PARLIAMENT AND OF THE COUNCIL,» [Online]. Available: http://eur-lex.europa.eu/legal-content/EN/TXT/HTML/?uri=CELEX:32009L0033&from=EN..

[43] «European Commission, “Guidelines on financial incentives: Promoting energy efficient vehicles”,» [Online]. Available: http://europa.eu/rapid/press-release_IP-13-174_en.htm.

[44] «European Enviroment Agency - ''Monitoring of CO2 emissions from passenger cars – Regulation 443/2009'',» [Online]. Available: https://www.eea.europa.eu/data-and-maps/data/co2-cars-emission-12.

[45] «DIRECTIVE 1999/94/EC OF THE EUROPEAN PARLIAMENT AND OF THE COUNCIL,» [Online]. Available: http://eur-lex.europa.eu/legal-content/EN/TXT/HTML/?uri=CELEX:01999L0094-20081211&from=EN.

[46] «European Comission - Vision 2020: CARS 21 Group delivers recommendations to help car industry reach new heights,» [Online]. Available: http://europa.eu/rapid/press-release_MEMO-12-419_en.htm?locale=en.

[47] E. Helmers e M. Weiss, «Advances and critical aspects in the life-cycle assessment of battery electric cars,» *Energy and Emission Control Technologies,* pp. 1-18, 1 February 2017.

[48] «DIRECTIVE 2014/94/EU OF THE EUROPEAN PARLIAMENT AND OF THE COUNCIL,» [Online]. Available: http://eur-lex.europa.eu/legal-content/EN/TXT/HTML/?uri=CELEX:32014L0094&qid=1507138109314&from=EN.

[49] «European Automobile Manufacturers Associaton,» [Online]. Available: www.acea.be/publications/article/fact-sheet-cars. .

[50] «Joint Research Center,» [Online]. Available: iri.jrc.ec.europa.eu/scoreboard16.html. .

[51] «Incentives & Legislation | EAFO | European Alternative Fuels Observatory,» [Online]. Available: http://www.eafo.eu/incentives-legislation.

[52] «Departement Omgeving Vlaamse Overheid - "Actieplan Clean Power for Transport Vlaanderen",» [Online]. Available: http://milieuvriendelijkevoertuigen.be/sites/default/files/atoms/files/Actieplan%20CPT.pdf.

[53] «LMC AUTOMOTIVE,» [Online]. Available: https://www.lmc-auto.com/.

[54] «European Alternative Fuel Observatory,» [Online]. Available: http://www.eafo.eu/eu..

[55] «European Alternatives Fuel Observatory | Norway,» [Online]. Available: www.eafo.eu/content/norway.

[56] «European Alternative Fuels Observatory,» [Online]. Available: http://www.eafo.eu/eu#eu_pev_mark_shr_graph_anchor.

[57] «EV Sales Down 80% In Denmark For 2016 After Tax Policy Change,» [Online]. Available: insideevs.com/ev-sales-down-80-in-denmark-for-2016-after-tax-policy-change/.

[58] [Online]. Available: http://business.time.com/2012/05/02/gen-ys-take-on-car-ownership-not-cool/.

[59] «Evaluation of the Impact that a Progressive Deployment of EV will Provoke on Electricity Demand, Steady State Operation, Market Issues, Generation Schedules and on the Volume of Carbon Emissions-Electric Vehicle Penetration Scenarios in Germany, UK, Spain,» in *EU MERGE project, Task 3.2, Part II of Deliverable D 3.2*.

[60] E. L. Karfopoulos, E. M. Vouvoulakis e N. Hatziargyriou, «Steady-state and dynamic impact analysis of the large scale integration of plug-in EV to the operation of the autonomous power system of Crete Island,» *MedPower ,* pp. 1-9, 2-5 November 2014.

[61] E. Karfopoulos e N. Hatziargyriou, «A Multi-Agent System For Controlled Charging of A Large Population of Electric Vehicles,» *Transactions on Power Systems, vol. 28, issue 2,* pp. 1196-1204, 2013.

[62] E. L. Karfopoulos, K. A. Panourgias e N. D. Hatziargyriou, «Distributed Coordination of Electric Vehicles providing V2G Regulation Services,» *IEEE Transactions on Power Systems ,* pp. 2834 - 2846, 15 September 2015.

[63] «5. TERNA Grid development plan. EN source ITA source. 2016».

[64] «A. Prudenzi, A. Silvestri, R. Lamedica, M. C. Falvo, and M. Regoli, "A domestic electric load simulator including psychological aspects of demand," 2010 IEEE PES General Meeting, Minneapolis (MN), United States, 25-29 July 2010.».

[65] «J. Li and M.A. Danzer, "Optimal charge control strategies for stationary photovoltaic battery systems," J. Power Sources, vol. 258, pp. 365-373, July 2014.».

[66] «M. Bruch and M. Müller, "Calculation of the cost-effectiveness of a PV battery system," Energy Proc., vol. 46, pp. 262-270, 2014.».

[67] «Y. Zong, L. Mihet-Popa, D. Kullmann, A. Thavlov, O. Gehrke, and H.W. Bindner, “Model predictive controller for active demand side management with PV selfconsumption in an intelligent building,” 2012 IEEE PES innovative smart grid technologies conferen».

[68] «P. Palensky and D. Dietrich, “Demand side management: demand response, intelligent energy systems, and smart loads,” IEEE Trans. Ind. Inform., vol. 7, pp. 381-388, August 2011.».

[69] «M. Castillo-Cagigal, E. Matallanas, A. Gutiérrez, F. Monasterio-Huelin, E. Caamaño-Martín, D. Masa-Bote, and J. Jiménez-Leube, “Heterogeneous collaborative sensor network for electrical management of an automated house with PV energy,” Sensors, vol. 1».

[70] «N. Femia, D. Toledo, and W. Zamboni, “Storage unit and load management in photovoltaic inverters for residential application,” in 39th Annual Conference of the IEEE Industrial Electronics Society (IECON 2013), Vienna (Austria), 2013, pp. 6800-6805.».

[71] «Italian Manager of Energy Services (GSE), “Rapporto statistico 2016 – solare fotovoltaico (in Italian),” available on line on https://www.gse.it/documenti_site/Documenti%20GSE/Rapporti%20statistici/Solare%20Fotovoltaico%20-».

[72] NOBEL Consortium, *NOBEL Annex I,* Valencia: EC, 2009.

[73] Consortium, WiseGRID, «Grant Agreement».

[74] DEFENDER Consortium, «http://defender-project.eu/».

[75] NRG-5, Project, «nrg.eu».

[76] «ELSA project - elsa.eu».

[77] inteGRIDy project, «http://www.integridy.eu/,» [Online].

[78] eDREAM project, «https://edream-h2020.eu/,» [Online].

[79] SOFIE project, «https://www.sofie-iot.eu/en,» [Online].

[80] «ARERA web site,» [Online]. Available: https://www.arera.it/it/inglese/index.htm. [Consultato il giorno 02 01 2018].

[81] ARERA, «Testo integrato della regolazione output-based dei servizi di distribuzione e misura dell’energia elettrica periodo di regolazione 2016-2023,» 2016.

[82] «IEEE-1366 2003 Guide for Electrique Power Distribution reliability indices».

[83] «SouthWell, P. Disaster recovery within a cigre strategic framework: Network resilience, trends and areas of future work,” CIGRE Study Committee C1, 2014,» 2014.

[84] «UNARETI, unit for Asset Management and Planning “Plan of interventions for increasing resilience of electrical distribution network of UNARETI (Development Plan unareti annex n.20)” In Italian https://www.unareti.it/unr/unareti/Piano-di-lavoro-per-increme».

[85] «A. Bosisio, A. Berizzi, C. Bovo, E. Amaldi, S. Fratti “GIS-based urban distribution networks planning with 2-step ladder topology considering electric power cable joints” AEIT International Conference Bari 2018.».

[86] «R.A. Jongen, P.H.F. Morshuis, J.J. Smit, A.L.J. Janssen, “Influence of ambient temperature on the failure behavior of cable joints” Annual Report Conference on Electrical Insulation and Dielectric Phenomena 2007».

[87] T. Bragatto, M. Cresta, F. M. Gatta, A. Geri, M. Maccioni, M. Paulucci, “Underground MV power cable joints: a nonlinear thermal circuit model and its experimental validation,” Electric Power System Research, vol. 149, pp. 190–197, Aug. 2017..

[88] T. Bragatto, M. Cresta, F. M. Gatta, A. Geri, M. Maccioni, M. Paulucci, “A 3-D nonlinear thermal circuit model of underground MT power cables and their joints” Electric Power System Research, vol. 173, pp. 112–121, Aug. 2019

[89] Bragatto, T.; Cerretti, A.; D’Orazio, L.; Gatta, F.M.; Geri, A.; Maccioni, M. Thermal Effects of Ground Faults on MV Joints and Cables. Energies 2019, 12, 3496.».

[90] «D. M. Simmons, “Calculation of the electrical problems of underground cables,” Elect. J., vol. 29, no. 8, pp. 395–398, 1932.».

[91] «J. H. Neher, M. H. McGrath, “The calculation of the temperature rise and load capability of cable systems,” AIEE Transactions Part III - Power Apparatus and Systems, vol. 76, pp. 752–764, Oct 1957.».

[92] «C. A. Bauer, R. J. Nease, “A study of the superposition of heat fields and the kennelly formula as applied to undergrounds cable systems,” Amer. Inst. Elect. Eng. Trans., pt. III, pp. 1330–1333, Feb. 1958.».

[93] «S.M. Sellers, W.Z. Black, “Refinements to the Neher-McGrath model for calculating the ampacity of underground cables,” IEEE Trans. Power Delivery, vol. 11, pp. 12–30, Jan. 1996.».

[94] «B. M. Weedy, “Air temperatures in a deep cable tunnel,” Elect. Power Syst. Res., vol. 15, pp. 229–232, Dec. 1988.».

[95] «F. C. Van Wormer, “An improved approximate technique for calculating cable temperature transients,” Amer. Inst. Elect. Eng. Trans., pt. III, vol. 74, pp. 277–281, April 1955.».

[96] «G. Gela, J. J. Dai, “Calculation of thermal fields of underground cables using the boundary element method,” IEEE Trans. Power Delivery, vol. 3, pp. 1341–1347, Oct. 1988.».

[97] «J. K. Mitchell, O. N. Abdel-Hadi, “Temperature distribution around buried cables,” IEEE Trans. Power Apparat. Syst., vol. PAS-98, pp. 1158–1166, Apr. 1979.».

[98] «M. A. Kellow, “A numerical procedure for the calculation of the temperature rise and ampacity of underground cables,” IEEE Trans. Power Apparat. Syst., vol. PAS-100, pp. 3322–3330, July 1981.».

[99] «T. A. Haskew, R. F. Carwile, L. L. Gribsby, “An algorithm for steady-state thermal analysis of electrical cables with radiation by reduced Newton-Raphson techniques,” IEEE Trans. Power Delivery, vol. 9, pp. 526–533, Jan. 1994.».

[100] «M. A. Hanna, A. Y. Chikhani, M. M. A. Salama, “Thermal analysis of power cables in multi-layered soil—Part 1: Theoretical model,” IEEE Trans. Power Delivery, vol. 8, pp. 761–771, July 1993.».

[101] «T. Bragatto, M. Cresta, F. M. Gatta, A. Geri, M. Maccioni, M. Paulucci, “Underground MV power cable joints: a nonlinear thermal circuit model and its experimental validation,” Electric Power System Research, vol. 149, pp. 190–197, Aug. 2017.».

[102] «G. J. Anders, Rating of electric power cables: ampacity computations for transmission, distribution, and industrial applications, IEEE Press Power Engineering Series, 1997.».

[103] «IEC 60287, Electric cables - Calculation of the current rating - Part 2-1: Thermal resistance - Calculation of the thermal resistance, 2015.».

[104] «C. Moreau, L. Courset, “Current rating of cables installed in plastic ducts,” Jicable 2007 – Session B8 – Design, Paris-Versailles, France, 24-28 June 2007.».

[105] «[29] F. Kreith, Principles of heat transfer, Third edition, Intext Educational Publisher, New York, 1973.».

[106] «[30] P. Berdahl, R. Fromberg, “The thermal radiance of clear skies,” Sol. Energy, vol. 29, pp. 299–314, 1982.».

[107] «R. de Lieto Vollaro, L. Fontana, A. Vallati, “Thermal analysis of underground electrical power cables buried in non-homogeneous soils,” App. Therm. Eng., vol. 31, pp. 772–778, April 2011.».

[108] «E. Kroener, A. Vallati, M. Bittelli, “Numerical simulation of coupled heat, liquid water and water vapor in soils for heat dissipation of underground electrical power cables,” App. Therm. Eng., vol. 70, pp. 510–523, Sept. 2014.».

[109] «P. Ocłoń, P. Cisek, M. Pilarczyk, D. Taler, “Numerical simulation of heat dissipation processes in underground power cable system situated in thermal backfill and buried in a multilayered soil,” Energy Conversion and Management, vol. 95, pp. 352–370, May».

[110] «O. Johansen, “Thermal conductivity of soils,” Ph.D. thesis, Trondheim, Norway; 1975.».

[111] «M. Ouzzane, P. Eslami-Nejad, M. Badache, Z. Aidoun, “New correlations for the prediction of the undisturbed ground temperature,” Geothermics, vol. 53, pp. 379–384, Jan. 2015.».

[112] «M. Badache, P. Eslami-Nejad, M. Ouzzane, Z. Aidoun, L. Lamarche, “A new modeling approach for improved ground temperature profile determination,” Renewable Energy, vol. 85, pp. 436–444, Jan. 2016.».

[113] «T. Sung, S. Y. Yoon, K. C. Kim, “A mathematical model of hourly solar radiation in varying weather conditions for a dynamic simulation of the solar organic Rankine cycle,” Energies, vol. 8, pp. 7058-7069, 2015.».

[114] «J. W. Spencer, “Fourier series representation of the position of the sun,” Search, vol. 2, pp. 162–172, May 1971.».

[115] «M. Krarti, C. Lopez-Alonzo, D.E. Claridge, J.F. Kreider, “Analytical model to predict annual soil surface temperature variation,” J. Sol Energy Eng., vol. 117, pp. 91–99, May 1995.».

[116] «G. Mihalakakou, “On estimating soil surface temperature profiles,” Energy Build., vol. 34, pp. 251–259, March 2005.».

[117] «L. O. Chua, P.-M. Lin, Computer–aided analysis of electronic circuits, Prentice-Hall, Inc. Englewood Cliffs, New Jersey, 1975.».

[118] «C. Cesaraccio, D. Spano, P. Duce, R. L. Snyder, “An improved model for determining degree-day values from daily temperature data,” Int. J. Biometeorology, vol. 45, pp. 161–169, Nov. 2001.».

[119] «11. Yang, F.; Zhu, N.; Liu, G.; Ma, H.; Wei, X.; Hu, C.; Wang, Z.; Huang, J. A new method for determining the connection resistance of the compression connector in cable joint. Energies, 2018, Volume 11, 1667, DOI: 10.3390/en11071667.».

[120] «9. Greenwood, J.A. Constriction resistance and the real area of contact. British Journal of Applied Physics 1966, Volume 17, 1621-1632,».

[121] «10. Boyer, L. Contact resistance calculations: generalizations of Greenwood's formula including interface films. Transactions on Components and Packaging Technologies 2001, Volume 24,».

[122] «11. Vogler, M.; Sheppard, S. Electric contact resistance under high loads and elevated temperatures. Welding Journal – Including Welding Research Supplement 1993, Volume 72, 231-238.».

[123] «4. Yang, F.; Cheng, P.; Luo, H.; Yang, Y.; Liu, H.; Kang, K. 3-D thermal analysis and contact resistance evaluation of power cable joint. Applied Thermal Engineering 2016, Volume 93, 1183-1192,».

[124] «12. CESI. PROVE DI DIAGNOSTICA SU GIUNTI DI CAVO MT – Prove di cortocircuito di giunti di cavi MT e servizio di Analisi. Technical Report for e-distribuzione, 2017 [B7013247].».

[125] «25. Gatta, F.M.; Geri, A. Studi di Rete Finalizzati all'Analisi ed alla Predizione delle Correnti di Corto Circuito e dei loro Effetti negli Schermi dei Cavi delle Reti di Distribuzione in MT a Seguito di Guasti Monofase o Polifase, Singoli o Multipli».

[126] L. A. Bollinger e D. G. P. J., «Evaluating infrastructure resilience to extreme weather - the case of the Dutch electricity transmission network,» *EJTIR,* vol. 16, n. 1567 - 7141, pp. 214 - 239, 2016.

[127] K. Forssén e K. Maki, «Resilience of Finnish electricity distribution networks against extreme weather conditions,» in *CIRED Workshop*, Helsinki 14-15 June 2016.

[128] E. Amicarelli, L. Ferri, M. De Masi e A. V. G. Suich, «Assessment of the resilience of the electrica distribution grid: e-distribuzione approach,» in *AEIT*, Bari, 2018.

[129] A. Kwansinski, «Quantitative model and metrics of electrical grids' resilience evaluated at a power distribution level,» *Energies,* vol. 9, p. 93, 2016.

[130] T. Bragatto, M. Cresta, F. Gatta, A. Geri, M. Maccioni e M. Paulucci, «Assessment and possible solution to increase the resilience of Terni distribution Grid: the ice sleeves formation threat,» in *AEIT*, Bari, 2018.

[131] «Bie, Z.H.; Lin, Y.L.; Li, G.F.; Li, F.R. Battling the Extreme: A Study on the Power System Resilience. Proc. IEEE 2017, 105, 1253–1266».

[132] L. Jiazheng, G. Jun, J. Zhou, Y. Yihao e W. T., «Resilience Assessment and Its Enhancement in Tackling Adverse Impact of Ice Disasters for Power Transmission Systems,» *Energies,* vol. 11, n. 2272, 2018.

[133] S. Espinozaa, M. Panteli, P. Mancarella e H. Rudnick, «Multi-phase assessment and adaptation of power systems resilience to natural hazards,» *EPSR,* vol. 136, pp. 352 - 361, 2016.

[134] «Yang, Y.H.; Tang,W.H.; Liu, Y.; Xin, Y.L.;Wu, Q.H. Quantitative Resilience Assessment for Power Transmission Systems Under TyphoonWeather. IEEE Access 2018, 6, 40747–40756».

[135] «Li, Z.; Shahidehpour, M.; Aminifar, F.; Alabdulwahab, A.; Al-Turki, Y. Networked Microgrids for Enhancing».

[136] «Engineering Technical Report 138 Issue 3 2018 Resilience to Flooding of Grid and Primary Substations PRODUCED BY THE OPERATIONS DIRECTORATE OF ENERGY NETWORKS ASSOCIATION».

[137] H. J. Murdock, K. M. de Bruijn e B. Gersonius, «Assessment of Critical Infrastructure Resilience to Flooding Using a Response Curve Approach,,» *Energies,* vol. 3470, 2018.

[138] «Arera, Resolution 646/2015/R/eel (in Italian)».

[139] F. Ciasca, A. Sallati e N. Tolu, «Italian National Resilience Plan 2017,» in *2017 AEIT International Annual Conference*, Florence.

[140] «Dulmage, A. L.; Mendelsohn, N. S. Coverings of bipartite graphs, Can. J. Math., 1958, 10, 517–534».

[141] O. o. c. p. Province of Terni, «Emergency plan of the province, hydro risk».

[142] A. o. T. basin, «Hydrogelogichal plan, Technical standards».

[143] « Ma, G. , Zhang, J. , Jiang, W. , Liu, J. , and Ma, L. GIS-Based Risk Assessment Model for Flood Disaster in China. Proc., 18th International Conference on Geoinformatics, Beijing, 2010, pp. 1–5.».

[144] «Dunn S, Wilkinson S, Alderson D, Fowler H, Galasso C. Fragility Curves for Assessing the Resilience of Electricity Networks Constructed from an Extensive Fault Database. Natural Hazards Review 2018,».

[145] «Bragatto, T.; Cresta, M.; Cortesi, F.; Gatta, F.M.; Geri, A.; Maccioni, M.; Paulucci, M. Assessment and Possible Solution to Increase Resilience: Flooding Threats in Terni Distribution Grid. Energies 2019, 12, 744.».

[146] «T. Bragatto, M. Cresta, F. M. Gatta, A. Geri, M. Maccioni, M. Paulucci, “Assessment and possible solution to increase the resilience of Terni distribution Grid: the ice sleeves formation threat” AEIT 2018, 110th International Conference, Bari, 2018.».

[147] «Bragatto, T.; Cresta, M.; Cortesi, F.; Gatta, F.M.; Geri, A.; Maccioni, M.; Paulucci, M. Assessment and Possible Solution to Increase Resilience: Flooding Threats in Terni Distribution Grid. AEIT 2019, 111th International Conference, Firenze, 2019.».

[148] «S. E. Perkins and L. V. Alexander, “On the measurement of heat waves,” Journal of Climate, 26 (13), 4500-4517, 2013.».

[149] «S. F. Kew, S. Y. Philip, G. J. Van Oldenborgh, F. E. L. Otto, R. Vautard, and G. Van Der Schrier, “The exceptional summer heat wave in southern europe 2017,” Bulletin of the American Meteorological Society, 100(1), S49-S53, 2019.».

[150] «R. B. P. Faggian, “Raising awareness on climate-change related hazards that might impact electric infrastructures,” in AEIT 2018, Bari, 2018.».

[151] «S. Dunn, S. Wilkinson, D. Alderson, H. Fowler, and C. Galasso, “Fragility Curves for Assessing the Resilience of Electricity Networks Constructed from an Extensive Fault Database,” Natural Hazards Review 2018, 19(1).».

[152] «F. Ciasca, A. Sallati, and N. Tolu, “Italian National Resilience Plan 2017,” AEIT International Conference, Florence, 2017.».

[153] «Aven, T., “On some recent definitions and analysis frameworks for risk, vulnerability, and resilience,” Risk Anal. 31 (4), 515–522, 2011.».

[154] «D. Meloni and F. Carpine, “50 Years of weather observation at Federico Cesi weather station (1953-2002)” - 2002 - Terni Province - In Italian.».

[155] «Sanduleac M, Eremia M. and all, Integrating the Electrical Vehicles in the Smart Grid through Unbundled Smart Metering and multiobjective Virtual Power Plants, IEEE PES, Manchester, December 201».

[156] «New Smart Meter Design in Nobel Grid,».

[157] «M. Sănduleac ; L. Alacreu ; L. Pons ; A. Solar ; R. Alemany ; C. Stănescu. “Medium/Low Voltage Smart Grid Observability and PQ assesment with Unbundled Smart Meters” 2016 IEEE International Energy Conference (ENERGYCON).».

[158] «M. M. Albu, M. Sanduleac, C. Stanescu, Syncretic Use of Smart Meters for Power Quality Monitoring in Emerging Networks IEEE TRANSACTIONS ON SMART GRID, VOL. 8, NO. 1, JANUARY 2017 485».

[159] «J. Ringelstein, M. Shalaby, M. Sanduleac, L. Alacreu, J. Martins, V. Delgado-Gomes, "Software-driven active customer interface for DER integration", CIRED - Open Access Proceedings Journal, vol. 2017, no. 1, pp. 2003-2006, 2017.».

[160] Nobel Grid Project, «D9.2 - G3M Framework development».

[161] «D. Lagutin, F. Bellesini, T. Bragatto, A. Cavadenti, V. Croce, Y. Kortesniemi, H. C. Leligou, Y. Oikonomidis, G. C. Polyzos, G. Raveduto, F. Santori, P. Trakadas, M. Verber "Secure Open Federation of IoT Platforms through Interledger Technologies - the SO».

[162] «N. Stifter, A. Judmayer, P. Schindler, A. Zamyatin, and E. Weippl, "Agreement with Satoshi - On the Formalization of Nakamoto Consensus," in Cryptology ePrint Archive, Report 2018/400, 2018.».

[163] «S. Voulgaris et al., “SOFIE Deliverable D2.1: State of the Art Report,” 2018, available at: https://media.voog.com/0000/0042/0957/files/SOFIE_D2.1-State_of_the_Art_Report.pdf (accessed 1.2.2019).».

[164] «BIG IoT - Bridging Interoperability Gap of the Internet of Things, available at: http://big-iot.eu/ (accessed 6.2.2019).».

[165] «M. P. Andersen et al., "WAVE: A Decentralized Authorization System for IoT via Blockchain Smart Contracts," University of California at Berkeley Technical Report UCB/EECS-2017-234, 2017, available at: http://www2.eecs.berkeley.edu/Pubs/TechRpts/2017/E».

[166] «LO3 Energy, available at: https://lo3energy.com/ (accessed 5.2.2019).».

[167] «Grid Singularity, available at: http://gridsingularity.com/ (accessed 5.2.2019).».

[168] «SolarCoin, available at: https://solarcoin.org/ (accessed 5.2.2019).».

[169] «D. Reed et al., “Decentralized Identifiers (DIDs) v0.11 - Data Model and Syntaxes for Decentralized Identifiers (DIDs),” Draft Community Group Report, January 2019, available at: https://w3c-ccg.github.io/did-spec/ (accessed 30.1.2019).».

[170] «D. Lagutin, Y. Kortesniemi, N. Fotiou, and V. A. Siris, "Enabling Decentralised Identifiers and Verifiable Credentials for Constrained Internet-of-Things Devices using OAuth-based Delegation," in proceedings of Workshop on Decentralized IoT Security».

[171] «N. Fotiou, V. A. Siris, S. Voulgaris, G. C. Polyzos, “Interacting with the Internet of Things using Smart Contracts and Blockchain Technologies,” in proceedings of 11th SpaCCS, Melbourne, Australia, December 2018.».

[172] «N. Fotiou, V. A. Siris, G. C. Polyzos, D. Lagutin, “Bridging the Cyber and Physical Worlds using Blockchains and Smart Contracts,” in proceedings of Workshop on Decentralized IoT Security and Standards (DISS 2019), in conjunction with the NDSS Sympo».

[173] «T. Bragatto, F. M. Gatta, S. Lauria, M. Lazzaro, A. Geri, M. Maccioni, M. Paulucci, G. Paternò “Flexibility services to power systems from smart rural microgrid prosumers” 2018 IEEE 18th EEEIC, Palermo, 2018,».

[174] «A. Majzoobi and A. Khodaei, “Application of microgrids in supporting distribution grid flexibility,” in IEEE Transactions on Power Systems, Vol. 32, Issue 5, pp. 3660-3669, Sept. 2017.».

[175] «EC Smart Grids Task Force, “Regulatory Recommendations for the Deployment of Flexibility,” European Commission, 2015.».

[176] «OpenADR 2.0 Profile Specification B Profile. Available; http://www.openadr.org/specification [accessed on December, 2017]».

[177] «T. Bragatto, F. Carere, M. Cresta, F. M. Gatta, A. Geri, S. Lauria, M. Maccioni, M. Paulucci, “Smart Grid and Microgrid Cooperation in a Real Distibution Network under Emergency Conditions” 2018 IEEE 18th EEEIC, Palermo, 2018,».

[178] «M- Lazzaro, G. Paternò, T. Bragatto, M. Paulucci, F. Santori, F. M. Gatta, A. Geri, S. Lauria, and M. Maccioni, “Flexibility Services to Power Systems from Smart Rural Microgrid Prosumers,” 2018 IEEE 18th International Conference on Environment and El».

[179] «T. Bragatto; V.Croce; M. Cresta; M. Paulucci; F. Santori; D. Ziu “A real-life experience on 2nd life batteries services for Distribution System Operator” 2019 IEEE EEEIC / I&CPS Europe.».

[180] «M. Sănduleac, A. Corsi, T. Bragatto, D. Stanescu, C. Stanescu, A. Sbarcea, C. Bulac "Using Frequency measurements for data consistency assessment related to malicious data injection in distribution related ICT systems" ISFEE 2018, Bucarest, 2018».

[181] «G. E. Suh and S. Devadas, “Physical unclonable functions for device authentication and secret key generation,” in Proceedings of the 44th annual Design Automation Conference, 2007».

[182] «S. Tajik, E. Dietz, S. Frohmann, J.-P. Seifert, D. Nedospasov, C. Helfmeier, C. Boit and H. Dittrich, “Physical characterization of Arbiter PUFs,” in 16th International Workshop on Cryptographic Hardware and Embedded Systems, New York, 2014.».

[183] «C. Gu, J. P. Murphy and M. O'Niell, “A unique and robust single slice FPGA identification generator,” in IEEE International Symposium on Circuits and Systems, Melbourne, Victoria, Australia, 2014».

[184] «Project H2020 SUCCESS, www.success-h2020.eu/».

[185] «Yao, X, Tan, B., Hu, C., Islanding detection for PV plant using instantaneous power theory, 2016 IEEE Advanced Information Management, Communicates, Electronic and Automation Control Conference (IMCEC)».

[186] «T. Bragatto; M. Cresta; C. Kalogiros; M. Paulucci; M. Sanduleac; F. Santori; V. Scotto di Carlo “Innovative Tools for Demand Response Strategies: a Real-Life Experience” 2019 IEEE EEEIC / I&CPS Europe.».

[187] «M. H. Shoreh, P. Siano, M. Shafie-Khah, V. Loia, J. P. S. Catalão, "A survey of industrial applications of demand response", Electr. Power Syst. Res., vol. 141, pp. 32-49, Dec. 2016.».

[188] «P. Siano, "Demand response and smart grids—A survey", Renew. Sustain. Energy Rev., vol. 30, pp. 461-478, Feb. 2014.».

[189] «T. Müller, D. Möst “Demand response potential: available when needed?” Energy Policy, 115 (2018), pp. 181-198».

[190] «T. Bragatto, M. Paulucci, G. Thanos, M. Minou, C. Kalogiros "DSOs Using Demand-Side Management Techniques For Reducing Congestion Issues: The Case of ASM Terni" HAEE 2019, Athens, 2019».